Methods in Molecular Biology 1439

Springer Protocols

William P. Janzen *Editor*

High Throughput Screening

Methods and Protocols

Third Edition

Humana Press

METHODS IN MOLECULAR BIOLOGY

Series Editor
John M. Walker
School of Life and Medical Sciences
University of Hertfordshire
Hatfield Hertfordshire, UK

For further volumes:
http://www.springer.com/series/7651

High Throughput Screening

Methods and Protocols

Third Edition

Edited by

William P. Janzen

Epizyme, Inc.
Cambridge, MA, USA

Humana Press

Editor
William P. Janzen
Epizyme, Inc.
Cambridge, MA, USA

ISSN 1064-3745 ISSN 1940-6029 (electronic)
Methods in Molecular Biology
ISBN 978-1-4939-3671-7 ISBN 978-1-4939-3673-1 (eBook)
DOI 10.1007/978-1-4939-3673-1

Library of Congress Control Number: 2016941460

Printed on acid-free paper

This Humana Press imprint is published by Springer Nature
The registered company is Springer Science+Business Media LLC New York

Preface

Everything changes and nothing stands still—Heraclitus of Ephesus

This quote from Heraclitus was written almost 2500 years ago but could not fit the modern world more clearly. It has definitely proven true of the field of High Throughput Screening (HTS). When I began to work in HTS in 1989 it was virtually unheard of outside of a few industrial research laboratories. As an illustration, there are nine citations in PubMed from that year that contain "HTS" or "High Throughput Screening" in the title or key words. In 2013 there were over 2000. HTS has become integrated with large segments of research and across many fields. It has evolved from a highly specialized and secretive activity to a function that is made available to researchers through academic core labs.

But, "the more things change the more they stay the same" (Jean-Baptiste Alphonse Karr). This quote is also true of HTS. The basic processes underlying HTS have not changed in the last 25 years. Test a large number of potential effectors of a biological system as rapidly as possible while maintaining sufficient rigor to allow conclusions to be drawn from the data that is generated. The size, quality, and complexity of the chemical libraries used in HTS have changed, growing into the millions of compounds with rapid QC of compound composition. HTS assays have expanded to include complex cellular systems, mass spectrometer techniques, microfluidics and, in the most telling change of all, many of these have become widely available as kits. Systems that are capable of capturing, calculating, and visualizing millions of data points have become competitive sets of commercial software rather than custom-built systems that often relied on spreadsheet calculators. And last, but certainly not least, the recognition that quality is paramount in all of these factors has become an accepted tenet of not only HTS, but drug discovery in general.

So, in short, HTS has become mainstream. It is an important part of the drug discovery process, but is integrated with many other tools and techniques. The road that HTS has traveled in this period is paralleled by the three editions of this book. The first edition was designed to introduce the reader to basic HTS techniques and the chapters were designed to cover broad applications while the second added more detail and included key chapters providing detailed protocols. In recognition of this evolution, I have tried to move this edition more towards the traditional format of Method in Molecular Biology and have asked the authors to present detailed protocols for the techniques that they describe. The introductory chapter (Chapter 1) still provides an overview of important assay development techniques, but the following chapters provide what is needed in HTS today: details on how to develop and execute screens at whatever throughput the user needs.

I hope you enjoy this volume and find it useful.

Cambridge, MA, USA *William P. Janzen*

Contents

Preface ..... *v*
Contributors ..... *ix*

1 Design and Implementation of High-Throughput Screening Assays 1
David J. Powell, Robert P. Hertsberg, and Ricardo Macarrón

2 Characterization of Inhibitor Binding Through Multiple Inhibitor Analysis: A Novel Local Fitting Method 33
Thomas V. Riera, Tim J. Wigle, and Robert A. Copeland

3 High-Throughput Screening Using Mass Spectrometry within Drug Discovery 47
Mattias Rohman and Jonathan Wingfield

4 Structure-Based Virtual Screening of Commercially Available Compound Libraries 65
Dmitri Kireev

5 AlphaScreen-Based Assays: Ultra-High-Throughput Screening for Small-Molecule Inhibitors of Challenging Enzymes and Protein-Protein Interactions 77
Adam Yasgar, Ajit Jadhav, Anton Simeonov, and Nathan P. Coussens

6 Instrument Quality Control 99
Chatura Jayakody and Emily A. Hull-Ryde

7 Application of Fluorescence Polarization in HTS Assays 115
Xinyi Huang and Ann Aulabaugh

8 Time-Resolved Fluorescence Assays 131
Chen-Ting Ma and Eduard A. Sergienko

9 Protein Kinase Selectivity Profiling Using Microfluid Mobility Shift Assays 143
Peter Drueckes

10 Screening for Inhibitors of Kinase Autophosphorylation 159
Bianca Heedmann and Martin Klumpp

11 A Fluorescence-Based High-Throughput Screening Assay to Identify Growth Inhibitors of the Pathogenic Fungus *Aspergillus fumigatus* 171
Thomas M. Smith, Daryl L. Richie, and Jianshi Tao

12 *Mycobacterium tuberculosis* High-Throughput Screening 181
E. Lucile White, Nichole A. Tower, and Lynn Rasmussen

13 Identification of State-Dependent Blockers for Voltage-Gated Calcium Channels Using a FLIPR-Based Assay 197
Alberto di Silvio, JeanFrancois Rolland, and Michela Stucchi

14 A Luciferase Reporter Gene System for High-Throughput Screening of γ-Globin Gene Activators 207
Wensheng Xie, Robert Silvers, Michael Ouellette, Zining Wu, Quinn Lu, Hu Li, Kathleen Gallagher, Kathy Johnson, and Monica Montoute

15 A High-Throughput Flow Cytometry Assay for Identification of Inhibitors of 3′, 5′-Cyclic Adenosine Monophosphate Efflux 227
Dominique Perez, Peter C. Simons, Yelena Smagley, Larry A. Sklar, and Alexandre Chigaev

16 High-Throughput Cell Toxicity Assays 245
David Murray, Lisa McWilliams, and Mark Wigglesworth

17 BRET: NanoLuc-Based Bioluminescence Resonance Energy Transfer Platform to Monitor Protein-Protein Interactions in Live Cells 263
Xiu-Lei Mo and Haian Fu

18 Application of Imaging-Based Assays in Microplate Formats for High-Content Screening 273
Adam I. Fogel, Scott E. Martin, and Samuel A. Hasson

Index *305*

Contributors

Ann Aulabaugh • *Immunology, Inflammation and Infectious Diseases Discovery and Translational Area Roche Pharma Research & Early Development, Roche Innovation Center Shanghai Roche R&D Center (China) Ltd, Pudong, Shanghai, P. R. China*

Alexandre Chigaev • *University of New Mexico Cancer Center, Center for Molecular Discovery, University of Mexico, Albuquerque, NM, USA*

Robert A. Copeland • *Epizyme, Inc., Cambridge, MA, USA*

Nathan P. Coussens • *Division of Pre-Clinical Innovation, National Center for Advancing Translational Sciences (NCATS), National Institute of Health (NIH), Rockville, MD, USA*

Alberto Di Silvio • *Screening Technologies Unit, AXXAM SpA, Bresso-Milan, Italy*

Peter Drueckes • *CPC Screening Sciences, Novartis Pharma AG, Novartis Institutes for Biomedical Research, Inc., Basel, Switzerland*

Adam I. Fogel • *Biogen, Cambridge, MA, USA*

Haian Fu • *Department of Pharmacology and Emory Chemical Biology Discovery Center, Emory University School of Medicine, Atlanta, GA, USA; Department of Hematology and Medical Oncology, Winship Cancer Institute, Emory University, Atlanta, GA, USA*

Kathleen Gallagher • *Department of Target & Pathway Validation, Target Sciences, GlaxoSmithKline, Collegeville, PA, USA*

Samuel A. Hasson • *National Center for Advancing Translational Sciences, National Institute of Health, Rockville, MD, USA; Pfizer, Inc., Cambridge, MA, USA*

Bianca Heedmann • *Center for Proteomic Chemistry, Novartis Institute for Biomedical Research Basel, Inc., Basel, Switzerland*

Robert P. Hertzberg • *GSK Pharmaceuticals R&D, retired, Philadelphia, PA, USA*

Xinyi Huang • *Immunology, Inflammation and Infectious Diseases Discovery and Translational Area Roche Pharma Research & Early Development, Roche Innovation Center Shanghai Roche R&D Center (China) Ltd, Pudong, Shanghai, P. R. China*

Emily A. Hull-Ryde • *Center for Integrative Chemical Biology and Drug Discovery, UNC Eshelman School of Pharmacy, University of North Carolina at Chapel Hill, Chapel Hill, NC, USA*

Ajit Jadhav • *National Center for Advancing Translational Sciences, National Institutes of Health, Rockville, MD, USA*

William P. Janzen • *Epizyme, Inc., Cambridge, MA, USA*

Chatura Jayakody • *Warp Drive Bio LLC, Cambridge, MA, USA*

Kathy Johnson • *Department of Target & Pathway Validation, Target Sciences, GlaxoSmithKline, Collegeville, PA, USA*

Dmitri Kireev • *Center for Integrative Chemical Biology and Drug Discovery, Eshelman School of Pharmacy, University of North Carolina at Chapel Hill, Chapel Hill, NC, USA*

Martin Klumpp • *Center for Proteomic Chemistry, Novartis Institute for Biomedical Research Basel, Basel, Switzerland*

Hu Li • *Department of Biological Sciences, Platform Technology and Science, GlaxoSmithKline, Collegeville, PA, USA*

Quinn Lu • *Department of Target & Pathway Validation, Target Sciences, GlaxoSmithKline, Collegeville, PA, USA*

Chen-Ting Ma • *Conrad Prebys Center for Chemical Genomics, Sanford-Burnham-Prebys Medical Discovery Institute, La Jolla, CA, USA*
Ricardo Macarrón • *Alternative Drug Discovery, GSK Pharmaceuticals, Upper Providence, PA, USA*
Scott E. Martin • *Department of Discovery Oncology, Genentech Inc., South San Francisco, CA, USA*
Lisa McWilliams • *Discovery Sciences, Innovative Medicine, AstraZeneca, Macclesfield, UK*
Xiu-Lei Mo • *Department of Pharmacology and Emory Chemical Biology Discovery Center, Emory University School of Medicine, Atlanta, GA, USA*
Monica Montoute • *Department of Biological Sciences, Platform Technology and Sciences, GlaxoSmithKline, Collegeville, PA, USA*
David Murray • *Discovery Sciences, Innovative Medicines, AstraZeneca, Macclesfield, UK*
Michael Ouellette • *Department of Biological Sciences, Platform Technology and Science, GlaxoSmithKline, Collegeville, PA, USA*
Dominique Perez • *University of New Mexico Cancer Center, Center for Molecular Discovery, University of New Mexico, Albuquerque, NM, USA*
David J. Powell • *Alternative Drug Discovery, GSK Pharmaceuticals, Stevenage, Herts, UK*
Lynn Rasmussen • *High Throughput Screening Center, Southern Research Institute, Birmingham, AL, USA*
Daryl L. Richie • *Department of Infectious Diseases, Novartis Institutes for Biomedical Research, Inc., Emeryville, CA, USA*
Thomas V. Riera • *Epizyme, Inc., Cambridge, MA, USA*
Mattias Rohman • *Reagent and Assay Development, AstraZeneca R&D, Mölndal, Sweden*
Jean Francois Rolland • *Electrophysiology Unit, AXXAM SpA, Bresso-Milan, Italy*
Eduard A. Sergienko • *Conrad Prebys Center for Chemical Genomics, Sanford-Burnham-Prebys Medical Discovery Institute, La Jolla, CA, USA*
Robert Silvers • *Department of Biological Sciences, Platform Technology and Sciences, GlaxoSmithKline, Collegeville, PA, USA*
Anton Simeonov • *National Center for Advancing Translational Sciences (NCATS), National Institutes of Health, Rockville, MD, USA*
Peter C. Simons • *University of New Mexico Cancer Center, Center for Molecular Discovery, University of New Mexico, Albuquerque, NM, USA*
Larry A. Sklar • *University of New Mexico Cancer Center, Center for Molecular Discovery, University of New Mexico, Albuquerque, NM, USA*
Yelena Smagley • *University of New Mexico Cancer Center, Center for Molecular Discovery, University of New Mexico, Albuquerque, NM, USA*
Thomas M. Smith • *Center for Proteomic Chemistry, Novartis Institutes for Biomedical Research, Inc., Cambridge, MA, USA*
Michela Stucchi • *Screening Technologies Unit, AXXAM SpA, Bresso-Milan, Italy*
Jianshi Tao • *Genomics Institute of the Novartis Research Foundation, San Diego, CA, USA*
Nichole A. Tower • *High Throughput Screening Center, Southern Research Institute, Birmingham, AL, USA*
E. Lucile White • *High Throughput Screening Center, Southern Research Institute, Birmingham, AL, USA*
Mark Wigglesworth • *Discovery Sciences, Innovative Medicine, AstraZeneca, Macclesfield, UK*
Tim J. Wigle • *Ribon Therapeutics, Cambridge, MA, USA*

Jonathan Wingfield • *Screening Sciences, AstraZeneca, Cambridge, UK*
Zining Wu • *Department of Biological Sciences, Platform Technology and Science, GlaxoSmithKline, Collegeville, PA, USA*
Wensheng Xie • *Department of Target & Pathway Validation, Target Sciences, GlaxoSmithKline, Collegeville, PA, USA*
Adam Yasgar • *National Center for Advancing Translational Sciences (NCATS), National Institute of Health, Rockville, MD, USA*

Chapter 1

Design and Implementation of High-Throughput Screening Assays

David J. Powell, Robert P. Hertzberg, and Ricardo Macarrón

Abstract

HTS remains at the core of the drug discovery process, and so it is critical to design and implement HTS assays in a comprehensive fashion involving scientists from the disciplines of biology, chemistry, engineering, and informatics. This requires careful consideration of many options and variables, starting with the choice of screening strategy and ending with the discovery of lead compounds. At every step in this process, there are decisions to be made that can greatly impact the outcome of the HTS effort, to the point of making it a success or a failure. Although specific guidelines should be established to ensure that the screening assay reaches an acceptable level of quality, many choices require pragmatism and the ability to compromise opposing forces.

Key words Bioassay, Phenotypic, Drug screening, Human, Methodology

1 Introduction to the HTS Process

High-throughput screening (HTS) is a central function in the drug discovery process [1]. As the availability of increasing numbers of discreet chemical compounds has driven the development of larger collections for use in screening campaigns, the complexity of the HTS process has also increased. A number of HTS approaches can be employed to identify compounds of interest which may positively modulate a disease process. In some cases, individual pharmacological targets have been associated with a disease mechanism or process and a target-based approach is initiated through rational design, focused screening, or HTS. In other cases, screening is undertaken at a much more holistic cellular level; phenotypic approaches seek to identify compounds that modulate known biological characteristics that may have a close association with the disease of interest. In any case, drug discovery groups often rely on HTS as the primary engine driving lead discovery from both phenotypic and target-based approaches.

William P. Janzen (ed.), *High Throughput Screening: Methods and Protocols*, Methods in Molecular Biology, vol. 1439,
DOI 10.1007/978-1-4939-3673-1_1,

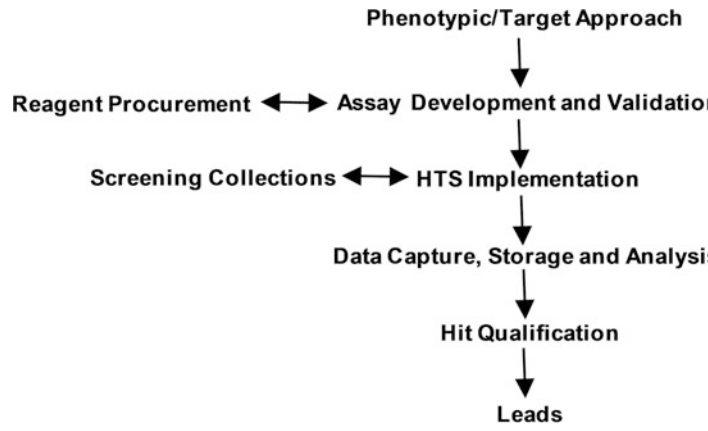

Fig. 1 Flow chart of the typical steps involved in the lead discovery process

The HTS process is a part of the lead discovery phase that includes the steps shown in Fig. 1. It is critically important to align the screening approach and assay method to ensure that a biologically relevant and robust screen is configured. The assay must be configured correctly so that compounds with the desired biological effect will be found if they exist in the screening collection. The assay would ideally demonstrate both low variability and a high signal window (SW) so that false negatives and false positives are minimized, although many assays have to strike a balance between these contributory elements. The screen must have sufficient throughput and low cost to enable screening of large compound collections. Considerable thought should also go into the experimental triaging which will clearly distinguish true pharmacological actives (qualified hits) from those which interfere in the assay detection system or act non-specifically. To meet these many requirements, organizations must ensure that communication between therapeutic departments (or principal investigators), assay development groups, and screening scientists occurs early - ideally at the initiation of the drug discovery program-and throughout the assay development phase.

Reagent procurement is often a major bottleneck in the HTS process. This can delay the early phases of assay development - e.g. when active protein cannot be obtained - and also delay HTS implementation if scale-up or supply of protein or cells fails to produce sufficient reagent to run the full screen. For efficient HTS operation for target-based screens, there must be sufficient reagent available to run the entire screening campaign before production HTS can start. This is not possible sometimes for phenotypic screens where the use of disease-relevant primary cells requires continuous resupply and quality control (QC); such demands often lead to longer and more resource-intensive campaigns.

These constraints also lead to sampling of the available chemical diversity or targeted screening using annotated compound sets as full-deck HTS might be too expensive or impossible to achieve when precious samples are used for screening [2]. Careful scheduling between reagent procurement departments and HTS functions is critical to ensure optimal use of robotics and personnel. Modern HTS laboratories have borrowed concepts from the manufacturing industry to smooth the flow of targets through the hit discovery process (e.g. supply chain management, constrained work-in-progress, and statistical quality control) and these ideas have paid off with higher productivity and shorter lead times.

Successful HTS implementation is multidisciplinary and requires close alignment of computational chemists directing the synthesis or acquisition of compound collections, sample management specialists maintaining and distributing screening decks, technology specialists responsible for setting up and supporting HTS automation, biologists and biochemists with knowledge of assay methodology, IT personnel capable of collecting and analyzing large datasets, and medicinal chemists capable of examining screening hits to look for patterns that define lead series. Through the marriage of these diverse specialties, therapeutic assays and targets can be put through the lead discovery engine called HTS and lead compounds will emerge.

2 Phenotypic Approaches to HTS

A phenotypic assay (or "black box" assay) measures an endogenous effect in a biological system, that effect being agnostic of a defined target but relevant in the context of reverting a disease state to a healthy state (e.g. a reduction of the secretion of pro-inflammatory cytokines is expected to have a therapeutic effect in pathological inflammation). Examples of such assays include secretion of protein factors, chemotaxis, apoptosis, cellular translocation, and cell shape change. Phenotypic assays are often favored for screening as the analyte or phenotype being measured is usually relevant for the disease indication or mechanism of interest, thus subsequent leads and candidates have a greater chance of translating to the patient. An advantage of phenotypic assays is the fact that multiple targets are screened at once, providing multiple chances for compounds to "find" the most tractable and biologically relevant target(s) in the cell system employed. However, phenotypic assays are more difficult to configure and more expensive to run, and hit deconvolution is time consuming and complex and may require a number of orthogonal approaches to confirm activity against a specific target. In addition, provision of cells for phenotypic screens can be challenging, particularly where primary cells are being used. Recent advances in stem cell and induced pluripotent stem cell (IPSC)

technologies have helped in the scalability of such assays and in driving the use of more complex 3D cell models for phenotypic screening [3].

In addition to lead discovery through HTS, phenotypic assays are being used for target identification and biology discovery through genetic or compound-based screening approaches. There is an increasing use of annotated compound sets to identify compounds with known target-based pharmacology in phenotypic assays to uncover novel cellular roles for those targets; such sets can also be used for drug repurposing. Genetic approaches are also becoming more sophisticated in this area; in addition to small inhibitory ribonucleic acid (siRNA) the use of viral based short hairpin ribonucleic acid (shRNA) allows the interrogation of disease-relevant cell systems at the genome level. Viral based CRISPR (clustered regularly interspersed palindromic repeats) screening is also now possible to explore gene function more rapidly in phenotypic assays [4].

The key considerations when contemplating a phenotypic HTS are the disease relevance of the analyte or phenotype being measured, the scalability of the cellular reagents (and its continued disease relevance), and the formatting of a robust screen that may have high variability due to the nature of the readout and the reagents being used. Post-screen triaging and deconvolution should be considered at the program outset as these may be highly challenging in themselves; it can often take many months or even years to fully confirm the exact pharmacological target or pathway that is modulating a phenotypic system.

While there has been an increase in screening more complex and disease-relevant systems in recent years, such assays nevertheless present complex challenges to reagent generation, assay development, and screening groups. As a consequence, many programs prefer to commit to the certainty of target-based screens, although their greater tractability and ease at which target activity can be confirmed can be offset by gaps in target biology knowledge leading to higher attrition downstream.

3 Choice of Therapeutic Target

There are three major considerations for choosing a therapeutic target destined for HTS: target validity (i.e. disease relevance), chemical tractability, and "screenability." Disease relevance is the most important consideration and also the most complex. Since there is an inverse relationship between target novelty and validity, organizations should choose a portfolio of targets which span the risk spectrum. Some targets will have a high degree of validation but low novelty (fast follower targets) and others will be highly novel but poorly linked to disease. Target validity can be assessed

with genetic approaches and/or compound-based experiments. Genetic approaches have advanced greatly in recent years to complement gene knockout and RNAi technologies which can be time consuming and sometimes lead to false conclusions. Newer additions to the repertoire of genome editing techniques such as transcription activator-like effector nucleases (TALENs), zinc finger nucleases, and the CRISPR/Cas9 system now allow researchers to quickly and selectively target specific genes to assess their functionality and involvement in disease mechanism. This has greatly increased the speed at which target disease hypotheses can be established and has allowed the study of functionality in more relevant models of human disease. Compound-based (chemical biology) target validation approaches require screening to identify tool compounds, followed by cell-based, Omic, or in-vivo experiments to assess functionality. Careful interpretation of cell-based and in-vivo data is required and selectivity might need to be assessed through further screening, e.g. in the kinase area, to confirm whether functionality can be attributed to a specific target. Both genetic and chemical biology approaches have their advantages and disadvantages, and most organizations use a combination. Many pharmaceutical companies are now refocusing efforts in the disease biology space to ensure that targets have a greater amount of disease association; running screens for "screenable" targets on the less validated end of the spectrum can subsequently increase attrition through the more expensive downstream translational part of the drug development process due to the absence of robust target validation.

While disease relevance should be the primary consideration when choosing a target, one should also consider technical factors important to the HTS process. Chemical tractability considerations relate to the probability that drug-like compounds capable of producing the therapeutically relevant effect against a specific target are present in the screening collection and can be found through screening. Years of experience in HTS within the industry have suggested that certain target classes are more chemically tractable than others, including G-protein-coupled receptors (GPCRs), ion channels, nuclear hormone receptors, and kinases. Enzymes generally are also very tractable targets; however screening collections might contain fewer potentially active compounds due to their wide diversity and bespoke biochemical reaction activities.

On the other side of the spectrum, targets that work via protein-protein interactions (PPI) have a lower probability of being successful in HTS campaigns. One reason for this is the fact that compound libraries often do not contain compounds of sufficient size and complexity to disrupt the large protein-protein interaction surface that is encountered in these targets. Natural products are one avenue that may be fruitful against protein-protein targets, since these compounds are often larger and more complex than those in traditional chemical libraries. The challenge for these

targets is finding compounds which have the desired inhibitory effect and also contain drug-like properties (e.g. are not too large in molecular weight). Nevertheless, natural products with undesirable physical-chemical properties from a lead perspective may still be suitable for tool compound use for target validation studies.

Certain subsets of PPI have been successful from an HTS point of view. For example, chemokine receptors are technically a protein-protein interaction (within the GPCR class) and there are several examples of successful lead compounds for targets in this class. Similarly, certain integrin receptors that rely on small epitopes (i.e. RGD sequences) have also been successful at producing lead compounds. More recently, compounds which inhibit the interactions of members of the bromodomain family of proteins with their interacting histone counterparts have been described [5], and some of these have already advanced to the clinic.

Despite the difficulties in identifying drug-like compounds from PPI screens, there will be a continuing demand for such screens based on the sheer number of disease-relevant mechanisms driven by such interactions; interest in this target class is expected to rise in coming years [6].

Based on the thinking that chemically tractable targets are easier to inhibit, some pharmaceutical companies have concentrated much of their effort on these targets and diminished work on more difficult targets. While this approach has some merit, one should be careful not to eliminate entirely target classes that would otherwise be extremely attractive from a biological point of view. Otherwise, the prophecy of chemical tractability will be self-fulfilled, since today's compound collections will not expand into new regions and we will never find leads for more difficult biologically relevant targets. There is clearly an important need for enhancing collections by filling holes that chemical history has left open [7]. There is evidence that continued attention in this area is yielding results as success rates for screens have increased in recent years to 75 % from about 60 % in the mid-2000s [6, 8].

A final factor to consider when choosing targets is "screenability" - the technical probability of developing a robust and high-quality screening assay. The impact of new assay technologies has made this less important, since there are now many good assay methods available for a wide variety of target types (*see* Subheading 3). Nevertheless, some targets are more technically difficult than others. Of the target types mentioned above, GPCRs, kinases, proteases, nuclear hormone receptors, and protein-protein interactions are often relatively easy to establish screens for. Screening ion channels continues to be challenging, although as mentioned later new technologies are being developed which make these more approachable from an HTS point of view. Enzymes other than kinases and proteases must be considered on a case-by-case basis, depending on the nature of the substrates involved.

A 2014 survey found an encouraging trend in target class selection [6]. Although GPCRs and kinases were still well represented, the most abundant target class reported by HTS labs was "other enzymes." Furthermore, a majority of labs were pursuing protein-protein interaction screens and this class was predicted to increase. This suggests that pharmaceutical researchers may be less risk averse than in the past and are now choosing targets based more on biological rationale than tractability or "screenability."

All of these factors must be considered on a case-by-case basis and should be evaluated at the beginning of a target-to-lead effort before making a choice to go forward. Working on an expensive and technically difficult assay must be balanced against the degree of validation and biological relevance. While the perfect target is chemically tractable, technically easy, inexpensive, and biologically relevant, such targets are rare. The goal is to work on a portfolio that spreads the risk among these factors and balances the available resources.

4 Choice of Assay Method

There are usually several ways of looking for hits of any given target. The first and major choice to make is between a biochemical and cell-based assay. Biochemical is generally understood to mean an assay developed to look for compounds that interact with an isolated target in an artificial environment. This was the most popular approach in the early 1990s, the decade in which HTS became a mature and central area of drug discovery. This bias toward biochemical assays for HTS was partly driven by the fact that cell-based assays were often more difficult to run in high throughput. However, advances in technology and instrumentation for cell-based assays that translated to commercial products around the early 2000s, together with disappointments with the success rates of molecular based hit discovery campaigns, changed the tilt toward cell-based HTS [6]. This theme has continued with the increase in phenotypic HTS in recent years as groups focus on more disease-relevant screens. A 2014 survey found that 63% of HTSs were being run in cell-based format, with a full 20% deemed to be phenotypic [6].

Projections foresee even greater use of cellular formats as technologies such as imaging, IPSC, and complex/3D models continue to evolve. For most drug discovery programs, both types of assay are required for hit discovery and characterization and subsequent lead optimization. Everything being equal (technical feasibility, cost, throughput), cell-based assays are often preferred for HTS because compounds tested will be interacting with a more realistic mix of protein target conformations in their physiological milieu, i.e. with the right companions (proteins, metabolites, etc.) at the

right concentration. Additionally, cell-based assays tend to avoid some common artifacts in biochemical assays such as aggregators [9] and other nonspecific effects which may require additional triaging to confirm true pharmacological activity at target [10]. On the other hand, cell-based assays may identify hits that do not act on the target or pathway of interest and may miss hits of interest that do not penetrate the cell membrane.

If a cell-based assay is chosen for primary screening, a biochemical assay will often be used as a secondary screen to characterize hits and help guide lead optimization (and vice versa). A wide variety of assay formats are now available at relatively affordable prices to cope with most needs in the HTS labs. The following sections provide a very succinct summary of some of the most popular choices. A comprehensive review by Inglese and co-workers is recommended for further reading [11].

4.1 Biochemical Assay Methods

Most biochemical screens today use simple homogeneous "mix-and-read" formats. This is particularly true for HTS assays run in industrial labs that are conducted on high-density microtiter plates (now predominantly at 1536 wells).

The most common assay readouts used in biochemical assay methods for HTS are optical, including absorbance, fluorescence, and luminescence. Among these, fluorescence-based techniques are amongst the most important detection approaches used for HTS with TR-FRET being the most common [6]. Fluorescence techniques give very high sensitivity, which allows assay miniaturization, and are amenable to homogeneous formats. One factor to consider when developing fluorescence assays for screening compound collections is wavelength; in general, short excitation wavelengths (especially those below 400 nm) should be avoided to minimize interference produced by test compounds.

Although fluorescence intensity measurements have been successfully applied in HTS, this format is mostly applied to a narrow range of enzyme targets for which fluorogenic substrates are available. A more widely used fluorescence readout is time-resolved fluorescence resonance energy transfer (TR-FRET). This is a dual-labeling approach that is based upon long-range energy transfer between fluorescent Ln^{3+}-complexes and a suitable resonance energy acceptor. These approaches give high sensitivity by reducing background and a large number of HTS assays have now been configured using TR-FRET [6]. This technique is highly suited to measurements of protein-protein interactions and has also been tailored to detect important metabolites such as cAMP. Bioluminescence resonance energy transfer (BRET) is an analogous technique which can also be used for cellular readouts. Another versatile fluorescence technique is fluorescence polarization (FP), which can be used to measure bimolecular association events. Immobilized metal-ion affinity-based FP (IMAP, Molecular Devices) is a

variation of FP that can be applied to test activity of kinases and other enzymes. The success of fluorescent techniques has seen a dramatic reduction in the use of radiometric formats, such as scintillation proximity assay (SPA), which now constitute only about 1% of screens run [6].

Other technologies able to circumvent technical hurdles for niche difficult assays are amplified luminescence proximity (AlphaScreen®/AlphaLisa®, Perkin Elmer) [12] and electrochemiluminescence (ECL, Meso Scale Discovery) [13].

Label-free assays are a diverse set of techniques of growing interest and demand. Many of the methods are modern adaptation to the high-throughput environment of well-established technologies such as mass spectroscopy or calorimetry. The mass spectrometry (MS) screening field in particular has made significant advances in recent years with the introduction of technologies such as RapidFire® (Agilent) which couples a high-throughput autosampler/desalting step with an integrated ms/MALDI. This technology can now be used for medium-throughput screens with an average read time of <10 s/sample [14]. Additional technology development in this space is ongoing, and there are realistic prospects that throughput will be sufficient for full-deck HTS in the near future.

As previously mentioned, biochemical assays are more prone to interference through non-specific effects, and there are known classes of pan-active interference compounds [9]. These can include compound-mediated aggregation, protein reaction, optical interference in fluorescent/Alpha readouts (e.g. quenching, compound absorbance) and other non-stoichiometric effects. Considerable thought should go into downstream confirmatory assays that will conclusively demonstrate binding of compound to the target to identify qualified hits.

4.2 Cell-Based Assay Methods

As recently as the mid-1990s, most cell-based assay formats were not consistent with HTS requirements. However, as recent technological advances have facilitated higher throughput functional assays, cell-based formats make up a reasonable proportion of screens performed today. One of the most important advances in cell-based assay methodology was the development of the FLIPR® (Molecular Devices), a fluorescence imaging plate reader with integrated liquid handling that facilitates the simultaneous fluorescence imaging of 384 samples to measure intracellular calcium mobilization in real time [15]. This format is now commonly used for GPCR and ion channel targets. Based on the success of the FLIPR®, several additional cell-based assays for GPCRs were developed including aequorin and assays to measure intracellular cAMP (TR-FRET, AlphaScreen® and enzyme fragment complementation) [16].

Significant advances in ion channel screening have occurred over the past decade. Calcium-sensing dyes read on FLIPR® are

commonly used to measure channels that conduct calcium, while voltage-sensing dyes are used to track changes in membrane potential. An important advance in high-throughput ion channel assays was the development of FRET-based voltage-sensing dyes, where a pair of molecules exhibit FRET which is disrupted when the membrane is depolarized. Ion flux assays using non-radioactive tracers analyzed by atomic absorbance spectroscopy (AAS) can now be run in HTS format using recently available instrumentation. And the standard for measuring ion channel activity, patch-clamp measurements, has been facilitated by the development of automated instrumentation such as Ionworks® Quattro, PatchXpress®, QPatch, and Barracuda® [17]. While these technologies have revolutionized ion channel research, further improvements are still necessary before patch-clamp measurements can be used for primary HTS other than focused libraries.

Cellular phenotypes and pathways are now routinely measured using a variety of techniques amenable to HTS. The reporter gene assay is the oldest and most well-studied method which allows the discovery of compounds that modulate a pathway resulting in changes in gene expression [16]. This method offers certain advantages relative to other cell-based assays, in that it requires fewer cells, is easier to automate, and can be performed in 1536-well plates. Descriptions of miniaturized reporter gene readouts include luciferase (the most popular reporter gene) [18], secreted alkaline phosphate, and beta-lactamase. However, reporter gene assays are relatively low resolution since they measure effects on an entire pathway at once. Advances in cellular imaging have allowed HTS of higher resolution phenomena such as protein secretion and redistribution, receptor internalization, and other cellular pathway events (Fig. 2 shows extracellular collagen deposition from primary human fibroblasts, such high-resolution images have become routine in cellular screening groups). There is now a wide range of imaging readers for use in screening which use both confocal and non-confocal methodologies; examples include the IN Cell reader series (GE Life Sciences), the Opera platform (Perkin Elmer), and the Acumen® Cellista (TTP Labtech). While high-content imaging readouts are now a mainstay for screens in the phenotypic area, they do come with a significant IT infrastructure requirement, particularly in terms of image storage and data transfer.

Another cellular phenotype that is commonly measured in HTS is protein secretion. Classical methods to measure protein secretion such as radioimmunoassay (RIA) and enzyme-linked immunosorbent assay (ELISA) are being replaced by improved techniques such as AlphaLisa® and MultiArray® or MultiSpot® electrochemiluminescence-based solutions (Meso Scale Discovery [13]).

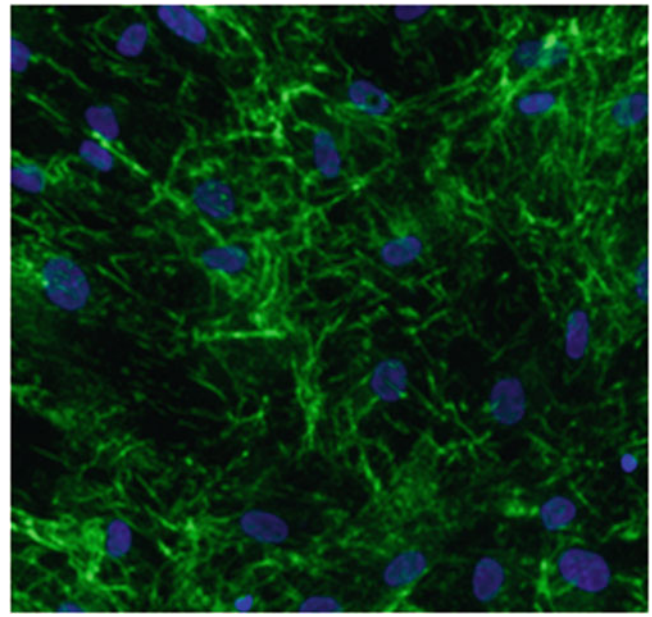

Fig. 2 Representative image of cellular information captured on high-content screening imagers. Primary pulmonary fibroblasts were treated with TGF-B in a Ficoll-containing media before staining with Hoechst dye (*blue*) and for mature collagen (*green*). Image was captured on an IN Cell 2000 series imager

4.3 Matching Assay Method to Target Type

Often, one has a choice of assay method for a given target type (Table 1). To illustrate the options that might be available when choosing an assay format for HTS a protein kinase target example will be considered. Kinases are most often screened in biochemical formats such as TR-FRET, AlphaLisa®, and IMAP FP, although cellular phospho-protein readouts using TR-FRET, MSD, or imaging are also possible but used much less routinely. Biochemical assay formats are very tractable with a high probability that a robust screen will be completed but with a wide range of development options available. Such assays can use isolated kinase domains or full-length proteins, and substrates can take the form of peptides or proteins which might be phosphorylated in-vivo. The concentration of the second substrate, ATP, can also be varied from concentrations at K_m (typically 1–100 μM) to endogenous cellular levels of ~2 mM. As a consequence of these many development options, the resulting HTS assay can be more or less easy to develop and scale and may be more or less representative of the physiological kinase setting.

This example illustrates some of the trade-offs one needs to consider when choosing an assay type. In general, one should choose the assay format that is easiest to develop, most predictable, most relevant biologically, and cheapest to run. These factors,

Table 1
The most important assay formats for various target types are shown

	Assay formats	
Target type	**Biochemical**	**Cell based**
GPCRs	SPA, FP, FIDA	FLIPR, reporter gene, aequorin, TR-FRET, AlphaScreen, EFCcell imaging
Ion channels	SPA, FP	FLIPR, FRET, AAS, automated patch clamp
Nuclear hormone receptor	FP, TR-FRET, SPA, AlphaScreen	Reporter gene, cell imaging
Kinases	FP, TR-FRET, SPA, IMAP, MS	Cellular phosphorylation, cell imaging
Protease	FLINT, FRET, TR-FRET, FP, SPA, MS	Reporter gene, cell imaging
Other enzymes	FLINT, FRET, TR-FRET, FP, SPA, absorbance, MS	
Protein-protein	TR-FRET, FRET, BRET, SPA, ECL, AlphaScreen	BRET, cell imaging, reporter gene

EFC enzyme fragment complementation, *FIDA* fluorescence intensity distribution analysis, *FLINT* fluorescence intensity

however, are not always known in advance. And even worse, they can be at odds with each other and thus must be balanced to arrive at the best option. Additional important quality considerations include compound interference issues and assay variability. It makes little sense to run a cheap and easy assay that is variable or overly sensitive to inhibition. In some cases it makes sense to parallel track two formats during the assay development phase and choose between them based on which is easiest to develop and most facile. Finally, in addition to these scientific considerations, logistical factors such as the number of specific readers or robot types available in the HTS lab and the queue size for these systems must be taken into account.

5 Assay Development and Validation

The final conditions of an HTS assay are chosen following the optimization of quality without compromising throughput while keeping costs as low as possible. The most critical points that must be considered in the design of a high-quality assay are biochemical data and statistical performance. Assay optimization is often required to achieve acceptable HTS performance while keeping assay conditions within the desired range. This usually significantly improves the stability and/or activity of the biological system studied, and has therefore become a key step in the development of screening assays [19].

5.1 Critical Biochemical Parameters in HTS Assays

The success of an HTS campaign in finding hits with the desired profile depends primarily on the presence of such compounds in the collection tested. But it is also largely dependent on the ability of the researcher to engineer the assay in accordance with that profile while reaching an appropriate statistical performance.

A classical example that illustrates the importance of the assay design is how substrate concentration determines the sensitivity for different kinds of enzymatic inhibitors. If we set the concentration of one substrate in a screening assay at ten times K_m, competitive inhibitors of that enzyme-substrate interaction with a K_i greater than 1/11 of the compound concentration used in HTS will show less than 50% inhibition and will likely be missed - i.e. competitive inhibitors with a K_i of 0.91 μM or higher would be missed when screening at 10 μM. On the other hand, the same problem will take place for uncompetitive inhibitors if substrate concentration is set at 1/10 of its K_m. Therefore, it is important to know what kind of hits are sought in order to make the right choices in substrate concentration; one often chooses a substrate concentration that facilitates discovery of both competitive and uncompetitive inhibitors.

In this section, we describe the biochemical parameters of an assay that have a greater influence on the sensitivity of finding different classes of hits and some recommendations about where to set them.

5.1.1 Enzymatic Assays

Substrate Concentration

The sensitivity of an enzymatic assay to different types of inhibitors is a function of the ratio of substrate concentration to K_m (S/K_m).

Competitive inhibitors: For reversible inhibitors that bind to a binding site that is the same as one substrate, the more of that substrate present in the assay, the less inhibition will be observed. The relationship between IC50 (compound concentration required to observe 50% inhibition of enzymatic activity with respect to an uninhibited control) and K_i (inhibition constant) is [20]

$$\mathrm{IC50} = (1 + S/K_m) \times K_i$$

As shown in Fig. 3, at S/K_m ratios less than 1 the assay is more sensitive to competitive inhibitors, with an asymptotic limit of $\mathrm{IC50} = K_i$. At high S/K_m ratios the assay becomes less suitable for finding this type of inhibitors. Knowledge of the physiological substrate concentration is useful in interpreting downstream pharmacology. For example, if a kinase with a low K_m for ATP, e.g. 10 μM, is screened for compounds in an assay where $[S] = K_m$, then ATP competitive compounds might show a significant pharmacology drop-off in cell-based assays where the intracellular ATP concentration is 1.5–2 mM (100–200 × K_m).

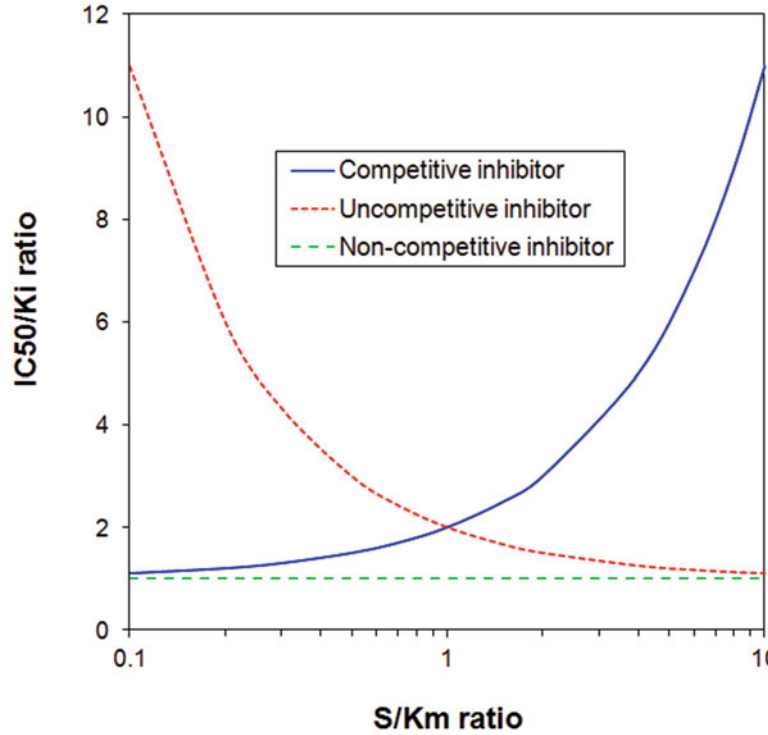

Fig. 3 Variation of IC50/K_i ratio with the S/K_m ratio for different type of inhibitors. At [S] = K_m, IC50 = 2K_i for competitive (*blue line*) and uncompetitive (*red line*) inhibitors. For noncompetitive inhibitors (*green line*) IC50 = K_i at all substrate concentrations

Uncompetitive inhibitors: If the inhibitor binds to the enzyme-substrate complex or any other intermediate complex but not to the free enzyme, the dependence on S/K_m is the opposite to what has been described for competitive binders. The relationship between IC50 and K_i is [20]

$$IC50 = (1 + K_m/S) \times K_i$$

High substrate concentrations make the assay more sensitive to uncompetitive inhibitors (Fig. 3).

Noncompetitive (allosteric) inhibitors: If the inhibitor binds with equal affinity of the free enzyme and to the enzyme-substrate complex, the inhibition observed is independent of the substrate concentration. The relationship between IC50 and K_i is [20]

$$IC50 = K_i$$

Mixed inhibitor: If the inhibitor binds to the free enzyme and to the enzyme-substrate complex with different affinities (K_i1 and K_i2, respectively), the relationship between IC50 and K_i is [21]

$$IC50 = (S + K_m)/(K_m/K_i1 + S/K_i2)$$

In summary, setting the substrate(s) concentration(s) at the K_m value is an optimal way of ensuring that all type of inhibitors exhibiting a K_i close to or below the compound concentration in the assay can be found in an HTS campaign. Nevertheless, if there is a specific interest in favoring or avoiding a certain type of inhibitor, then the S/K_m ratio would be chosen considering the information provided above. For instance, many ATP-binding enzymes are tested in the presence of saturating concentrations of ATP to minimize inhibition from compounds that bind to the ATP-binding site.

Quite often the cost of one substrate or the limitations of the technique used to monitor enzymatic activity (Table 2) may preclude setting the substrate concentration at its ideal point.

As in many other situations found while implementing an HTS assay, the screening scientist must consider all factors involved and look for the optimal solution. For instance, if the sensitivity of a detection technology requires setting $S = 10 \times K_m$ to achieve an acceptable signal to background, competitive inhibitors with a K_i greater than 1/11 of the compound concentration tested will not likely be identified and will limit the campaign to finding more potent inhibitors. In this case, working at a higher compound concentration would help to find some of the weak inhibitors otherwise missed. If this is not feasible, it is better to lose weak inhibitors while running a statistically robust assay, rather than making the assay more sensitive by lowering substrate concentration to a point of unacceptable signal to background. The latter approach is riskier since a bad statistical performance would jeopardize the discovery of more potent hits (*see* Subheading 4.3).

Table 2
Examples of limitations to substrate concentration imposed by some popular assay technologies

Assay technology	Limitations
Fluorescence	Inner filter effect at high concentrations of fluorophore (usually >1 μM)
Fluorescence polarization	>30 % substrate depletion required
Capture techniques (ELISA, SPA, FlashPlate, others)	Antibody availability. Concentrations of the reactant captured must be in alignment with the upper limit of binding capacity
Capture techniques and assay monitoring binding	Nonspecific binding (NSB) of the product or of any reactant to the capture element (bead, plate, membrane, antibody, etc.) may result in misleading activity determinations
All	Sensitivity limits impose a lower limit to the amount of product detected

These limitations also apply to ligand in binding assays or other components in assay monitoring any kind of binding event

Enzyme Concentration

The accuracy of inhibition values calculated from enzymatic activity in the presence of inhibitors relies on the linear response of activity to the enzyme concentration. Therefore, an enzyme dilution study must be performed in order to determine the linear range of enzymatic activity with respect to enzyme concentration; this is important when single end-point reads are being used for screening.

As shown in the mass spectrometry-based readout in Fig. 4a for kynurenine mono-oxygenase (KMO), at high enzyme concentrations there is typically a loss of linearity due to substrate depletion (although protein aggregation or limitations in the detection system could cause similar effects in biochemical assay systems). If the enzyme is not stable at low concentrations, or if the assay method does not respond linearly to product formation or substrate depletion, there could also be a lack of linearity in the lower end.

In addition, enzyme concentration marks a lower limit to the accurate determination of inhibitor potency. IC50 values lower than one half of the enzyme concentration cannot be measured; this tight binding effect is often referred to as "bottoming out." As the quality of compound collections improves, this could be a real problem since SAR trends cannot be observed among the more potent hits. Obviously, enzyme concentration must be kept far below the concentration of compounds tested in order to find any inhibitor. In general, compounds are tested at micromolar concentrations (1–100 μM) and, as a rule of thumb, it is advisable to work at enzyme concentrations below 100 nM.

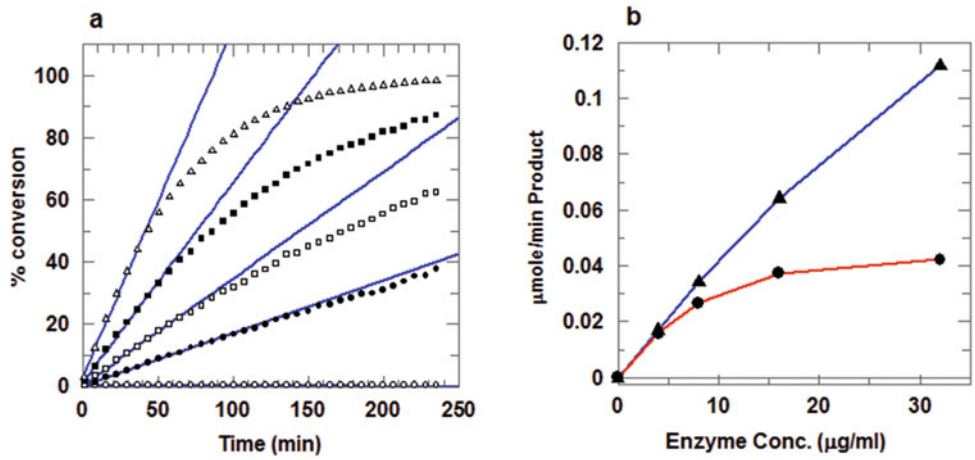

Fig. 4 (**a**) Enzyme dilution (in μg protein/ml) curve for kynurenine monooxygenase (KMO). Enzyme activity was measured by mass spectrometry following the methodology described [14]. *Open circle*—0 μg/ml, *filled diamond*—4 μg/ml, *open square*—8 μg/ml, *filled square*—16 μg/ml, *open triangle*—32 μg/ml. (**b**) Product formation for KMO in μmoles/min at varying enzyme concentration (in μg protein/ml) at $T = 50$ min (*blue line*) and $T = 250$ min (*red line*)

On the other hand, the assay can be made insensitive to certain undesired hits (such as inhibitors of enzymes added in coupled systems) by using higher concentrations of these proteins. In any case, the limiting step of a coupled system must be the one of interest, and thus the auxiliary enzymes should always be in excess.

Incubation Time and Degree of Substrate Depletion

As described above for enzyme concentration, it is important to assess the linearity versus time of the reaction analyzed. HTS assays are often end-point and so it is crucial to select an appropriate incubation time. Although linearity versus enzyme concentration is not achievable if the end-point selected does not lie in the linear range of the progress curves for all enzyme concentrations involved, exceptions to this rule do happen, and so it is important to check it as well.

To determine accurate kinetic constants, it is crucial to measure initial velocities. However, for the determination of acceptable inhibition values it is sufficient to be close to linearity. Therefore, the classical rule found in biochemistry textbooks of working at or below 10% substrate depletion (e.g., [22]) does not necessarily apply to HTS assays and such considerations may be challenging with some formats such as FP. Provided that all compounds in a collection are treated in the same way, if the inhibitions observed are off by a narrow margin it is not a problem. As shown in Fig. 5, at 50% substrate depletion with an initial substrate concentration at its K_m, the inhibition observed for a 50% real inhibition is 45%, an

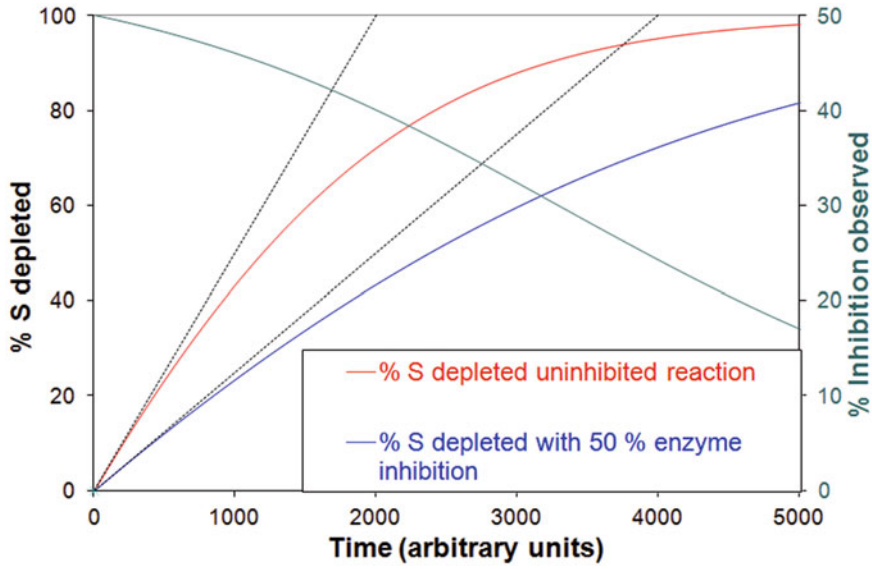

Fig. 5 Theoretical progress curves at $S = K_m$ of an uninhibited enzymatic reaction (*red*) and a reaction with an inhibitor at its IC50 concentration (*blue*). The inhibition values determined at different end-points throughout the progress curve are shown in *green*. Initial velocities are represented by *dotted lines*

acceptable error. For higher inhibitions the errors are lower (e.g., instead of 75% inhibition 71% would be observed). At lower S/K_m ratios the errors are slightly higher (e.g., at $S = 1/10\ K_m$, a 50% real inhibition would yield an observed 42% inhibition, again at 50% substrate depletion). Figure 4b shows the effect on KMO product formation when comparing product formation at 50 and 250 min; in this case, substrate depletion at longer incubation times could desensitize compound inhibition at the higher enzyme concentrations as depicted.

This flexibility to work under close-to-linearity but not truly linear reaction rates makes it feasible to use certain assay technologies in HTS - e.g. fluorescence polarization (FP) - that require a high proportion of substrate depletion in order to produce a significant change in signal. Secondary assays configured within linear rates should allow a more accurate determination of IC50s for hits.

In reality, the experimental progress curve for a given enzyme may differ from the theoretical one depicted here for various reasons such as non-Michaelis-Menten behavior, reagent deterioration, product inhibition, and detection artifacts. In view of the actual progress curve, practical choices should be made on experimental kinetic data to avoid missing interesting hits.

Order of Reagent Addition

The order of addition of reactants and putative inhibitors is important to modulate the sensitivity of an assay for slow binding and irreversible inhibitors.

A preincubation (usually 5–10 min) of enzyme and test compound favors the finding of slow-binding competitive inhibitors. If the substrate is added first, these inhibitors have a lower probability of being found. Assays should ideally have many enzyme/kinase turnovers during the time course to minimize the complications of single/low-turnover reactions.

In some cases, especially for multisubstrate reactions, the order of addition can be engineered to favor certain uncompetitive inhibitors.

5.1.2 Binding Assays

Although this section is focused on receptor binding, other binding reactions (protein-protein, protein-nucleic acid, etc.) are governed by similar laws, and so assays to monitor these interactions should follow the guidelines hereby suggested.

Ligand Concentration

The equation that describes binding of a ligand to a receptor, developed by Langmuir to describe adsorption of gas films to solid surfaces, is virtually identical to the Michaelis-Menten equation for enzyme kinetics:

$$BL = B_{max} \times L/(K_d + L)$$

where BL = bound ligand concentration (equivalent to v0), B_{max} = maximum binding capacity (equivalent to maximum velocity (V_{max})), L = total ligand concentration (equivalent to S), and K_d = equilibrium affinity constant also known as dissociation constant (equivalent to K_m).

Therefore, all equations disclosed in Subheading "Substrate Concentration" can be directly translated to ligand (L)-binding assays. For example, for competitive binders,

$$IC50 = (1 + L/K_d) \times K_i$$

Uncompetitive binders cannot be detected in binding assays; functional assays must be performed to detect this inhibitor class. Allosteric binders could be found if their binding modifies the receptor in a fashion that prevents ligand binding.

Typically, ligand concentration is set at the K_d concentration as an optimal way to attain a good signal (50% of binding sites occupied). This results in a good sensitivity for finding competitive binders.

Receptor Concentration

The same principles outlined for enzyme concentration in Subheading 5.1.1 apply to receptor concentration, or concentration of partners in other binding assays. In most cases, especially with membrane-bound receptors, the nominal concentration of receptor is not known but can be determined by measuring the proportion of bound ligand at the K_d. In any case, linearity of response (binding) with respect to receptor (membrane) concentration should be assessed.

In traditional radiofiltration assays it was recommended to set the membrane concentration so as to reach at most 10% of ligand bound at the K_d concentration, i.e., the concentration of receptor present should be below 1/5 of K_d [23]. Although this is appropriate to get accurate binding constants, it is not absolutely required to find competitive binders in a screening assay. Some formats (FP, SPA in certain cases) require a higher proportion of ligand bound to achieve acceptable statistics, and receptor concentrations close or above the K_d value have to be used.

Another variable to be considered in ligand-binding assays is nonspecific binding (NSB) of the labeled ligand. NSB increases linearly with membrane concentration. High NSB leads to unacceptable assay statistics, but this can often be improved with various buffer additives (*see* Subheading 5.2).

Preincubation and Equilibrium

As discussed for enzymatic reactions, a preincubation of test compounds with the receptor would favor slow binders. After the preincubation step, the ligand is added and the binding reaction should be allowed to reach equilibrium in order to ensure a proper calculation of displacement by putative inhibitors. Running

binding assays at equilibrium is convenient for HTS assays, since one does not have to carefully control the time between addition of ligand and assay readout as long as the equilibrium is stable.

5.1.3 Cell-Based Assays

The focus of the previous sections has been on cell-free systems. Cell-based assays offer different challenges in their setup with many built-in factors that are out of the scientist's control. Nevertheless, some of the points discussed above apply to them, *mutatis mutandi*.

One of the most important considerations is cell type. The most physiologically relevant cells are primary human cells (disease cells are even better), but these are very difficult and expensive to procure. Advances in stem cell/IPSC science are facilitating the provision of cells for HTS that are closer to the primary human cell. However, despite increases in the level of phenotypic screening and the use of more complex cellular models [3, 6], transformed/recombinant cells remain the most commonly used cell type for HTS.

Important considerations when developing cell-based assays include the following [19, 24]:

1. Cell culture details should be well documented and reproducible. Most problems with cell-based assays can be traced to problems with the cells.
2. Consider using cryopreserved cells as an assay source to reduce variability and improve screening scheduling logistics. Many primary cell types can now be cryopreserved.
3. Adherent cells or suspension cells can be used, and the choice is based on the cell type and assay readout method. In general, try to mimic the physiological conditions as much as possible while considering assay logistics.
4. Either stable cell lines or transient transfection can be used. Expression levels of the recombinant protein(s) should be confirmed. Extremely high expression levels should generally be avoided.
5. Consider using modified baculovirus (BacMam virus) gene delivery technology for transient expression of target proteins in mammalian cells [25].
6. When using stable cell lines, use early passages to avoid cells losing their responsiveness.
7. Lower numbers of cells are preferred for cost reasons, but at least 1000 cells per well should generally be used to minimize stochastic single-cell events. The response observed should be linear with respect to the number of cells.

8. Pay attention to cell clumps which can cause variability.
9. Preincubation of cells with compounds should be considered when applicable (e.g., assays in which a ligand is added).
10. Optimal incubation time should be selected in accordance to the rule of avoiding underestimation of inhibition or activation values (*see* Subheading "Incubation Time and Degree of Substrate Depletion"). All other factors being equal, shorter incubation times minimize cytotoxic interference problems.
11. Cell-based assays tend to be more sensitive to dimethyl sulfoxide (DMSO) than biochemical assays. Determine the DMSO sensitivity of the assay and configure the protocol to remain well below this level.
12. Use standard inhibitors and/or activators during the screening run to confirm that the desired signal is observed.
13. Pay attention to edge effects which occur commonly in cell-based assays due to problems with incubators or uneven cell distribution of cells in the well. Incubating seeded plates at room temperature before placing them in the incubator can help this problem [26].

5.2 Assay Optimization

In-vitro assays are performed in artificial environments in which the biological system studied could be unstable or exhibiting an activity below its potential. The requirements for stability are higher in HTS campaigns than in other areas of research. In HTS runs, diluted solutions of reagents are used throughout long periods of time (typically 4–12 h) and there is a need to keep both the variability low and the signal to background high. Additionally, several hundreds of thousands of samples are usually tested, and economics often dictates one to reduce the amount of reagents required. In this respect, miniaturization of assay volumes has been in continuous evolution, from tubes to 96-well plates to 384-well plates to 1536 and beyond. Many times, converting assays from low-density to high-density formats is not straightforward. Thus, in order to find the best possible conditions for evaluating an HTS target, optimization of the assay should be accomplished as part of the development phase.

HTS libraries contain synthetic or natural compounds that in most cases are dissolved in DMSO. The tolerance of the assay to DMSO must be considered. Typically, compounds are stored at concentrations ranging between 1 and 30 mM. Test compound concentrations in primary screening are in the 1–30 μM range. Therefore, DMSO concentrations from 0 to 10% are tested. It is critical to work at DMSO concentrations in a region of minimal

variation, as otherwise compound effects can be obscured by variability in the addition of compound stocks (typically the smallest volume in the assay mix, and thus the most sensitive liquid-handling step).

If a significant decrease of activity/binding is observed at the standard solvent concentration - typically 0.5–1% (v/v) DMSO - lower test compound concentrations may be required. In some cases the detrimental effect of solvent can be circumvented by optimizing assay conditions. In all cases, key biochemical parameters (e.g. K_m) should be checked in the final assay conditions (DMSO concentration) before starting the screening campaign.

Though unusual, DMSO may sometimes increase the apparent activity or reduce variability in some biochemical assays; this may be due to increased solubility of substrates or other assay constituents in the presence of small amounts of solvent.

The stability of reagents should be tested using the same conditions intended for HTS runs, including solvent concentration, stock concentration of reagents, reservoirs, and plates. Quite often signal is lost with time not because of degradation of one biological partner in the reaction but because of its adsorption to the plastics used (reservoir, tips, or plates) (Fig. 6). Addition of detergents below their critical micellar concentration (CMC) and/or carrier

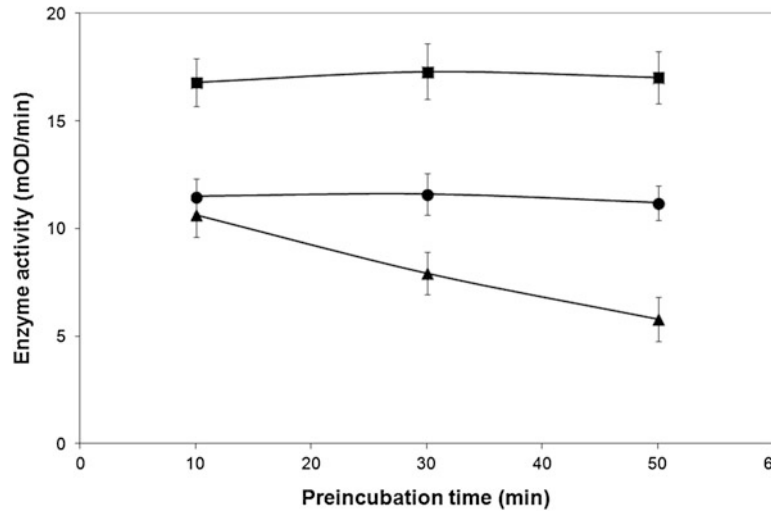

Fig. 6 Example of loss of signal in an enzymatic reaction related with adsorption of enzyme (or substrate) to plasticware. The data is from a real assay performed in our lab. Stability of reagents was initially measured using polypropylene tubes and 384-well polystyrene plates, without CHAPS (*circles*). Once HTS was started, using polypropylene reservoirs and polystyrene 384-well plates (*triangles*), a clear loss of signal was observed. Addition of 0.01% w/v CHAPS not only solved the problem but also improved the enzyme activity (*squares*). Reactions were initiated at 10, 30, and 50 min after preparation of diluted stocks of reagents that remained at 4 °C before addition to the reaction wells

proteins (e.g. bovine serum albumin (BSA)) is a common technique to minimize this undesirable phenomenon. These assay components can also aid in reducing nonspecific enzymatic inhibition caused by aggregation of test compounds [9].

The number of factors that can be tested in an optimization process is immense. Nevertheless, initial knowledge of the system (optimal pH, metal requirements, sensitivity to oxidation, etc.) can help to select the most appropriate ones. Factors to be considered can be grouped as follows:

- Buffer composition
- pH
- Temperature
- Ionic strength
- Osmolarity
- Monovalent ions (Na^+, K^+, Cl^-)
- Divalent cations (Mn^{2+}, Mg^{2+}, Ca^{2+}, Zn^{2+}, Cu^{2+}, Co^{2+})
- Reological modulators (glycerol, polyethylene glycol)
- Polycations (heparin, dextran)
- Carrier-proteins (BSA, casein)
- Chelating agents (ethylenediamine-*N*,*N*,*N*′,*N*′-tetraacetic acid (EDTA))
- Blocking agents (polyethylene imine (PEI), milk powder)
- Reducing agents (dithiothreitol (DTT), β-mercaptoethanol)
- Protease inhibitors (phenylmethylsulfonyl fluoride (PMSF), leupeptin)
- Detergents (Triton, Tween, 3-([3-cholamidopropyl] dimethylammonio)-1-propanesulfonate (CHAPS))

Cell-based assays are usually conducted in cell media of complex formulation. Factors to be considered in this case are mainly medium, supplier, selection, and concentration of extra protein (human serum albumin, BSA, gelatin, collagen). One also needs to take into account cell density, plate type, plate coatings, incubation time, temperature, and atmosphere. Since cell-based assays generally have more variables than biochemical assays, care must be taken when documenting and reproducing the cell culture and assay conditions. This is even more critical when IPSC differentiation protocols are being used.

Besides analyzing the effect of factors individually, it is important to consider interactions between factors because synergies and antagonisms can commonly occur [27]. Full-factorial or partial factorial designs can be planned using several available statistical

packages (e.g., JMP, Statistica, and Design Expert) and automated hardware and software solutions are available for more complex combinations of assay constituents. The Dragonfly® system from TTPLabTech is a non-contact dispenser designed specifically for optimization experiments while Beckman Coulter have continued to develop the SAGIAN™ SAMI® software system for full automated assay optimization (AAO) on the Biomek series of liquid handlers [28].

Usually the focus of optimization is on activity (signal or signal to background), but statistical performance should also be taken into account when doing assay optimization. Though this is not feasible when many factors and levels are scrutinized without replicates, whenever possible duplicates or triplicates should be run and the resulting variability measured for every condition. Some buffer ingredients make a reproducible dispensement very difficult, and so should only be used if they are really beneficial (e.g. glycerol).

For some factors it is critical to run the HTS assay close to physiological conditions (e.g. pH) in order to avoid missing interesting leads for which the chemical structure or interaction with the target may change as a function of that factor.

5.3 Statistical Evaluation of HTS Assay Quality

The quality of an HTS assay must be determined according to its primary goal, i.e. to distinguish accurately hits from non-hits in a vast collection of samples.

In the initial evaluation of assay performance, several plates are filled with positive controls (signal; e.g. uninhibited enzyme reaction) and negative controls or blanks (background; e.g. substrate without enzyme). Choosing the right blank is sometimes not so obvious. In ligand-receptor binding assays, the blanks referred to as NSB controls are prepared traditionally by adding an excess of unlabeled (cold) ligand; the resulting displacement could be unreachable for some specific competitors that would not prevent nonspecific binding of the labeled ligand to membranes, or labware. A better blank could be prepared with membranes from the same cell line not expressing the receptor targeted. Though this is not always practical in the HTS context, it should be at least tested in the development of the assay, and compared with the NSB controls to which they should be ideally pretty close.

A careful analysis of these control plates allows identifying errors in liquid handling or sample processing. For instance, an assay with a long incubation typically produces plates with edge effects due to faster evaporation of the external wells even if lids are used, unless the plates are placed in a chamber with humidity control. Analysis of patterns (per row, per column, per quadrant) helps to identify systematic liquid-handling errors.

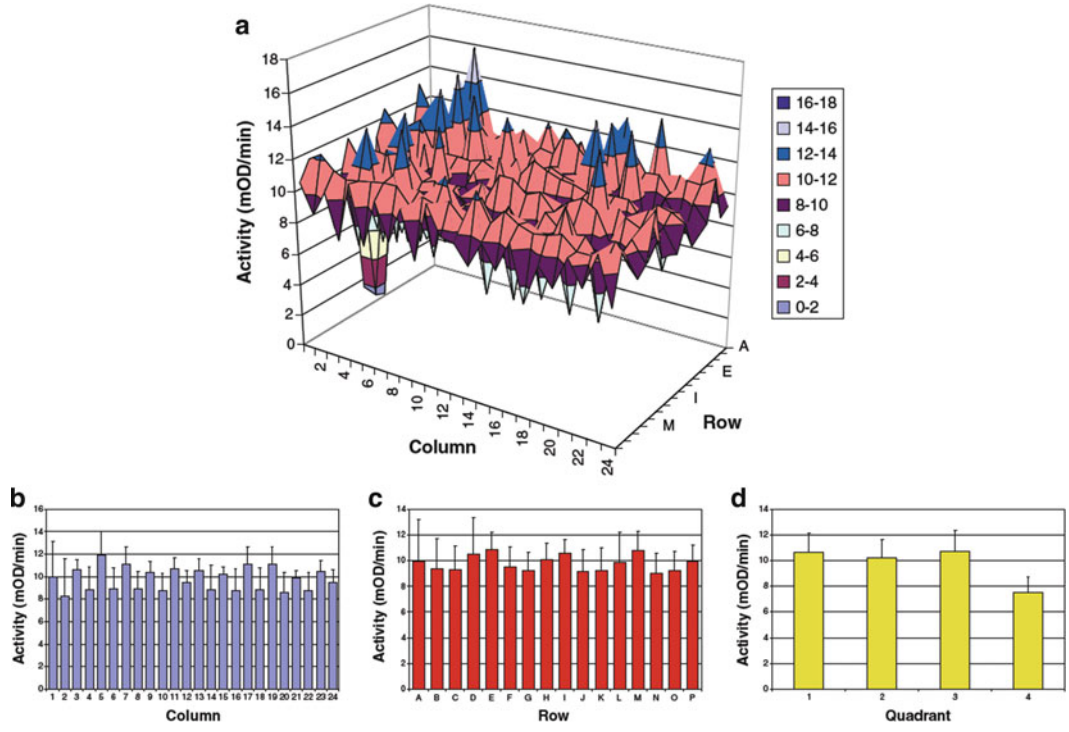

Fig. 7 Graphical analysis of a 384-well plate of positive controls of an enzymatic reaction monitored by absorbance (continuous readout). The plate was filled using a pipettor equipped with a 96-well head and indexing capability. (**a**) 3-D plot of the whole plate showing that four wells (I1, I2, J1, and J2) had a dispensement problem. The corresponding tip may have been loose or clogged. Analysis by columns (**b**), rows (**c**), and quadrants (**d**) reveals that the 4th quadrant was receiving less reagent

Obvious problems must be solved before evaluating the quality of the assay. After troubleshooting, random errors are still expected to happen due to instrument failure or defects in the labware used. They should be included in the subsequent analysis of performance (removing outliers is a misleading temptation equivalent to hiding the dirt under the rug).

The analysis of performance can be accomplished by several means. Graphical analysis helps to identify systematic errors (e.g. Fig. 7). The statistical analysis of raw data involves the calculations of a number of parameters, starting with mean (M) and standard deviations (SD) for signal and background, and combinations of these as follows:

5.3.1 Signal-to-Background Ratio (S/B)

$$S/B = M_{signal}/M_{background}$$

S/B provides an indication of the separation of positive and negative controls. It can be useful in early assay development to understand the potential of an assay format or to validate reagents under

development. But it is a poor indicator of assay quality as it is independent of variability [29].

5.3.2 Coefficient of Variation (CV) of Signal and Background

$$CV = 100 \times SD/M(\%)$$

A relative measure of variability, it provides a good indication of variability. Variability is a function of the assay stability and precision of liquid-handling and detection instruments.

5.3.3 Signal to Noise

$$S/N = (M_{signal} - M_{background})/SD_{background}$$

This classic expression of signal-to-noise ratio (S/N) provides an incomplete combination of signal window and variability. Its original purpose was to assess the separation between signal and background in a radio signal [29]. It should not be used to evaluate performance of HTS assays.

Another parameter referred to as *S/N* by some authors is

$$S/N = (M_{signal} - M_{background})/\sqrt{(SD_{signal})^2 + (SD_{background})^2}$$

This second expression provides a complete picture of the performance of an HTS assay but as discussed below the field has converged in using Z′ as the standard measure of HTS assay quality.

5.3.4 Z′ Factor

$$Z' = 1 - 3 \times (SD_{signal} + SD_{background})/|M_{signal} - M_{background}|$$

Since its publication in 1999 [29] the Z′ factor has been widely accepted by the HTS community as a very useful way of assessing the statistical performance of an assay [30]. Z′ is an elegant combination of signal window and variability, the main parameters used in the evaluation of assay quality. The relationship between Z′ factor and S/B is not obvious from its definition but can be easily derived as

$$Z' = 1 - 0.03 \times (|S/B| \times CV_{Signal} + CV_{Background})/(|S/B| - 1)$$

The value of Z′ factor is a relative indication of the separation of the signal and background populations. It is assumed that there is a normal distribution for these populations, as it is the case if the variability is due to random errors.

Z′ factor is a dimensionless parameter that ranges from 1 (infinite separation) to <0. Signal and background populations start to overlap when $Z' = 0$. In our screening groups, the minimal acceptable value for an assay is $Z' > 0.4$, although in practice the majority of our assays demonstrate $Z' > 0.6$. A Z′ of 0.4 is

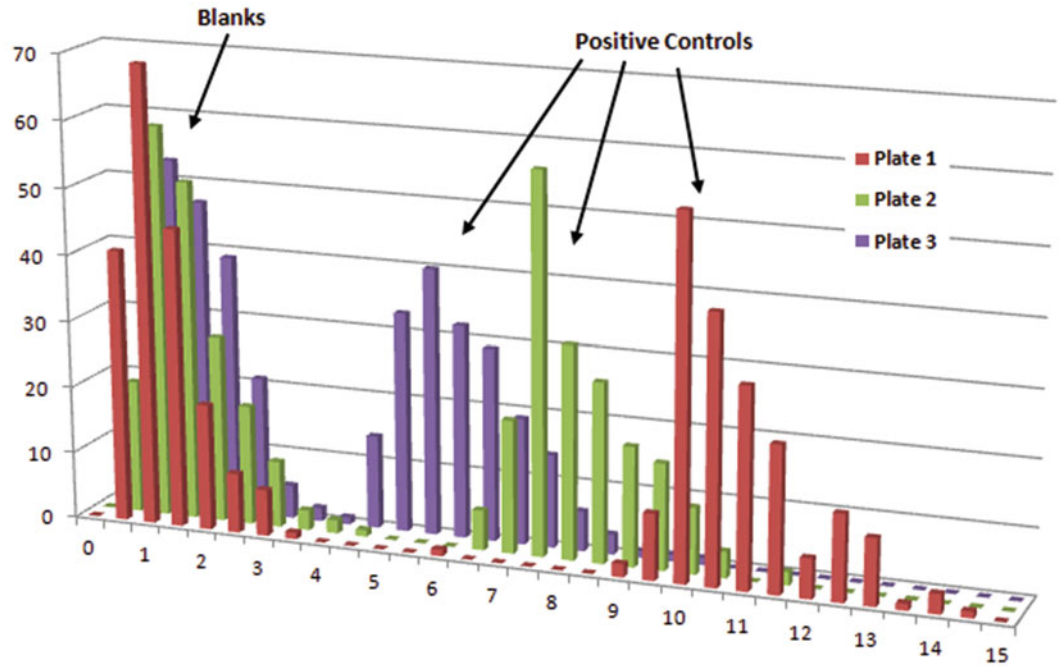

Fig. 8 Distribution of activity values (bins of 0.5 mOD/min) for three 384-well plates half-filled with blanks and half-filled with positive controls of an enzymatic reaction monitored by absorbance (continuous readout). Z′ factors were 0.59 for plate 1, 0.42 for plate 2, and 0.10 for plate 3. A complete analysis of performance is shown in Table 3

equivalent to having a S/B of 3 and a CV of 10%. Low variability allows for a lower S/B, but a minimum of 2 is usually required provided that CVs are rarely below 5%. Figure 8 shows Z′ at work in three different scenarios. Full analysis of the corresponding data is collected in Table 3.

Z′ should be evaluated during assay development and validation, and also throughout HTS campaigns on a per plate basis to assess the quality of dispensement and reject data from plates with errors. Further reading on statistic analyses of screening data is also available [31].

For cellular assays, particularly using patient-derived cells or other human cells, there will be intrinsic variability in response and quite often in-well, well-to-well, or plate-to-plate variation arising from this intrinsic variability and/or batch changes. New literature is arising to help dissect and understand these sources of variability [32].

5.4 Assay Validation

Once an assay optimized to find compounds of interest passes its quality control with a Z′ greater than 0.6 (or whatever is the applied acceptance criteria), a final step must be done before starting an HTS campaign. The step referred to here as assay validation consists

Table 3
Statistical analysis of data from the three plates described in Fig. 8

Parameter	Plate 1	Plate 2	Plate 3
M_{signal} (mOD/min)	10.09	7.77	5.84
SD_{signal} (mOD/min)	0.84	0.81	0.96
M_{bckg} (mOD/min)	0.30	0.69	0.74
SD_{bckg} (mOD/min)	0.51	0.57	0.57
S/B	34	11	8
SW (mOD/min)	9.80	7.08	5.09
S/N[a]	19	12	9
S/N[b]	10.0	7.1	4.6
CV_{signal} (%)	8	10	16
CV_{bckg} (%)	173	82	77
Z′ factor	0.59	0.42	0.10

[a] $S/N = (M_{signal} - M_{background})/SD_{background}$
[b] $S/N = (M_{signal} - M_{background})/\sqrt{(SDsignal)^2 + (SDbackground)^2}$

of testing a representative sample of the screening collection in the same way HTS plates will be treated, i.e. on the same robotic system using protocols identical to the HTS run. The purposes of this study are to:

- Obtain production data on assay performance
- Assess interferences from screening samples
- Evaluate the reproducibility of results obtained in a production environment
- Estimate the hit rate and determination of optimal sample concentration

A dramatic example of how the test of a pilot collection helps to detect interferences is shown in Fig. 9. This target, HCV RNA-dependent RNA polymerase, had been found to be slightly unstable at room temperature (Fig. 9b, without BSA). Nevertheless, the effect of 352 mixtures of 11 compounds each was tested and an extremely high hit rate was observed (45% of the mixtures inhibited the enzyme activity greater than 70%). The problem was solved by stabilization of the system using BSA 0.05%. Similar effects have been observed in several other targets.

It is therefore advisable to run a few plates with 500–2000 random samples just to spot any major interference as soon as possible. The size of the pilot collection can be as small as 1% of the total collection. Its usefulness to predict hit rates and interferences

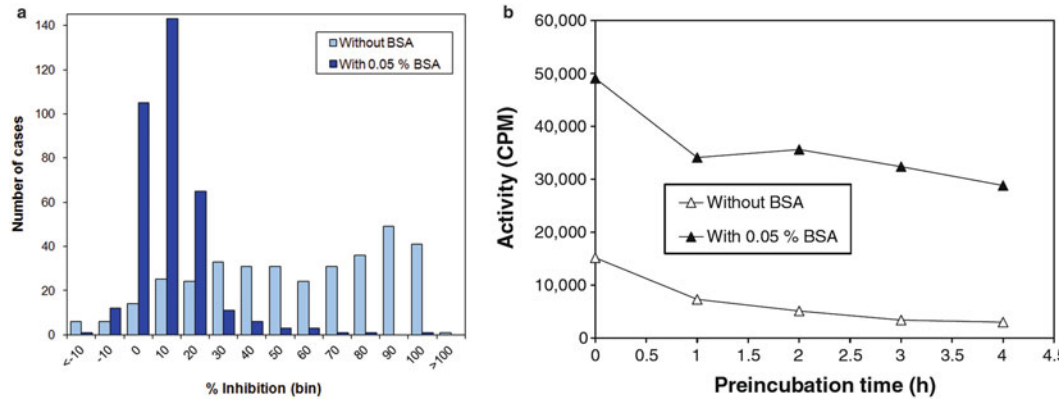

Fig. 9 (**a**) Distribution of inhibition values (10% bins) in the validation of an HTS assay of HCV RNA-dependent RNA polymerase tested with and without 0.05% w/v BSA. The samples were 352 representative mixtures of compounds (11 components at 9.1 μM each). (**b**) It was shown that the stability and activity of the enzyme were greatly improved in the presence of BSA

increases with its size. On the other hand, too many plates worth of work and reagents can be lost if any major problem is found in this step, as often happens. Therefore, it is not advisable to go beyond a 5% representation of the collection.

With a randomized sample of 1% of a collection of 50,000 compounds, a hit rate of 1% can be estimated with an SD of 0.5%. For a 5% rate, the estimation's SD would be 1%. These approximate figures have been calculated as described by Barnett [33].

Irrespective to the size of the pilot collection, at least 10–20 plates should be run to test the HTS system in real action. Duplicates of the same samples run in independent experiments provide a way to evaluate the reproducibility of results (Fig. 10). In a duplicated experiment without further retest false negatives and false positives will be indistinguishable, and will all appear as discrepant results. A third replica allows an estimation of the rates of false positives and negatives; additionally hit rate and confirmation rate after retest can be estimated providing the level of information required to assess the quality of the assay and achieve the level of performance required prior to initiation of the HTS efforts [34].

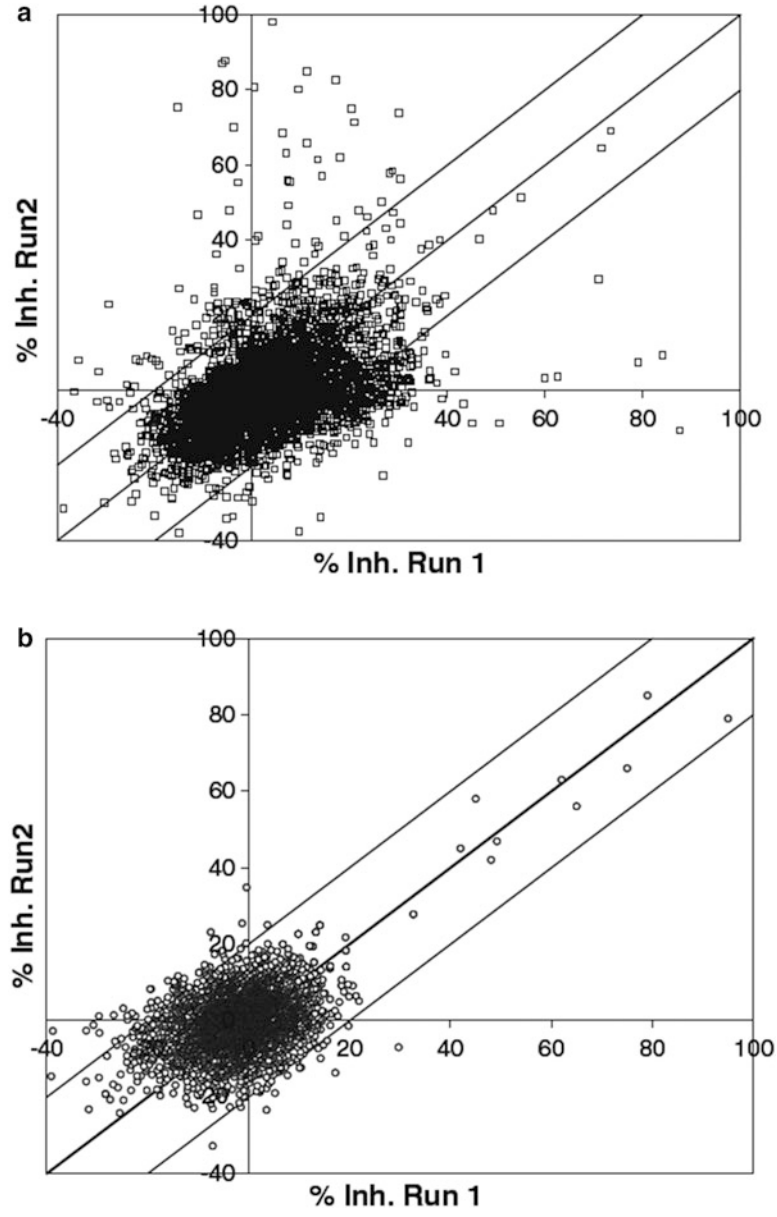

Fig. 10 Comparison of duplicates from validation for two HTS assays. (**a**) This enzymatic assay showed a significant number of mismatched results between duplicate runs of the same 4000 samples. Two actions should be taken in a case like this: liquid-handling errors have to be avoided, and the assay quality must be improved. (**b**) The data corresponds to a ligand-binding assay that showed a good reproducibility

Acknowledgements

The authors are grateful to the many colleagues at GlaxoSmithKline past and present who helped over the years to shape the screening process and to build the collective knowledge succinctly described in this introduction.

References

1. Macarrón R, Banks MN, Bojanic D *et al.* (2011) Impact of high-throughput screening in biomedical research. Nat Rev Drug Discov 10:188–195
2. Wassermann AM, Camargo LM, Auld DS (2014) Composition and applications of focus libraries to phenotypic assays. Front Pharmacol 5:1–12
3. Horman SR, Hogan C, Delos Reyes C, Lo F, Antzcak C (2015) Challenges and opportunities towards enabling phenotypic screening of complex and 3D cell models. Future Med Chem 7(4):513–525
4. Shalem O, Sanjana NE, Hartenian E *et al.* (2014) Genome-scale CRISPR-Cas9 knockout screening in human cells. Science 343 (6166):84–87
5. Nicodeme E, Jeffrey KL, Shaefer U *et al.* (2010) Suppression of inflammation by a synthetic histone mimic. Nature 468:1119–1123
6. Comley J (2014) HTS Metrics and future directions trends 2014. http://www.htstec.com/consultancyitem.aspx?Item=408
7. Drewry D, Macarrón R (2010) Enhancements of screening collections to address areas of unmet medical need: an industry perspective. Curr Opin Chem Biol 14:289–298
8. Macarrón R (2006) Critical review of the role of HTS in drug discovery. Drug Discov Today 11:277–279
9. Shoichet BK (2006) Screening in a spirit haunted world. Drug Discov Today 11:607–615
10. Baell J, Holloway G (2010) New substructure filters for removal of pan assay interference compounds (PAINS) from screening libraries and for their exclusion in bioassays. J Med Chem 53:2719–2740
11. Inglese J, Johnson RL, Simeonov A *et al.* (2007) High-throughput screening assays for the identification of chemical probes. Nat Chem Biol 3:466–479
12. Wigle T, Herold JM, Senisterra GA *et al.* (2010) Screening for inhibitors of low-affinity epigenetic peptide-protein interactions. J Biomol Screen 15(1):62–71
13. Debad JD, Glezer EN, Wohlstadter JN, Sigal GB (2004) Clinical and biological applications of ECL. In: Bard AJ (ed) Electrogenerated chemiluminescence. Marcel Dekker, New York, pp 43–78
14. Lowe DM, Gee M, Hasmam C *et al.* (2014) Lead discovery for human kynurenine 3-monooxygenase by high-throughput rapidfire mass spectrometry. J Biomol Screen 19:508–515
15. Schroeder KS, Neagle BD (1996) FLIPR: a new instrument for accurate, high throughput optical screening. J Biomol Screen 1:75–80
16. Thomsen W, Frazer J, Unett D (2005) Functional assays for screening GPCR targets. Curr Opin Biotechnol 16:655–665
17. Farre C, Fertig N (2012) HTS techniques for patch clamp-based ion channel screening—advances and economy. Expert Opin Drug Discov 7(6):515–524
18. Fan F, Wood KV (2005) Bioluminescent assays for high-throughput screening. Assay Drug Dev Technol 5:127–136
19. Assay Guidance Manual Version 4.1 (2005) Eli Lilly and Company and NIH Chemical Genomics Center. http://www.ncbi.nlm.nih.gov/books/NBK53196/. Accessed Jun 2015
20. Cheng YC, Prussof W (1973) Relationship between the inhibition constant (K_i) and the concentration of inhibitor which causes 50 per cent inhibition (I50) of an enzymatic reaction. Biochem Pharmacol 22:3099–3108
21. Bush K (1983) Screening and characterization of enzyme inhibitors as drug candidates. Drug Metab Rev 14:689–708
22. Tipton KF (1980) Kinetics and enzyme inhibition studies. In: Sandler M (ed) Enzyme inhibitors as drugs. University Park Press, Baltimore, pp 1–23
23. Burt D (1986) Receptor binding methodology and analysis. In: O'Brien RA (ed) Receptor binding in drug research. Decker, New York, pp 4–29
24. Gupta S, Indelicato S, Jethwa V *et al.* (2007) Recommendations for the design, optimization, and qualification of cell-based assays used for the detection of neutralizing antibody

responses elicited to biological therapeutics. J Immunol Methods 321:1–18

25. Airenne KJ, Hu YC, Kost T *et al.* (2013) Baculovirus: an insect-derived vector for diverse gene transfer applications. Mol Ther 21 (4):739–749
26. Lundholt B, Scudder K, Pagliaro L (2003) A simple technique for reducing edge effect in cell-based assays. J Biomol Screen 8:566–570
27. Lutz MW, Menius JA, Choi TD *et al.* (1996) Experimental design for high-throughput screening. Drug Discov Today 1:277–286
28. Taylor P, Stewart F, Dunnington DJ *et al.* (2000) Automated assay optimization with integrated statistics and smart robotics. J Biomol Screen 5:213–225
29. Zhang JH, Chung TDY, Oldenburg KR (1999) A simple statistical parameter for use in evaluation and validation of high throughput screening assays. J Biomol Screen 4:67–73
30. Iversen PW, Eastwood BJ, Sittampalam GS, Cox KL (2006) A comparison of assay performance measures in screening assays: signal window, Z′ factor, and assay variability ratio. J Biomol Screen 11:247–252
31. Malo N, Hanley JA, Cerquozzi S, Pelletier J, Nadon R (2006) Statistical practice in high-throughput screening data analysis. Nat Biotechnol 24:167–175
32. Gough AH, Chen N, Shun TY *et al.* (2014) Identifying and quantifying heterogeneity in high content analysis: application of heterogeneity indices to drug discovery. PLoS One 9 (7):1932–6203
33. Barnett V (1974) Elements of sampling theory. The English Universities Press, London, pp 42–46
34. Coma I, Clark L, Diez E *et al.* (2009) Process validation and screen reproducibility in high-throughput screening. J Biomol Screen 14:66–76

Chapter 2

Characterization of Inhibitor Binding Through Multiple Inhibitor Analysis: A Novel Local Fitting Method

Thomas V. Riera, Tim J. Wigle, and Robert A. Copeland

Abstract

Understanding inhibitor binding modes is a key aspect of drug development. Early in a drug discovery effort these considerations often impact hit finding strategies and hit prioritization. Multiple inhibitor experiments, where enzyme inhibition is measured in the presence of two simultaneously varied inhibitors, can provide valuable information about inhibitor binding. These experiments utilize the inhibitor concentration dependence of the observed combined inhibition to determine the relationship between two compounds. In this way, it can be determined whether two inhibitors bind exclusively, independently, synergistically, or antagonistically. Novel inhibitors can be tested against each other or reference compounds to assist hit classification and characterization of inhibitor binding. In this chapter, we discuss the utility and design of multiple inhibitor experiments and present a new local curve fitting method for analyzing these data utilizing IC_{50} replots. The IC_{50} replot method is analogous to that used for determining mechanisms of inhibition with respect to substrate, as originally proposed by Cheng and Prusoff (Cheng and Prusoff Biochem Pharmacol 22: 3099–3108, 1973). The IC_{50} replot generated by this method reveals distinct patterns that are diagnostic of the nature of the interaction between two inhibitors. Multiple inhibition of the histone methyltransferase EZH2 by EPZ-5687 and the reaction product *S*-adenosylhomocysteine is presented as an example of the method.

Key words Enzyme inhibition, Multiple inhibitor, Binding site, Yonetani-Theorell, IC_{50} replot, Local curve fitting

1 Introduction

The inhibitor-binding pocket on a target enzyme is a fundamental determinant of its inhibition properties. Consequently, the identification and characterization of an inhibitor's binding site is a key focal point of drug development efforts and a valuable means to classify inhibitors. A conventional method to assess the binding mode is with respect to substrate through mechanism of inhibition experiments where inhibitor and substrate are simultaneously varied. The resulting dependence of inhibition on substrate concentration indicates whether inhibitor and substrate bind exclusively and may or may not share a binding pocket.

William P. Janzen (ed.), *High Throughput Screening: Methods and Protocols*, Methods in Molecular Biology, vol. 1439,
DOI 10.1007/978-1-4939-3673-1_2,

An analogous approach is a multiple inhibitor experiment, where enzyme activity is measured in the presence of varying concentrations of two inhibitors. Testing inhibitors of interest against each other is a useful means to group chemical matter by shared sites as well as to identify the number of inhibitor-binding sites present on a target enzyme. Multiple inhibitor experiments can also be used to characterize an inhibitor of interest's binding pocket by testing it against compounds of known binding sites and/or inhibition mechanisms. Furthermore, knowledge of these relationships can facilitate inhibitor-linking efforts where two inhibitors are selected to be covalently attached as a means to increase potency [1].

This information can be similarly derived from competitive binding assays where a compound of interest is tested for displacement of a probe with a known binding site. Examples of such approaches are presented in Chapter 8 of this volume and elsewhere [1] and are valuable as an orthogonal determination of inhibitor binding. However, this latter approach requires a suitable probe molecule which is often not available early in a drug discovery effort. Moreover, additional probes and assays must be developed for every binding site of interest. In contrast, an enzyme activity-based method can in most cases utilize the existing assay employed for compound screening and is applicable for all binding sites producing inhibition.

Figure 1a depicts the binding of two inhibitors, I and J, to a catalytically competent form of enzyme to form EI, EJ, and EIJ inhibited complexes. K_I and K_J are the apparent dissociation

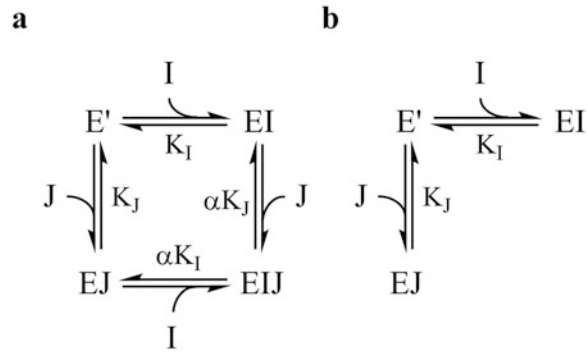

Fig. 1 Scheme for inhibitors I and J binding to a catalytically competent form of enzyme, E' (**a**), forming an EIJ ternary complex. K_I and K_J are the apparent dissociation constants for I and J, respectively, and α is the interaction constant describing the relationship between I and J. When inhibitors bind independently, $\alpha = 1$ ($\alpha K_I = K_I$). When inhibitor binding is synergistic, the binding of one inhibitor is enhanced by the presence of the other inhibitor and $0 < \alpha < 1$ ($\alpha K_I < K_I$). Conversely, when inhibitors are antagonistic, $\alpha > 1$ ($\alpha K_I > K_I$). In the extreme case of antagonism (**b**), I and J are mutually exclusive and no EIJ ternary complex forms ($\alpha = \infty$)

constants for I and J, respectively, at the given assay conditions and α is the interaction constant describing the relationship between I and J binding. When inhibitors bind independently, $\alpha = 1$ ($\alpha K_I = K_I$) and inhibition is simply additive. If inhibitor binding is synergistic, the binding of one inhibitor is enhanced by the presence of the other inhibitor and $0 < \alpha < 1$ ($\alpha K_I < K_I$). Conversely, when I and J bind antagonistically the inhibition by one inhibitor is attenuated by the presence of the second inhibitor producing an α value >1 ($\alpha K_I > K_I$). This condition can arise when two inhibitors have partially overlapping binding sites. Binding is still permitted but at a penalty to the compounds' apparent affinity. In the extreme case of antagonism, I and J are mutually exclusive and no EIJ ternary complex forms (Fig. 1b, $\alpha = \infty$). This case will arise when the binding site for two compounds is highly overlapping, such that binding of one inhibitor occludes binding of the second inhibitor. It is important to note that synergistic, antagonistic, and exclusive binding can also stem from allostery where distinct binding sites are conformationally linked. In this case, binding at one site affects the protein conformation and thereby compound affinity at a second site.

This analysis makes the simplifying assumptions that in the absence of enzyme, I and J do not interact with each other or substrates. Because apparent rather than intrinsic binding constants are used, this analysis does not require knowledge of the inhibition mechanism with respect to substrate, making it useful for investigation of early-stage compounds including HTS hits. Moreover, inhibitors with differing mechanisms may be evaluated in this way. For mechanism-specific equations, the reader is referred elsewhere [2].

The relationship between I and J can be derived from the measurement of the enzymatic activity in the presence of varying amounts of both inhibitors. A popular graphical method to analyze these data was proposed in 1964 by Yonetani and Theorell [3]. Using this method, a plot of the reciprocal initial velocity versus the concentration of I at varied J transforms the data into a series of lines which are locally fit by linear regression analyses. The resulting series of lines will be parallel if I and J are mutually exclusive (Fig. 2a) or intersecting if an EIJ ternary complex can form (Fig. 2b). When non-exclusive, the lines will intersect at a point above, on, or below the x-axis for synergistic, independent, and antagonistic binding, respectively, and the concentration of I at the intersection point will equal $-\alpha K_I$; if the value of K_I is already known, α may be easily calculated. While the method of Yonetani and Theorell produces patterns diagnostic of exclusive or non-exclusive binding, it suffers from the imprecision common to linear transformations and compounded by the use of reciprocal velocity. The data are unevenly weighted in a linear regression where the highest y values carry the most weight. The greatest values of $1/v_i$

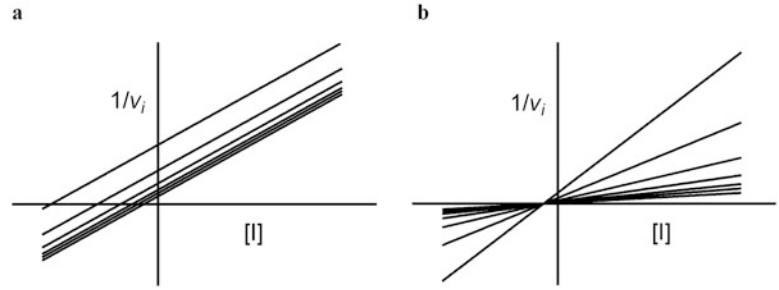

Fig. 2 Yonetani-Theorell plots for multiple inhibitor data. Plotting $1/v_i$ versus the concentration of I at fixed concentrations of J transforms the data into a series of lines. (**a**) Mutually exclusive inhibitors produce a series of parallel lines. (**b**) Non-exclusive inhibitors produce a series of intersecting lines ($\alpha = 1$ shown). The intersection point will occur above, on, and below the *x*-axis for synergistic, independent, and antagonistic binding, respectively, and the x-coordinate of the intersection point is equal to $-\alpha K_I$

arise from the lowest velocities which are prone to greater error. Thus, it is the lowest velocities with the greatest error which have the most influence on the fit. As a result, these linear transformations may provide useful visualizations of the data but nonlinear regression methods should be used for more accurate determination of the fitting parameters.

A more contemporary approach to the analysis of these data is to globally fit by nonlinear regression the fraction of remaining enzyme activity (v_i/v_0) using Eq. 1 to determine values for K_I, K_J, and α:

$$\frac{v_i}{v_0} = \frac{1}{1 + \frac{I}{K_I} + \frac{J}{K_J} + \frac{IJ}{\alpha K_I K_J}} \tag{1}$$

As a consequence of fitting an entire data set simultaneously, global fit analyses have the advantage of a high data-to-parameter ratio, permitting determination of the fitted parameters with increased accuracy. However, visual inspection of globally fitted data is made difficult by the resulting plots containing all of the actual and fitted data on one scale. As a result, the quality of the fit over all data points cannot be resolved and non-ideal behaviors and deviations of the data from the fit due to mechanistic features not captured in the model may be missed.

An alternative method is local curve fitting, in which subsets of the data are analyzed independently to produce apparent values for a fit parameter which are then replotted to determine the global parameter value. As a consequence of this deconvoluted approach, these methods provide superior visualization of the fitted data allowing facile evaluation of both the data quality and fit to the

modeled mechanism. Replots from these data often produce diagnostic, mechanism-specific patterns. The disadvantage of this method is that because subsets of the data are represented by apparent fit parameters, the final analysis has a lower data-to-parameter ratio compared with global fitting. For high-quality data sets, globally and locally fitted values will be in good agreement. Importantly, local curve fitting provides an excellent means to interrogate the veracity of a fitted model.

A local curve fitting analysis exploiting nonlinear regression methods has not previously been proposed for multiple inhibitor data. Here, we present such a method based on IC_{50} replots analogous to the Cheng-Prusoff method for determining mechanisms of inhibition with respect to substrate [4]. The multiple inhibitor data are analyzed in two stages. First, the IC_{50} values for inhibitor I are determined for each concentration of J and then those IC_{50} values for I are plotted as a function of the concentration of J to determine the relationship between I and J. It should be noted that the choice of whether to plot the IC_{50} of I versus the concentration of J or the IC_{50} of J versus the concentration of I is arbitrary as both will give the same value for α due to the nature of the thermodynamic box created by inhibitor binding (Fig. 1a).

To derive an expression for the IC_{50} value for I (IC_{50}^{i}) in the presence of J, Eq. 1 is first rearranged to solve for the concentration of I (Eq. 2):

$$I = K_I\left(\frac{1}{1+\frac{J}{\alpha K_J}}\right)\left(\left(\frac{v_0}{v_i}\right)-\left(1+\frac{J}{K_J}\right)\right) \tag{2}$$

In the absence of I, the starting v_i/v_0 will be determined by the concentration of J and K_J according to Eq. 3:

$$\frac{v_i}{v_0} = \left(\frac{1}{1+\frac{J}{K_J}}\right) \tag{3}$$

The IC_{50} value for I will equal the concentration of I that results in one-half the starting v_i/v_0 (Eq. 4):

$$IC_{50}^{i} \quad \text{when} \quad \frac{v_i}{v_0} = \frac{1}{2}\left(\frac{1}{1+\frac{J}{K_J}}\right) \tag{4}$$

Finally, substituting the reciprocal of Eq. 4 into Eq. 2 for v_0/v_i produces Eq. 5 for the IC_{50}^{i} which can be simplified to Eq. 6:

$$IC_{50}^{i} = K_I\left(\frac{1}{1+\frac{J}{\alpha K_J}}\right)\left(2\left(1+\frac{J}{K_J}\right)-\left(1+\frac{J}{K_J}\right)\right) \tag{5}$$

$$IC_{50}^{i} = K_I \left(\frac{1 + \frac{J}{K_J}}{1 + \frac{J}{\propto K_J}} \right) \tag{6}$$

This is the general equation which can be used to determine the interaction constant for I and J. A plot of the IC_{50} values for I as a function of the concentration of J will produce a pattern that is diagnostic of the relationship between I and J. A hyperbolic dependence is observed when I and J are synergistic or antagonistic where the y-intercept is equal to the value of K_I and the asymptotic limit is equal to the value of αK_I. A descending hyperbola is observed for synergistic inhibitors (Fig. 3a, $\alpha K_I < K_I$) whereas an ascending hyperbola is produced for antagonistic inhibitors (Fig. 3c, $\alpha K_I > K_I$). When I and J bind independently, $\alpha = 1$ and Eq. 6 reduces to Eq. 7 producing a horizontal line equal to the K_I (Fig. 3b):

$$IC_{50}^{i} = K_I \tag{7}$$

When I and J are mutually exclusive, α equals infinity and Eq. 6 reduces to Eq. 8:

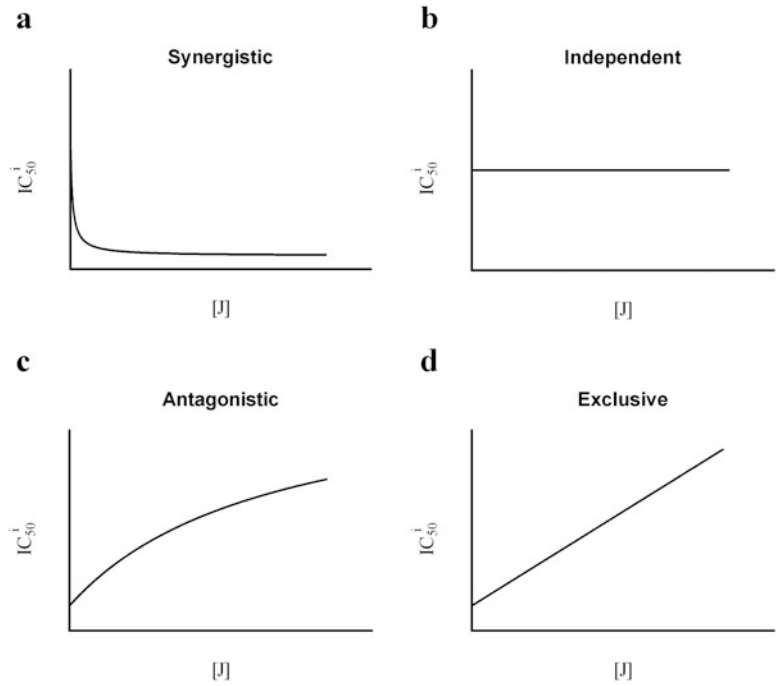

Fig. 3 IC_{50} replot patterns for synergistic, independent, antagonistic, and exclusive binding. Simulated replots of the IC_{50} value for inhibitor I (IC_{50}^{i}) at various concentrations of inhibitor J when the relationship is (**a**) synergistic ($\alpha = 0.1$ shown), (**b**) independent ($\alpha = 1$ shown), (**c**) antagonistic ($\alpha = 10$ shown), or (**d**) exclusive ($\alpha =$ infinite)

$$IC_{50}^{i} = K_I\left(1 + \frac{J}{K_J}\right) \tag{8}$$

Re-expression of Eq. 8 as Eq. 9 reveals the linear dependence between the IC_{50} value for I and the concentration of J (Fig. 3d):

$$IC_{50}^{i} = K_I + \left(\frac{K_I}{K_J}\right)J \tag{9}$$

As these equations are general in form for two ligand-binding enzyme, they are analogous to the Cheng-Prusoff equations for mixed-type (Eq. 6), noncompetitive (Eq. 7), and competitive (Eqs. 8 and 9) inhibition with respect to substrate [4].

As discussed above, when the series of dose–response curves is plotted as v_i/v_0 as a function of I at fixed concentrations of J, the starting fractional activity will decrease with increasing J as shown in Fig. 4. Using Eq. 10 will account for the variable starting point and amplitude:

$$\frac{v_i}{v_0} = (\max - \min)\left(\frac{1}{1 + \left(\frac{I}{IC_{50}}\right)^{h}}\right) + \min \tag{10}$$

Here, max and min are the maximum and minimum values of v_i/v_0, respectively, and h is the Hill slope. Relative to the case where I and J are independent (Fig. 4b), the curves will be shifted to lower and higher midpoint values of [I] for synergism (Fig. 4a) and antagonism (Fig. 4c), respectively. These shifts should be considered when selecting inhibitor concentrations to be tested. Ultimately however, low initial remaining activity will limit the data that is usable at higher concentrations of J (*see* **Notes 1–4**).

The IC_{50} replot method presented here is applicable to any multiple inhibitor, biochemical experiment, regardless of assay format. We have chosen to illustrate this method using our previously

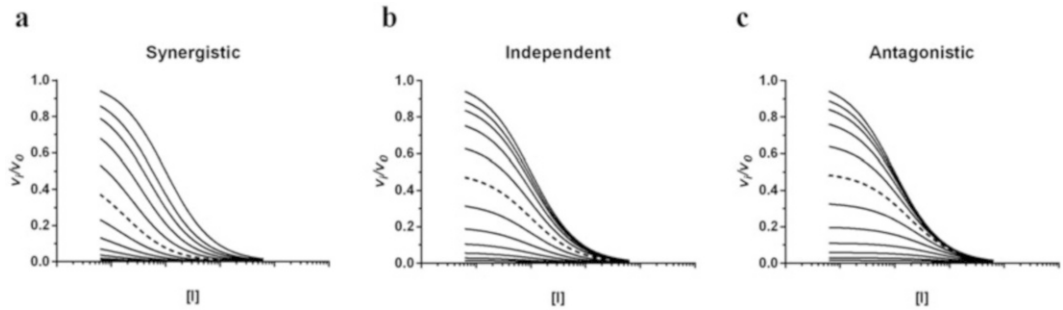

Fig. 4 Simulated IC_{50} curves for inhibitor I in the presence of varying concentrations of inhibitor J shown using Eq. 1 for examples where I and J binding is (**a**) synergistic ($\alpha = 0.1$ shown), (**b**) independent ($\alpha = 1$ shown), or (**c**) antagonistic ($\alpha = 10$ shown). A twofold dilution series for J is shown with the curve where [J] = K_J is represented as a *dashed line*

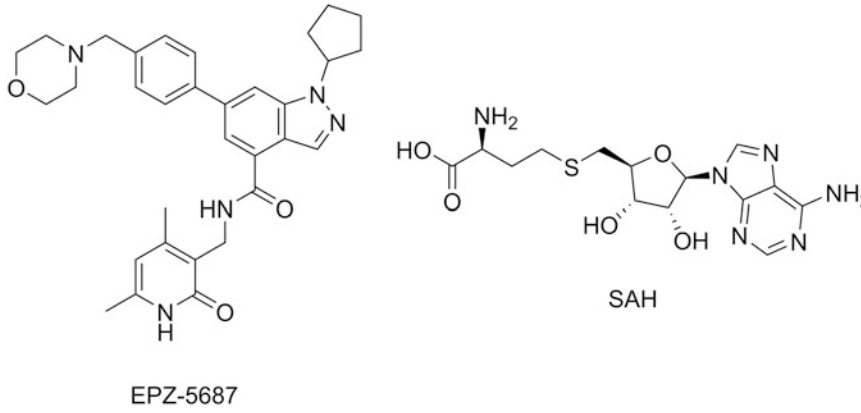

Fig. 5 Inhibitor structures for EPZ-5687 and SAH

published data characterizing an inhibitor developed from an HTS hit against the histone methyltransferase, EZH2 [5]. EZH2 is the enzymatic subunit of the polycomb repressive complex 2 (PRC2) which catalyzes the mono- through tri-methylation of lysine 27 of histone 3 (H3K27) with the concomitant conversion of the methyl donor *S*-adenosylmethionine (SAM) to *S*-adenosylhomocysteine (SAH). EZH2 has been found to be amplified in several cancers and overexpression has been correlated with a poor prognosis [6, 7] making it an attractive target in human cancers. Moreover, genetic alterations, including gain-of-function point mutants, have been reported in hematologic and solid tumors which confer an oncogenic dependency on EZH2 [8–16].

EPZ-5687 is a SAM-competitive inhibitor of EZH2 with a K_i value of 24 nM suggesting that it may bind in the SAM pocket of the enzyme (Fig. 5) [5]. Efforts to obtain an EPZ-5687-bound crystal structure were unsuccessful; hence, crystallographic identification of the inhibitor-binding site was not possible. In other protein methyltransferases, crystallographic analyses of SAM- and SAH-bound structures demonstrate a shared binding site (reviewed in [9]). Consistent with these observations, SAH displays SAM-competitive inhibition of EZH2 with a K_i value of 7.5 μM [17]. To test the hypothesis that EPZ-5687 binds in the SAM pocket of EZH2, a multiple inhibitor experiment was performed to determine whether SAH and EPZ-5687 were mutually exclusive. For these studies, a discontinuous, radiometric assay was utilized to measure the EZH2-catalyzed incorporation of a tritiated methyl group from ^{3}H-labeled SAM to a histone peptide substrate in a 384-well flashplate format. The following is a general protocol which may be readily adapted to accommodate other assay formats. The assay was run with substrate concentrations equal to their K_M values so as to maintain a balanced sensitivity to all inhibition mechanisms (balanced conditions, [1]). The assay end point was

within the linear phase of product formation. Unless noted, a Multidrop (Thermo Scientific) was used for liquid transfer steps.

2 Materials

1. Recombinant purified human PRC2 complex containing EZH2 [5].
2. Histone 3 peptide substrate: Corresponding to residues 21–44, C-terminally amide capped, and biotinylated (ATKAARKSA-PATGGVKKPHRYRPGGK(biotin)-$CONH_2$).
3. ^{3}H-SAM: ^{3}H-S-adenosylmethionine, labeled on the sulfonium methyl group.
4. SAM: *S*-adenosylmethionine.
5. 1× Assay buffer: 20 mM Bicine, pH 7.6, 0.002 % Tween-20, 0.005 % bovine skin gelatin, and 0.5 mM DTT.
6. 1.25 × PRC2 solution: 5 nM PRC2 complex in 1× assay buffer.
7. 5× Substrate mix: 0.925 μM peptide, 0.75 μM ^{3}H-SAM, 9 μM SAM in 1× assay buffer.
8. Stop buffer: 600 μM SAM.

3 Methods

3.1 Assay Method

1. Spot a matrix of varying concentrations of both compounds onto a 384-well plate such that all combinations of EPZ-5687 and SAH concentrations are obtained (1 μL total in 100 % DMSO) using a Hewlett Packard D300 digital dispenser (*see* **Notes 1** and **5**).
2. Add 40 μL 1.25 × PRC2 solution and incubate for 30 min at room temperature.
3. Initiate reactions with 10 μL of 5× substrate mix (*see* **Note 3**).
4. Incubate for 90 min at room temperature.
5. Add 10 μL of stop buffer to quench the reaction.
6. Transfer 50 μL of the quenched reactions to a 384-well, streptavidin-coated flashplate to capture the biotinylated peptide.
7. Incubate for 30 min at room temperature.
8. Wash plates three times with 150 μL/well of 0.1 % Tween-20 using a BioTek ELx-405 plate washer.
9. Read plate using a Perkin Elmer Topcount NXT HTS plate reader (*see* **Note 6**).

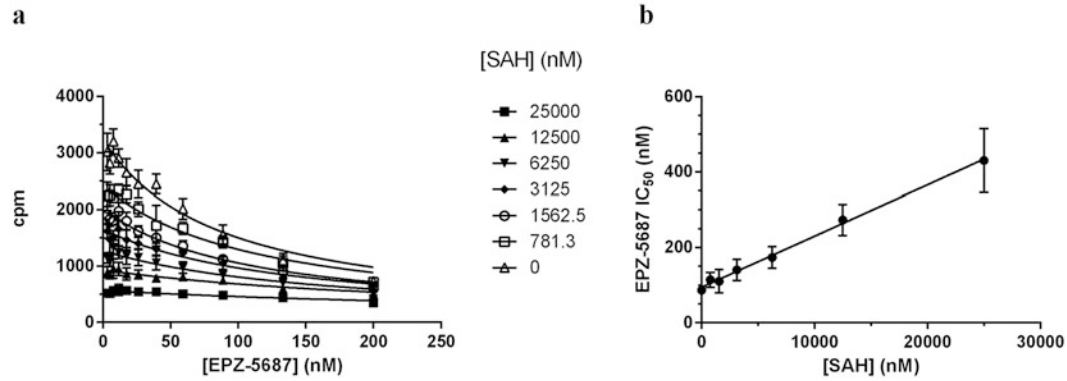

Fig. 6 Multiple inhibitor data for EPZ-5687 and SAH inhibition of the EZH2-containing PRC2 complex. (**a**) Dose–response curves for EPZ-5687 at varying concentrations of SAH. The lines show the fit by Eq. 10 in the text to determine the IC_{50} value. These data are excerpted from Knutson et al. [5]. (**b**) Replot of the EPZ-5687 IC_{50} values from (**a**) versus SAH concentration. The linear dependence indicates mutually exclusive binding and the line is the fit of the data by Eq. 9 from the text. The apparent binding constants for EPZ-5687 and SAH are 94 ± 4 nM and 7.0 ± 0.4 μM, respectively

3.2 Data Analysis

The series of dose–response curves for EPZ-5687 at varying concentrations of SAH were plotted and individually fit using Eq. 10 (Fig. 6a). The resulting IC_{50} values for EPZ-5687 were plotted against the concentration of SAH producing a linear relationship indicating mutually exclusive binding (Fig. 6b). A fit of the data by Eq. 9 gave apparent binding constants for EPZ-5687 and SAH of 94 ± 4 nM and 7.0 ± 0.4 μM, respectively, in good agreement with the published values [5, 10]. The original analysis using the Yonetani-Theorell method [3] produced a 1/velocity versus [SAH] plot with a series of parallel lines also indicating mutually exclusive binding between EPZ-5687 and SAH [5].

4 Notes

1. A minimal recommended concentration range for each inhibitor is 0.1×–4 × IC_{50}. Low assay signal becomes a greater issue at inhibitor concentrations above the IC_{50} values in a multiple inhibitor experiment. Usable data is limited by the quality of the assay at low remaining activity of the enzyme and the relationship between the inhibitors tested. For example, when two independent inhibitors are present at their IC_{50} concentrations, only 25 % of enzyme activity will remain according to Eq. 1. This value will be lower and higher for synergistic and antagonistic inhibitors, respectively. Thus, additional concentrations greater than the IC_{50} values can be tested though the data may not be useful. Measures can be taken to increase the assay signal in order to get more usable data at low remaining

percent activities. First, the enzyme concentration may be increased as long as it remains well below substrate concentrations (maintain initial velocity conditions). Second, the assay time may be increased while still within the linear range of product production (initial velocity conditions).

2. Some enzymes exhibit substrate inhibition. For these cases, I and J IC_{50}s should be measured at substrate concentrations well below the substrate K_i. Otherwise, α will reflect interactions not only between inhibitors but between inhibitor and substrate, if they exist, as well.
3. Zero inhibitor groups should be included as controls. In addition to the enzyme activity control (absence of I and J), varied I in the absence of J and varied J in the absence of I serve as controls for each compound in the experiment. The fitted values for K_I and K_J should be in agreement with the IC_{50} values from the single inhibitor groups.
4. Most current graphing programs allow for new equations to be created so that Eqs. 1, 6, 7, 9, and 10 may be added for analysis of multiple inhibitor data.

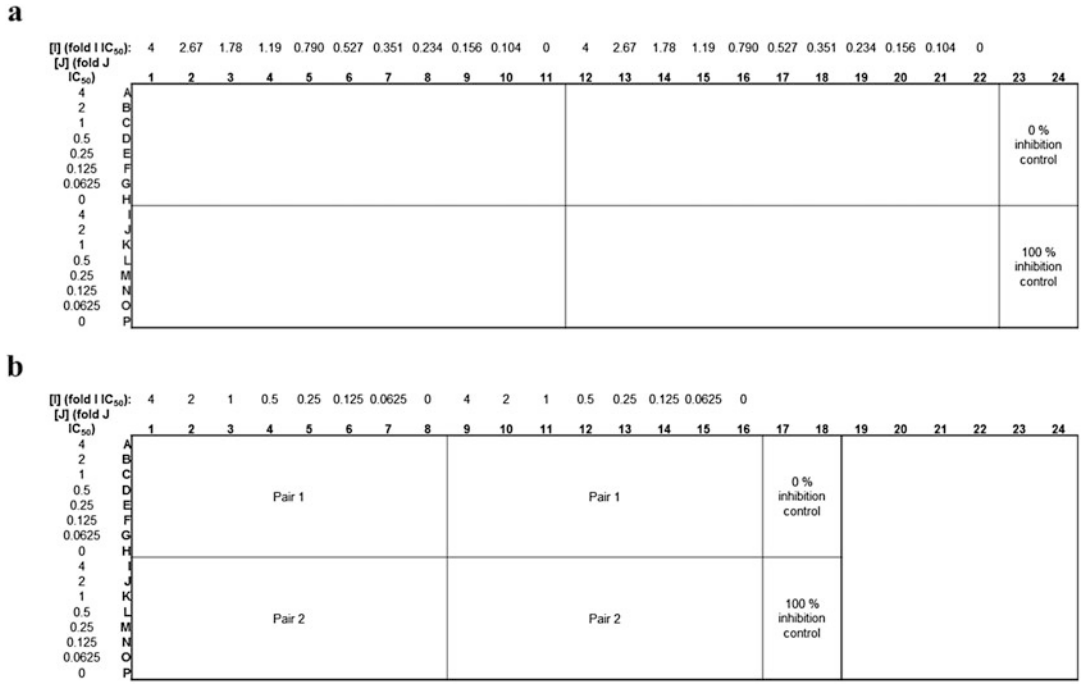

Fig. 7 Sample plate layout for the matrix of inhibitors I and J including controls using a 384-well plate. This layout tests every combination of inhibitor concentrations (**a**) in quadruplicate for one pair of compounds or (**b**) in duplicate for two pairs of compounds. Inhibitor concentrations are listed as the final concentration in the assay as fold IC_{50}. DMSO is used in place of compound for the 0 % inhibition wells and a saturating concentration of a control inhibitor is used for 100 % inhibition control wells

5. Compound serial dilutions may be performed by manual pipetting. However, the availability of digital liquid dispensers such as the HP D300 automates this step vastly improving the ease and throughput. Using a digital dispenser, we have configured plate layouts in which two pairs of compounds were tested on each 384-well plate and have exploited the increased throughput to evaluate several compound pairs (Fig. 7).
6. Alternate radiometric plate readers may be used such as Perkin Elmer's MicroBeta^2 plate counter.

Acknowledgements

We acknowledge William Janzen for helpful discussions in the preparation of this chapter and Suzanne Jacques for providing data for test fitting.

References

1. Copeland RA (2013) Evaluation of enzyme inhibitors in drug discovery : a guide for medicinal chemists and pharmacologists, 2nd edn. Wiley, Hoboken, NJ
2. Segel IH (1975) Enzyme kinetics : behavior and analysis of rapid equilibrium and steady state enzyme systems. Wiley, New York
3. Yonetani T, Theorell H (1964) Studies on liver alcohol hydrogenase complexes. 3. Multiple Inhibition kinetics in the presence of two competitive inhibitors. Arch Biochem Biophys 106:243–251
4. Cheng Y, Prusoff WH (1973) Relationship between the inhibition constant (Ki) and the concentration of inhibitor which causes 50 per cent inhibition (I50) of an enzymatic reaction. Biochem Pharmacol 22(23):3099–3108
5. Knutson SK, Wigle TJ, Warholic NM, Sneeringer CJ, Allain CJ, Klaus CR, Sacks JD, Raimondi A, Majer CR, Song J, Scott MP, Jin L, Smith JJ, Olhava EJ, Chesworth R, Moyer MP, Richon VM, Copeland RA, Keilhack H, Pollock RM, Kuntz KW (2012) A selective inhibitor of EZH2 blocks H3K27 methylation and kills mutant lymphoma cells. Nat Chem Biol 8 (11):890–896. doi:10.1038/nchembio.1084, nchembio.1084 [pii]
6. Chase A, Cross NC (2011) Aberrations of EZH2 in cancer. Clin Cancer Res 17(9): 2613–2618. doi:10.1158/1078-0432.CCR-10-2156, 1078–0432.CCR-10-2156 [pii]
7. Simon JA, Lange CA (2008) Roles of the EZH2 histone methyltransferase in cancer epigenetics. Mutat Res 647(1–2):21–29. doi:10.1016/j.mrfmmm.2008.07.010, S0027-5107(08)00142-5 [pii]
8. Knutson SK, Warholic NM, Wigle TJ, Klaus CR, Allain CJ, Raimondi A, Porter Scott M, Chesworth R, Moyer MP, Copeland RA, Richon VM, Pollock RM, Kuntz KW, Keilhack H (2013) Durable tumor regression in genetically altered malignant rhabdoid tumors by inhibition of methyltransferase EZH2. Proc Natl Acad Sci U S A 110(19):7922–7927. doi:10.1073/pnas.1303800110, 1303800110 [pii]
9. Majer CR, Jin L, Scott MP, Knutson SK, Kuntz KW, Keilhack H, Smith JJ, Moyer MP, Richon VM, Copeland RA, Wigle TJ (2012) A687V EZH2 is a gain-of-function mutation found in lymphoma patients. FEBS Lett 586 (19):3448–3451. doi:10.1016/j.febslet.2012.07.066, S0014-5793(12)00634-5 [pii]
10. Sneeringer CJ, Scott MP, Kuntz KW, Knutson SK, Pollock RM, Richon VM, Copeland RA (2010) Coordinated activities of wild-type plus mutant EZH2 drive tumor-associated hypertrimethylation of lysine 27 on histone H3 (H3K27) in human B-cell lymphomas. Proc Natl Acad Sci U S A 107(49): 20980–20985. doi:10.1073/pnas.1012525107 1012525107 [pii]
11. Wigle TJ, Knutson SK, Jin L, Kuntz KW, Pollock RM, Richon VM, Copeland RA, Scott MP (2011) The Y641C mutation of EZH2 alters substrate specificity for histone H3 lysine 27 methylation states. FEBS Lett 585(19): 3011–3014. doi:10.1016/j.febslet.2011.08.018, S0014-5793(11)00608-9 [pii]

12. McCabe MT, Graves AP, Ganji G, Diaz E, Halsey WS, Jiang Y, Smitheman KN, Ott HM, Pappalardi MB, Allen KE, Chen SB, Della Pietra A, 3rd, Dul E, Hughes AM, Gilbert SA, Thrall SH, Tummino PJ, Kruger RG, Brandt M, Schwartz B, Creasy CL (2012) Mutation of A677 in histone methyltransferase EZH2 in human B-cell lymphoma promotes hypertrimethylation of histone H3 on lysine 27 (H3K27). Proc Natl Acad Sci U S A 109 (8):2989–2994. doi:10.1073/pnas.1116418109 [pii]
13. Morin RD, Johnson NA, Severson TM, Mungall AJ, An J, Goya R, Paul JE, Boyle M, Woolcock BW, Kuchenbauer F, Yap D, Humphries RK, Griffith OL, Shah S, Zhu H, Kimbara M, Shashkin P, Charlot JF, Tcherpakov M, Corbett R, Tam A, Varhol R, Smailus D, Moksa M, Zhao Y, Delaney A, Qian H, Birol I, Schein J, Moore R, Holt R, Horsman DE, Connors JM, Jones S, Aparicio S, Hirst M, Gascoyne RD, Marra MA (2010) Somatic mutations altering EZH2 (Tyr641) in follicular and diffuse large B-cell lymphomas of germinal-center origin. Nat Genet 42(2):181–185. doi:10.1038/ng.518ng.518 [pii]
14. Morin RD, Mendez-Lago M, Mungall AJ, Goya R, Mungall KL, Corbett RD, Johnson NA, Severson TM, Chiu R, Field M, Jackman S, Krzywinski M, Scott DW, Trinh DL, Tamura-Wells J, Li S, Firme MR, Rogic S, Griffith M, Chan S, Yakovenko O, Meyer IM, Zhao EY, Smailus D, Moksa M, Chittaranjan S, Rimsza L, Brooks-Wilson A, Spinelli JJ, Ben-Neriah S, Meissner B, Woolcock B, Boyle M, McDonald H, Tam A, Zhao Y, Delaney A, Zeng T, Tse K, Butterfield Y, Birol I, Holt R, Schein J, Horsman DE, Moore R, Jones SJ, Connors JM, Hirst M, Gascoyne RD, Marra MA (2011) Frequent mutation of histone-modifying genes in non-Hodgkin lymphoma. Nature 476(7360):298–303. doi:10.1038/nature10351nature10351 [pii]
15. Ryan RJ, Nitta M, Borger D, Zukerberg LR, Ferry JA, Harris NL, Iafrate AJ, Bernstein BE, Sohani AR, Le LP (2011) EZH2 codon 641 mutations are common in BCL2-rearranged germinal center B cell lymphomas. PLoS One 6(12):e28585. doi:10.1371/journal.pone.0028585, PONE-D-11-17903 [pii]
16. Yap DB, Chu J, Berg T, Schapira M, Cheng SW, Moradian A, Morin RD, Mungall AJ, Meissner B, Boyle M, Marquez VE, Marra MA, Gascoyne RD, Humphries RK, Arrowsmith CH, Morin GB, Aparicio SA (2011) Somatic mutations at EZH2 Y641 act dominantly through a mechanism of selectively altered PRC2 catalytic activity, to increase H3K27 trimethylation. Blood 117(8):2451–2459. doi:10.1182/blood-2010-11-321208blood-2010-11-321208 [pii]
17. Richon VM, Johnston D, Sneeringer CJ, Jin L, Majer CR, Elliston K, Jerva LF, Scott MP, Copeland RA (2011) Chemogenetic analysis of human protein methyltransferases. Chem Biol Drug Des 78(2):199–210. doi:10.1111/j.1747-0285.2011.01135.x

Chapter 3

High-Throughput Screening Using Mass Spectrometry within Drug Discovery

Mattias Rohman and Jonathan Wingfield

Abstract

In order to detect a biochemical analyte with a mass spectrometer (MS) it is necessary to ionize the analyte of interest. The analyte can be ionized by a number of different mechanisms, however, one common method is electrospray ionization (ESI). Droplets of analyte are sprayed through a highly charged field, the droplets pick up charge, and this is transferred to the analyte. High levels of salt in the assay buffer will potentially steal charge from the analyte and suppress the MS signal. In order to avoid this suppression of signal, salt is often removed from the sample prior to injection into the MS. Traditional ESI MS relies on liquid chromatography (LC) to remove the salt and reduce matrix effects, however, this is a lengthy process. Here we describe the use of RapidFire™ coupled to a triple-quadrupole MS for high-throughput screening. This system uses solid-phase extraction to de-salt samples prior to injection, reducing processing time such that a sample is injected into the MS ~every 10 s.

Key words Mass spectrometry, RapidFire™, Electrospray (ESI), High-throughput screening, Triple-quadrupole mass spectrometry, Mass charge (m/z), Ionization

1 Introduction

Mass spectrometry has been an integral part of drug discovery [1–4] for many years, being a key technology in target discovery, translational science, and ADME/Tox. However, until recently, the use of mass spectrometry in screening larger compound libraries has been limited. The main limitation has been throughput, HPLC-MS, or UPLC-MS which typically have processing times of multiple minutes/sample [5, 6]. Matrix-assisted laser desorption ionization (MALDI)-MS has been successfully used for higher throughput screening, but the drawback is multiple transfer steps of reaction mixture and potentially significant matrix effects [7]. It was not until the introduction of RapidFire™-MS, integration of automated plate handling, and simple sample preparation with a standard MS that high-throughput screening (HTS) could really

William P. Janzen (ed.), *High Throughput Screening: Methods and Protocols*, Methods in Molecular Biology, vol. 1439,
DOI 10.1007/978-1-4939-3673-1_3,

access MS end points [8–10]. Sample processing time was reduced to seconds; hence the throughput was increased significantly. Importantly, screening could be performed without any compromises regarding buffers or modifiers in line with traditional LC-MS. Here we describe the development and experimental setup of a RapidFire™-MS screen.

1.1 RapidFire™ System Overview

The system (Fig. 1) comprises a simple automation plate mover which picks plates from a hotel and moves them to an X/Y stage. The plate stage is positioned to allow an auto sampler to address each well of the 96- or 384-well plate. An injection needle mounted on the auto sampler can pierce the plate seal and aspirate samples

Fig. 1 RapidFire™ 365 automated MS preparations system. Image shown is the latest high-throughput MS screening system from Agilent. The different components of the system are labeled: (**a**) Plate carrier and sample injection system. (**b**) Direct drive plate handling robot. (**c**) RapidFire™ control PC. (**d**) Pump system for solvents. (**e**) Mobile-phase storage and waste bottles. This sample preparation front end can be connected to a range of mass spectrometry detectors. Image provided courtesy of Agilent Technologies

from the source plate. The sample is then driven through a simple solid-phase extraction (SPE) column. A series of pumps enable solvents to bind, wash, and elute the analyte of interest from the column; the sample is then injected into a MS source. The column is washed and then the next sample is aspirated from the plate. Once each well has been sampled the plate handler returns the source plate to the plate store and the cycle starts again with the next plate from the batch.

2 Buffer Preparation

2.1 Ligand Optimization Buffer

In order to detect a known ligand using mass spectrometry it is necessary to understand how the ligand can be ionized and how it will fragment in the mass spectrometer. There are several parameters which need to be optimized to ensure successful quantification of any ligand. Multiple reaction monitoring (MRM) is essential when using a triple-quadrupole (QqQ) instrument and usually requires direct infusion of the pure ligand into the mass spectrometer. The optimization buffer typically contains a small volatile component to assist in generating a charged state. A mix of organic solvent/water is recommended to maintain the ligand in solution and ensure good desolvation in the detector.

1. 5 M Ammonium acetate: Add 19.25 g of ammonium acetate to a 50 mL Pyrex glass bottle. Add about 30 mL of water and stir using a magnetic stirrer until dissolved. Add solution to a measuring cylinder and adjust volume to 50 mL using water (*see* **Note 1**).
2. Ligand optimization solution: Add 60 μL of 5 M ammonium acetate to 50 mL of water in a Pyrex glass flask. Finally add 50 mL of methanol and mix using a magnetic stirrer (*see* **Note 2**).

2.2 RapidFire™-MS Running Buffers

Typically the RapidFire™-MS system requires two running buffers, one aqueous and another solvent. One buffer allows the analyte of interest to adsorb to the chromatography material while the unwanted salts are washed through. The second buffer disrupts the interaction between the analyte and the chromatography material enabling the analyte to be eluted into the mass spectrometer.

1. Mobile phase A: Add 4 L water to a 5 L Pyrex glass flask. Add 8 mL of formic acid and mix by shaking (*see* **Note 3**). Final concentration becomes 0.2 % formic acid.
2. Mobile phase B: Add 4 L MeOH to a 5 L Pyrex glass flask. Add 8 mL of formic acid and mix by shaking (*see* **Notes 2** and **3**). Final concentration becomes 0.2 % formic acid.

3 Methods

3.1 Optimization of Ligand by Direct Infusion

There are two principal methods to optimize the mass spectrometer parameters for a ligand, one uses an auto-injector and the other a syringe pump. Using an LC-programed auto-injector is particularly useful if one has a large number of ligands to optimize. However, one needs to have a fully functioning HPLC and auto-injector system setup to achieve this. Since a RapidFire™-MS system normally does not normally include an HPLC system, direct infusion of ligand using a syringe pump is more common. Although direct infusion is a slower approach, the number of ligands to be optimized for an HTS project is usually limited to a substrate and product.

Very little optimization of a ligand is required for a time-of-flight (ToF) mass spectrometer as this type of instrument can see a very wide range of mass charged ions. The description below is limited to QqQ instruments which are effectively gated to look at a much smaller range of mass charge ions in each injection. (Discussion of mass spectrometer options is included in Subheading 3.2.)

1. Dissolve the ligand in ligand optimization buffer (*see* **Note 4**). Draw the sample into a glass syringe and load into a syringe pump. Connect tubing directly to the mass spectrometer source inlet with the appropriate connector.
2. Prepare the mass spectrometer for optimization of ligand. Ensure that the appropriate nebulizing gas is enabled. Set the flow rate of the syringe pump to 10 μL/min and start the pump running (*see* **Note 5**).
3. Manual ligand optimization: The mass detector needs to be gated so that the instrument is acquiring over the appropriate mass over charge (m/z) range to cover the ligand of interest (*see* **Note 6**). Set quadrupole 1 to a narrow range around the expected ligand m/z.
4. Ensure that the signal is stable by inspecting the total ion count (TIC). The length of time required to establish a stable signal is dependent on the length of tubing between the syringe and the detector and the pump speed (*see* **Note 7**).
5. Optimize the potential difference between the ground and the orifice plate (de-clustering potential, also called fragment voltage or cone voltage, depending on mass spectrometer manufacturer). Observe how TIC and the m/z of the ligand changes as the de-clustering potential is adjusted (*see* **Note 8**). Set to the optimal de-clustering potential for the ligand.
6. Optimize the collision energy for the ligand of interest (*see* **Note 9**). Using the optimum m/z of the product ion and de-clustering potential, change the collision energy in quadrupole 2 and observe the changes in fragment pattern (*see* **Note 10**).

7. Once the optimal fragment has been selected the essential parameters for multiple reaction monitoring (MRM) have been established (*see* **Note 11**).

3.2 Setup of RapidFire™-MS

One important aspect to consider before starting mass spectrometry-based screening is the type of mass spectrometer to use. The two most common types of detector are ToF or QqQ. Both types of mass spectrometers have advantages and disadvantages as HTS tools.

Using a ToF-based system allows very easy optimization of detection. In particular, high-resolution instruments provide a very accurate mass of the ligand, which is important in order to distinguish between ions with very similar masses. Additionally one can, in the spectra, observe adduct formation and potentially adapt buffers to reduce adducts. A TOF instrument is ideal for detection of very large molecules such as proteins, although a special column is probably required. However, ToF instruments are not as sensitive as QqQ, although the difference is not large on modern instruments. The data files from ToF detectors can be very large as they are typically acquiring across a large spectrum of m/z ions; this can lead to issues with data storage.

QqQ instruments provide highly selective detection of ligands when using MRM. MRM is usually very sensitive and allows detection and quantification for a range of small molecules and peptides. Due to the sensitivity, QqQ instruments can often quantify in sub nM region although this is ligand dependent. The data files are small; hence data storage is not an issue. Some ligands do not fragment well, which is problematic. One solution is to use the same m/z both for product and fragment ion while keeping the collision energy to a minimum. However, this can result in rather high background signals. QqQ instruments are not particularly suited for larger molecules.

Selection of the correct column is essential to get good results. There are several columns commercially available ranging from reverse phase (RP) to hydrophilic interaction chromatography (HILIC). Column selection is dependent on ligand; for example a hydrophobic ligand requires an RP column such as C4 or C18 (*see* **Note 12**). A very hydrophilic ligand such as arginine may require an HIILC column (*see* **Note 13**). A curious phenomenon, probably due to the solid-phase extraction methodology used by RapidFire™, is that many ligands can be detected using either reverse phase or HILIC. This is different from traditional liquid chromatography and it is therefore advisable to test the ligand on different columns. In our experience, we start using RP and test all columns; if this is not successful then we resort to HILIC.

Selection of buffers is, in our experience, a less critical component than the column selection. Although one can change the solvents and the modifier, this is unlikely to result in a dramatic

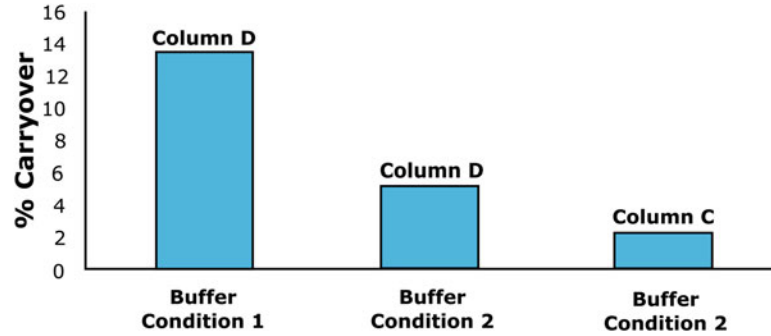

Fig. 2 Carryover analysis. A ligand was injected at high concentration followed by a blank injection. The percentage of signal in the blank injection was calculated for each ligand concentration. Condition 1—Buffer A = water, Buffer B = 5 mM ammonium acetate in water:CH2CN:acetone (2:1:1 v/v). Condition 2—Buffer A = water + 0.2 % acetic acid (v/v), Buffer B = methanol + 0.2 % acetic acid (v/v)

improvement in detection of a ligand. However, the combination of buffer and the column can impact on sample carryover, i.e., sample being retained in the system and being eluted in the next injection (Fig. 2).

1. Prime the pumps with the solvents of choice (*see* **Note 14**). Open the RapidFire™-MS software (Fig. 3). Manually open the valves on the pumps and use the RapidFire™-MS software to set the flow rates to 10 mL/min. Allow 2 min of priming and then turn off the flow rate and close the valves on the pumps.
2. Selection of column: The correct column is essential for good results. For reverse-phase applications, a good starting point is to use a C18 column (Fig. 2 Column C).
3. Selection of flow rates: In our experience, changing the flow rates from the standard settings can have a positive effect. However, if the flow rate is reduced it may be necessary to increase the elution time. This will increase the total sample time and therefore reduce the throughput. A reduction in flow rate will significantly reduce the solvent usage.
4. Selection of cycle durations: Any changes in cycle duration times will have a significant impact on throughput. For instance in Fig. 3, increasing the load and elute duration twofold will increase the processing time per plate by approximately 40 min.
5. Managing carryover: Including blank injections between samples is useful if sample carryover is an issue. It will increase the batch time significantly; however, this is usually effective in removing carryover since the system does a full blank load/elution cycle. The recommendation is, therefore, to use blank injections instead of increased cycle duration if carryover cannot be reduced to an acceptable level.

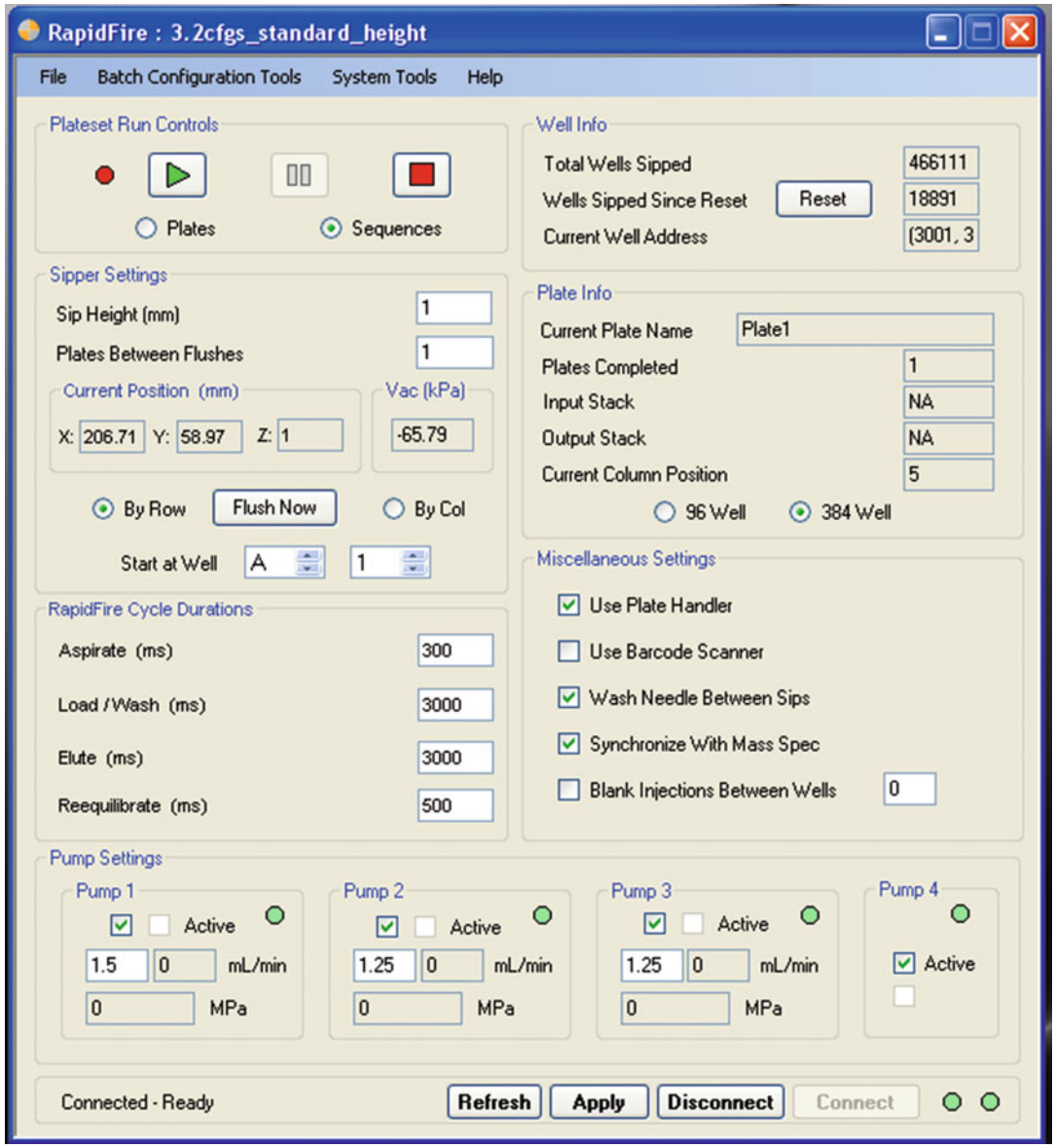

Fig. 3 RapidFire™-MS control software

6. Multiplexing in order to increase throughput: If throughput is an issue, multiplexing can significantly increase throughput. We have successfully screened two different targets simultaneously. Each target was tested independently. Once the reactions were stopped, an aliquot was removed from each target test plate, transferred, and pooled in a new plate and the resulting mixture was then analyzed. Another approach is to use different peptides for the same target. This has successfully been done using four different peptides followed by pooling into one plate and analysis on the RapidFire™-MS [11].

3.3 Experimental

Before commencing with screening, there are several important parameters to be determined.

1. Establishing the linear range for ligand detection: For any screening assay it is necessary to understand the linear dynamic range of the end point of interest. Since the amount of product generated in the assay is being used as a surrogate for target enzyme activity, it is really important that the amount of product formed is within the linear range of detection. A product stock solution should be made from which a standard curve can be generated with threefold dilutions. The buffers should be matched to the buffer that will be used in future experiments and screening (*see* **Note 15**). Plot the standard curve to establish linearity of the ligand (Fig. 4a). Always use one or two blank injections after the highest concentration (*see* **Note 16**). If there are any carryover issues, try using a different column and/or a different mobile-phase composition (*see* **Note 17**).

   Once the optimum mobile phase and column have been determined, assay development to establish the parameters for HTS can begin; some of the key experiments are described.

2. Establish the enzyme concentration. It is important to ensure that a minimum amount of enzyme is used per reaction. Excessive use of enzyme increases the assay cost; the most important

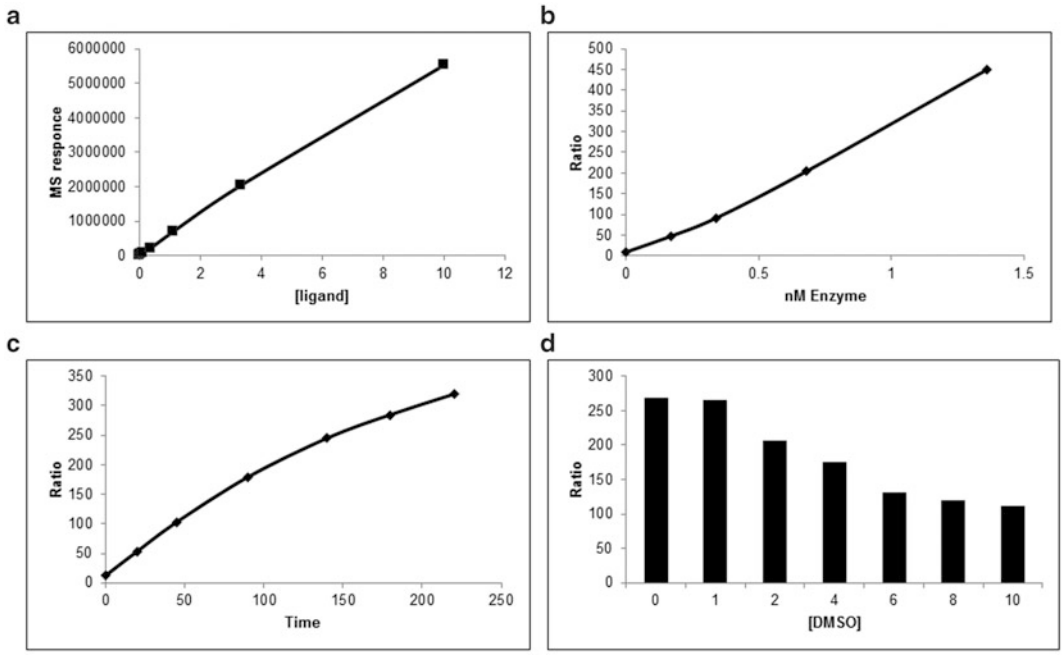

Fig. 4 Key assay development parameters. (**a**) Linearity of a ligand detected by RapidFire™-MS. (**b**) Linearity with enzyme concentration. (**c**) Linearity of reaction progress with time. (**d**) DMSO sensitivity of an enzyme. Each bar is the turnover and a reduction in turnover indicates a reduction in enzyme activity

factor is to have sufficient enzyme concentration to accurately measure the effect of a compound on the target enzyme (*see* **Note 18**). Enzyme at different concentrations is added to test wells of a 96- or 384-well plate (*see* **Note 19**) followed by substrate (*see* **Note 20**). After a set time period, the reactions are stopped (*see* **Note 21**) and substrate/product conversion is analyzed (Fig. 4b).

3. Establish linearity of the reaction. Using the information from previous experiments, the appropriate enzyme concentration can be selected. If the reaction rate is slow, one can increase the reaction time (*see* **Note 22**). For each time point the reaction is stopped and substrate/product conversion is analyzed (Fig. 4c).
4. Establishing solvent tolerance of the target enzyme: Compound libraries are typically stored in an organic solvent such as dimethyl sulfoxide (DMSO) and hence it is important to establish the solvent sensitivity of the target enzyme. In our example, different volumes of DMSO are preincubated with the target enzyme before the reaction is initiated with substrate (*see* **Note 23**). The effect of DMSO on enzyme activity can be expressed graphically (Fig. 4d). Where possible, the concentration of solvent within the reaction needs to be maintained at the lowest possible level to minimize the impact on the assay. Maintaining a standard level of solvent in every well is important to minimize inter-well variability; no compound control wells need to contain solvent.
5. Determination of substrate affinity: To maximize the sensitivity of an enzyme assay it is necessary to understand the kinetics of the assay. The first step is to measure the affinity between the enzyme and substrate (Km). The affinity is calculated using the initial reaction rate of the enzyme at various substrate concentrations (*see* **Note 24**); it is important to take measurements where the reaction is within the linear range. When reaction rate (*see* **Note 25**) is plotted against substrate concentration, the Km is the concentration of substrate where the enzyme is working at half the maximum velocity (Vmax/2) (Fig. 5).
6. Determination of the stability of the ligand after addition of the stop: Typically HTS runs generate a large number of plates; therefore, it is important to be sure that the ligand is stable in the stop solution for a prolonged time. Each plate takes around 45–60 min to analyze and one usually will have 18 plates in a batch run. Therefore, the ligand needs to be stable for 18–20 h at room temperature. If plates are frozen for analysis at a later stage, signal stability during freeze/thaw cycles needs to be established. This is done by analyzing the ligand directly, after 20 h at room temperature as well as after freeze/thaw cycle (*see* **Note 26**).

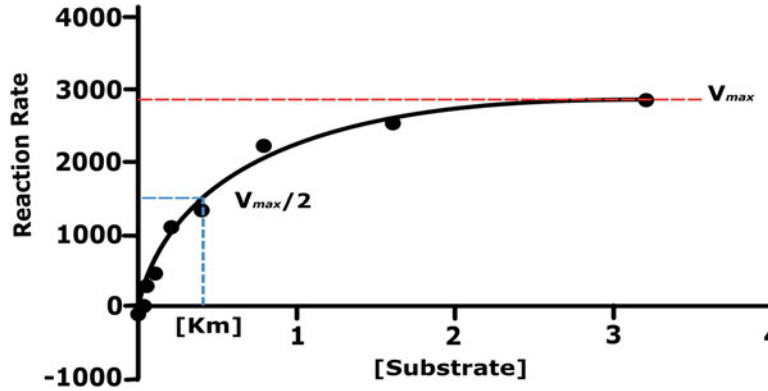

Fig. 5 Km determination for a substrate. Km is defined as the substrate concentration where the enzyme reaction is running at half the maximum rate (Vmax/2). The graph shows the reaction rates for a fixed concentration of enzyme where substrate concentration is varied

7. Reference and standard compounds: Having established the basic parameters of the assay, enzyme and substrate concentration (*see* **Note 27**), duration of assay, and reagent stability, it is appropriate to try and identify both a reference and standard compound(s) for the assay. A reference compound is one which is tested at a single concentration, whereas a standard is tested across a range of concentrations to enable calculation of an IC_{50}. It is important that both reference and standard compounds behave reproducibly in the assay. In order to minimize the interassay variability all reagent additions should be made using the same liquid-handling tools that will be used within the HTS. Using established reference and standard compounds allows comparison with previous in-house or published data. Concentration response analysis should be performed on at least three different occasions in order to evaluate the inter-experiment variability of the assay (*see* **Note 28**). Typical IC_{50} data is shown in Fig. 6.
8. Determination of the robustness of the screen: To establish the robustness of the assay several plates are prepared containing either DMSO (maximum signal), inhibitor compound (minimum signal) (*see* **Note 29**), or reference compound (at a concentration which inhibits enzyme by ~50 %). These plates are tested over several occasions; analysis of robustness is determined statistically and expressed as Z' [12] (*see* **Note 30**). In addition the intraplate signal variability can be calculated.

3.4 HTS Screening Using RapidFire™

Once the assay development is complete, the HTS can be started. There are several ways of performing HTS but typically the sample library is tested at a single compound concentration, followed by confirmation of the actives. Hit confirmation is most generally carried out by retesting actives in concentration response.

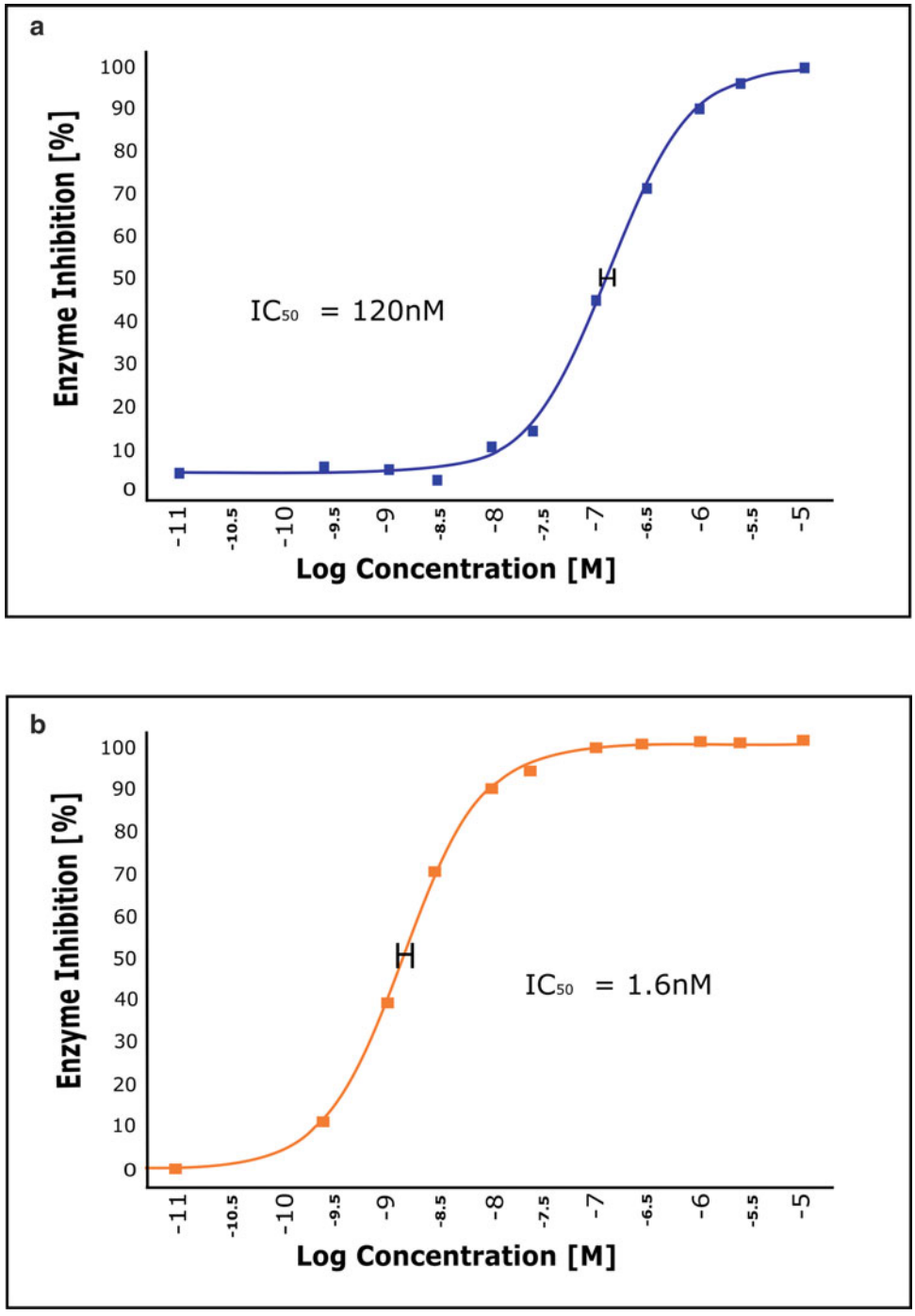

Fig. 6 Typical IC_{50} data generated by RapidFire™-MS. Compounds were tested over a half log dilution series on multiple occasions; only one example curve is shown for each compound. The use of half log dilutions enables a wide range of potencies to be addressed

This method works well even with limited medicinal chemistry input as the primary screen can progress with actives being confirmed at the end of the process. However, we found it to be very effective to have close contact with medicinal chemistry during the HTS. The throughput of the RapidFire™ forces screening to be carried out in batches; therefore concentration response data for actives from the previous batch can be generated with the current single concentration test batch. Near neighbors of confirmed actives can be included in subsequent batches and therefore structural activity relationships can start to be established during the primary screen. Using this approach can reduce the amount of screening required as interesting series can be quickly identified.

Another method to increase the throughput, discussed above, is to multiplex. One can run multiple projects at the same time and pool a plate from each project into one analysis plate. This method is particularly effective if one completes the assay development of one project before the HTS is finished for another project. One can simply start pooling at that time without waiting for the completion of the HTS. However, to multiplex in this way there must be a significant difference in the m/z of each of the ligands and both ligands need to be compatible with the buffer and column selection (*see* **Note 31**).

Multiplexing within a single HTS using different isotopically labeled substrates has been successfully described [11]. Although this can increase throughput around fourfold, there will be increased assay development time. The affinity of each isotopically labeled substrate will need to be measured and a final check to ensure that the standard compound behaves exactly the same with all substrates.

The detection using RapidFire™-mass spectrometry is usually straightforward:

1. After the reactions have been stopped, the plates are loaded into the stacker (*see* **Note 32**).
2. Create a batch containing the correct number of plates.
3. Make sure that there is sufficient quantity of mobile phases (*see* **Note 33**) for the entire batch.
4. Start the batch and once the pumps are running, make sure that the back pressure is not too high (*see* **Note 34**).

3.5 Data Handling

Data processing is carried out after completion of a batch. The area of the peaks, both for substrate and product, is calculated using the provided software (*see* **Note 35**).

After integration the system generates a single data file per ligand per plate; within each of these files is the area of the ligand peak in each well, either as a list or in plate matrix format. When using a QqQ mass spectrometer the data files are small; thus data storage is not an issue. The data can then be further processed on

line or directly imported into a third-party or in-house data analysis package. The calculation of turnover of substrate to product is usually performed using the following equation: product area/(product area + substrate area) (*see* **Note 36**). Turnover calculation effectively eliminates the need for internal standards. Any changes in the injected volume will effect both substrate and product, and thus will not affect the calculation.

Although screening using RapidFire™-MS is not as high throughput as traditional HTS assays, the data quality is usually unprecedented. As with any other assay technology, compounds which nonspecifically bind to proteins and cause aggregation will result in a false-positive result. However, false positives and false negatives are otherwise restricted to compounds that have the same m/z as either the substrate or the product. This is usually a very small fraction of a compound library, so the false-positive/negative compounds are very few. In fact, RapidFire™-MS has been successfully used to remove false positives from traditional assay formats [13]. A further method to identify false-positive/negative compounds is to inspect the substrate and product data separately. Any abnormal value is due to compound interference and can be either removed if it is a false-positive or rescued if it is a false-negative compound.

Many groups are working to address the throughput limitations of MS so that it can be applied more widely across HTS. Removing or reducing the sample preparation step is one obvious way to address throughput. Direct infusion of samples into the MS detector will allow sampling rates to reach or exceed 1 per second; this approach is widely used in the metabolomics field [14]. The use of acoustics to fire samples directly from a microtiter plate has shown some promise; loading time can be as fast as 3 samples/s (reading a full 384-well plate in under 2 min). This level of throughput would be equivalent to existing HTS assay technologies but being label free significantly reduces the cost. Acoustic transfer has several potential advantages; the sample volumes are very small and there is no mechanical contact with the samples (no sample carryover). Direct sample infusion coupled to an electrospray MS system does have limitations, ion suppression being one of the major problems. The use of alternative ionization strategies in combination with modifications to the assay buffer may provide some solutions.

4 Notes

1. No requirement to set pH of the solution.
2. Use MS-grade methanol. Use of other grade methanol can cause high background signal and potentially suppress the ligand signal.

3. Addition of strong acid to water and methanol should be carried out in a fume hood taking appropriate safety measures.
4. A good starting concentration is 100 nM.
5. If the signal is weak, one can reduce the flow rate. However, the use of correct concentration is far more effective.
6. Use software on the mass spectrometer or freeware on the Web to calculate the exact monoisotopic mass from the molecular formula. For instance the peptide with molecular formula $C_{205}H_{340}N_{60}O_{53}$ has got an average Mw of 4493.27 whereas the monoisotopic Mw is 4490.57. The use of correct Mw is imperative in order to obtain ligand signal.
7. 2 min is usually sufficient, unless the tubing is extremely long.
8. If ions are not generated in positive mode, try switching to negative mode. Also check to see if adducts have formed; these will fly with higher m/z charges. Lists of adducts can be found online. A note of caution: While adducts may be easier to obtain during optimisation, even a strong adduct MRM can be lost running in screening mode when using the column. In order to promote adducts, one can add the adduct salt to the running buffers. For instance, if the dominating species is an ammonium adduct, one can try to promote adduct formation by addition of ammonium to the running buffer. Alternatively switch to ammonium acetate or ammonium formate. Adducts can be erratic and, where possible, should be avoided.
9. If a larger peptide is used, it is advisable to optimize using several m/z. Peptides larger than 1000 molecular weight may have two or more charges as the product ion. The software provided with Analyst can calculate the expected m/z for each charge state. We routinely optimize on two different charges for a larger peptide.
10. The fragment ion can be larger than the product ion. It is important to set the stop to cover the monoisotopic mass of the ligand. For instance, phosphatidylinositol-4,5-bisphosphate (1,2-dioctanoyl) has a product ion of 372.4 (negative mode, $z = 2$) whereas one of the fragment ions is 665.3.
11. The settings for an instrument will be dependent on multiple factors, for example the gas pressure and purity.
12. For RP, the sample is introduced with aqueous solution and binds to the resin. After desalting the interaction between the column and ligand(s) is disrupted by the organic solvent.
13. For HILIC, the sample is introduced with organic solvent. After desalting the interaction between the column and ligand(s) is disrupted by the aqueous solution. It is important to realize that buffer components such as HEPES will elute with the ligand. Hence buffer suppression can be more pronounced when using HILIC resins.

14. If the systems have not been used for a period of time or a different buffer system is to be used, proper priming of the pumps is required. Solvent quality is a critical factor for generating reproducible results.
15. If water is used to prepare standard curves this can result in an overestimation of the signals. This is most likely due to the fact that ions present in the buffers can contribute to ion suppression, especially if buffer concentrations are high. It is therefore good practice to use the same screening buffer when preparing standard curves. This suppression of signal is less pronounced in LC-MS, due to improved wash and separation conditions.
16. Carryover, normally not a big issue in LC-MS, can be problematic when using RapidFire™-MS. Hence, to estimate the carryover and therefore also the signal to background, a blank injection is used.
17. Organic mobile phase can be switched to acetonitrile from methanol. Changing the modifier can also be successful, switching between ammonium formate and ammonium acetate for example. However, the organic mobile phase requires at least 5 % water to prevent precipitation of the modifier. Care should be taken with the use of high pH, since this can cause some columns to dissolve over time.
18. If the enzyme concentration is 100 nM, the theoretical tight binding limit would be 50 nM, the amount of compound required to inhibit half of the enzyme (assuming 100 % active protein). While this may not be an issue for primary screening it may become an issue when concentration response data is being generated as the maximum achievable IC_{50} will be 50 nM.
19. A good range to start with is 0.1–10 nM.
20. Good practice is to use the liquid-handling dispenser that is to be used in the screen as early as possible in assay development. Some enzymes lose significant activity when handled by automated dispensers; this could be due to protein binding to tubing or physical shear forces applied to proteins as they transit the dispense head. Addition of 0.01 % BSA or detergents can reduce the problem of nonspecific protein binding.
21. Stop solution can be an equal volume of acetonitrile, pH reduction using 0.2 % formic acid, or an inhibitor. Make sure to include stability experiments for the chosen stop solution. This can be done by analyzing one plate directly, a similar plate after 24 h at room temperature. If plates are to be frozen for storage, the effect of freeze/thaw should also be included.
22. Although 1 h is convenient, the reaction time can be extended to several hours, depending on enzyme stability.

23. Preincubation times should at least mirror what is to be used in the screen. A guideline is to use 15–30 min.
24. Substrate concentration in the range of 0.1–10 Km is ideal.
25. The rate is easiest calculated by $(\text{signal}_{t2} - \text{signal}_{t1})/(t2 - t1)$.
26. Using several freeze/thaw cycles as well as prolonged storage at room temperature is advised. This will simulate an automation issue during a run and plates being stored for prolonged periods of time.
27. Most screens tend to use substrate concentration around Km; although other substrate concentrations can be used it will impact the sensitivity of the assay. Enzyme concentration should be as low as possible to maximize sensitivity.
28. We perform dose–response analysis in singlicate ($n = 1$) on at least three separate occasions, using five or more standard compounds where possible. Preferably, the potency of the compounds falls within a range from nM to μM.
29. If solubility and availability are not limited, using $50 \times IC_{50}$ ensures that the enzyme is completely inhibited. A reduction to $10\times$ can be tolerated but less can cause problems, for instance if the compound is unstable. Another strategy can include using wells without enzyme.
30. A $Z' > 0.5$ is considered acceptable though >0.7 should be achievable for most biochemical assays.
31. Detection of multiple ligands in positive and negative mode is only achievable using a fast-scanning mass spectrometer.
32. Make sure to add the plates in the correct orientation.
33. A 20-h batch requires around 1800 mL of mobile phase A and 3000 mL of mobile phase B using the flow rates described in Fig. 3.
34. If the back pressure at the start of the run is over 14–15 MPa, it is very likely that this will result in an over-pressure alarm which will stop the batch at some point during the run. It is advised to locate the source of the increased back pressure and resolve the issue before staring the batch.
35. Data files are generated after each plate completes processing. At the end of a batch the RapidFire™ PC will copy the timing files to the appropriate directory to enable integration. In order to complete integration it is necessary to manually identify the peak width of interest from the first well within each plate file.
36. RapidFire™-MS is primarily used for measuring substrate-to-product conversions. Monitoring increase in product can generate reasonable quality data provided that there is sufficient sensitivity in the MS detector. However, calculations based only on substrate depletion are not advisable.

References

1. Awad H, Khamis MM, El-Aneed A (2015) Mass spectrometry. Review of the basics: ionization. Appl Spectrosc Rev 50(2):158–175
2. Trufelli H, Palma P, Famiglini G et al (2011) An overview of matrix effects in liquid chromatography–mass spectrometry. Mass Spectrom Rev 30(3):491–509
3. van Breemen RB (2010) Mass spectrometry and drug discovery. Burger's medicinal chemistry and drug discovery. Wiley, Hoboken, NJ
4. Zhang J, Shou WZ (2012) Mass spectrometry for quantitative in vitro ADME assays. Mass spectrometry for drug discovery and drug development. Wiley, Hoboken, NJ, pp 97–113
5. Benkestock K, Van Pelt CK, Akerud T et al (2003) Automated nano-electrospray mass spectrometry for protein-ligand screening by noncovalent interaction applied to human H-FABP and A-FABP. J Biomol Screen 8(3):247–256
6. Yang M, Brazier M, Edwards R et al (2005) High-throughput mass-spectrometry monitoring for multisubstrate enzymes: determining the kinetic parameters and catalytic activities of glycosyltransferases. ChemBioChem 6(2): 346–357
7. Donegan M, Tomlinson AJ, Nair H et al (2004) Controlling matrix suppression for matrix-assisted laser desorption/ionization analysis of small molecules. Rapid Commun Mass Spectrom 18(17):1885–1888
8. Özbal CC, LaMarr WA, Linton JR et al (2004) High throughput screening via mass spectrometry: a case study using acetylcholinesterase. Assay Drug Dev Technol 2(4): 373–382
9. Quercia AK, LaMarr WA, Myung J et al (2007) High-throughput screening by mass spectrometry: comparison with the scintillation proximity assay with a focused-file screen of AKT1/PKB alpha. J Biomol Screen 12(4):473–480
10. Forbes CD, Toth JG, Ozbal CC et al (2007) High-throughput mass spectrometry screening for inhibitors of phosphatidylserine decarboxylase. J Biomol Screen 12(5):628–634
11. Leveridge M, Buxton R, Argyrou A et al (2014) Demonstrating enhanced throughput of RapidFire mass spectrometry through multiplexing using the JmjD2d demethylase as a model system. J Biomol Screen 19(2):278–286
12. Zhang JH, Chung TD, Oldenburg KR (1999) A simple statistical parameter for use in evaluation and validation of high throughput screening assays. J Biomol Screen 4(2):67–73
13. Adam GC, Meng J, Rizzo JM et al (2015) Use of high-throughput mass spectrometry to reduce false positives in protease uHTS screens. J Biomol Screen 20(2):212–222
14. Fuhrer T, Zamboni N (2015) High-throughput discovery metabolomics. Curr Opin Biotechnol 31:73–78

Chapter 4

Structure-Based Virtual Screening of Commercially Available Compound Libraries

Dmitri Kireev

Abstract

Virtual screening (VS) is an efficient hit-finding tool. Its distinctive strength is that it allows one to screen compound libraries that are not available in the lab. Moreover, structure-based (SB) VS also enables an understanding of how the hit compounds bind the protein target, thus laying ground work for the rational hit-to-lead progression. SBVS requires a very limited experimental effort and is particularly well suited for academic labs and small biotech companies that, unlike pharmaceutical companies, do not have physical access to quality small-molecule libraries. Here, we describe SBVS of commercial compound libraries for Mer kinase inhibitors. The screening protocol relies on the docking algorithm Glide complemented by a post-docking filter based on structural protein-ligand interaction fingerprints (SPLIF).

Key words Structure-based virtual screening, Commercially available compounds, Docking, Scoring function, Triage, Procurement, Experimental testing

1 Introduction

Over the last decade, virtual screening (VS) proved to be a useful hit-finding technology and became an integral part of the drug discovery process. In many respects, VS mimics its experimental counterpart and is used to rank/filter large compound libraries in order to yield a compound set "enriched" in hits for experimental testing. Its most remarkable virtues include the possibility (1) to screen against targets, which are not amenable to high-throughput screening (HTS) assays, and (2) to identify hits in compound collections not available in the lab. VS techniques rely on various kinds of algorithms that take the structure of a chemical compound as an input and deliver some measure of the compound's biological activity as an output. In particular, structure-based (SB) screening, considered in this account, involves docking of a chemical compound into the protein-binding pocket [1] followed by assessment of the binding affinity (called scoring) [2]. Structure-based methods need a high-resolution protein structure, but do not require

William P. Janzen (ed.), *High Throughput Screening: Methods and Protocols*, Methods in Molecular Biology, vol. 1439,
DOI 10.1007/978-1-4939-3673-1_4,

knowledge of existing active compounds. A beneficial side effect of SBVS is that, in addition to tractable hits, it also brings in understanding of how these hits interact with their respective targets and, hence, providing guidance for a rational hit-to-lead progression. While there is now a general consensus that the popular docking algorithms perform fairly well, the scoring functions most often fail to adequately evaluate the binding affinity [3–9], which rarely allows a success rate (i.e., the percentage of experimentally confirmed virtual hits) higher than 5 %. Therefore, all possible means must be deployed to improve the odds of getting a sizable number of confirmed actives out of very small sets of virtual hits. We have recently demonstrated that a post-docking score based on *s*tructural *p*rotein-*l*igand *i*nteraction *f*ingerprints (SPLIF) can greatly improve VS success rates [10, 11]. The SPLIF-based score exploits the idea that a compound that can mimic "native" ligand-protein interactions (e.g., enzyme-substrate interactions) is more likely to be a true hit than a random compound with a decent docking score. It has also been shown that simulation-based post-docking scores can be useful in the latest selection step due to more accurate protein-ligand affinity prediction (with respect to empirical docking scores) [12, 13].

On the whole, despite all the unresolved issues, the hit rates in VS are substantially higher than those observed in diversity-based HTS (~0.1 %). Due to a limited experimental effort and the possibility to use commercial compound libraries, VS is particularly suited for academic labs and small biotech companies that, unlike pharmaceutical companies, do not have physical access to rich small-molecule libraries. Here, we describe an SBVS protocol that has been used to identify inhibitors of Mer kinase, a promising therapeutic target against acute lymphoblastic leukemia (ALL) [10, 14]. Prior to the start of this campaign, we had already identified a lead series of potent Mer inhibitors [15–18] and the objective of this VS campaign was to identify backup leads whose structures would significantly differ from the lead compound, UNC2025 [19]. This SBVS project features all critical screening and confirmation steps, including docking, scoring, post-scoring, triage, procurement, and experimental testing. Eventually, of 62 experimentally tested compounds, 15 demonstrated consistent dose-dependent responses in the Mer microfluidic capillary electrophoresis assay with inhibitory potencies ranging from 0.46 to 9.9 μM, resulting in a high success rate of 25 %. It is remarkable for a virtual screen (and HTS in general) that two (of 15) hits demonstrated mid-nanomolar potencies of 0.46 and 0.60 μM. We were also able to assess the overall efficiency of our virtual screening run to that of a random diversity screen. To this end, we have screened ten randomly selected 384-well (320-ligand) plates in a single-dose run (at 10 μM; in duplicate) in the Mer microfluidic capillary electrophoresis assay. Only four compounds of the 3200

screened have shown activity above a threshold of 30 % resulting in a hit rate of 0.12 % (4 hits/3200 tested). Therefore, our VS approach has demonstrated an ~200-fold (24 %/0.12 %) improvement over a random screen [10]. This study also exemplifies that screening of commercial catalogs can yield tractable hits appropriate as starting points for the hit-to-lead progression.

2 Materials

2.1 Software

The docking algorithm used in this study is Glide [20] from the Maestro software suite commercialized by Schrodinger Inc. (www.shrodinger.com). Our criteria for choosing this software were (1) a good overall reputation (based on publications and the author's industrial experience) and (2) availability (UNC has a campus-wide license for the Maestro suite).

Pipeline Pilot (BIOVIA; accelrys.com) was used for all data processing purposes, including data-format conversion, compound structure cleaning, filtering, and clustering. All SPLIF-related code was written using Pipeline Pilot script, a scripting language that can be interpreted by Pipeline Pilot when a data-processing protocol is being executed.

See **Note 1** for alternative choices of docking and data-pipelining software.

2.2 Databases

The virtual collection of commercially available compounds was created from five large catalogs: Asinex, ChemDiv, Enamine, IBS, and Life Chemicals. These vendors have been selected because they have their own, up-to-date stocks, and offer affordable prices and high availability rates. Structures were obtained in the form of SD files downloaded from the vendors' websites. The resulting collection features ~3.8 million compounds and is updated on a semiannual basis via SD files provided by the vendors. The files used in this study have been uploaded between July and December of 2011. Virtually all compounds satisfied our usual pre-screening filters, i.e., a softened version of the Lipinski rules [21] (2 + violations of Number of H-bond donors <6, Number of H-bond acceptors <12, Molecular Weight between 200 and 600, ALogP < 5.5) and REOS [22]. Chemical structures of all screened compounds were cleaned using Pipeline Pilot software [23]. The cleaning protocol included salt stripping, mixture splitting, functional group standardization, and charge neutralization. Ionizable compounds were converted to their most probable charged species at pH 7.4. Pipeline Pilot was then used for 3D conversion.

See **Note 2** for details on a new, more extended and timely source of compound procurement.

3 Methods

3.1 Workflow

The overall screening process is outlined in Fig. 1. In the current case study, the VS protocol comprised the following steps:

1. Docking and scoring.
2. SPLIF-based re-scoring.
3. Hit selection based on the analysis of the Glide (G-score) and SPLIF scores.
4. Hit triage.

The triage procedure involved the three following components:

1. Cluster-based selection.
2. Visual inspection (in order), for example, to remove clusters that the chemists would not like to follow up.
3. Miscellaneous elimination criteria, such as compound price or stock depletion.

In the Mer VS study, Glide docking of 3.8 million commercial compounds resulted in three million poses (1.56 million unique compounds) with G-scores < 0 kcal/mol. The G-score approximates the ligand-binding free energy, taking into consideration

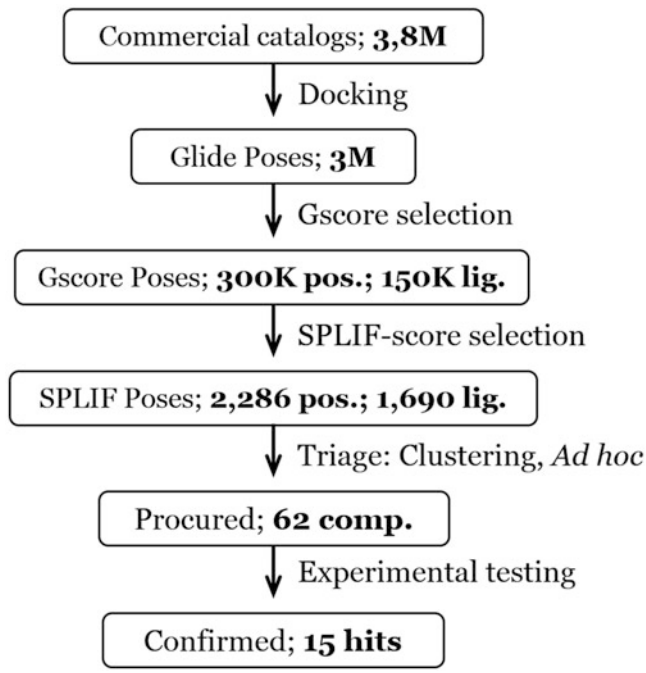

Fig. 1 The milestones and outcomes of the reported structure-based VS study

force field (electrostatic, van der Waals) contributions and terms rewarding or penalizing interactions known to influence ligand binding. As has been shown in an earlier benchmark study [11], the SPLIF-based ranking yields higher hit rates, if these "raw" docking poses are pre-filtered using a certain G-score threshold. This threshold was set in such a way that it would eliminate up front the least likely Mer inhibitors. To determine the value of the threshold, we used the probability density distribution of G-scores for known Mer actives and that for the inactives. At this point, our chemical optimization program had generated 385 Mer actives ($IC_{50} < 1$ μM) and 409 inactives ($IC_{50} > 30$ μM). Both actives and inactives were docked using the same protocol as described in the *Docking* subsection of Subheading 3. The G-score distributions (*see* Fig. 2a) indicate that a G-score threshold of −6 kcal/mol

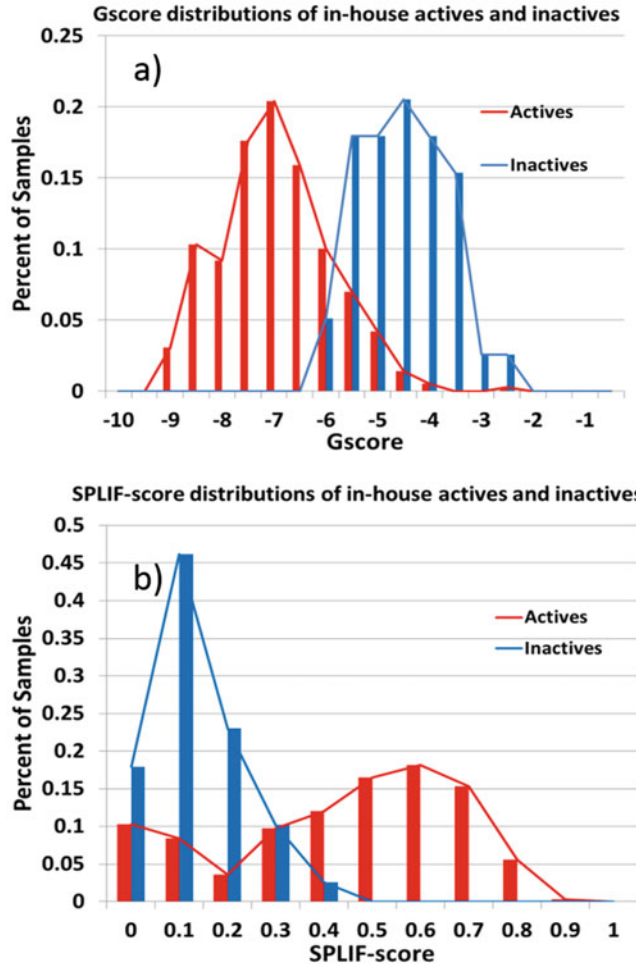

Fig. 2 (**a**) The distributions of Gscores of in-house-identified Mer actives and inactives; (**b**) the distribution of SPLIF scores of in-house-identified Mer actives and inactives

adequately separates actives from inactives with optimal false-positive vs. false negative rates. Therefore, assuming similar distributions for the 1.5 million scored compounds from the commercial screening collection, the G-score threshold for the virtual screening campaign was set to −6 kcal/mol, which resulted in a selection of 403,581 compounds.

In **step 2**, for all poses from the G-score selection, SPLIF scores have been calculated and used as filters with the ultimate goal of obtaining a manageable list of hit candidates to submit to the triage step. Again, known Mer actives and inactives were used (as described in the previous paragraph) to determine an optimal SPLIF-score threshold. As can be seen in Fig. 2b, an optimal active/inactive separation occurs at a threshold of ~0.35. The retained SPLIF score threshold of 0.35 resulted in a selection of 10,862 SPLIF-based hit candidates.

In **step 3**, the 10,862 hit candidates were first subjected to a cluster-based selection as described in the *Clustering* subsection of Subheading 3. A total of 544 clusters were identified. All cluster centers were visually inspected and a few clusters dropped as inappropriate lead candidates (e.g., nucleotides, steroids). A few more hit candidates were reported as unavailable following a quote request. Eventually, 62 compounds were purchased and tested in the Mer microfluidic capillary electrophoresis assay.

This study pointed out the importance of using heuristic post-docking filters, such as SPLIF score, for achieving acceptable hit rates. However, it also demonstrated that the SPLIF score alone was not enough to efficiently rank docking poses and that the standard docking score, such as G-score, is very helpful in eliminating the bulk of the most awkward ligand poses.

3.2 Docking

Small-molecule structures were docked into the active site of the target proteins using the Glide program [20] in standard docking precision (Glide SP). The binding region was defined by a 20 Å × 20 Å × 20 Å box centered on a reference ligand. A scaling factor of 0.8 was applied to the van der Waals radii. Default settings were used for all the remaining parameters. The top three poses were generated for each ligand and subjected to SPLIF scoring.

3.3 Structural Protein-Ligand Interaction Fingerprints

SPLIF scoring consists of two steps:

1. Generating SPLIF for the current docking pose.
2. Calculating similarity between the current and reference SPLIFs.

The details of the technique have been described in our earlier work [11]. In this study, functional connectivity fingerprints up to the second closest neighbor (FCFP4) from the Pipeline Pilot

software [23] were used as SPLIF bits. The SPLIF-based similarity score was calculated as follows:

$$\text{SPLIF-Sim} = \sqrt{\frac{N_{\text{UMLA}} N_{\text{UMPA}}}{N_{\text{ULA}} N_{\text{UPA}}}} \quad (1)$$

where N_{UMLA} is the number of unique matching ligand atoms, i.e., atoms constituting the matching circular fragments of the docking pose compared to the reference (on the ligand side); N_{ULA} is the number of unique ligand atoms, i.e., atoms constituting all interaction fingerprints of the docking pose (on the ligand side); N_{UMPA} is the number of unique matching protein atoms, i.e., atoms constituting the matching circular fragments of the docking pose compared to the reference (on the protein side); and N_{UPA} is the number of *u*nique *p*rotein *a*toms, i.e., atoms constituting all interaction fingerprints of the docking pose (on the protein side). The whole workflow was implemented in Pipeline Pilot [23]. The current implementation allows processing of ~10 poses per second in screening mode.

3.4 SPLIF Reference Structures

Three high-resolution crystal structures of the Mer protein kinase domain were used in this study. The reference ligand structures are shown in Fig. 3.

1. In complex with adenosine diphosphate (ADP) (resolution 1.90 Å; PDB code: 3BRB) [24].
2. In complex with a weakly potent inhibitor C-52 (Fig. 3, 1) (resolution 2.80 Å; PDB code: 3BPR) [24].
3. In complex with a highly potent inhibitor UNC569 (Fig. 3, 2), previously reported by us (resolution 2.69 Å; PDB code: 3TCP) [25].

Because it was not our intention to mimic the phosphate groups of ATP, we stripped them off to yield the reference ligand (Fig. 3, 3).

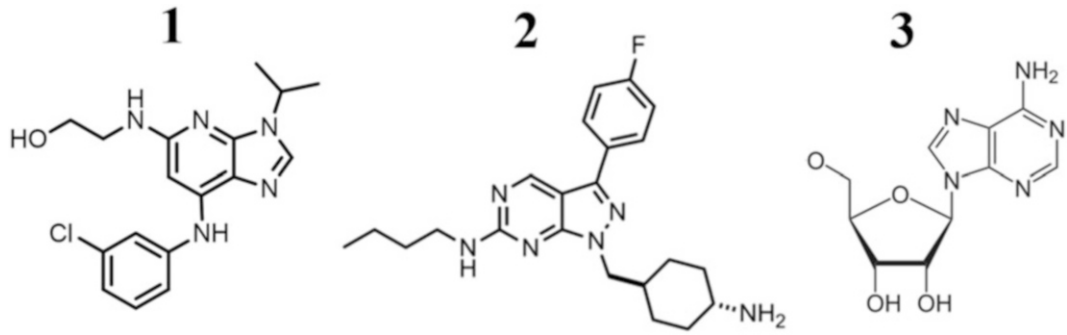

Fig. 3 Reference ligand structures for SPLIF scoring

The corresponding PDB files were processed as follows. Hydrogen atoms were added to the protein, the active site was visually inspected, and appropriate corrections were made for tautomeric states of histidine residues, orientations of hydroxyl groups, and protonation states of basic and acidic residues. The hydrogen atoms were energy minimized in the MMFF force field [26] using the Macromodel software with the Maestro graphics interface [27] with all the non-hydrogen atoms constrained to their original positions.

3.5 Hit Analysis and Selection

After potential hits were selected using a combination of Glide and SPLIF scores, we subjected them to a hit triage process. The triage was based upon a number of objective and subjective criteria. The objective criteria included redundancy reduction and elimination of singletons (a singleton is a compound that is not similar to any other potential hit). The redundancy reduction consisted in elimination of some compounds belonging to large clusters, i.e., groups of chemically similar compounds. Redundancy reduction consisted of two steps. First, the virtual hits were grouped into clusters with members similar at $\geq$45 % (Tanimoto; ECFP4 fingerprints). The clustering method used at this step was maximum dissimilarity clustering without limitation on the maximum number of clusters and with the number of re-center steps set to zero [23]. In the next step, 20–50 % of compounds were then selected from each cluster in such a way that larger clusters contributed smaller percentages. The output ligands were aligned to their respective maximum common substructures to facilitate the subsequent visual ad hoc selection. To facilitate an ad hoc hit selection/elimination we created a hit list, in which each cluster was represented by a single (central) compound.

We also visually inspected 3D poses of each cluster representative in the protein-binding pocket. Multiple criteria were applied to infer whether a pose was relevant. For example, we privileged poses with hydrogen bonds buried deep within the pocket over poses with solvent-exposed hydrogen bonds. Similarly, ligands featuring relatively large hydrophobic moieties complementary in shape to the respective protein pockets were preferred to highly polar ligands. Additionally, we assessed whether a ligand's binding is meaningfully similar to that of an SPLIF reference. For example, Fig. 4 shows that, despite very different chemical structures, both the SPLIF-reference compound and the virtual hit show highly similar binding signatures.

3.6 Mer Microfluidic Capillary Electrophoresis Assay

Inhibitory potency of the procured virtual hits was tested using a microfluidic capillary electrophoresis (MCE) assay. In MCE, phosphorylated and unphosphorylated substrate peptides were separated and analyzed through a LabChip EZ Reader [28, 29]. Compound testing was performed in a 384 well, polypropylene

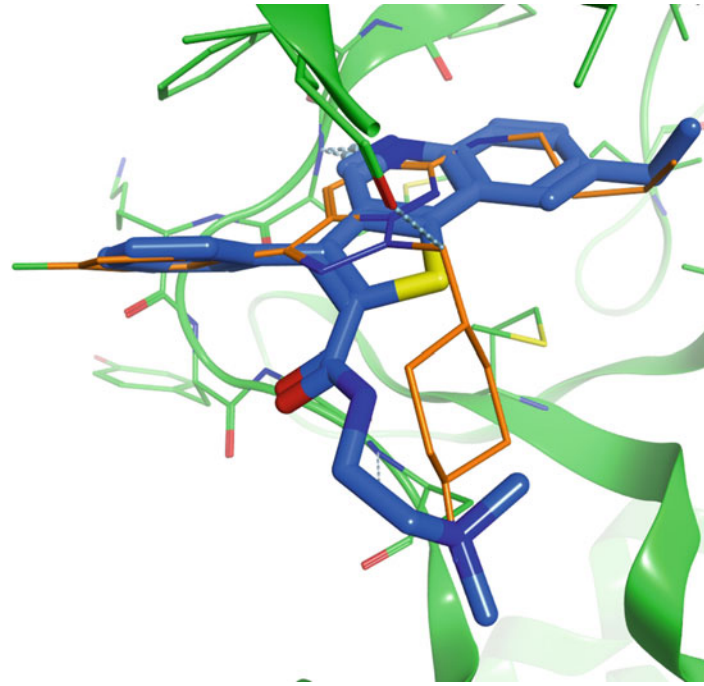

Fig. 4 A docking pose of the most potent hit (*blue*) overlaid with the reference ligand **2** (*brown*)

microplate in a final volume of 50 μL in 50 mM Hepes, Ph 7.4 containing 0.1 % bovine serum albumin (BSA), 0.1 % Triton X-100, 10 mM $MgCl_2$, and ATP at 5 μM. All reactions were terminated by addition of 50 μL of 70 mM EDTA. Phosphorylated and unphosphorylated substrate peptides were separated following a 180-min incubation on a LabChip EZ Reader equipped with a 12-sipper chip in separation buffer supplemented with CR-8 and analyzed using EZ Reader software. The reaction was run at 2 nM enzyme concentration. More details can be found in our previous work [16, 25].

3.7 Quality Control of Compound Samples

Quality control of the purchased and screened compounds was performed by diluting 1 μL of DMSO stock solution (10 mM concentration) with 49 μL of MeOH. The sealed plate was then directly used to inject 5 μL from each well onto an Agilent 6110 Series LC/MS system with the UV detector set to 220 nm. Samples were injected onto an Agilent Eclipse Plus 4.6 × 50 mm, 1.8 μM, C18 column at room temperature. A mobile phase of A being H_2O + 0.1 % acetic acid and B being MeOH + 0.1 % acetic acid was used. A linear gradient from 10 to 100 % B in 5.0 min was followed by pumping 100 % B for another 2 min with a flow rate of 1.0 mL/min. Mass spectra (MS) data were acquired in positive ion mode using an Agilent 6110 single-quadrupole mass spectrometer with an electrospray ionization (ESI) source. The purity of all

compounds was found to be 95 % or higher by UV absorption at 220, 254, and 280 nm and the MS^{+1} peak was consistent for the purchased structure.

3.8 Post-screening Follow-Up

Experimental testing is often followed by an optional (although highly recommended) step of hit expansion. Hit expansion comprises searching for and procurement of chemical analogs of those virtual hits whose activity has been confirmed in experimental testing. Simple 2D similarity (e.g., Tanimoto metrics in combination with structural fingerprints) is usually utilized to search for hit analogs. In general, the likelihood that close structural analogs of confirmed actives would also be active is quite high (10–30 %). Having more actives representing each chemical series would allow the medicinal chemists to infer early structure-activity relationships (SAR), which will be very helpful to initiate the hit-to-lead process.

4 Notes

1. Glide is obviously not the only docking software on the market. There are plausible free alternatives to Glide, such as AutoDock [30], developed by the Scripps Research Institutes, or DOCK, maintained at UCSF (dock.compbio.ucsf.edu/dock_6) and a number of commercial analogs, such as GOLD (CCDC; www.ccdc.cam.ac.uk), ICM (MolSoft, www.molsoft.com), or FlexX (BioSolveIT; www.biosolveit.de). Free data-pipelining software, close analogs of Pipeline Pilot, exist as well: KNIME (www.knime.com) and CDK-Taverna [31].
2. At the time of the study, we used to use a database of commercially available compounds that we compiled ourselves. Currently, there is a better solution. Molport (www.molport.com) is a compound ordering service that combines over 100 commercial catalogs with a total of ~5,000,000 unique compounds. MolPort takes orders in a form of a random compound lists, places respective orders to the original suppliers, and aggregates those orders (for an affordable fee) into a single shipping accompanied by an SD file containing a box/plate mapping.

References

1. Meng X-Y, Zhang H-X, Mezei M, Cui M (2011) Molecular docking: a powerful approach for structure-based drug discovery. Curr Comput Aided Drug Des 7(2):146
2. Jain AN (2006) Scoring functions for protein-ligand docking. Curr Protein Pept Sci 7 (5):407–420
3. Kirchmair J, Markt P, Distinto S, Wolber G, Langer T (2008) Evaluation of the performance of 3D virtual screening protocols: RMSD comparisons, enrichment assessments, and decoy selection—what can we learn from earlier mistakes? J Comput Aided Mol Des 22(3): 213–228. doi:10.1007/s10822-007-9163-6

4. Scior T, Bender A, Tresadern G, Medina-Franco JL, Martínez-Mayorga K, Langer T, Cuanalo-Contreras K, Agrafiotis DK (2012) Recognizing pitfalls in virtual screening: a critical review. J Chem Inf Model 52(4):867–881. doi:10.1021/ci200528d
5. Warren G, Andrews C, Capelli A, Clarke B, LaLonde J (2005) A critical assessment of docking programs and scoring functions. J Med Chem 49:5912–5931
6. Kitchen DB, Decornez H, Furr JR, Bajorath J (2004) Docking and scoring in virtual screening for drug discovery: methods and applications. Nat Rev Drug Discov 3(11):935–949. doi:10.1038/nrd1549, nrd1549 [pii]
7. Ferrara P, Gohlke H, Price D, Klebe G, Brooks CI (2004) Assessing scoring functions for protein-ligand interactions. J Med Chem 47:3032–3047
8. Cross JB, Thompson DC, Rai BK, Baber JC, Fan KY, Hu Y, Humblet C (2009) Comparison of several molecular docking programs: pose prediction and virtual screening accuracy. J Chem Inf Model 49(6):1455–1474. doi:10.1021/ci900056c
9. Kellenberger E, Rodrigo J, Muller P, Rognan D (2004) Comparative evaluation of eight docking tools for docking and virtual screening accuracy. Proteins 57(2):225–242. doi:10.1002/prot.20149
10. Da C, Stashko M, Jayakody C, Wang X, Janzen W, Frye S, Kireev D (2015) Discovery of Mer kinase inhibitors by virtual screening using structural protein–ligand interaction fingerprints. Bioorg Med Chem 23(5):1096–1101. doi:10.1016/j.bmc.2015.01.001
11. Da C, Kireev D (2014) Structural protein–ligand interaction fingerprints (SPLIF) for structure-based virtual screening: method and benchmark study. J Chem Inf Model 54 (9):2555–2561. doi:10.1021/ci500319f
12. Mortier J, Rakers C, Bermudez M, Murgueitio MS, Riniker S, Wolber G (2015) The impact of molecular dynamics on drug design: applications for the characterization of ligand–macromolecule complexes. Drug Discov Today 20 (6):686–702. doi:10.1016/j.drudis.2015.01.003
13. Gao C, Herold JM, Kireev D (2012) Assessment of free energy predictors for ligand binding to a methyllysine histone code reader. J Comput Chem 33(6):659–665. doi:10.1002/jcc.22888
14. Graham DK, Salzberg DB, Kurtzberg J, Sather S, Matsushima GK, Keating AK, Liang X, Lovell MA, Williams SA, Dawson TL, Schell MJ, Anwar AA, Snodgrass HR, Earp HS (2006) Ectopic expression of the proto-oncogene mer in pediatric T-cell acute lymphoblastic leukemia. Clin Cancer Res 12 (9):2662–2669. doi:10.1158/1078-0432.ccr-05-2208
15. Christoph S, DeRyckere D, Sather S, Wang XD, Kireev D, Janzen W, Liu J, Yang C, van Deusen A, Simpson C, Norris-Drouin J, Frye S, Earp HS, Johnson GL, Graham DK (2011) UNC569 as novel small molecule mer receptor tyrosine kinase inhibitor for treatment of ALL. Blood 118(21):1111–1112
16. Liu J, Zhang W, Stashko MA, Deryckere D, Cummings CT, Hunter D, Yang C, Jayakody CN, Cheng N, Simpson C, Norris-Drouin J, Sather S, Kireev D, Janzen WP, Earp HS, Graham DK, Frye SV, Wang X (2013) UNC1062, a new and potent Mer inhibitor. Eur J Med Chem 65:83–93. doi:10.1016/j.ejmech.2013.03.035
17. Zhang W, McIver AL, Stashko MA, DeRyckere D, Branchford BR, Hunter D, Kireev D, Miley MJ, Norris-Drouin J, Stewart WM, Lee M, Sather S, Zhou Y, Di Paola JA, Machius M, Janzen WP, Earp HS, Graham DK, Frye SV, Wang X (2013) Discovery of Mer specific tyrosine kinase inhibitors for the treatment and prevention of thrombosis. J Med Chem 56 (23):9693–9700. doi:10.1021/jm4013888
18. Zhang WH, Zhang DH, Stashko MA, DeRyckere D, Hunter D, Kireev D, Miley MJ, Cummings C, Lee M, Norris-Drouin J, Stewart WM, Sather S, Zhou YQ, Kirkpatrick G, Machius M, Janzen WP, Earp HS, Graham DK, Frye SV, Wang XD (2013) Pseudocyclization through intramolecular hydrogen bond enables discovery of pyridine substituted pyrimidines as new mer kinase inhibitors. J Med Chem 56(23):9683–9692. doi:10.1021/Jm401387j
19. Zhang W, DeRyckere D, Hunter D, Liu J, Stashko MA, Minson KA, Cummings CT, Lee M, Glaros TG, Newton DL, Sather S, Zhang D, Kireev D, Janzen WP, Earp HS, Graham DK, Frye SV, Wang X (2014) UNC2025, a potent and orally bioavailable MER/FLT3 dual inhibitor. J Med Chem 57 (16):7031–7041. doi:10.1021/jm500749d
20. Friesner RA, Banks JL, Murphy RB, Halgren TA, Klicic JJ, Mainz DT, Repasky MP, Knoll EH, Shelley M, Perry JK, Shaw DE, Francis P, Shenkin PS (2004) Glide: a new approach for rapid, accurate docking and scoring. 1. Method and assessment of docking accuracy. J Med Chem 47(7):1739–1749. doi:10.1021/jm0306430
21. Lipinski CA (2000) Drug-like properties and the causes of poor solubility and poor

permeability. J Pharmacol Toxicol Methods 44 (1):235–249, S1056-8719(00)00107-6 [pii]
22. Walters WP, Murcko MA (2002) Prediction of 'drug-likeness'. Adv Drug Deliv Rev 54 (3):255–271
23. (2009) Pipeline Pilot, ver 85, Accelrys Software Inc
24. Huang X, Finerty P Jr, Walker JR, Butler-Cole C, Vedadi M, Schapira M, Parker SA, Turk BE, Thompson DA, Dhe-Paganon S (2009) Structural insights into the inhibited states of the Mer receptor tyrosine kinase. J Struct Biol 165(2):88–96. doi:10.1016/j.jsb.2008.10.003, S1047-8477(08)00249-9 [pii]
25. Liu J, Yang C, Simpson C, Deryckere D, Van Deusen A, Miley MJ, Kireev D, Norris-Drouin J, Sather S, Hunter D, Korboukh VK, Patel HS, Janzen WP, Machius M, Johnson GL, Earp HS, Graham DK, Frye SV, Wang X (2012) Discovery of novel small molecule mer kinase inhibitors for the treatment of pediatric acute lymphoblastic leukemia. ACS Med Chem Lett 3(2):129–134
26. Halgren TA (1996) Merck molecular force field. I. Basis, form, scope, parameterization, and performance of MMFF94. J Comput Chem 17(5-6):490–519
27. (2009) Maestro Suite, Schrodinger LLC
28. Bernasconi P, Chen M, Galasinski S, Popa-Burke I, Bobasheva A, Coudurier L, Birkos S, Hallam R, Janzen WP (2007) A chemogenomic analysis of the human proteome: application to enzyme families. J Biomol Screen 12 (7):972–982. doi:10.1177/1087057107306759
29. Pommereau A, Pap E, Kannt A (2004) Two simple and generic antibody-independent kinase assays: comparison of a bioluminescent and a microfluidic assay format. J Biomol Screen 9(5):409–416. doi:10.1177/1087057104264175
30. Morris GM, Huey R, Lindstrom W, Sanner MF, Belew RK, Goodsell DS, Olson AJ (2009) Autodock4 and autodocktools4: automated docking with selective receptor flexibility. J Comput Chem 30(16):2785–2791
31. Kuhn T, Willighagen EL, Zielesny A, Steinbeck C (2010) CDK-Taverna: an open workflow environment for cheminformatics. BMC Bioinformatics 11(1):159

Chapter 5

AlphaScreen-Based Assays: Ultra-High-Throughput Screening for Small-Molecule Inhibitors of Challenging Enzymes and Protein-Protein Interactions

Adam Yasgar, Ajit Jadhav, Anton Simeonov, and Nathan P. Coussens

Abstract

AlphaScreen technology has been routinely utilized in high-throughput screening assays to quantify analyte accumulation or depletion, bimolecular interactions, and post-translational modifications. The high signal-to-background, dynamic range, and sensitivity associated with AlphaScreens as well as the homogenous assay format and reagent stability make the technology particularly well suited for high-throughput screening applications. Here, we describe the development of AlphaScreen assays to identify small-molecule inhibitors of enzymes and protein-protein interactions using the highly miniaturized 1536-well format. The subsequent implementation of counter assays to identify false-positive compounds is also discussed.

Key words AlphaLISA, AlphaScreen, High-throughput screening, Assay, ELISA, HTS, Enzyme, Protein-protein interaction

1 Introduction

The AlphaScreen (Amplified Luminescent Proximity Homogenous Assay Screen) and AlphaLISA technologies have enabled the development of robust proximity-based assays to identify small-molecule modulators for a variety of biological targets from high-throughput screening (HTS) of compound libraries. AlphaScreen technology was developed from a methodology for diagnostic assays called luminescent oxygen channeling immunoassay (LOCI) that was described in 1994 by Ullman et al. [1]. This method was based on the nonenzymatic channeling of singlet oxygen species, generated from a photoexcitable latex bead, to a second latex bead located in close proximity in order to induce a chemiluminescent signal. Ullman and colleagues demonstrated that the short diffusion distance of singlet oxygen prior to its spontaneous decay could be exploited to detect biological analytes and molecular interactions. Similarly, the AlphaScreen approach

William P. Janzen (ed.), *High Throughput Screening: Methods and Protocols*, Methods in Molecular Biology, vol. 1439,
DOI 10.1007/978-1-4939-3673-1_5,

reports on the proximity of "donor" and "acceptor" beads induced by the presence and co-recognition of an analyte of interest, which can include molecules, post-translational modifications to proteins, and molecular interactions. The donor beads contain a phthalocyanine photosensitizer that excites ambient oxygen into a singlet state following high-energy irradiation at 680 nm. Excitation of the donor beads generates about 60,000 oxygen singlets per second, which can diffuse to a maximum distance of about 200 nm [2]. A chemiluminescent signal is generated within an AlphaScreen acceptor bead if it is located in close enough proximity to receive singlet oxygen. Because AlphaScreen acceptor beads contain three chemical dyes, Thioxene, Anthracene, and Rubrene, they are sometimes referred to as "TAR" beads. The singlet oxygen initially reacts with thioxene to generate light that is transferred to anthracene and then to rubrene, resulting in a broad emission from 520 to 620 nm. In AlphaLISA and AlphaPlex acceptor beads, anthracene and rubrene are substituted by either europium, terbium, or samarium chelates, which are directly excited upon fragmentation of the dioxetane intermediate formed by the reaction of thioxene with singlet oxygen. AlphaLISA (Europium, $\lambda em = 615$ nm), AlphaPlex 545 (Terbium, $\lambda em = 545$ nm), and AlphaPlex 645 (Samarium, $\lambda em = 645$ nm) acceptor beads emit intense and spectrally defined emission signals. Therefore, it is possible to develop multiplex assays by incorporating multiple acceptor beads into the assay design. The lifetime of singlet oxygen is relatively short in aqueous solutions (~4 ms) and the beads are generally introduced at low concentrations, so nonspecific interactions among bead pairs are rare and the background is very low [3]. Due to the very high signal and very low background, AlphaScreen technology is easily adaptable to the highly miniaturized 1536-well plates. Additionally, the convenient homogenous assay format and excellent reagent stability make the AlphaScreen technology particularly well suited for high-throughput applications. The surfaces of the hydrophilic AlphaScreen, AlphaLISA, and AlphaPlex beads are coated with latex-based hydrogels with reactive aldehydes to allow the attachment of assay-specific molecules such as antibodies, ligands, substrates, and binding partners. In addition to the widely used biotin-streptavidin pair, frequently utilized are recognition pairs based on protein affinity purification handles, such as hexahistidine, FLAG, and GST tails, as well as specific antibodies targeting post-translational modifications, such as various histone methylation loci. This flexibility in bead conjugation has enabled the development of a variety of assays suitable for different biological applications. For example, a number of diagnostic approaches have been reported that utilize AlphaLISA to measure biomarkers from human saliva, plasma, and serum [4–8]. Additionally, the technology has been applied extensively to investigate a wide variety of biological processes, including the activities of purified enzymes, the generation of second messengers, post-

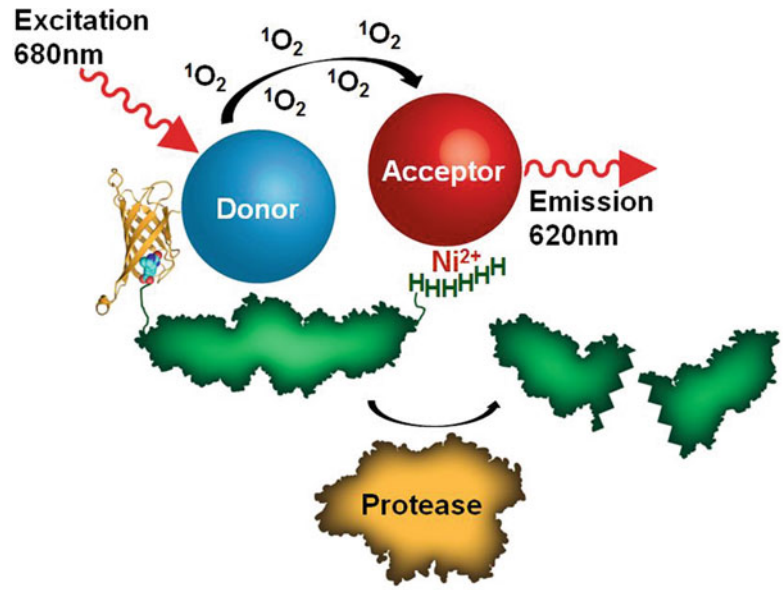

Fig. 1 Diagram of an AlphaScreen assay strategy to follow the depletion of substrate due to enzymatic activity. The activity of a protease (represented in *orange*) is measured by the loss of a protein substrate (represented in *green*) due to proteolytic cleavage. The biotinylated substrate also contains a polyhistidine tag, which brings streptavidin donor beads and nickel chelate acceptor beads into close proximity to generate a high signal prior to cleavage. The streptavidin-biotin complex (Protein Data Bank ID 3RY2) is represented with streptavidin as a *ribbon* diagram and biotin as *spheres* and was generated with the program PyMOL

translational modifications to proteins, and different types of molecular interactions (for a review, *see* [3]).

There are a multitude of examples reported in the literature where AlphaScreen/AlphaLISA technology has been utilized to develop sensitive and robust assays for HTS. In general, the basic paradigms of these different HTS assays are to detect either the depletion of a substrate (Fig. 1), the formation of a product (Fig. 2), or interactions between molecules (Fig. 3). At our center, we have utilized all of these approaches to develop miniaturized assays for diverse biological applications that ultimately enabled the identification of small-molecule modulators from large compound libraries. For example, based on a substrate depletion approach, we developed an AlphaScreen assay to identify inhibitors of tyrosyl-DNA phosphodiesterase I (Tdp1), which is involved in DNA repair [9]. For this assay, a reporter substrate for Tdp1 was generated by coupling fluorescein isothiocyanate (FITC) to the amino group of a phosphotyrosine-containing deoxyoligonucleotide biotinylated at its 5′-end. Thus, the intact substrate would yield a high signal due to the close proximity of streptavidin-conjugated donor beads and

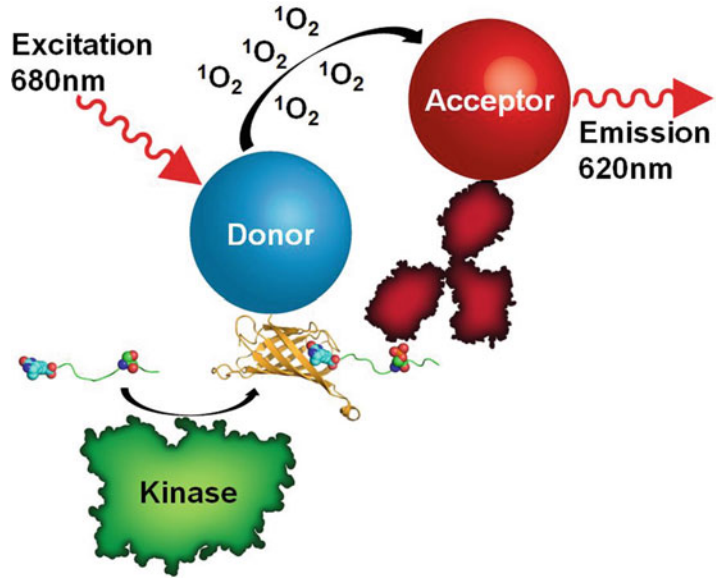

Fig. 2 Diagram of an AlphaScreen assay strategy to follow the generation of a reaction product due to enzymatic activity. Here, the activity of a kinase (represented in *green*) is followed by the phosphorylation of a biotinylated peptide substrate (represented as a *green ribbon*). A phospho-specific antibody (*red*), conjugated to an acceptor bead, recognizes the phosphorylated substrate and places the acceptor bead in close proximity to the streptavidin donor bead to generate a signal. The streptavidin-biotin complex (Protein Data Bank ID 3RY2) is represented with streptavidin as a *ribbon* diagram and biotin as *spheres* and was generated with the program PyMOL

anti-FITC-conjugated acceptor beads. In contrast, hydrolysis of the substrate by Tdp1 resulted in a loss of signal. This approach enabled the identification of previously unreported inhibitors of Tdp1. In another example, the strategy of following substrate depletion was utilized to develop an assay to investigate the activity of human flap endonuclease 1 (FEN1), which is involved in DNA replication and repair [10]. A substrate for FEN1 was assembled from three oligodeoxynucleotides, including an unlabeled template strand, a flap strand labeled on the 5′-end with FITC, and an upstream strand biotinylated at the 5′-end. Prior to cleavage, the three oligodeoxynucleotides associate and bring the streptavidin donor beads and anti-FITC-conjugated acceptor beads into close proximity, thereby generating a strong signal. Upon cleavage of the flap substrate by FEN1, the signal is reduced due to separation of the bead pairs as the biotin and FITC tags are no longer contained within the singular substrate molecule. The assay allowed identification of previously unreported FEN1 inhibitors with submicromolar potency. AlphaScreen/AlphaLISA assays also routinely report on the generation of a product, which can be from complex

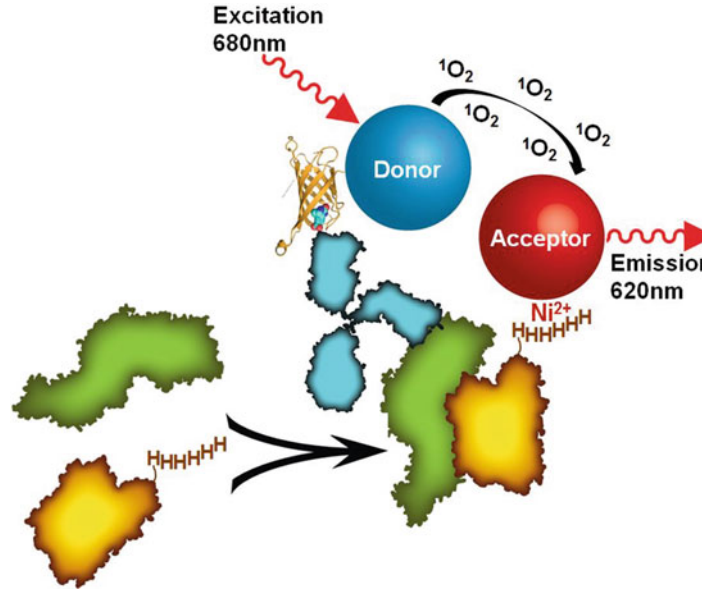

Fig. 3 Diagram of an AlphaScreen assay strategy to detect protein-protein interactions. In this scheme, the association between two proteins (represented in *green* and *orange*) is followed by pairing each molecule with a donor or acceptor bead, respectively. While the *orange* protein contains a polyhistidine tag and associates with nickel chelate acceptor beads, the *green* protein is recognized by a biotinylated antibody (*blue*) that binds a streptavidin donor bead. The protein complex places the bead pair into close proximity to generate a signal. The streptavidin-biotin complex (Protein Data Bank ID 3RY2) is represented with streptavidin as a *ribbon* diagram and biotin as *spheres* and was generated with the program PyMOL

systems, such as from intact or lysed cells in media. In one such example, our center took advantage of the commercially available AlphaLISA TNF-α assay to identify inhibitors of TNF-α secreted from THP-1 cells that were stimulated with lipopolysaccharide in 1536-well plates [11]. The detection reagents included two anti-TNF-α antibodies that recognize different epitopes of TNF-α. While one is directly conjugated to acceptor beads, the other antibody is biotinylated and therefore binds donor beads in solution. A signal is generated in the presence of TNF-α, which brings the bead pairs into close proximity. The optimized assay was robust and allowed us to identify novel inhibitors of TNF-α. In a different example, we used a commercially available AlphaLISA Tau assay to measure total cellular levels of the microtubule-associated protein, Tau, from SH-SY5Y neuroblastoma cell lysates in 1536-well plates [12]. As with the AlphaLISA TNF-α assay, the Tau assay utilized two antibodies that recognize different epitopes of the target. Measuring product formation can also be used to investigate the activity of purified enzymes in buffered solutions. We have used

this strategy to follow the enzymatic activities of the histone methyltransferases, G9a and EHMT1 (also known as GLP) [13, 14]. For these assays, the substrate was a biotinylated histone peptide. Methylation of the histone peptide by either G9a or EHMT1 was recognized by a primary antibody against methyllysine, which resulted in an increased signal due to the induced proximity of secondary antibody-coated acceptor beads and streptavidin donor beads. AlphaScreen assays can also be developed to report on associations between molecules and this approach enabled our group to investigate interactions between biotinylated trimethyllysine histone peptides that represent different histone epigenetic marks and glutathione S-transferase (GST) chimeras of chromodomains (MPP8, HP1β, and CHD1), the JMJD2A tudor domain, and RAG2, a plant homeodomain [15]. Such interactions are generally weak (having dissociation constants in the micromolar range) and therefore are challenging to interrogate by other assay technologies, such as fluorescence polarization. The AlphaScreen approach utilized commercially available streptavidin donor and anti-GST acceptor beads to yield a signal as a consequence of protein-peptide interactions. Ultimately, the optimized assay enabled the characterization of binding specificities for the different domains to multiple histone marks. Another example of a protein-peptide interaction that was adapted to an AlphaScreen format is the association between a C-terminal peptide of heat-shock protein 90 (Hsp90) and the TPR2A domain of the Hsp90 cochaperone, Hsp-organizing protein (HOP) [16]. As before, the assay incorporated a biotinylated peptide, while the TPR2A protein contained a hexahistidine tag. Therefore, streptavidin donor beads and nickel chelate acceptor beads are brought together through the Hsp90/TPR2A interaction to generate a signal. The optimized assay was robust and allowed identification of a novel class of Hsp90 inhibitors [17]. Similarly, we developed a high-throughput AlphaScreen assay to identify inhibitors of the interaction between the malaria parasite proteins, AMA1 and RON2, which is essential for parasite invasion into red blood cells. The assay was developed with a biotinylated RON2L peptide, which binds streptavidin donor beads and AMA1 with a hexahistidine tag that binds nickel chelate acceptor beads. Inhibitors of the AMA1-RON2 interaction reduced the proximity of donor and acceptor beads along with the signal. The assay enabled our discovery of the first small-molecule inhibitor for this interaction [18]. In addition to peptide-protein interactions, we have also developed AlphaScreen assays to report on protein-protein interactions. An excellent example of this is an assay to detect heterodimerization of the transcription factors RUNX1 and CBFβ, which has been shown to be critical for the pathogenesis of CBF leukemias [19]. In this case, the RUNX1 protein was biotinylated and the CBFβ protein was expressed to

include a hexahistidine tag. Inhibitors were identified that prevented heterodimerization of the proteins and thus a loss of pairing between the streptavidin donor and nickel chelate acceptor beads. We have also used an AlphaScreen format to interrogate other types of interactions, such as an RNA-protein interaction that is relevant to the pathology of myotonic dystrophy type 1 [20]. For this assay, it was possible to utilize the same AlphaScreen reagents described in the previous example, due to the use of biotinylated RNA molecules and polyhistidine-tagged muscleblind-like 1 protein. The remainder of this chapter is intended to provide useful guidelines for the development of different types of AlphaScreen assays suitable for the identification of small-molecule inhibitors of targets such as purified enzymes, protein-protein interactions, and targets within whole cells from high-throughput screens in the highly miniaturized 1536-well format.

2 Materials

The following three protocols for detecting substrate depletion by an enzymatic reaction, detecting protein-protein interactions, and detecting product formation from live cells have each been optimized for unpublished projects that are currently active in our laboratory. Therefore, the names of the specific proteins or targets are unidentified to maintain confidentiality.

2.1 Materials for Detecting Substrate Depletion from AlphaScreen Assays

1. Medium-binding white solid-bottom 1536-well plates.
2. Plate reader capable of 1536-well AlphaScreen detection (such as the EnVision Plate Reader equipped with a 1536 HTS AlphaScreen aperture).
3. Assay buffer (PBS pH 7.4, 0.01 % Tween-20, or another preferred buffer, *see* **Note 1**).
4. Enzyme at double the final concentration in assay buffer.
5. Substrate at fourfold the final concentration in assay buffer.
6. Mixture of nickel chelate acceptor beads (20 μg/mL working stock for 5 μg/mL, final) and streptavidin donor beads (20 μg/mL working stock for 5 μg/mL, final) suspended in assay buffer (or beads conjugated for the preferred specificity, such as anti-GST) (*see* **Note 2**).
7. Experimental compounds suspended in DMSO (stock concentrations of 640 nM–10,000 μM for a working concentration range of 3.7 nM–57.5 μM after a 174-fold dilution into the assay mixture).
8. Liquid transfer pin tool (such as a Kalypsys automated pin-tool station) (*see* **Note 3**).

9. Centrifuge equipped with a rotor that will accommodate plates.
10. Liquid dispenser capable of delivering small volumes (such as a BioRAPTR Flying Reagent Dispenser).

2.2 Materials for Detecting Protein-Protein Interactions from AlphaScreen Assays

1. Medium-binding white solid-bottom 1536-well plates.
2. Plate reader capable of 1536-well AlphaScreen detection (such as the EnVision Plate Reader equipped with a 1536 HTS AlphaScreen aperture).
3. Assay buffer (15 mM HEPES pH 7.5, 150 mM NaCl, and 0.01 %Tween-20 or preferred buffer, *see* **Note 1**).
4. Polyhistidine-tagged protein at double the final concentration in assay buffer.
5. Biotinylated protein at fourfold the final concentration in assay buffer.
6. A mixture of streptavidin donor beads (80 μg/mL working stock for 20 μg/mL, final) and nickel chelate acceptor beads (80 μg/mL working stock for 20 μg/mL, final) suspended in assay buffer (or beads conjugated for the preferred specificity, such as anti-GST) (*see* **Note 2**).
7. Experimental compounds suspended in DMSO (stock concentrations of 640 nM–10,000 μM for a working concentration range of 3.7 nM–57.5 μM after a 174-fold dilution into the assay mixture).
8. Liquid transfer pin tool (such as a Kalypsys automated pin-tool station) (*see* **Note 3**).
9. Centrifuge equipped with a rotor that will accommodate plates.
10. Liquid dispenser capable of delivering small volumes (such as a BioRAPTR Flying Reagent Dispenser).

2.3 Materials for Detection of Product Formation from Live Cells by AlphaScreen Assays

1. Medium-binding white solid-bottom tissue culture-treated 1536-well plates.
2. Plate reader capable of 1536-well AlphaScreen detection (such as the EnVision Plate Reader equipped with a 1536 HTS AlphaScreen aperture).
3. THP-1 cells in media with 5 % serum (*see* **Note 4**).
4. Media with 5 % serum.
5. Lipopolysaccharide (LPS) (4 μg/mL working stock for 1 μg/mL, final) in media with 5 % serum.
6. Mixture of biotinylated anti-TNF-α antibody (4.66 nM working stock for 1 nM, final) and anti-TNF-α-conjugated acceptor beads (46.66 μg/mL working stock for 10 μg/mL, final) in AlphaLISA immunoassay buffer.

7. Streptavidin donor beads (186.4 μg/mL working stock for 40 μg/mL, final) in AlphaLISA immunoassay buffer (*see* **Note 2**).
8. Experimental compounds suspended in DMSO (stock concentrations of 640 nM–10,000 μM for a working concentration range of 3.7 nM–57.5 μM after a 174-fold dilution into the assay mixture).
9. Liquid transfer pin tool (such as a Kalypsys automated pin-tool station) (*see* **Note 3**).
10. Centrifuge equipped with a rotor that will accommodate plates.
11. Liquid dispenser capable of delivering small volumes (such as a Multidrop Combi Reagent Dispenser).

3 Methods

3.1 Methods for Detecting Substrate Depletion from AlphaScreen Assays

1. Before beginning assay development and regularly thereafter, verify that the plate reader settings are optimized for the AlphaScreen assay (*see* **Note 5**).
2. Determine the enzymatic assay conditions, including the buffer composition, concentration of enzyme, and the K_M of the substrate under those conditions (*see* **Note 6**).
3. Perform a titration of the substrate with fixed concentrations of AlphaScreen reagents in order to determine the saturation point of the beads and the dynamic range of the assay (*see* **Note 7**).
4. Perform a titration of enzyme with fixed concentrations of substrate and AlphaScreen reagents (*see* **Note 8**).
5. After assay optimization, establish DMSO tolerance (or appropriate vehicle) by performing a titration. Secondly, perform the assay in a 1536-well plate where the wells have only been treated with DMSO and control compound(s) (*see* **Note 9**).
6. Dispense 2 μL of a buffered enzyme solution, into columns 1, 2, and 5–48 of a 1536-well plate (*see* **Note 10**).
7. Dispense 2 μL of buffer (the same buffer that the enzyme has been diluted into) into columns 3 and 4 of the plate (*see* **Note 11**).
8. Spin the plate in a centrifuge for 15 s at 161 × *g*.
9. Deliver 23 nL of DMSO vehicle, control (if available), and library compounds to the appropriate wells of the 1536-well plate (*see* **Note 12**).
10. Incubate the plate at room temperature for 15 min to allow time for the compounds to bind the target (the time period can be optimized for different assays).

11. Dispense 1 μL of the concentrated substrate into the wells of columns 1–48 (*see* **Note 13**).
12. Spin the plate in a centrifuge for 15 s at 161 × *g*.
13. Incubate the plate at room temperature for 30 min (or a predetermined amount of time).
14. Dispense 1 μL of a 20 μg/mL mixture of AlphaScreen streptavidin donor and nickel chelate acceptor beads (or beads with the preferred specificity) into columns 1–48 (*see* **Note 2**).
15. Spin the plate in a centrifuge for 15 s at 161 × *g*.
16. Incubate the plate at room temperature for 30 min (this incubation time can be optimized for individual assays).
17. Read the plate on an EnVision Reader equipped with a 1536 HTS AlphaScreen aperture using an 80 ms excitation time and 240 ms measurement (or another reader appropriately set up to measure AlphaScreen assays) (*see* **Note 14**).

3.2 Methods for Detecting Protein-Protein Interactions from AlphaScreen Assays

1. Before beginning assay development and regularly thereafter, verify that the plate reader settings are optimized for the AlphaScreen assay (*see* **Note 5**).
2. Establish the lowest concentration of each protein required to obtain robust assay results (*see* **Note 15**).
3. Verify that titration with an unlabeled version of each protein results in assay signal reduction (this can also be used as a control).
4. After assay optimization, establish DMSO tolerance (or appropriate vehicle) by performing a titration. Secondly, perform the assay in a 1536-well plate where the wells have only been treated with DMSO and control compound(s) (*see* **Note 9**).
5. Dispense 2 μL of concentrated polyhistidine-tagged protein into columns 1–48 of a 1536-well plate.
6. Deliver 23 nL of DMSO vehicle, control (if available), and library compounds to the appropriate wells of the 1536-well plate (*see* **Note 12**).
7. Spin the plate in a centrifuge for 15 s at 161 × *g*.
8. Incubate the plate at room temperature for 15 min to allow time for the compounds to bind the target (the time period can be optimized for different assays).
9. Dispense 1 μL of concentrated biotinylated-protein into columns 1, 2, and 5–48 of the plate.
10. Dispense 1 μL of buffer into columns 3 and 4 of the plate (*see* **Note 16**).
11. Spin the plate in a centrifuge for 15 s at 161 × *g*.

12. Incubate the plate at room temperature for 15 min to allow time for the proteins to bind (the time period can be optimized for different assays).
13. Dispense 1 μL of 80 μg/mL mixture of streptavidin donor beads and nickel chelate acceptor beads (or beads with the preferred specificity) into columns 1–48 of the plate (*see* **Note 2**).
14. Spin the plate in a centrifuge for 15 s at 161 × *g*.
15. Incubate the plate at room temperature for 30 min (this incubation time can be optimized for individual assays).
16. Read the plate on an EnVision Reader equipped with a 1536 HTS AlphaScreen aperture using an 80 ms excitation time and 240 ms measurement (or another reader appropriately set up to measure AlphaScreen assays) (*see* **Note 14**).

3.3 Methods for Detection of Product Formation from Live Cells by AlphaScreen Assays

1. Before beginning assay development and regularly thereafter, verify that the plate reader settings are optimized for the AlphaScreen assay (*see* **Note 5**).
2. Optimize the assay parameters for detection of preferred product from preferred cell line (*see* **Note 17**).
3. After assay optimization, establish DMSO tolerance (or appropriate vehicle) by performing a titration. Secondly, perform the assay in a 1536-well plate where the wells have only been treated with DMSO and control compound(s) (*see* **Note 9**).
4. Dispense 3 μL containing 3000 THP-1 (or preferred cell type and optimized concentration) into columns 1–48 of a 1536-well plate.
5. Spin the plate in a centrifuge for 15 s at 161 × *g*.
6. Deliver 23 nL of DMSO vehicle, control (if available), and library compounds to the appropriate wells of the 1536-well plate (*see* **Note 12**).
7. Incubate the plate at 37 °C with 5 % CO_2 for 60 min to allow time for the compounds to enter the cells and bind a target (the time period can be optimized for different assays).
8. Dispense 1 μL of LPS (4 μg/mL working stock for 1 μg/mL, final or preferred stimulation reagent suspended in media to obtain the optimized final concentration) into columns 1, 2, and 5–48.
9. Dispense 1 μL of media with 5 % serum into columns 3 and 4 (*see* **Note 18**).
10. Spin the plate in a centrifuge for 15 s at 161 × *g*.
11. Incubate the plate at 37 °C with 5 % CO_2 for 16 h.
12. Dispense 1.5 μL containing a mixture of biotinylated anti-TNF-α antibody (1 nM, final) and anti-TNF-α-conjugated acceptor beads (10 μg/mL, final) into columns 1–48.

13. Spin the plate in a centrifuge for 15 s at 161 × *g*.
14. Incubate the plate at room temperature for 1 h (this incubation time can be optimized for individual assays).
15. Dispense 1.5 μL donor beads (40 μg/mL, final) into columns 1–48 (*see* **Note 2**).
16. Spin the plate in a centrifuge for 15 s at 161 × *g*.
17. Incubate the plate at room temperature for 30 min (this incubation time can be optimized for individual assays).
18. Read the plate on an EnVision Reader equipped with a 1536 HTS AlphaScreen aperture using an 80 ms excitation time and 240 ms measurement (or another reader appropriately set up to measure AlphaScreen assays) (*see* **Note 14**).

3.4 Identifying False-Positive Hit Compounds

In screening AlphaScreen/AlphaLISA assays against libraries of small-molecule compounds, it is probable that some of the hit compounds identified will be due to activity of the compound against the assay technology, rather than the biological system under investigation. Such compounds are commonly referred to as "false-positive hits" or "assay artifacts" and it is important to identify these compounds early on to avoid spending additional time and money in follow-up. The TruHit kit, available from PerkinElmer, was developed to detect compounds that interfere with the assay technology by four mechanisms, including those mimicking biotin, quenching singlet oxygen, quenching light, and scattering light. The TruHit kit simply contains streptavidin donor beads and biotinylated acceptor beads, which bind directly to one another, bypassing the requirement for an analyte (Fig. 4).

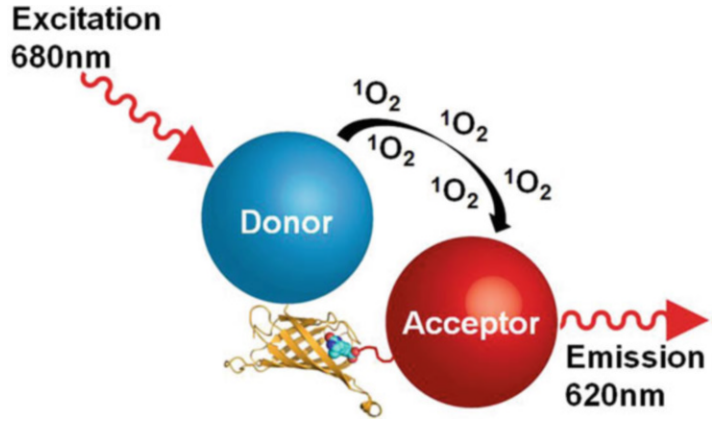

Fig. 4 Diagram of an AlphaScreen TruHit kit. A streptavidin donor bead interacts directly with a biotinylated acceptor bead to generate a signal in the absence of ligand. The kit can be used to identify false-positive hits from a screen by detecting interference from compounds that mimic biotin, quench singlet oxygen, quench light, and scattering light. The streptavidin-biotin complex (Protein Data Bank ID 3RY2) is represented with streptavidin as a *ribbon* diagram and biotin as *spheres* and was generated with the program PyMOL

To identify compounds that interfere by all four of the mechanisms listed above, it is necessary to perform the assay by two separate methods. To distinguish biotin mimetics, hit compounds are incubated with the streptavidin donor beads prior to the addition of biotinylated acceptor beads. These interference molecules will bind to streptavidin and prevent subsequent pairing of the donor and acceptor beads, which is indicated by a reduced AlphaScreen signal. The remaining interference mechanisms, singlet oxygen and light quenchers as well as light scatterers, are identified by incubating the hit compounds with beads that have been premixed. Examples of singlet oxygen quenchers include ascorbate, azide, and metals such as Zn^{2+}, Cu^{2+}, Fe^{2+}, and Fe^{3+}. Color quenchers or inner filters, such as malachite green and blue dextran, interfere with the assay by absorbing either the light used to excite the donor beads or the light emitted by the acceptor beads. Finally, compounds that form insoluble aggregates can cause interference by scattering light from both the excitation and emission wavelengths. Depending on the strategy of a particular AlphaScreen/AlphaLISA assay, additional experiments might need to be performed to identify other types of false-positive compounds that cannot be revealed by the TruHit kit. For instance, in the case of an AlphaScreen assay designed to detect an analyte using two antibodies, such as the secreted cytokine TNF-α, it is possible for a compound to act as a false-positive hit by disrupting the interactions of either antibody with the analyte. These interference compounds can be distinguished by performing the AlphaScreen assay in the presence of purified TNF-α after the other false-positive hits have been identified from the TruHit kit. In other cases, where a fusion protein has been linked to a bead through the use of an affinity tag, such as GST or polyhistidine, compounds could potentially disrupt those secondary detection interactions. If the other binding partner is biotinylated, products such as AlphaScreen Biotinylated-GST and Biotinylated-HIS are available to directly couple the donor and accepter beads and thus allow screening for interference compounds. In addition to the TruHit approach, cheminformatics filters can be applied using chemical substructure features such as the pan assay interference compounds (PAINS) filters identified by Baell et al. [21].

4 Notes

1. Buffer conditions that have already been established for a particular enzymatic reaction or protein-protein interaction can serve as a starting point for assay development. Sometimes it is possible to further improve an assay signal with modifications to the assay buffer, such as pH, buffering compound, salt, divalent cations, reducing agents, EDTA, and BSA [22]. Also, the addition of a detergent, such as Triton X-100, Tween 20,

NP-40, or Brij-35, at a concentration of ~0.01 % will sometimes improve the assay signal by reducing protein adsorption to the surface of plate wells. Within the online technical resources under, "Bead selection and bead interference," PerkinElmer provides detailed information about interferences caused by different buffer components for various bead types.

2. Note that any assay procedures which involve donor beads need to be performed under low-light conditions (<100 lx).
3. Accommodations can be made if a pin-tool, acoustic liquid dispenser, or other liquid-handling device capable of accurately transferring nanoliter volumes is not available. In this case, one could achieve the 174-fold dilution from a DMSO stock solution by making appropriate dilutions into the assay buffer or media. Each compound should be delivered as a four- or five-fold concentrated solution in a 1 μL volume to assay volumes of 3 μL or 4 μL, respectively, to achieve the final concentration. The delivery could be made with a 16-channel pipettor.
4. The use of media that contains biotin, such as RPMI, should be avoided as it will compete with the biotin-conjugated antibodies for the streptavidin donor beads and ultimately reduce the assay signal (Fig. 5). Also, when working with terbium-containing acceptor beads, which emit at 545 nm, we have observed a 50 % decrease in signal when using media containing phenol red as compared to phenol red-free media. Finally, before preparing cells for an experiment, it is recommended to use a cell strainer.

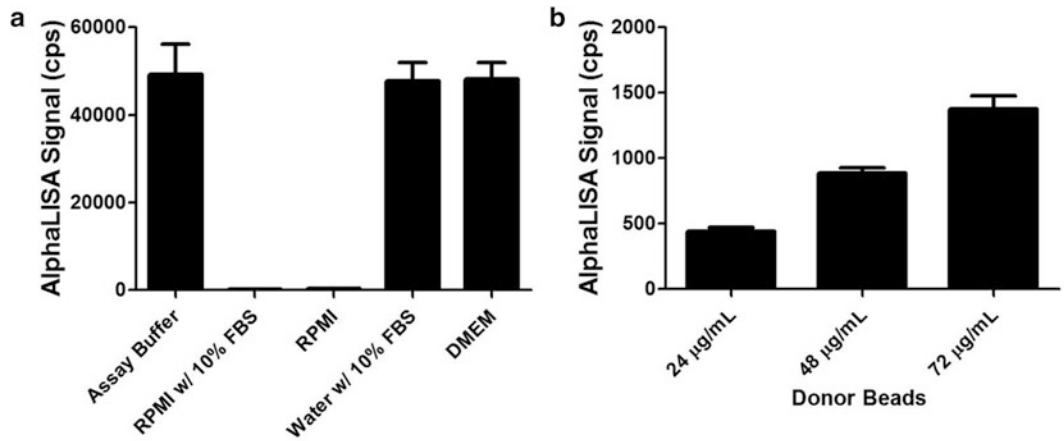

Fig. 5 Media containing biotin, such as RPMI, should be avoided when working with AlphaScreen reagents, due to interference with the streptavidin donor beads. Purified IL-1β (5.36 ng/mL) was suspended in the indicated solutions and detection was carried out with 6 μg/mL anti-IL-1β acceptor beads, 0.6 nM biotinylated anti-IL-1β antibody, and 24 μg/mL donor beads in the wells of a 1536-well plate (**a**). Increasing the concentration of streptavidin donor beads in the RPMI media (**b**), while maintaining the concentrations of the other AlphaLISA reagents as in (**a**), improves IL-1β detection, which is consistent with interference by biotin in the media

5. It is important to verify both prior to and throughout the process of working with AlphaScreen/AlphaLISA assays that the plate reader settings have been optimized for use with the assay being developed. AlphaScreen Omnibeads are intended to provide a strong signal in the absence of acceptor beads and therefore can be used to calibrate instruments. The importance of instrument optimization can be illustrated with an example from our center, where the same 1536-well plate was read before and after optimizing the settings of the plate reader. In this example, the wells of the AlphaScreen assay plate were treated with only control compound ($n = 32$) and DMSO ($n = 1408$). Optimization of the reader for the plate dimensions improved the %CV from 9.6 to 2.5 % and the Z' value from 0.68 to 0.9 (Fig. 6).
6. Detailed information about developing enzymatic assays for high-throughput screening, including measuring the K_M, can be found in the Assay Guidance Manual [22].
7. Low concentrations of substrate will result in low signal, which will increase with substrate concentration. At high substrate concentrations, the signal will again be reduced due to competition with substrate that does not result in bead pairing, which has been referred to as the "hook effect" (Fig. 7) [23]. Also, the concentration of donor and acceptor beads can be optimized for individual assays.
8. This experiment will determine the amount of enzyme required to achieve a robust assay signal (Fig. 8). In principle, this experiment could be performed as a two-dimensional matrix

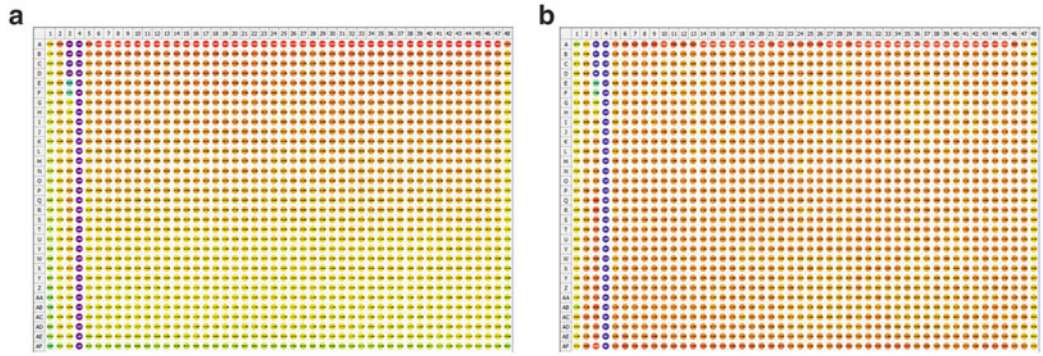

Fig. 6 Comparison of AlphaScreen data from the same plate before (**a**) and after (**b**) optimization of the plate reader. In this example, the wells of the plate were treated with only control compound (columns *3* (titration) and *4* (100 % inhibition, $n = 32$)) and DMSO ($n = 64$, columns *1* and *2*; $n = 1408$, columns *5–48*). The signal from the wells is represented as a heat map, with *red* and *purple* corresponding to high and low signal, respectively. A gradient of signal is apparent prior to plate reader optimization (**a**) causing a %CV of 9.6 % for 1408 wells and a Z' value of 0.68. Optimization of the reader for the plate dimensions clearly improved the results as seen by the uniform signal (**b**), a lowered %CV of 2.5 % and an increased Z' value of 0.9

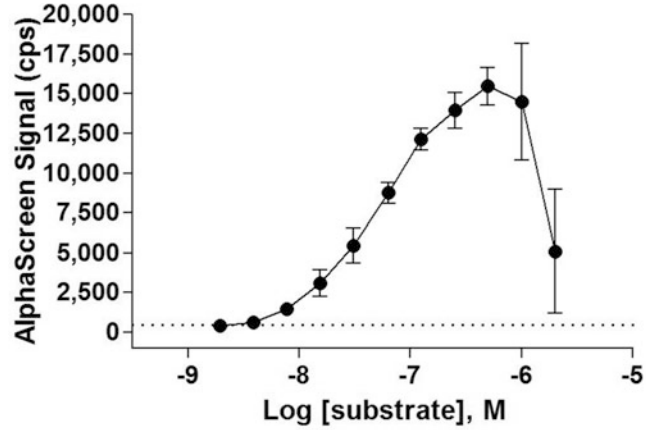

Fig. 7 Results of a substrate titration for an AlphaScreen enzymatic assay to detect substrate depletion. With this assay format, substrate depletion causes a loss of signal. As expected, the signal is low with low substrate concentrations and increases until the point where the AlphaScreen beads are saturated. At high substrate concentrations, the signal is also reduced due to competition among substrate molecules that interferes with bead pairing, which has been referred to as the "hook effect"

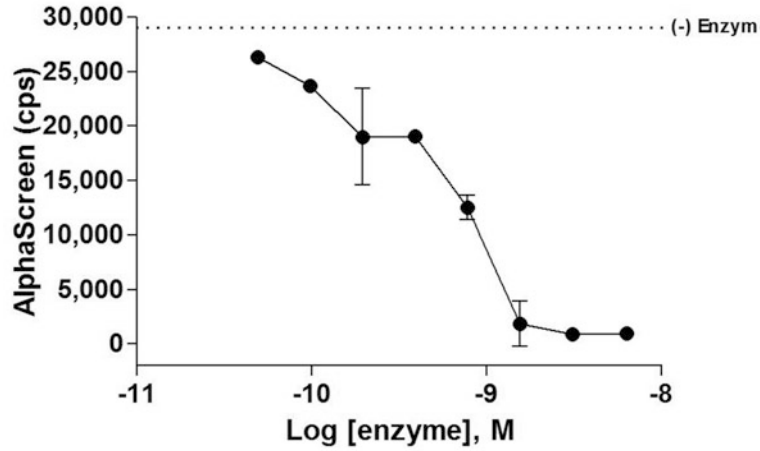

Fig. 8 Results of an enzyme titration for an AlphaScreen enzymatic assay to detect substrate depletion after 30 min. The level of the "no-enzyme control" (no substrate cleavage) is indicated by a *dashed line*. The results of this experiment can be used to determine the amount of substrate turnover for different concentrations of enzyme and various incubation periods. Thirty minutes was chosen as an incubation period for this assay to accommodate automation on a large scale

that also incorporates the substrate titration described in the previous note; however, the substrate will need to be applied with a liquid dispenser capable of delivering reagent to each of the wells simultaneously to allow comparison of the kinetics.

9. After an assay has been optimized, the tolerance to DMSO (or another vehicle used to solubilize compounds) should be established with a titration of vehicle into the assay mixture. Also, prior to screening with an optimized AlphaScreen/AlphaLISA assay, it is critical to evaluate the results of a plate treated with only DMSO and control compound(s). In one instance, we were able to link an irregular pattern in the DMSO-treated plate to inconsistent vehicle transfer by the automated pin-tool used to deliver compounds. The AlphaLISA assay results showed a low signal on the right side of the plate (Fig. 9a), whereas pin-transferring dye into PBS with the same pin tool showed a higher transfer of dye on the right side (Fig. 9b).

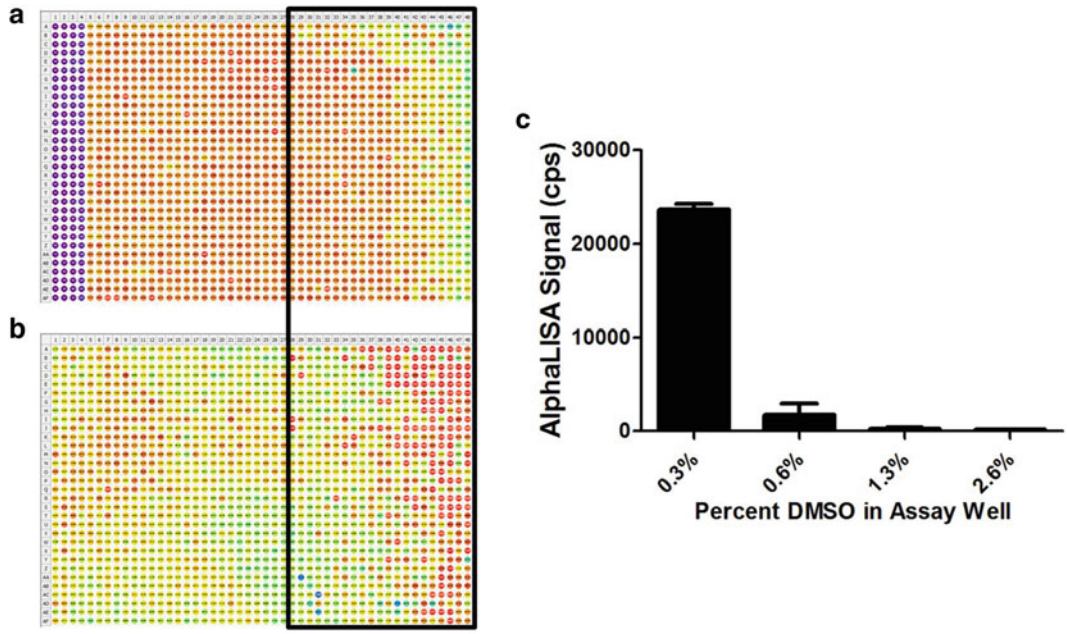

Fig. 9 Evaluation of an assay plate treated with only control compound(s) and vehicle can help to identify sources of error. In this example, an AlphaLISA IL-1β assay was performed and the wells of the plate were treated with only control compound ($n = 128$, columns *1–4*) and DMSO ($n = 1408$, columns *5–48*) (**a**). The signal from the wells is represented as a heat map, with *red* and *purple* corresponding to high and low signal, respectively. An irregular pattern associated with a lower signal was observed on the *right side* of the plate. After pin transferring dye into PBS buffer, a similar pattern was also observed that was consistent with greater delivery of dye on the *right side* of the plate (**b**). Therefore, the pattern in (**a**) was attributed to a greater delivery of DMSO to the wells on the *right side* of the plate based on the results in (**b**) and the DMSO sensitivity of the assay (**c**)

The DMSO tolerance experiment demonstrated that the assay signal was inhibited by and sensitive to DMSO (Fig. 9c).

10. The final enzyme concentration will need to be predetermined based on the enzymatic activity (*see* **Note 6**), which might vary among preparations/batches.
11. This protocol suggests a "no-enzyme control" in columns 3 and 4, which can be used if there are no known inhibitors. Alternatively, if an inhibitor exists, enzyme would be included in all columns and the inhibitor compound(s) would be applied in columns 3 and 4. For instance, a titration series might be introduced in column 3 and the wells of column 4 would contain a concentration that results in 100 % inhibition (*see* **Note 12**).
12. At our center, we include high and low controls in columns 1–4 with library compounds in columns 5–48. A range for final library compound concentrations would be 3 nM–57 μM after a 174-fold dilution.
13. The final substrate concentration will need to be predetermined (*see* **Note 6**) and is often used at the K_M in order to be optimally sensitive to different mechanisms of inhibition [22].
14. The suggested excitation and measurement times will allow sensitive detection at the expense of time. Therefore, the settings can be optimized for individual assays depending on the assay signal. When using white plates, high signals will carry over to some extent into neighboring wells.
15. Depending on the chosen affinity tags for each protein, it is possible to evaluate the signal window before assay optimization by using commercially available products, such as AlphaScreen Biotinylated-GST and Biotinylated-HIS. We have observed that the assay signal window for a protein-protein interaction can vary depending on the affinity tag selected [15]. Therefore, one might choose to test several affinity tags before beginning the process of assay optimization. After the affinity tags for the two proteins have been selected, assay development can proceed. In order to determine the minimal concentrations of each protein required to achieve robust assay results, one should first perform a matrix titration in a 1536-well plate to systematically determine the assay signal from different concentrations of each protein in assay buffer with a fixed concentration of AlphaScreen reagents. The plate can be set up to compare eight concentrations, including zero, of each protein in a matrix with 16 replicates per condition (Fig. 10). Mean values and standard deviations for each of the 16 replicates will then be calculated from the data (Fig. 11). This information allows calculation of the Z' statistic, which can be used to select the minimal protein concentrations that result

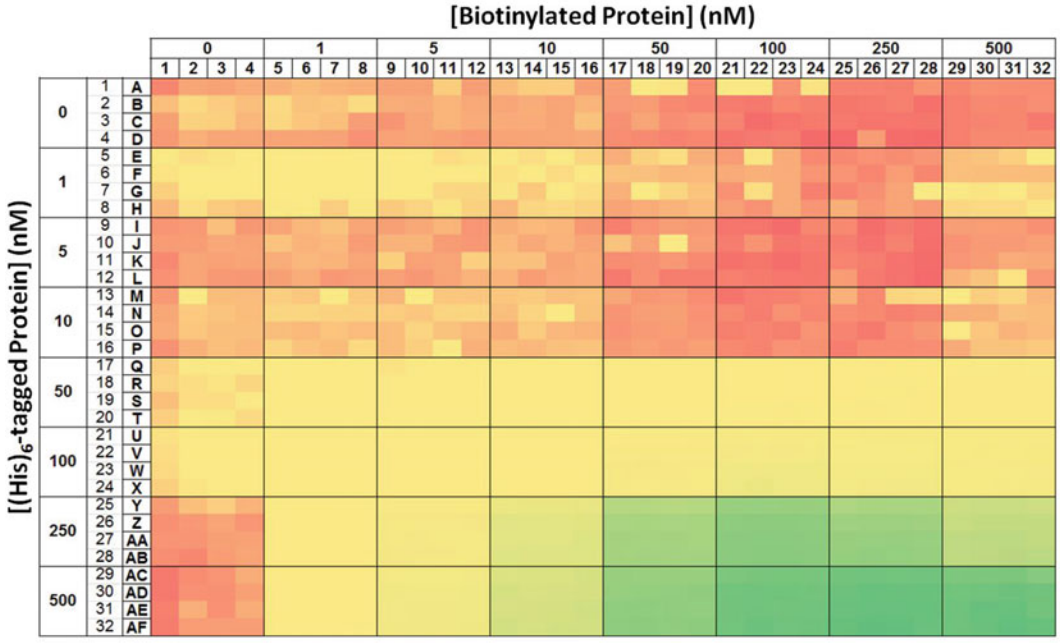

Fig. 10 Results of an experiment to determine optimal concentrations of two proteins for an AlphaScreen assay. Eight concentrations of both hexahistidine-tagged protein (*vertical axis*) and biotinylated protein (*horizontal axis*) were examined in a matrix arrangement with 16 replicates per condition in a 1536-well plate. The signals from the wells are represented by a heat map, with *red* and *green* corresponding to low and high signal, respectively

[Biotinylated Protein] (nM)

[(His)6-tagged Protein] (nM)	0	1	5	10	50	100	250	500
0	-	-	-	-	-	-	-	-
1	-1	-10	-6	16	8	-1	3	-80
5	10	-4	4	16	41	73	78	-14
10	12	-7	37	134	394	646	766	798
50	17	40	886	2,733	6,757	10,398	11,938	10,644
100	21	114	3,814	10,507	23,104	32,632	36,391	33,416
250	19	537	13,771	32,017	59,244	76,455	80,365	83,285
500	24	35	1,907	8,541	35,171	63,477	78,510	98,322

Fig. 11 Mean signals from various combinations of protein concentrations were calculated from the data shown in Fig. 10. The mean signals ($n = 16$) are colored as a heat map, with *red* and *green* corresponding to low and high signal, respectively

[(His)$_6$-tagged Protein] (nM) \ [Biotinylated Protein] (nM)	1	5	10	50	100	250	500
1	-9.79	-14.23	-11.81	-14.29	-85.96	-54.01	-9.03
5	-25.24	-24.92	-4.73	-1.55	-0.58	-1.04	-64.86
10	-14.76	-2.28	-1.08	0.51	0.51	0.54	-0.44
50	-4.43	0.65	0.83	0.86	0.88	0.86	-0.78
100	-0.35	0.74	0.84	0.87	0.85	0.92	-0.28
250	0.41	0.82	0.88	0.93	0.94	0.93	0.32
500	-2.40	0.28	0.47	0.76	0.85	0.91	0.63

Fig. 12 The *Z'* values resulting from various combinations of protein concentrations were calculated from the data shown in Fig. 10. The *Z'* values are colored as a heat map, with *red* and *green* corresponding to low and high, respectively. Based on these data, we chose to use 250 nM of polyhistidine-tagged protein and 100 nM of biotinylated protein

in robust assay performance (Fig. 12) [24]. Based on the example data shown, we chose to use 250 nM of polyhistidine-tagged protein and 100 nM of biotinylated protein. Secondly, the concentrations of donor and acceptor beads can be optimized.

16. This example suggests a "no-protein partner control." Alternatively, if an inhibitor compound or peptide is used, the protein will be delivered to columns 1–48. In that case, the inhibitor can be applied to columns 3 and 4. For instance, a titration series might be introduced in column 3 and the wells of column 4 would contain a concentration that results in 100 % inhibition (*see* **Note 12**).
17. Optimizations include determining the optimal cell number per well, the optimal concentration of stimulation compound (Fig. 13), and the optimal incubation period following cell stimulation. Additionally, the concentrations of donor and acceptor beads can be optimized.
18. This example suggests an "unstimulated control." Alternatively, if an inhibitor compound is used, LPS can be delivered to columns 1–48. In that case, the inhibitor can be applied to columns 3 and 4. For instance, a titration series might be introduced in column 3 and the wells of column 4 would contain a concentration that results in 100 % inhibition (*see* **Note 12**).

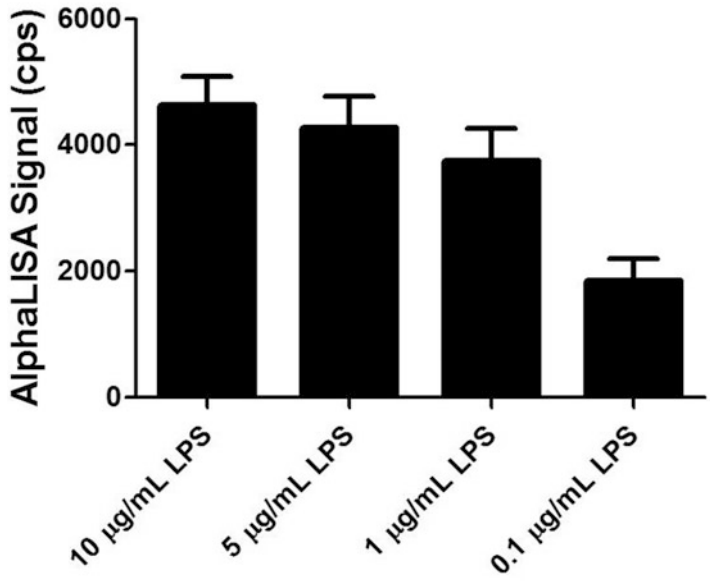

Fig. 13 A titration of stimulation reagent should be performed to establish an optimal assay concentration. This graph shows the AlphaLISA signal associated with IL-1β detection from 3000 THP-1 cells stimulated in 1536-well plates with different concentrations of lipopolysaccharide (LPS) and incubated for 16 h

Acknowledgement

This work was supported by the NCATS Division of Pre-Clinical Innovation Intramural Program.

References

1. Ullman EF, Kirakossian H, Singh S, Wu ZP, Irvin BR, Pease JS, Switchenko AC, Irvine JD, Dafforn A, Skold CN et al (1994) Luminescent oxygen channeling immunoassay: measurement of particle binding kinetics by chemiluminescence. Proc Natl Acad Sci U S A 91 (12):5426–5430
2. Peppard J, Glickman F, He Y, Hu SI, Doughty J, Goldberg R (2003) Development of a high-throughput screening assay for inhibitors of aggrecan cleavage using luminescent oxygen channeling (AlphaScreen). J Biomol Screen 8 (2):149–156. doi:10.1177/1087057103252308
3. Eglen RM, Reisine T, Roby P, Rouleau N, Illy C, Bosse R, Bielefeld M (2008) The use of AlphaScreen technology in HTS: current status. Curr Chem Genomics 1:2–10. doi:10.2174/1875397300801010002
4. Wan Y, Xhang X, Atherton JJ, Kostner K, Dimeski G, Punyadeera C (2015) A multimarker approach to diagnose and stratify heart failure. Int J Cardiol 181:369–375. doi:10.1016/j.ijcard.2014.12.052
5. Zhang X, Dimeski G, Punyadeera C (2014) Validation of an immunoassay to measure plasminogen-activator inhibitor-1 concentrations in human saliva. Biochem Medica 24 (2):258–265, 10.11613/BM.2014.028
6. Zhang X, Wan Y, Cooper-White J, Dimeski G, Atherton J, Punyadeera C (2013) Quantification of D-dimer levels in human saliva. Bioanalysis 5(18):2249–2256. doi:10.4155/bio.13.190
7. He A, Liu TC, Dong ZN, Ren ZQ, Hou JY, Li M, Wu YS (2013) A novel immunoassay for the quantization of CYFRA 21-1 in human serum.

J Clin Lab Anal 27(4):277–283. doi:10.1002/jcla.21597

8. Dynon K, Heng S, Puryer M, Li Y, Walton K, Endo Y, Nie G (2012) HtrA3 as an early marker for preeclampsia: specific monoclonal antibodies and sensitive high-throughput assays for serum screening. PLoS One 7(9): e45956. doi:10.1371/journal.pone.0045956
9. Marchand C, Lea WA, Jadhav A, Dexheimer TS, Austin CP, Inglese J, Pommier Y, Simeonov A (2009) Identification of phosphotyrosine mimetic inhibitors of human tyrosyl-DNA phosphodiesterase I by a novel AlphaScreen high-throughput assay. Mol Cancer Ther 8(1):240–248. doi:10.1158/1535-7163.MCT-08-0878
10. Dorjsuren D, Kim D, Maloney DJ, Wilson DM 3rd, Simeonov A (2011) Complementary non-radioactive assays for investigation of human flap endonuclease 1 activity. Nucleic Acids Res 39(2), e11. doi:10.1093/nar/gkq1082
11. Leister KP, Huang R, Goodwin BL, Chen A, Austin CP, Xia M (2011) Two high throughput screen assays for measurement of TNF-alpha in THP-1 cells. Curr Chem Genomics 5:21–29. doi:10.2174/1875397301105010021
12. Dehdashti SJ, Zheng W, Gever JR, Wilhelm R, Nguyen DT, Sittampalam G, McKew JC, Austin CP, Prusiner SB (2013) A high-throughput screening assay for determining cellular levels of total tau protein. Curr Alzheimer Res 10 (7):679–687
13. Liu F, Chen X, Allali-Hassani A, Quinn AM, Wigle TJ, Wasney GA, Dong A, Senisterra G, Chau I, Siarheyeva A, Norris JL, Kireev DB, Jadhav A, Herold JM, Janzen WP, Arrowsmith CH, Frye SV, Brown PJ, Simeonov A, Vedadi M, Jin J (2010) Protein lysine methyltransferase G9a inhibitors: design, synthesis, and structure activity relationships of 2,4-diamino-7-aminoalkoxy-quinazolines. J Med Chem 53 (15):5844–5857. doi:10.1021/jm100478y
14. Quinn AM, Allali-Hassani A, Vedadi M, Simeonov A (2010) A chemiluminescence-based method for identification of histone lysine methyltransferase inhibitors. Mol Biosyst 6(5):782–788. doi:10.1039/b921912a
15. Quinn AM, Bedford MT, Espejo A, Spannhoff A, Austin CP, Oppermann U, Simeonov A (2010) A homogeneous method for investigation of methylation-dependent protein-protein interactions in epigenetics. Nucleic Acids Res 38(2):e11. doi:10.1093/nar/gkp899
16. Yi F, Zhu P, Southall N, Inglese J, Austin CP, Zheng W, Regan L (2009) An AlphaScreen-based high-throughput screen to identify inhibitors of Hsp90-cochaperone interaction. J Biomol Screen 14(3):273–281. doi:10.1177/1087057108330114
17. Yi F, Regan L (2008) A novel class of small molecule inhibitors of Hsp90. ACS Chem Biol 3(10):645–654. doi:10.1021/cb800162x
18. Srinivasan P, Yasgar A, Luci DK, Beatty WL, Hu X, Andersen J, Narum DL, Moch JK, Sun H, Haynes JD, Maloney DJ, Jadhav A, Simeonov A, Miller LH (2013) Disrupting malaria parasite AMA1-RON2 interaction with a small molecule prevents erythrocyte invasion. Nat Commun 4:2261. doi:10.1038/ncomms3261
19. Cunningham L, Finckbeiner S, Hyde RK, Southall N, Marugan J, Yedavalli VR, Dehdashti SJ, Reinhold WC, Alemu L, Zhao L, Yeh JR, Sood R, Pommier Y, Austin CP, Jeang KT, Zheng W, Liu P (2012) Identification of benzodiazepine Ro5-3335 as an inhibitor of CBF leukemia through quantitative high throughput screen against RUNX1-CBFbeta interaction. Proc Natl Acad Sci U S A 109 (36):14592–14597. doi:10.1073/pnas.1200037109
20. Chen CZ, Sobczak K, Hoskins J, Southall N, Marugan JJ, Zheng W, Thornton CA, Austin CP (2012) Two high-throughput screening assays for aberrant RNA-protein interactions in myotonic dystrophy type 1. Anal Bioanal Chem 402(5):1889–1898. doi:10.1007/s00216-011-5604-0
21. Baell JB, Holloway GA (2010) New substructure filters for removal of pan assay interference compounds (PAINS) from screening libraries and for their exclusion in bioassays. J Med Chem 53(7):2719–2740. doi:10.1021/jm901137j
22. Brooks HB, Geeganage S, Kahl SD, Montrose C, Sittampalam S, Smith MC, Weidner JR (2004) Basics of enzymatic assays for HTS. In: Sittampalam GS, Gal-Edd N, Arkin M et al (eds) Assay Guidance Manual. Eli Lilly & Company and the National Center for Advancing Translational Sciences, Bethesda, MD
23. Newton P, Harrison P, Clulow S (2008) A novel method for determination of the affinity of protein: protein interactions in homogeneous assays. J Biomol Screen 13(7): 674–682. doi:10.1177/1087057108321086
24. Zhang JH, Chung TD, Oldenburg KR (1999) A simple statistical parameter for use in evaluation and validation of high throughput screening assays. J Biomol Screen 4(2):67–73

Chapter 6

Instrument Quality Control

Chatura Jayakody and Emily A. Hull-Ryde

Abstract

Well-defined quality control (QC) processes are used to determine whether a certain procedure or action conforms to a widely accepted standard and/or set of guidelines, and are important components of any laboratory quality assurance program (Popa-Burke et al., J Biomol Screen 14: 1017–1030, 2009). In this chapter, we describe QC procedures useful for monitoring the accuracy and precision of laboratory instrumentation, most notably automated liquid dispensers. Two techniques, gravimetric QC and photometric QC, are highlighted in this chapter. When used together, these simple techniques provide a robust process for evaluating liquid handler accuracy and precision, and critically underpin high-quality research programs.

Key words Quality control, Liquid-handling variability, Assay performance, High-throughput screening QC, Gravimetric quality control, Photometric quality control

1 Introduction

Quality control (QC) procedures for plate-based controls and calculation of Z' factors are now standard practice in high-throughput screening [1, 2]. However, Z' factors may not reveal small changes in assay component volumes resulting from systematic (e.g., positional) or calibration errors by liquid-handing dispensers that can significantly affect assay results [3]. Further, incorporating dose responses into the plate controls, while good practice, may still miss systematic dispense errors. Since liquid-handling capabilities form the core component of most high-throughput screening and lead discovery assays, routine monitoring and maintenance of these automated platforms are essential to ensure their accurate and precise functioning. In most cases, liquid handlers are used to repeatedly pipette millions of samples in the picoliter (pL) to microliter (μL) range. Thus, optimal functioning of these instruments directly impacts assay reproducibility and ultimately the success of drug discovery campaigns. Multiple groups have described QC procedures for various automated liquid handlers

William P. Janzen (ed.), *High Throughput Screening: Methods and Protocols*, Methods in Molecular Biology, vol. 1439,
DOI 10.1007/978-1-4939-3673-1_6,

[4–8]. The intent of this chapter is to detail two cost-effective and simple QC techniques that together can be used by both novices and experts to ensure accurate and precise automated liquid dispensing for a broad range of instrumentation.

The gravimetric QC technique utilizes the known weight of a volume of water (or any other liquid) to determine pipetting accuracy for an intended volume. Taking into account the density and specific weight of water (density of water at 21 °C = 0.99802 g/cm^3) and assuming that 1 μL of water is roughly equal to 1 milligram (mg), the performance of a liquid handler dispensing a certain volume of liquid can be determined by measuring the weight of the liquid [9]. Photometric QC techniques typically employ dyes and absorbance measurements to determine the precision of liquid handler dispensing. For the method detailed below, tartrazine (yellow food dye #5) is used to profile pipetting performance for multichannel dispensers such as 384 and 96 multichannel liquid handlers. This technique helps gauge precision on a channel-to-channel basis by analyzing absorbance on a well-to-well level. Together, these simple yet robust techniques not only ensure reproducibility, but can also serve as early warning indicators of deteriorating liquid handler performance.

2 Materials

Two different liquid handlers, a 384 multichannel workstation and an independent 8-tip liquid-handling workstation, have been highlighted to illustrate the use of these techniques. Data from both gravimetric and photometric techniques can be analyzed using a LIMS system or a spreadsheet.

2.1 Gravimetric Quality Control

Materials Required

1. Distilled or ultrapure water (18 MΩ cm).
2. Analytical balance in the milligram range.
3. Assay plate, well polypropylene microplate.
4. Lid for assay plate.

2.2 Photometric Quality Control

Materials Required

1. Tartrazine, yellow food color dye #5.
2. Dimethyl sulfoxide.
3. Tartrazine stock solution—a stock solution at a concentration of 2 mg/mL was prepared by dissolving 1 g of tartrazine in 500 mL of dimethyl sulfoxide.
4. Assay plate, 384-well clear polystyrene flat-bottom plate.
5. Absorbance plate reader.

3 Methods

3.1 Gravimetric Quality Control

Gravimetric quality control utilizes the relationship of volume to mass to determine pipetting accuracy by measuring the weight of the dispensed volume. A 384 multichannel dispenser was chosen to illustrate the principles of gravimetric quality control. With regard to multichannel dispensers, gravimetric QC measures the volume dispensed as a whole. For example, a 384 multichannel dispenser will pipette 1 μL of liquid into each well of a 384-well plate with a total final volume of 384 μL. Gravimetric QC will identify how close the total volume pipetted is equal to the mass of 384 μL (*see* **Notes 1** and **2**).

1. A 384 multichannel liquid dispenser.
2. A set of routinely used volumes that will be used for quality control should be determined. For example, the 384 multichannel liquid handler routinely dispenses 1, 5, 10, and 20 μL amounts. Therefore, these volumes (1, 5, 10, and 20 μL) were chosen for QC determination.
3. Start by taring a 384 multiwell plate with a lid using an analytical balance. Note the importance of the lid, as it is used to prevent evaporation at low volumes (1–5 μL) (*see* **Note 3**).
4. Use one of the predetermined volumes (e.g., 1 μL) and dispense a set volume (e.g., 1 μL) of distilled water into a 384-well plate. Place the lid on the plate immediately after dispensing and measure the new weight of the plate (*see* **Note 3**).
5. Record the weight of the plate and repeat the steps above for all the other QC volumes (5, 10, and 20 μL).
6. Compare the measured weight of each volume to the standard/expected weight using the Microsoft Excel®-based data analysis tool to determine whether the plate passed or failed QC (Fig. 1).
7. The tool (represented in Fig. 1) works by comparing the "Measured Weight" (column C) to a calculated standard weight ("Expected Weight," Column B). Given that the weight of 1 μL of water is roughly equal to 1 mg (density of water at 21 °C = 0.99802 g/cm^3), the weight of 1 μL of water dispensed 384 times should roughly be equal to 384 mg [9].
8. Enter the measured weight into the "Measured Weight" column for the corresponding volume in the Microsoft Excel®-based data analysis tool. The tool will then calculate the percent error (column D) and will return a result of "PASS" or "FAIL" for that particular QC volume.
9. The calculations necessary to create a similar spreadsheet depicted in Fig. 1 are shown in Fig. 2.

	A	B	C	D	E
1	**Gravimetric Quality Control Data Analysis**				
2	**96 Multichannel Dispense Head**				
3	**Volume (µL)**	**Expected Weight (mg)**	**Measured Weight (mg)**	**Percent Error (%)**	**Gravimetric QC PASS/FAIL**
4	10	960	900	6.25%	PASS
5	20	1920	1900	1.04%	PASS
6	40	3840	3800	1.04%	PASS
7	80	7680	7600	1.04%	PASS
8					
9					
10	**384 Multichannel Dispense Head**				
11	**Volume (µL)**	**Expected Weight (mg)**	**Measured Weight (mg)**	**Percent Error (%)**	**Gravimetric QC PASS/FAIL**
12	1	384	347	9.64%	PASS
13	2	768	730	4.95%	PASS
14	5	1920	1700	11.46%	FAIL
15	10	3840	3800	1.04%	PASS
16	20	7680	7600	1.04%	PASS

Fig. 1 Microsoft Excel-based gravimetric quality control (QC) data analysis tool. The spreadsheet includes QC for 96-well and 384-well liquid handlers. Highlighting the 1 µL QC for a 384-well liquid handler, the tool will give information pertaining to the "Calculated Weight" which is calculated based on the density of water at room temperature (density of water at 21 °C = 0.99802 g/cm^3) of the total volume pipetted. With respect to the 1 µL dispense volume, this would equal 384 milligrams (mg) since 384 µL was dispensed. The user will enter the "Measured Weight" which is the total weight measured using a balance. The "Percent Error" is then calculated automatically and based on this value a "PASS or FAIL" criteria will be assigned to that particular QC. The upper limit for passing QC is set at 10 % (≤10 %) and any value higher (>10 %) is considered a failed QC

Accuracy is reported as percent error (%) and can be calculated using the following equation:

$$\text{Percent Error} = \left(\frac{|\text{Expected Weight} - \text{Actual Weight}|}{\text{Expected Weight}}\right) \times 100$$

The spreadsheet depicted in Fig. 2 provides a data template for information about the QC quality and pass/fail criteria. The criteria for passing QC is a percent error equal to or less than 10 %, while the criteria for failing QC is a percent error greater than 10 %.

10. Gravimetric QC provides overall accuracy data for automated liquid dispensers and can serve as an early warning system to detect deteriorating liquid handler performance(*see* **Note 4**). However, there is no way to ascertain the dispensing precision of each channel in a multichannel liquid dispenser (*see* **Note 2**). This highlights the need for a secondary method which can

Gravimetric Quality Control Data Analysis

96 Multichannel Dispense Head

Volume (µL)	Expected Weight (mg)	Measured Weight (mg)	Percent Error (%)	Gravimetric QC PASS/FAIL
10	=A4*96	900	=(ABS(B4-C4))/((B4))	=IF(D4<=10%,"PASS","FAIL")
20	=A5*96	1900	=(ABS(B5-C5))/((B5))	=IF(D5<=10%,"PASS","FAIL")
40	=A6*96	3800	=(ABS(B6-C6))/((B6))	=IF(D6<=10%,"PASS","FAIL")
80	=A7*96	7600	=(ABS(B7-C7))/((B7))	=IF(D7<=10%,"PASS","FAIL")

384 Multichannel Dispense Head

Volume (µL)	Expected Weight (mg)	Measured Weight (mg)	Percent Error (%)	Gravimetric QC PASS/FAIL
1	=A12*384	347	=(ABS(B12-C12))/((B12))	=IF(D12<=10%,"PASS","FAIL")
2	=A13*384	730	=(ABS(B13-C13))/((B13))	=IF(D13<=10%,"PASS","FAIL")
5	=A14*384	1700	=(ABS(B14-C14))/((B14))	=IF(D14<=10%,"PASS","FAIL")
10	=A15*384	3800	=(ABS(B15-C15))/((B15))	=IF(D15<=10%,"PASS","FAIL")
20	=A16*384	7600	=(ABS(B16-C16))/((B16))	=IF(D16<=10%,"PASS","FAIL")

Fig. 2 Microsoft Excel®-based gravimetric quality control (QC) data analysis tool with calculations

identify well-to-well variation. Photometric QC provides a solution to this problem and offers a way to track well-to-well variation with coefficient of variation data.

3.2 Photometric Quality Control

While gravimetric QC utilizes mass to determine accuracy of the total amount of liquid dispensed, photometric QC determines pipetting precision for each channel by measuring individual well absorbance(*see* **Note 5**). Thus, photometric QC enables determination of well-to-well variability for a 384 multichannel dispense head and allows for the analysis of each channel individually (*see* **Notes** 6 and 7). Photometric analysis incorporates the use of a dye with convenient spectral and physiochemical properties for measurement. We use tartrazine (yellow food dye #5) which has an absorbance in the range 400–460 nm and a peak absorbance at 425 nm. In order to conduct photometric analysis, an absorbance assay needs to be optimized for the plate reader that is to be used to ensure that readings are in the linear range of the detector. This is achieved by first setting up a standard curve.

3.2.1 Tartrazine Standard Curve

1. The purpose of setting up a standard curve is to test the dynamic range of the plate reader in order to determine linear range and the saturation point of the detectors.
2. Table 1 is an example of a tartrazine standard curve. A standard stock solution of tartrazine at a concentration of 2 mg/mL was diluted twofold to yield a 10-point serially diluted curve. Next, choose an appropriate final volume for your standard curve; for the purpose of this experiment the final volume was set at 20 µL.

Table 1
Tartrazine standard curve mg/mL

Tartrazine concentration (mg/mL)
2.0
1.0
0.5
0.25
0.13
0.063
0.031
0.0156
0.0078
0.0039

The curve starts at a concentration of 2 mg/mL and a twofold serial dilution is performed nine times to yield a 10-point serially diluted curve. Dimethyl sulfoxide was used to prepare the 2 mg/mL tartrazine stock solution as well as the diluent for the serial dilution. All samples were carefully diluted by hand using a multichannel pipette (16 channels). Each curve was replicated three times. The serial dilution was performed in a clear 384-well polystyrene plate

The appropriate way to select a final volume is to base it on the liquid handling capacity of the instruments undergoing QC. Dimethyl sulfoxide was the primary vehicle transferred by the liquid handlers; therefore it was used to prepare the 2 mg/mL tartrazine stock solution as well as the diluent for the serial dilutions. Choose a liquid that best fits your applications (e.g., DMSO, aqueous buffer).

3. Perform the standard curve in a clear, flat-bottomed 384-well polystyrene plate suitable for reading absorbance. Use this plate for all subsequent QC applications with all liquid handlers.
4. Measure absorbance using a plate reader. Absorbance for this standard curve was measured at 405 nm.
5. Plot the graph (Fig. 4) to identify the linear range of the curve which in this case was determined to be between the concentrations of 0.015625 and 0.25 mg/mL. Choose a concentration within the linear part of the curve for photometric QC. Based on Figs. 3 and 4 a final concentration of 0.1 mg/mL was chosen as the optimal final concentration for testing.
6. The 0.1 mg/mL concentration of tartrazine was chosen as the final concentration. For example, if testing a 1 μL dispense with a 20 μL final volume, 1 μL of tartrazine at 2 mg/mL is

[Tartrazine] mg/mL	2	1	0.5	0.25	0.125	0.0625	0.03125	0.015625	0.007813	0.003906
Replicate 1	2.167	2.176	2.167	1.755	0.971	0.512	0.311	0.185	0.118	0.076
Replicate 2	2.164	2.186	2.175	1.791	1.004	0.553	0.329	0.196	0.127	0.086
Replicate 3	2.171	2.174	2.166	1.752	1.051	0.531	0.314	0.183	0.107	0.074

Fig. 3 Absorbance data obtained using an absorbance-based plate reader for three replicates of the tartrazine standard curve. Absorbance was measured at 405 nm. The standard curve was prepared by serially diluting a 2 mg/mL tartrazine stock dissolved in 100 % dimethyl sulfoxide nine times to yield a 10-point standard curve

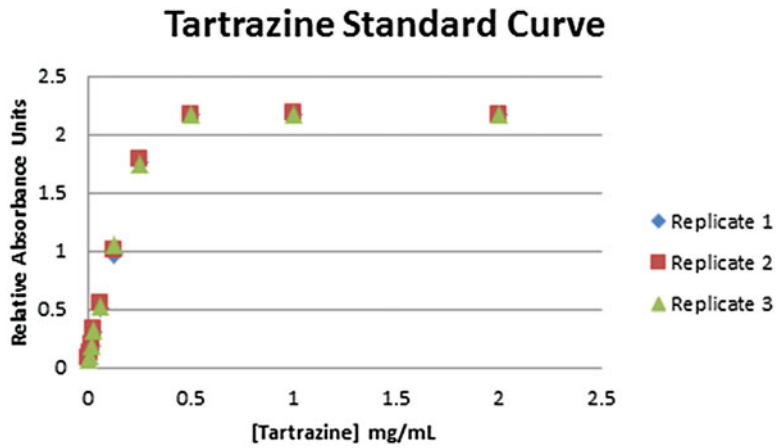

Fig. 4 Tartrazine standard curve illustrated graphically. Based on the graph, the linear range is determined to be in between 0.015625 and 0.25 mg/mL. The tartrazine concentration chosen for quality control was 0.1 mg/mL

transferred into a plate containing 19 µL of diluent. This will yield a final concentration of 0.1 mg/mL.

7. It is important to note that different plate readers have varying dynamic ranges and saturation points. Thus, alterations need to be made to the standard curve highlighted above to best suit the plate reader being utilized. Once optimized, use the same plate reader for all quality control applications.

3.2.2 Photometric QC Setup

Two liquid handlers are outlined in this section to illustrate the versatility of photometric QC analysis. A 384 multichannel liquid handler and a liquid-handling arm with eight independently operating tips were chosen as examples.

3.2.3 Photometric Quality Control of a 384 Multichannel Liquid Handler

1. Determine the operating range of the 384 multichannel liquid handler. This is the same liquid handler detailed in the gravimetric QC section and is constantly used in the 1–20 µL volume range. Thus the same volumes are tested for accuracy (1, 5, 10, and 20 µL). The final total volume for each well was

Table 2
384 multichannel liquid handler QC protocol, detailing the stock concentration (mg/mL) and diluent volume (μL) required in ascertaining pipetting accuracy at 1, 5, 10, and 20 μL

384 Multichannel liquid handler QC				
Starting tartrazine concentration (mg/mL)	**Final tartrazine concentration (mg/mL)**	**Volume diluent (μL)**	**Volume of diluent (μL)**	**Final volume (μL)**
2.0	0.1	1	19	20
1.0	0.1	2	18	20
0.4	0.1	5	15	20
0.2	0.1	10	10	20

Dimethyl sulfoxide was used to prepare all the tartrazine stock solutions and was also used as the diluent

set at 20 μL and the 384 multichannel liquid handler was used to transfer the tartrazine and the diluent.

2. As the final concentration for tartrazine absorbance testing was chosen as 0.1 mg/mL, four stock concentrations of tartrazine were prepared for each volume tested. Table 2 represents the stock solutions prepared for the 384 multichannel liquid handler QC.
3. The 384 multichannel liquid handler used for this QC is mainly used to transfer compounds dissolved in dimethyl sulfoxide. Thus, dimethyl sulfoxide was used to prepare all the tartrazine stocks and was also used as the diluent.
4. Use the liquid handler to transfer the tartrazine stock (1, 5, 10, and 20 μL) and the diluent (19, 15, and 10 μL). Using the same liquid handler to perform both transfers (tartrazine and diluent) helps avoid introducing bias related to a second liquid handler. If a second liquid handler is used to transfer the diluent, operational biases of that particular dispenser would have to be taken into consideration as well.
5. The 1 μL QC is used as an example to detail the technique and analyze data of photometric QC. Transfer 1 μL of the 2.0 mg/mL tartrazine stock to a 384-well clear polystyrene plate followed by 19 μL of dimethyl sulfoxide diluent to the same plate. This dilutes the 1 μL of 2.0 mg/mL tartrazine stock to 0.1 mg/mL which is well within the linear range of the plate reader.
6. Centrifuge the QC plate at a suitable speed (250 × *g*) and use a plate reader to measure absorbance (405 nm).

```
----- LOCAL PlateQC Run "NewRun" -----

Sat Aug 22 13:52:26 2015

----- PlateType = 384-well, Number Plates = 1 -----

Summary Statistics by Plate

    RESPONSE.1 = RawData

, , RESPONSE.1

   Mean     SD  CV  Max   Min UpperAdj UpperQuar Median LowerQuar LowerAdj UpperConf LowerConf NumOutliers
1 0.833 0.0408 4.9 0.98 0.753    0.891     0.841  0.823     0.806    0.755     0.826      0.82          42
```

Fig. 5 Screenable™ data output for a 1 μL QC of a 384 multichannel liquid handler. 1 μL of tartrazine stock dissolved in dimethyl sulfoxide at 2 mg/mL was diluted with 19 μL of dimethyl sulfoxide using the liquid handler to yield a final concentration of 0.1 mg/mL. The data indicates the mean, standard deviation (SD), coefficient of variation (CV), maximum read, minimum read, and the number of outliers. QC standards are set at a CV of 10 (pass $\leq$ 10, fail $>$ 10) and given that the CV in this instance is 4.9, the 1 μL dispense is considered successful

7. Determine the mean, standard deviation, coefficient of variation, maximum value, minimum value, and the number of outliers (*see* **Notes 8** and **9**).
8. Figures 5, 6, 7, and 8 illustrate a comparison of data analysis using the *Screen*Able™ LIMS system (Figs. 5 and 6) and the Microsoft Excel®-based data analysis system (Figs. 7 and 8).
9. Figures 7 and 8 illustrate the Excel®-based data analysis tool including all calculations so it can be used as a template. The tool allows for identifying outliers and also provides the mean, standard deviation, minimum read, maximum read, and the coefficient of variation for 384 multichannel liquid handlers. The equations detailed in Fig. 8 can be reconfigured to QC any type of liquid handler (96 well, 16 channel, 8 channel, etc.).
10. The pass/fail determination is based on the % coefficient of variation (CV): any QC run with a CV equal to or less than 10 % is considered successful (PASS) and any run with a CV greater than 10 % is considered unsuccessful (FAIL):

$$\text{Coefficient of Variance} = \frac{\text{Standard Deviation}}{\text{Average}} \times 100$$

3.2.3.1 Quality Control of Liquid Handler with Eight Independently Operating Tips

1. The same methodology and data analysis can be used to QC other liquid handlers. The following example represents a liquid handler with eight independently operating liquid-detecting tips. QC for the liquid handler is determined at 7, 14, 21, and 30 μL. The data analysis is conducted using Microsoft Excel® with the same principles highlighted in the previous section.

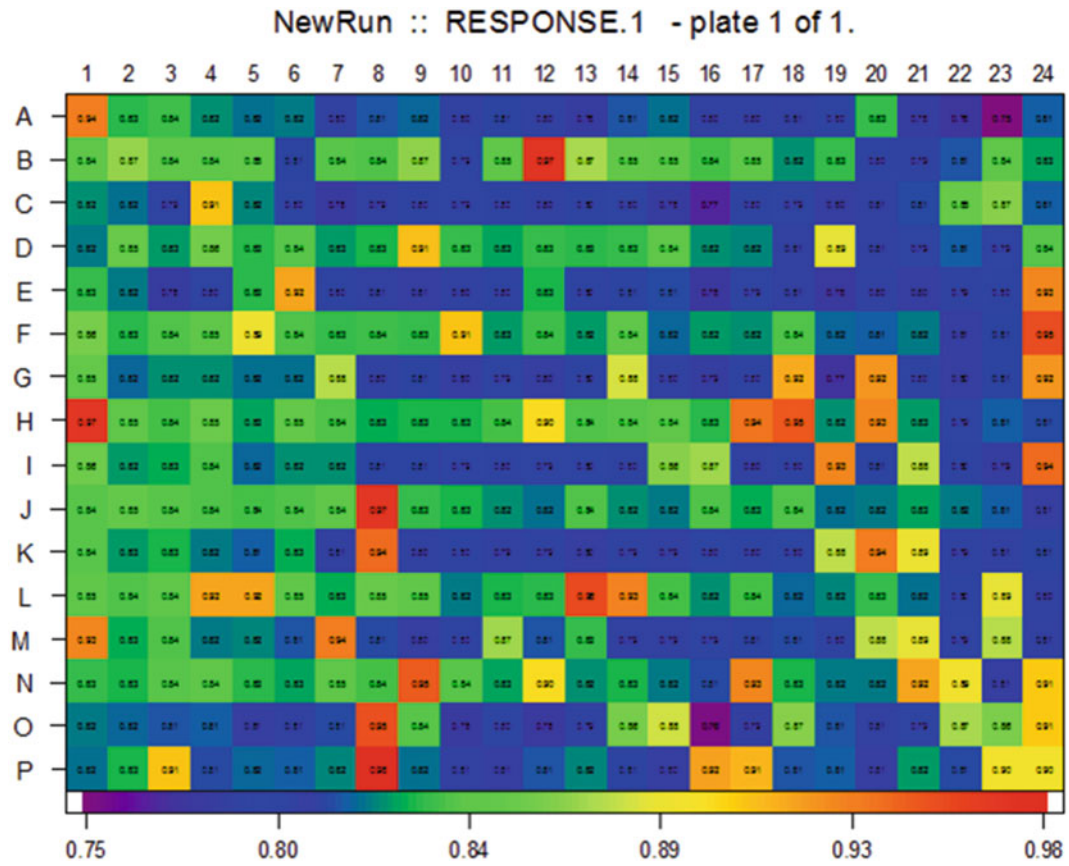

Fig. 6 Plate image of 1 μL QC detailing the 42 outliers. This image helps determine which channels are performing optimally. Repeated QCs will help identify frequent bad actors which could point to specific channel failure

2. A 384-well clear, flat-bottom polystyrene plate is used and each volume is added to six columns on the same plate. Columns 1–6 contain 7 μL of tartrazine (with 23 μL of diluent), 7–12 contain 14 μL of tartrazine (with 16 μL diluent), 13–18 contain 21 μL of tartrazine (with 9 μL diluent), and 19–24 contain 30 μL of tartrazine. Dimethyl sulfoxide is used to prepare all tartrazine stocks and is also used as the diluent. The final concentration of the tartrazine in 30 μL was 0.1 mg/mL in keeping with the plate reader dynamic range as explained in previous sections.
3. Table 3 represents the starting tartrazine stock concentration and the dilutions performed to get to a final concentration of 0.1 mg/mL. The same liquid handler is used for both the tartrazine stock and diluent addition.
4. The calculations for % CV and those to determine outliers are similar to those highlighted in the previous section.

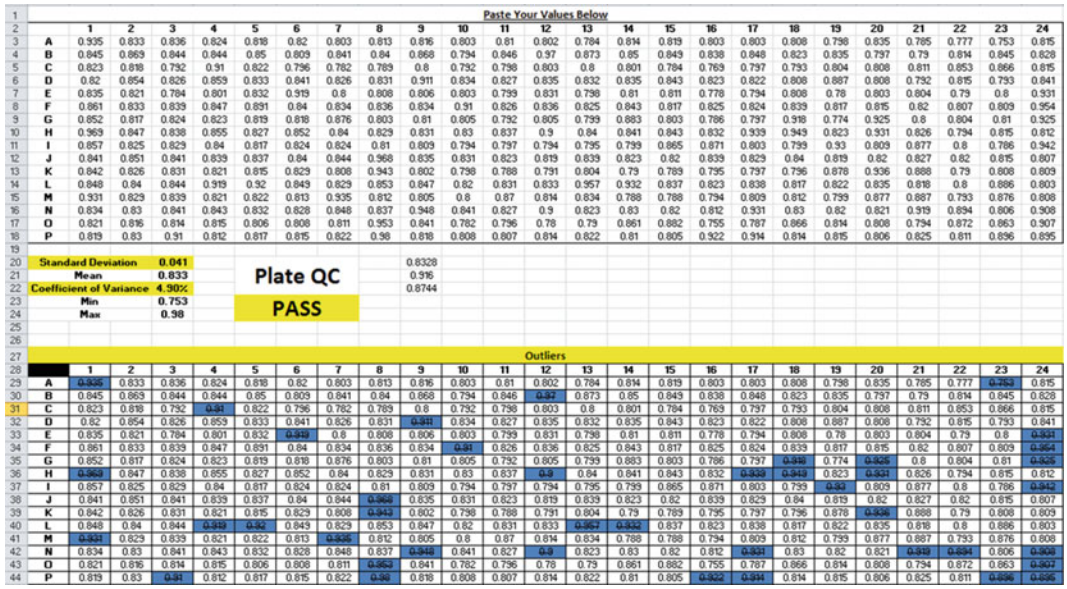

Fig. 7 Microsoft Excel®-based data analysis tool. Data from the plate reader is added in the section below (paste your values) and the standard deviation, mean, coefficient of variation, minimum read (Min), and maximum read (Max) are automatically calculated. Additionally the tool displays pass/fail criteria based on a 10 % limit for coefficient of variation where values equal to or less than 10 % will "PASS" QC and values more than 10 % will "FAIL" QC. The tool also displays all outliers, which in this case is 4

Figures 9 and 10 give an overview of the calculations used to determine the % CV and outliers for the 7 μL transfer. These calculations are similar for the 14, 21, and 30 μL volumes with a change in the sourced cells.

4 Notes

1. Gravimetric QC is based on the relationship of liquid volume and weight. It assumes that 1 μL of water weighs roughly 1 mg [9]. With this knowledge in hand, a 384 multichannel dispenser would pipette 1 μL of water from each of its 384 channels dispensing a total of 384 μL which should approximate 384 mg. When QC is conducted the goal is to see a measured value of 384 mg.
2. One major drawback for gravimetric QC is that it does not detect channel-to-channel variation with respect to multichannel dispensers. For example, when pipetting a certain volume (1 μL) using a 384 multichannel dispenser, one may encounter a situation where a channel is blocked but a different channel over-pipettes (2 μL) compensating for the blocked channel. So when the final weight is measured, it may be very close to the

a

Paste Your Values Below

	1	2	3	4	5	6	7	8	9	10	11	12	13	14	15	16	17	18	19	20	21	22	23	24
A	0.935	0.833	0.836	0.824	0.818	0.82	0.803	0.813	0.816	0.803	0.81	0.802	0.784	0.814	0.819	0.803	0.803	0.808	0.798	0.835	0.785	0.777	0.753	0.815
B	0.845	0.869	0.844	0.844	0.85	0.809	0.841	0.84	0.868	0.794	0.846	0.97	0.873	0.85	0.849	0.838	0.848	0.823	0.835	0.797	0.79	0.814	0.845	0.828
C	0.823	0.818	0.792	0.91	0.822	0.796	0.782	0.789	0.8	0.792	0.798	0.803	0.8	0.801	0.784	0.769	0.797	0.793	0.804	0.808	0.811	0.853	0.866	0.815
D	0.82	0.854	0.826	0.859	0.833	0.841	0.826	0.831	0.911	0.834	0.827	0.835	0.832	0.835	0.843	0.823	0.822	0.808	0.887	0.808	0.792	0.815	0.793	0.841
E	0.835	0.821	0.784	0.801	0.832	0.919	0.8	0.808	0.806	0.803	0.799	0.831	0.798	0.81	0.811	0.778	0.794	0.808	0.78	0.803	0.804	0.79	0.8	0.931
F	0.861	0.833	0.839	0.847	0.891	0.84	0.834	0.836	0.834	0.91	0.826	0.836	0.825	0.843	0.817	0.825	0.824	0.839	0.817	0.815	0.82	0.807	0.809	0.954
G	0.852	0.817	0.824	0.823	0.819	0.818	0.876	0.803	0.81	0.805	0.792	0.805	0.799	0.883	0.803	0.786	0.797	0.918	0.774	0.925	0.8	0.804	0.81	0.925
H	0.969	0.847	0.838	0.855	0.827	0.852	0.84	0.829	0.831	0.83	0.837	0.9	0.84	0.841	0.843	0.832	0.939	0.949	0.823	0.931	0.826	0.794	0.815	0.812
I	0.857	0.825	0.829	0.84	0.817	0.824	0.824	0.81	0.809	0.794	0.797	0.794	0.795	0.799	0.865	0.871	0.803	0.799	0.93	0.809	0.877	0.8	0.786	0.942
J	0.841	0.851	0.841	0.839	0.837	0.84	0.844	0.968	0.835	0.831	0.823	0.819	0.839	0.823	0.82	0.839	0.829	0.84	0.819	0.82	0.827	0.82	0.815	0.807
K	0.842	0.826	0.831	0.821	0.815	0.829	0.808	0.943	0.802	0.798	0.788	0.791	0.804	0.79	0.789	0.795	0.797	0.796	0.878	0.936	0.888	0.79	0.808	0.809
L	0.848	0.84	0.844	0.919	0.92	0.849	0.829	0.853	0.847	0.82	0.831	0.833	0.957	0.932	0.837	0.823	0.838	0.817	0.822	0.835	0.818	0.8	0.886	0.803
M	0.931	0.829	0.839	0.821	0.822	0.813	0.935	0.812	0.805	0.8	0.87	0.814	0.834	0.788	0.788	0.794	0.809	0.812	0.799	0.877	0.887	0.793	0.876	0.808
N	0.834	0.83	0.841	0.843	0.832	0.828	0.848	0.837	0.948	0.841	0.827	0.9	0.823	0.83	0.82	0.812	0.931	0.83	0.82	0.821	0.919	0.894	0.806	0.908
O	0.821	0.816	0.814	0.815	0.806	0.808	0.811	0.953	0.841	0.782	0.796	0.78	0.79	0.861	0.882	0.755	0.787	0.866	0.814	0.808	0.794	0.872	0.863	0.907
P	0.819	0.83	0.91	0.812	0.817	0.815	0.822	0.98	0.818	0.808	0.807	0.814	0.822	0.81	0.805	0.922	0.914	0.814	0.815	0.806	0.825	0.811	0.896	0.895

Standard Deviation	=STDEV(B3:Y18)
Mean	=AVERAGE(B3:Y18)
Coefficient of Variance	=(E20/E21)
Min	=MIN(B3:Y18)
Max	=MAX(B3:Y18)

Plate QC

=IF(E22<=10%,"PASS","FAIL")

Outliers	
Quartile 1	=QUARTILE(B29:Y44,1)
Quartile 3	=QUARTILE(B29:Y44,3)
Interquartile Range (IQR)	=V22-V21
Upper Fence	=V22+(V23*1.5)
Lower Fence	=V21-(V23*1.5)

Outliers

	1	2	3	4	5	6	7	8	9	10	11	12	13	14	15	16	17	18	19	20	21	22	23	24
A	=B3	=C3	=D3	=E3	=F3	=G3	=H3	=I3	=J3	=K3	=L3	=M3	=N3	=O3	=P3	=Q3	=R3	=S3	=T3	=U3	=V3	=W3	=X3	=Y3
B	=B4	=C4	=D4	=E4	=F4	=G4	=H4	=I4	=J4	=K4	=L4	=M4	=N4	=O4	=P4	=Q4	=R4	=S4	=T4	=U4	=V4	=W4	=X4	=Y4
C	=B5	=C5	=D5	=E5	=F5	=G5	=H5	=I5	=J5	=K5	=L5	=M5	=N5	=O5	=P5	=Q5	=R5	=S5	=T5	=U5	=V5	=W5	=X5	=Y5
D	=B6	=C6	=D6	=E6	=F6	=G6	=H6	=I6	=J6	=K6	=L6	=M6	=N6	=O6	=P6	=Q6	=R6	=S6	=T6	=U6	=V6	=W6	=X6	=Y6
E	=B7	=C7	=D7	=E7	=F7	=G7	=H7	=I7	=J7	=K7	=L7	=M7	=N7	=O7	=P7	=Q7	=R7	=S7	=T7	=U7	=V7	=W7	=X7	=Y7
F	=B8	=C8	=D8	=E8	=F8	=G8	=H8	=I8	=J8	=K8	=L8	=M8	=N8	=O8	=P8	=Q8	=R8	=S8	=T8	=U8	=V8	=W8	=X8	=Y8
G	=B9	=C9	=D9	=E9	=F9	=G9	=H9	=I9	=J9	=K9	=L9	=M9	=N9	=O9	=P9	=Q9	=R9	=S9	=T9	=U9	=V9	=W9	=X9	=Y9
H	=B10	=C10	=D10	=E10	=F10	=G10	=H10	=I10	=J10	=K10	=L10	=M10	=N10	=O10	=P10	=Q10	=R10	=S10	=T10	=U10	=V10	=W10	=X10	=Y10
I	=B11	=C11	=D11	=E11	=F11	=G11	=H11	=I11	=J11	=K11	=L11	=M11	=N11	=O11	=P11	=Q11	=R11	=S11	=T11	=U11	=V11	=W11	=X11	=Y11
J	=B12	=C12	=D12	=E12	=F12	=G12	=H12	=I12	=J12	=K12	=L12	=M12	=N12	=O12	=P12	=Q12	=R12	=S12	=T12	=U12	=V12	=W12	=X12	=Y12
K	=B13	=C13	=D13	=E13	=F13	=G13	=H13	=I13	=J13	=K13	=L13	=M13	=N13	=O13	=P13	=Q13	=R13	=S13	=T13	=U13	=V13	=W13	=X13	=Y13
L	=B14	=C14	=D14	=E14	=F14	=G14	=H14	=I14	=J14	=K14	=L14	=M14	=N14	=O14	=P14	=Q14	=R14	=S14	=T14	=U14	=V14	=W14	=X14	=Y14
M	=B15	=C15	=D15	=E15	=F15	=G15	=H15	=I15	=J15	=K15	=L15	=M15	=N15	=O15	=P15	=Q15	=R15	=S15	=T15	=U15	=V15	=W15	=X15	=Y15
N	=B16	=C16	=D16	=E16	=F16	=G16	=H16	=I16	=J16	=K16	=L16	=M16	=N16	=O16	=P16	=Q16	=R16	=S16	=T16	=U16	=V16	=W16	=X16	=Y16
O	=B17	=C17	=D17	=E17	=F17	=G17	=H17	=I17	=J17	=K17	=L17	=M17	=N17	=O17	=P17	=Q17	=R17	=S17	=T17	=U17	=V17	=W17	=X17	=Y17
P	=B18	=C18	=D18	=E18	=F18	=G18	=H18	=I18	=J18	=K18	=L18	=M18	=N18	=O18	=P18	=Q18	=R18	=S18	=T18	=U18	=V18	=W18	=X18	=Y18

b

Outliers	
Quartile 1	=QUARTILE(B29:Y44,1)
Quartile 3	=QUARTILE(B29:Y44,3)
Interquartile Range (IQR)	=V22-V21
Upper Fence	=V22+(V23*1.5)
Lower Fence	=V21-(V23*1.5)

Fig. 8 (**a**) Equations for standard deviation, mean, coefficient of variation, minimum read, maximum read, pass/fail criteria, and outliers. (**b**) Outlier calculation incorporating the Quartile 1 and 3 was used to calculate the upper and lower fence in order to determine the outliers. The *upper* and *lower* fences were calculated by multiplying the IQR by 1.5

"desired" weight while the blocked and over-pipetting channels are not identified.

3. When pipetting low volumes such as 1–5 μL, place a lid on the plate as soon as the liquid transfer is complete. At low volumes, liquid continues to evaporate rapidly even with a lid, so it is also imperative that the plate be measured right after dispensing the liquid. The weight measured can also vary on the balance due to evaporation of the liquid during the weighing process and this highlights the need to measure the weight immediately.

Table 3
Starting tartrazine concentration (mg/mL), final tartrazine concentration (mg/mL), testing and diluent volumes (μL) for QC

Independent eight-tip liquid handler quality control				
Starting tartrazine concentration (mg/mL)	**Final tartrazine concentration (mg/mL)**	**Volume tested (μL)**	**Volume diluent (μL)**	**Final volume (μL)**
0.43	0.1	7	23	30
0.21	0.1	14	16	30
0.14	0.1	21	9	30
0.10	0.1	30	0	30

Dimethyl sulfoxide is used to prepare all tartrazine stocks and it is also used as the diluent. The table provides a rubric for liquid dispensing; for example the liquid handler will dispense 7 μL of tartrazine stock at 0.43 mg/mL and dilute it with 23 μL of dimethyl sulfoxide to yield a final volume of 30 μL at a 0.1 mg/mL tartrazine concentration. This final concentration is mimicked by all three other QC volumes and is within the dynamic range of the plate reader used

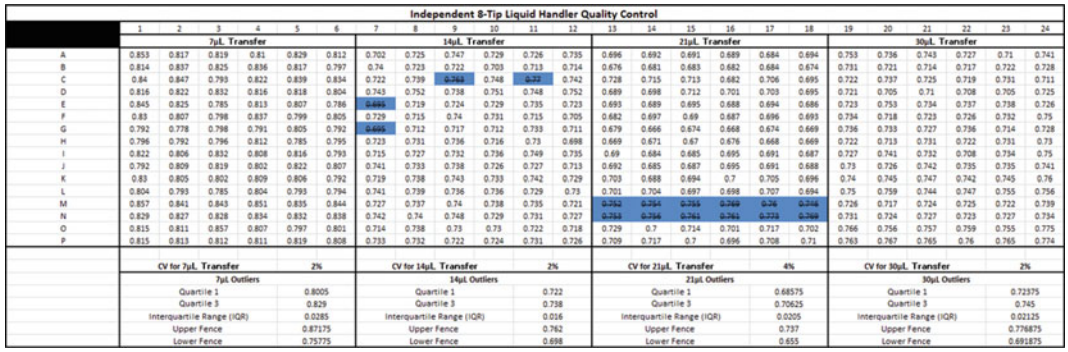

Fig. 9 QC conducted using a liquid handler with eight independent liquid detecting tips. The figure represents QC conducted with 7, 14, 21, and 30 μL which are the most commonly used volumes. All solutions were prepared and diluted using dimethyl sulfoxide. The data displays the coefficient of variation (CV) and outliers (highlighted in blue) for each QC'd volume. Coefficient of variation (CV) is used to determine pass/fail criteria where a CV equal to or less than 10 % will "PASS" QC and a CV greater than 10 % will "FAIL" QC

CV for 7μL Transfer	=((STDEV(C24:H39))/(AVERAGE(C24:H39)))
7μL Outliers	
Quartile 1	=QUARTILE(C24:H39,1)
Quartile 3	=QUARTILE(C24:H39,3)
Interquartile Range (IQR)	=G44-G43
Upper Fence	=G44+(G45*1.5)
Lower Fence	=G43-(G45*1.5)

Fig. 10 Calculations for CV and outliers for the 7 μL transfer. The calculations are similar for all QC'd volumes (14, 21, and 30 μL), with a change in the sourced cells

4. Gravimetric QC could be used with any type of liquid handler and any type of liquid can be used as long as its specific weight can be calculated easily.
5. Photometric QC requires the use of a dye and while tartrazine was used in this instance, any solution with a fluorescence or absorbance can be used. Having a suitable reader with a wide dynamic range for the dye chosen is critical for robust and reliable photometric QC.
6. Photometric QC is primarily used to determine channel-to-channel pipetting precision. It is also useful for profiling pipetting trends and performance throughout all 384 channels. More importantly, photometric QC can pinpoint pipetting inaccuracies that fail to be identified through gravimetric QC. Consider a 1 μL dispense where the channel is completely blocked and pipettes nothing (0 μL) and another channel over-pipettes (2 μL). The net result would not be identified by gravimetric QC, but absorbance readings from photometric QC will correctly identify this discrepancy.
7. Photometric QC can also be used to gauge the accuracy of the volume pipetted with the aid of a standard curve. A final tartrazine concentration chosen within the linear range of the standard curve (0.1 mg/mL) can be used for this purpose by tracking its signal strength or relative absorbance units (RAU). By example, if 0.1 mg/mL tartrazine routinely gives a signal of 0.8 RAU, you can use this knowledge to pipette 1 μL of tartrazine stock and dilute it to 0.1 mg/mL and measure absorbance. The absorbance signal should be in the range of 0.8 RAU. Any abnormal values (e.g., 1.2 RAU) would suggest an error in pipetting. It is important to note that RAU values will vary due to plate reader bias and other external factors (*see* **Note 10**).
8. It is also recommended to track well-to-well variation over multiple runs. If a certain well is a constant outlier over multiple runs, it could point to the degradation of that particular pipetting channel.
9. We use *Screen*Able™, developed by Screenable Solutions, but a Microsoft Excel®-based data analysis tool that incorporates the same logic can also be used. The logic for this calculation is provided in Figs. 5, 6, 7, 8, 9, and 10.
10. Both gravimetric QC and photometric QC while robust are not always foolproof. There will be instances where QC fails in part due to procedural complications unrelated to instrument performance. One example would be the presence of bubbles in the troughs containing diluents and tartrazine stocks. Air bubbles can act as barriers and impede aspiration, resulting in pipetting errors. This scenario does not necessarily indicate

instrument malfunction. For this reason it is always good to practice caution while conducting QC and if the need arises repeat the QC to avoid unintended assumptions.

Acknowledgements

We would like to thank Catherine Simpson and Alice Cheng for technical support; and Drs. Kenneth Pearce and Stephen Frye, and William Janzen for manuscript advice.

References

1. Zhang J-H, Chung TDY, Oldenburg KR (1999) A simple statistical parameter for use in evaluation and validation of high throughput screening assays. J Biomol Screen 4:67–73
2. Sittampalam GS, Coussens NP, Nelson H et al (2004) Assay guidance manual. Eli Lilly & Company and the National Center for Advancing Translational Sciences, Bethesda, MD
3. Hentz NG, Knaide TR (2014) Effect of liquid-handling accuracy on assay performance. J Lab Autom 19:153–162
4. Popa-Burke I, Lupotsk B, Boyer J, Gannon W, Hughes R, Kadwill P, Lylerly D, Nichols J, Nixon E, Rimmer D, Saiz-Nicolas I, Sanfiz-Pinto B, Holland S (2009) Establishing quality assurance criteria for serial dilution operations on liquid-handling equipment. J Biomol Screen 14:1017–1030
5. Taylor BP, Ashman S, Baddeley SM, Bartram SL, Battle CD, Bond BC, Clements YM, Gaul NJ, McAllister WE, Mostacero JA, Ramon F, Wilson JM, Hertzberg RP, Pope AJ, Macarron R (2002) A standard operating procedure for assessing liquid handler performance in high-throughput screening. J Biomol Screen 7:554–569
6. Astle TW, Akowitz A (1996) Accuracy and tip carryover contamination in 96-well pipetting. J Biomol Screen 1:212–216
7. Ouyang Z, Federer S, Porter G, Kaufmann C, Jemal M (2008) Strategies to maintain sample integrity using a liquid-filled automated liquid-handing system with fixed pipetting tips. J Lab Autom 13:24–32
8. Quintero C, Tran K, Szewczak AA (2013) High-throughput quality control of DMSO acoustic dispensing using photometric dye methods. J Lab Autom 18:296–305
9. Water - Density and Specific Weight. In: The Engineering ToolBox. Available via www.EngineeringToolBox.com. http://www.engineeringtoolbox.com/water-density-specific-weight-d_595.html. Accessed 4 June 2015

Chapter 7

Application of Fluorescence Polarization in HTS Assays

Xinyi Huang and Ann Aulabaugh

Abstract

Steady-state measurements of fluorescence polarization have been widely adopted in the field of high-throughput screening for the study of biomolecular interactions. This chapter reviews the basic theory of fluorescence polarization, the underlying principle for using fluorescence polarization to study interactions between small-molecule fluorophores and macromolecular targets, and representative applications of fluorescence polarization in high-throughput screening.

Key words FP, Polarization, Anisotropy, Competition binding, High-throughput screening

1 Introduction

Fluorescence polarization (FP) is a powerful fluorescence-based technique for the study of biomolecular interactions in aqueous solution. For a small-molecule fluorophore or a small molecule labeled with a fluorescent moiety, the interaction with a macromolecule can be monitored through the increase in FP that occurs with the change in fluorophore mobility upon complex formation. Perrin first described the quantitative relationship of the observed polarization with molecular size and solution viscosity in 1926 [1], and Weber subsequently applied FP to biological systems (for a review, *see* [2]). FP has since been applied to a wide range of interactions including DNA-DNA interactions, DNA-protein interactions, protein-protein interactions, and small molecule-protein interactions [3–7]. Migration of high-throughtput screening (HTS) in the biopharmaceutical industry to fluorescence and luminescence formats and development of commercial microplate FP instruments in the mid 1990s have resulted in the explosive growth of FP applications in HTS over the last decade.

William P. Janzen (ed.), *High Throughput Screening: Methods and Protocols*, Methods in Molecular Biology, vol. 1439,
DOI 10.1007/978-1-4939-3673-1_7,

1.1 Fluorescence Polarization Basic Theory

Fluorescence polarization, or anisotropy, is a property of fluorescent molecules that can be measured using an FP instrument. A polarized light is utilized to excite a fluorescent sample and the emission light intensities of the channels that are parallel (I_S) and perpendicular (I_P) to the electric vector of polarized excitation light are collected. The difference, $I_S - I_P$, can be normalized by the total fluorescence intensity of the emission beam, $I_S + I_P$ (polarization), or by the total fluorescence emission intensity from the sample, $I_S + 2I_P$ (anisotropy). Polarization (P) is then defined as $(I_S - I_P)/(I_S + I_P)$ and anisotropy (A) is defined as $(I_S - I_P)/(I_S + 2I_P)$. Both polarization (P) and anisotropy (A) terms have been widely used. Polarization and anisotropy can be interconverted by the following equation $A = 2P/(3 - P)$. Anisotropy is preferred for analyzing complex systems because the equations are considerably simpler when expressed in this term [8]. Since polarization (P) is nearly linearly correlated with anisotropy (A) because of a limiting anisotropy value of 0.4 (vide infra; Fig. 1), applications expressed in polarization are still valid in practical terms.

In order to more fully comprehend FP, one needs to start with the absorption of excitation light by a fluorophore. When a fluorescent sample is illuminated by polarized light, those molecules with their absorption transition dipole aligned parallel to the electric vector of the polarized excitation have the highest probability of absorption, resulting polarized emission light that is also parallel to the polarized excitation. Had all molecules in this sample been fully aligned parallel to excitation, the sample would have had anisotropy of 1. In reality, fluorescent molecules in solution are completely randomized relative to excitation. The probability of absorption is proportionally dependent on the angle between the fluorophore absorption dipole and the polarized excitation. This photo-selection process results in polarized emission with a theoretical maximum

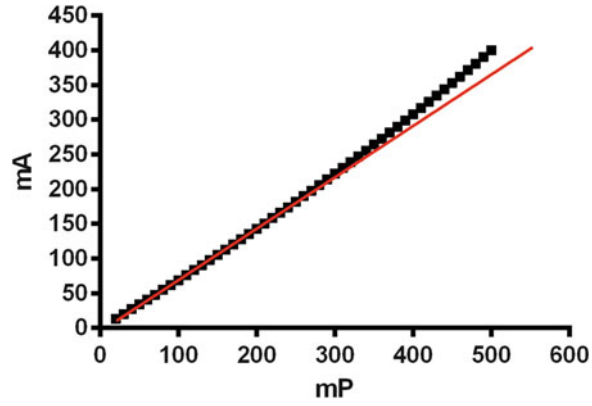

Fig. 1 The relationship between polarization and anisotropy. The data are generated by the following equation $A = 2P/(3 - P)$. The *red line* depicts theoretic perfect linear correlation

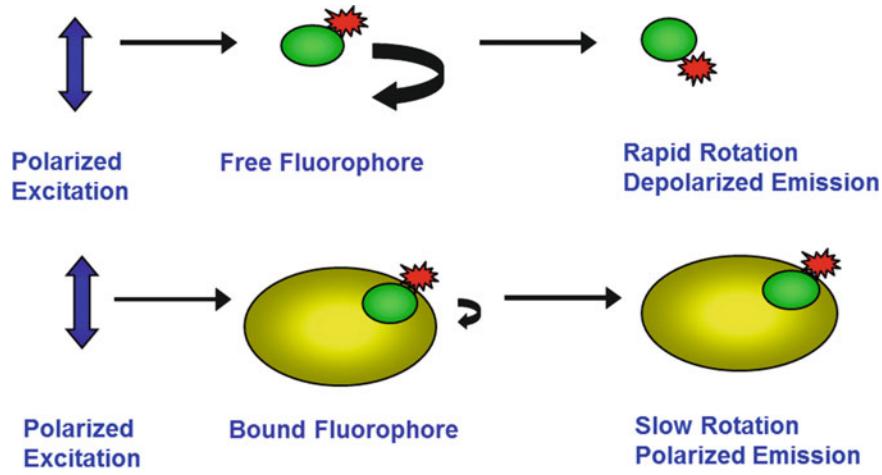

Fig. 2 The basics of fluorescence polarization binding assays. The small molecule fluorophores free or bound to macromolecules can be excited by vertically polarized light, resulting in polarized emission. The observed steady-state polarization of the sample depends on the extent of fluorophores bound to macromolecules. Free fluorophores have low observed polarization due to fast rotation relative to fluorescence lifetime, while bound fluorophores have high observed polarization due to slow rotation

anisotropy of 0.4 [8] (*see* **Note 1**). The observed anisotropy of a given sample falls between 0 and 0.4, depending on many extrinsic factors at play during the fluorescence lifetime of the fluorophore. The primary determinant of fluorescence depolarization in dilute solutions is the rotational diffusion of the fluorophore [1, 9, 10]. For ideal spherical rotors, anisotropy measured under steady-state conditions follows the Perrin equation (Eq. 1) where A_0 is the intrinsic anisotropy, τ is the fluorescence lifetime, and θ is the rotational correlation time of the fluorophore (the time the fluorophore rotates through an angle of 1 rad), which in turn is proportional to the viscosity of the solution (η) and the molecular volume of the rotor (V) and inversely proportional to the temperature (T) (Eq. 2).

$$A = \frac{A_0}{1 + \tau/\theta} \tag{1}$$

$$\theta = \frac{\eta V}{RT} \tag{2}$$

The consequence of this in practical terms is that fluorescence anisotropy can be used to measure changes in the rotational diffusion rate of a fluorophore as illustrated in Fig. 2. As a result, FP measurements can yield information on the size and shape of the fluorophore and the molecule complexed with the fluorophore. In aqueous nonviscous solutions, a typical small molecule fluorophore rotates on a time scale of 40 ps or less [11], much faster than a typical fluorescence lifetime of 10 ns [11], which results in

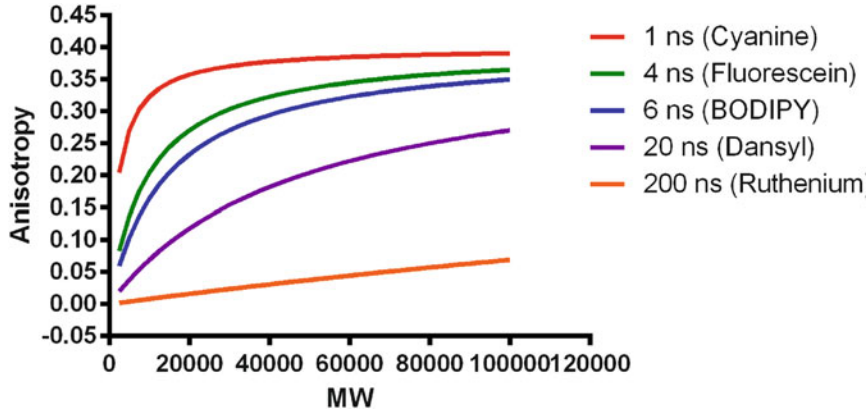

Fig. 3 Simulated graph illustrating the dependence of fluorescence anisotropy on fluorescence lifetime of the fluorophore and molecular size of the carrier macromolecule. Data are generated by Eq. 1

depolarized emission. Upon fluorophore binding to a macromolecule, the complex will rotate much slower with a rotational correlation time on par with the time scale of typical fluorescence lifetime, resulting in polarized emission. This forms the basis for quantifying the fraction of the fluorophore bound to the macromolecule. Figure 3 delineates the relationship between fluorescence anisotropy, carrier molecular weight, and fluorescence lifetime (simulated data using Eq. 1 assuming a limiting anisotropy of 0.4 and assuming the fluorophore is rigidly attached to a spherical carrier) [12]. It is evident that typical fluorophores such as fluorescein and BODIPY have ideal fluorescence lifetimes that allow FP measurements between a small labeled probe (<~1500 Da) and a macromolecule receptor (>~15,000 Da).

2 Methods

Numerous FP applications have been developed for HTS based on the principles described above and shown in Fig. 2. Because fluorescence polarization is a ratiometric measurement, in theory the FP signal should have less interference from background fluorescence of the assay plate and buffer. Because of this advantage, FP has become a popular technique for HTS assays. FP can be determined by steady-state measurements or time-resolved measurements [13]. In the time-resolved FP measurement, a short pulse of light excites the sample and the emission is recorded with a high-speed detection system that allows measurements on the nanosecond scale. In a steady-state FP measurement, the sample is illuminated by continuous excitation light and the measurement is an average of the time-resolved phenomenon over the intensity decay of the sample. The steady-state FP averaging over a single

exponential decay may thus mask complex exponential delays in some systems, and could be one of reasons for some nonideal steady-state FP data observed. The overwhelming majority of FP applications in HTS are steady-state measurements using commercial fluorescence plate readers. The scope of this chapter is limited only to steady-state FP measurements. This chapter will take a look at three steady-state FP applications in HTS: (1) Direct FP competition binding assay; (2) FP used as a detection method in a functional assay; (3) Determination of binding mechanism from a FP competition binding assay. Representative examples of the applications are presented where applicable.

2.1 Direct FP Competition Assay

The objective of a direct FP competition assay is to identify compounds that compete with the small-molecule fluorescent probe for binding to the macromolecular target. This approach is a quick and easy method that has been extensively used to identify active site binders of enzyme targets and small-molecule binders of nuclear receptors (NR). The disadvantage is that the assay may not identify compounds that bind at sites remote from the fluorescent probe (Subheading 2.3). In addition to active site binders, fluorescent probes prepared from allosteric ligands can be used to identify compounds that bind to regulatory sites outside of the target enzyme active site. In the following sections, the process for developing a FP competition assay for the exosite of a protease (FVIIa) and the utilization of a quality control parameter instead of an interference assay (counter-screen) in a direct nuclear receptor FP competition assay to identify false positive hits are described.

2.1.1 Design and Synthesis of an Appropriate Fluorescent Probe

FP assay development begins with designing a fluorescent probe. There are no universal rules for how to design an ideal probe for FP. When a label is attached to a known ligand to prepare a probe, the probe will work in FP assays only when the following conditions are satisfied: (1) the attachment of the label does not significantly alter how the ligand binds to the target; (2) the label cannot have a strong propeller effect, i.e., the rotational diffusion motion of the label needs to be restricted upon the binding of the probe to the target. A routine practice in our lab is to design probes with various linkers (both type and length) and to experimentally determine if the probes have the expected potency in the activity assay relative to the unmodified ligand, and if the probes work in the FP assay.

We applied the above approach to design a probe to identify compounds that bind at an allosteric site on the protease factor VIIa (FVIIa) in complex with its cofactor, tissue factor (TF). TF/FVIIa is a well-validated anticoagulant target [14, 15]. E-76, Ac-ALCDDPRVDRWYCQFVEG-NH2 (disulfide bond), is a reported partial inhibitor of TF/VIIA amidolytic behavior that binds to an exosite outside of the active site of FVIIa with a reported IC_{50} of 9.7 nM [16]. The mechanism of inhibition was

confirmed in our lab, though an IC_{50} of 2.3 nM was obtained under our assay conditions. Next, the reported crystal structure of the FVIIa/E-76 complex was examined to determine the residues on E-76 that are solvent exposed and potential sites for probe attachment. Based on solvent accessibility in the three-dimensional structure, the Glu residue at the C-terminal end was mutated to a Lys residue for the covalent attachment of Hilyte Fluor 488. The designed probe retained the same interactions with FVIIa as E-76 in a computer model. The probe was then custom-synthesized by Anaspec (San Jose, CA).

2.1.2 Determination of K_d Between the Fluorescent Probe and the Target

An appropriate concentration of the probe to use in the K_d determination is dependent upon several factors including the linearity of the fluorescent response with probe concentration, quantum yield of the probe, the K_d between the probe and target, and instrument sensitivity. The FVIIa experiments were carried out in an assay buffer containing 50 mM HEPES, pH 7.4, 100 mM NaCl, 5 mM $CaCl_2$, and 0.005 % (w/v) Triton X-100. Samples were prepared at a volume of 20 μl in a black 384-well low-volume polypropylene Matrical plate (cat# MP101-1-PP). Fluorescence intensity and anisotropy were measured on an Analyst AD plate reader (Molecular Devices). A probe dose titration was initially performed to determine the linearity of the fluorescent signal with probe concentration, and the probe fluorescence intensity was linear up to 500 nM. The probe concentration for the K_d determination should not be much greater than $2K_d$ to avoid stoichiometric titration [17]. A concentration of the probe corresponding to the IC_{50} in the functional assay is often chosen as the initial concentration for the binding assay. In this case, an initial probe concentration of 5 nM was selected, which yielded a fluorescence intensity S/B of 70.

Because there are intrinsic differences in instrument sensitivity for measuring the S channel and P channel, all plate readers need to be checked and calibrated for the instrument "*G*" or grating factor before obtaining any polarization data. The revised equation for polarization incorporating the *G* factor term is $P = (I_S - G \times I_P)/(I_S + G \times I_P)$. In this example, the *G* factor for the Analyst AD instrument was calibrated to achieve an mP of ~60 for the free probe (*see* **Note 2** for details on *G* factor calibration).

Next, a FVIIa concentration dependence was performed in the presence of 5 nM fixed probe concentration and 2000 nM sTF (Fig. 4a). Fitting the anisotropy data to Eq. 3a, where L_0 is the total probe concentration, R_0 is the total enzyme concentration, a is the probe signal in the absence of ligand, and b is the probe signal in the presence of saturating concentrations of ligand, yields A1 (free probe), A2 (bound probe), and an approximate K_d value of 0.6 nM. Identical results were observed after 10-min incubation

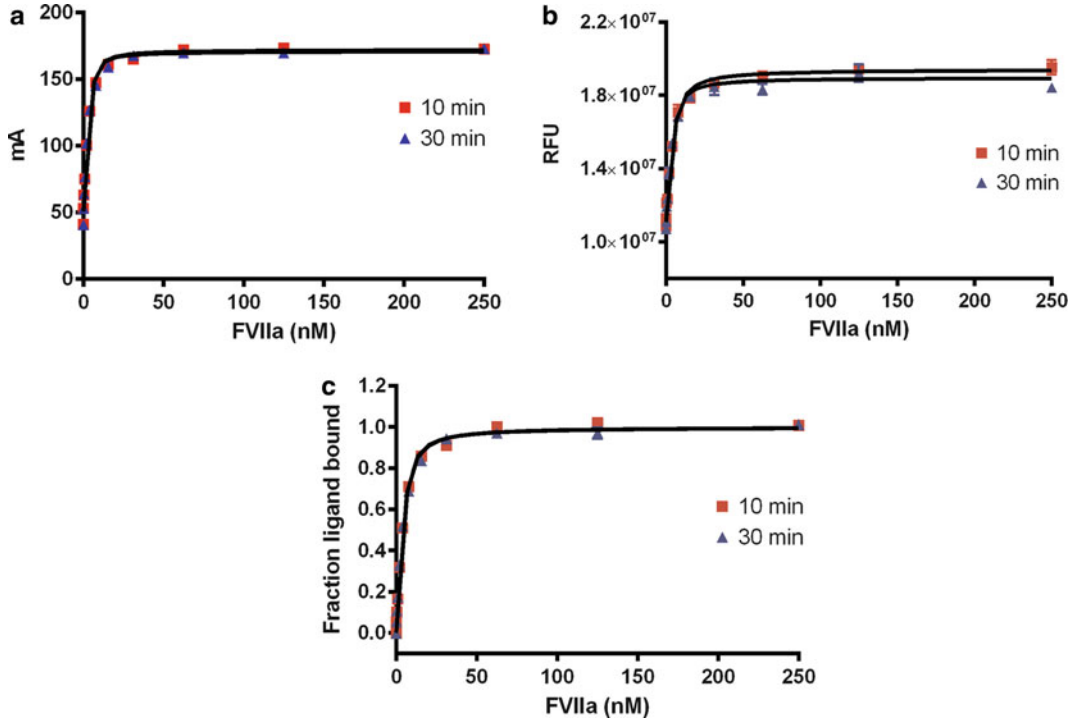

Fig. 4 The dose titration of FVIIa in the presence of fixed probe. The assay contained 5 nM probe, 2000 nM sTF and various concentrations of FVIIa and was measured for anisotropy and fluorescence intensity on Analyst AD after 10 and 30 min incubation at room temperature. (**a**) anisotropy measurement; (**b**) fluorescence measurement; (**c**) fb data converted from anisotropy data using Eq. 4

and 30-min incubation, indicating the binding equilibrium was reached quickly. The same dose titration was also measured by fluorescence intensity. Fitting of the fluorescence intensity data to Eq. 3a yielded a K_d of 1.3–1.8 nM (Fig. 4b). The discrepancy in K_d values obtained from anisotropy and fluorescence intensity measurements is attributed to the change in quantum yield of the probe upon binding to FVIIa. The quantum yield ratio (Q) of the bound probe to the free probe can be calculated from the ratio of fluorescence intensity of the bound probe to the fluorescence intensity of the free probe. A Q of 1.78 was obtained from the fluorescence data in Fig. 4b. The FP data in Fig. 4a was converted to the fraction bound probe (fb) by Eq. 4. Fitting of the FP fb data to Eq. 3b (where $a = 0$ and $b = 1$) yielded a K_d of 1.5–1.6 nM (Fig. 4c), which now agrees with the K_d calculated from the fluorescence intensity measurement. In addition, the selected probe concentration of 5 nM satisfies the non-stoichiometric conditions (i.e., the probe concentration not much greater than $2K_d$). Had the probe concentration been much greater than two times the calculated K_d value, a lower probe concentration would need to be selected and the K_d measurement repeated.

$$y = a + (b - a)\frac{(K_d + R_0 + L_0) - \sqrt{(K_d + R_0 + L_0)^2 - 4R_0L_0}}{2L_0} \tag{3a}$$

$$y = \frac{(K_d + R_0 + L_0) - \sqrt{(K_d + R_0 + L_0)^2 - 4R_0L_0}}{2L_0} \tag{3b}$$

$$\text{fb} = \frac{(A - A_1)}{(A - A_1) + Q(A_2 - A)} \tag{4}$$

Parallel with the determination of K_d between the fluorescent probe and the target, additional HTS assay optimization should be performed. As mentioned above, FP is a ratiometric method and background fluorescence effects are expected to be minimal. However, in practice, a number of experimental details including the chemical and physical properties of the test compounds can introduce artifacts into the results. Some plate types yield significantly larger assay windows for a given FP assay. Buffer optimization including detergent and carrier protein screening should be performed to select assay conditions that minimally affect the aggregation state of the probe and maximally enhance the stability of the target protein. For DMSO tolerance, it is critical that not only the assay signal window is maintained but also the interactions between the probe and the target protein are not adversely affected. The order of reagent addition and the equilibration time need to be evaluated and optimized for FP competition assays that do exhibit time-dependent binding between the probe and the target.

When multiple fluorescent probes are available, the most potent probe with a reasonable fluorescence quantum yield should be selected for the FP competition assay. In general, the most potent probe affords the best chance to identify compounds with the widest potency range [17].

2.1.3 Selection of Appropriate Screen Conditions for Direct FP Competition Assay

An fb of 0.5–0.8 is recommended for direct FP competition assays, which is a compromise between achieving a reasonable anisotropy signal window and adequate sensitivity to detect small-molecule compounds [17]. An fb value higher than 0.8 will decrease the assay sensitivity to identify weakly active compounds, while an fb value less than 0.5 often leads to an assay with an inadequate anisotropy signal window.

Based on data in Fig. 4c, the FVIIa concentration corresponding to an fb of 0.8 was selected for the TF/FVIIa FP competition assay. The optimized competition screen contains 5 nM probe and 12.5 nM FVIIa. The FP measurements are taken after 20 min incubation at room temperature. Upon finalization of the

screen conditions, reagent working stock stability is then determined to ensure the screen is conducted within the time constraints of reagent stability.

2.1.4 Validation of Direct FP Competition Assay

Validation of the FP competition assay can be achieved by use of a nonfluorescent counterpart of the probe or a known positive control that binds at the same site as the probe. In this case, we performed the dose titrations with E-76 (Fig. 5a) as a positive control and compound 1, which binds to the FVIIa active site, as a negative control (Fig. 5b).

E-76 is fully competitive with the probe, consistent with E-76 and the probe binding to the same exosite on FVIIa. The IC_{50} of E-76 in the FP competition assay (23 nM) is several-fold higher than the IC_{50} in the activity assay (2.3–9.7 nM), which is typical for FP competition assays. A lower starting fb will lead to an FP-derived IC_{50} closer to the functional assay IC_{50} but with the disadvantage of a smaller FP assay window [17].

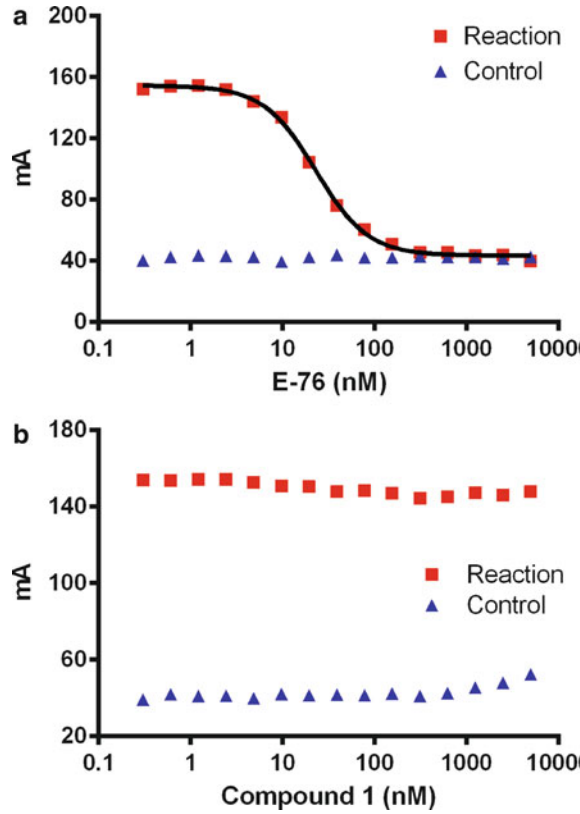

Fig. 5 The dose titration of E-76 and compound 1 in FVIIa FP competition assay. The assay contained 5 nM probe, 12.5 nM FVIIa, 37.5 nM sTF, and various concentrations of compound and was read for anisotropy on Analyst AD after 20 min incubation at RT. (**a**) E-76; (**b**) Compound 1

Compound 1 showed a minor degree of displacement with the probe, consistent with compound 1 and the probe binding at distinct sites on the target [18] and also consistent with partial inhibition of TF/FVIIa amidolytic activity by E-76. In the single-dose screen, this direct FP competition assay would be unlikely to identify hits that bind to alternate sites, such as compound 1 in this example. In Fig. 5a, b, a control reaction was performed in parallel to the competition reaction. The control reaction contains only the probe and the compound, and is helpful in identifying compound interference issues.

A screen was performed at 300 μM using a set of compounds identified by virtual screening. A limited number of hits were identified and then followed up with dose titration in parallel with a control reaction as described above. Three hits were confirmed while the other hits were identified as false positives in the control titration due to compound interference including compound interactions with the probe, compound solubility/aggregation, and compound fluorescence. The three confirmed hits were followed up for further characterization.

2.1.5 A Quality Control Parameter for a Direct FP Competition Screen

A HTS campaign was run using one of the NR FP competition red assays from Invitrogen. The compound library was tested at 10 μM in singlet in a 20 μl assay in a 384-well black Nunc polypropylene plate (cat# 267461). The screen was carried out on a Thermo-CRS platform and read on Envision plate readers (Perkin Elmer). 24,256 hits were identified in the primary assay based on 3× inter-quartile range standard deviation (IQR-SD) above the median. Next, an interference screen (counter-screen) would be performed to determine if the hits are selective or just interfering in the assay. For direct FP competition assays, there are no good options for a counter-screen. For this NR FP assay, the total fluorescence intensity (FLINT) was calculated from the S and P channel fluorescence and used for the calculation of a new quality control (QC) parameter, mP/total FLINT. We found that total fluorescence intensity of the bound probe is about 2× that of the free probe in this assay, resulting in a relatively constant mP/total FLINT regardless of the free and bound states of the probe. When mP/total FLINT is significantly below the median of the screen, the sample well likely contains a fluorescent compound. When mP/total FLINT is significantly above the median, the sample well either has a fluorescent quencher or has under-delivery of the probe. We did not identify many fluorescent compounds, likely due to the fact that the red probe was used in the assay. By applying a 3× IQR-SD cutoff above the median for mP/total FLINT, we were able to eliminate 22 % of the primary hits due to fluorescence quenching or probe under-delivery. The remaining primary hits were tested in a confirmation assay in triplicate and a large majority of hits (74 %) were confirmed as active. Total fluorescence intensity has also been reported as a QC parameter for FP screens [19].

2.2 FP as a Detection Method in Enzymatic Assays

Another application of FP assays in HTS is its use as a detection method in enzymatic assays. The detection methods can be divided into two types: (1) direct measurement of the product formation, (2) measurement of the product via FP competition. The pros and cons of these two types are discussed. Since these assays still measure FP, the standard practices for selection of the probe concentration, determination of K_d between the probe and the detection macromolecule, selection of the detection macromolecule concentration, optimization of reader protocols, optimization of plate, buffer, and other assay parameters as described earlier for direct FP competition assays (Subheading 2.1) still apply.

2.2.1 FP Method That Directly Measures the Product

The IMAP kinase and PDE assays (Molecular Devices) are examples of FP assays that directly measure the product of an enzyme reaction. In an IMAP kinase assay, the fluorescently labeled phosphopeptide product is detected by IMAP beads (IMAP beads serve as the macromolecules). The advantages of assays such as IMAP include: (1) measures the product directly; the signal increases with the product; (2) compound potency (%inhibition and IC_{50}) does not change significantly with the assay conversion rate when the conversion rate is not greater than 50 % [20]; and (3) an interference assay is available to remove false positive hits due to interference with the detection system. The latter is easily accomplished by using the detection reagents plus the substrate and the product mixed at a ratio that mimics the amount of product formed during the assay. The disadvantages of IMAP assay include: (1) use of labeled substrate instead of the "native" substrate; (2) the assay requires relatively higher conversion (20–50 %) of substrate than conventional functional assays using more traditional detection schemes to achieve a reasonable assay mP window.

2.2.2 FP Method That Measures the Product via Competition

Transcreener PDE assay (Bellbrooke), PolarScreen kinase FP assay (Invitrogen), and PI3K FP assay (Echelon Biosciences) are examples of assays that measure the product via competition. In a Transcreener PDE assay, the product (GMP or AMP) is detected by competition with the fluorescently labeled probe for binding to the antibody. The advantages of competition detection assays such as Transcreener include: (1) uses the non-labeled substrate; (2) interference assay is available to remove false positive hits due to interference with the detection system (using the detection reagents plus the substrate and the product mixed at the assay conversion ratio). The disadvantages of competition detection assays include: (1) measures the product through competition; the signal decreases with increasing product; (2) it is difficult to accurately determine the Km for the substrate because the product standard curve is nonlinear due to nonlinear competition detection of the product; (3) the assay window is typically selected between the EC50 and

EC90 of the enzyme dose titration curve; however, compound potency (%inhibition and IC_{50}) can change significantly with the assay conversion rate. These disadvantages are universal to all competition detection assays, and by no means unique to FP competition detection assays. For example, in a simple rapidly reversible competition model, the observed compound potency (IC_{50}) determined from the competition assay deviates from the true IC_{50} (50 % inhibition of the enzyme activity) [21]. The observed compound IC_{50} is 2× the true IC_{50} when the assay is conducted at EC50. However, the observed IC_{50} is 10× the true IC_{50} if the assay is performed at EC90. The actual assay is a compromise of an acceptable assay signal window and workable assay sensitivity, knowing the caveat that a larger assay signal window comes at the price of possibly not identifying weakly active compounds.

2.3 Determination of Binding Mechanism from FP Competition Binding Assay

The compound binding mechanism can be derived from a compound dose titration in a FP competition binding assay [18]. Figure 6 shows three of the most common mechanisms for compound binding: competitive, uncompetitive, and noncompetitive binding. The α value in Fig. 6 describes cooperativity between the probe binding and the inhibitor binding in a noncompetitive mechanism. A plot of the fraction bound versus compound concentration in Fig. 7 shows the diagnostic displacement curves of compounds that bind competitively, uncompetitively, or noncompetitively to the macromolecule target [18]. A competitive inhibitor fully displaces the probe resulting in a decrease in the fraction of ligand bound with increasing inhibitor concentration. In contrast, an uncompetitive compound increases the fraction of bound ligand resulting in a higher polarization value. The displacement of probe

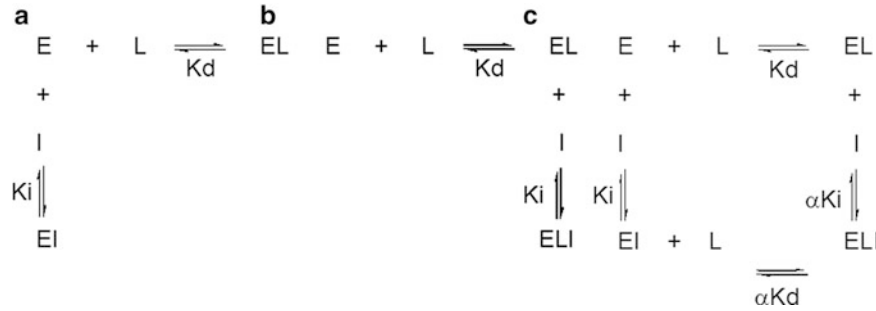

Fig. 6 Three common mechanisms for compound binding: (**a**) competitive mechanism; (**b**) uncompetitive mechanism; (**c**) noncompetitive mechanism where the α value describes cooperativity between the probe binding and the inhibitor binding. In a noncompetitive mechanism, $\alpha = 1$ represents no cooperativity between the probe binding and the inhibitor binding, $\alpha > 1$ represents negative cooperativity (the inhibitor binds weaker to the receptor-probe complex than to the free receptor), while $\alpha < 1$ represents positive cooperativity (the inhibitor binds stronger to the complex than to the free receptor). *R* is the receptor, *L* is the probe, and *I* is the inhibitor

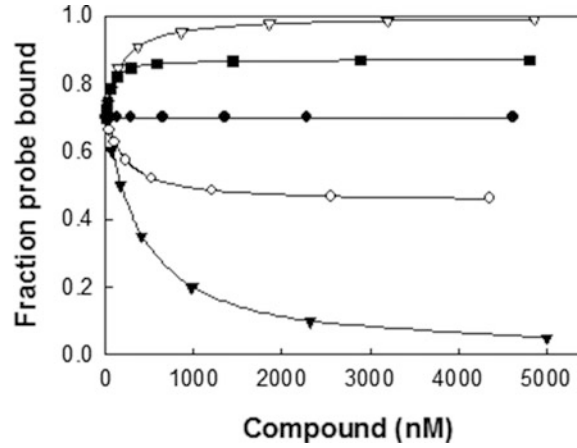

Fig. 7 Theoretical plots of competitive (▼), uncompetitive (▽), and noncompetitive ($\alpha = 1$ (●), 3 (○) and 0.33 (■)) inhibitors. The receptor and probe concentrations are 53.7 nM and 10 nM, respectively. The K_d for the probe is 20 nM. The K_i for compounds in cases of competitive and uncompetitive mechanisms is 100 nM, while the K_i values in cases of noncompetitive mechanism are 100 and 100α nM

by a noncompetitive compound is more complex and is dependent upon the degree of cooperatively. When the compound reduces ($\alpha > 1$), increases ($\alpha < 1$), or has no effect on probe affinity ($\alpha = 1$), the resulting fraction bound will decrease, increase, or not change, respectively (Fig. 7).

2.4 Limitations of Steady-State FP Measurements

As with any technique, fluorescence polarization has its share of limitations. General FP complications include interactions between the fluorescent probe and the compound, compound aggregation, scattered light, sample turbidity, plate or buffer polarization, compound fluorescence, fluorescence quenching due to various factors, and instrument detector saturation. Probe-target (or compound-target) interactions may also not fully mimic the native interactions, in cases including labeled probes having altered affinity/binding mode relative to unlabeled counterparts; using mutant enzymes in place of active enzymes; multiple enzyme conformations; and enzymes with multiple substrates. In addition, nonideal FP data can result from steady-state FP measurements of systems that possess multiple fluorescence lifetimes and/or multiple rotational correlation times and thus complex exponential decays, which may only be accurately determined by time-resolved FP measurements. Finally, because the FP assay signal window does not change significantly with the G factor and the starting polarization value is in practice set arbitrarily, the standard S/B parameter no longer indicates the robustness of the assay. For FP assays, the meaningful statistical parameters are assay signal window (mP) and Z'.

3 Notes

1. Fluorescence polarization measurements on commercial fluorescence plate readers follow one-photon excitation, which has a maximum anisotropy of 0.4. Anisotropy values higher than 0.4 indicate misalignment in the instrument or the presence of scattered light. Excitation with two photons or multiple photons by picosecond or femtosecond laser sources uses different photo-selection processes, which can lead to a maximum anisotropy greater than 0.4 [22].
2. The common practice is to set the instrument to 27 mP for 1 nM fluorescein and to subtract the background fluorescence (buffer only) from the I_S and I_P values as the background fluorescence is often polarized. I recommend adjusting the G factor of the instrument such that the probe mP is between 50 and 100 mP instead. Empirical results have shown that a FP assay signal window (probe bound minus probe free) does not vary significantly with the G factor. A higher initial mP for the probe can avoid situations in screens where polarization values are close to zero or turn negative. When the assay fluorescence intensity S/B is low (<20), background fluorescence due to buffer should be subtracted from the I_S and I_P values during calibration, and buffer only controls added to the assay plate. There are some commercial FP assays that have a FLINT S/B as low as 5. These assays are much more prone to larger CVs when implemented in screens without designated buffer only wells. If the probe concentration yields a fluorescence intensity S/B > 50, background effects are minimized and background subtraction is not required.

4 Summary

Fluorescence polarization is a powerful technique for the study of biomolecular interactions in solution, and has been widely used in biochemical high-throughput screens. This chapter reviewed three representative steady-state FP applications and good practices in the development and execution of FP-based HTS assays. After hits are obtained from FP-based HTS assays, a good practice is to always confirm the hits in a secondary assay. For direct FP competition binding assays, an orthogonal functional assay may be used. For FP detection assays, a second functional assay that employs a different detection method is recommended.

Acknowledgments

The authors would like to thank Ray Unwalla of Wyeth Research for molecular modeling of E-76 and the E-76 based probes, and would like to thank Rebecca Shirk and Belew Mekonnen of Wyeth Research for collaboration on the TF/FVIIa, and would like to thank Shannon Stahler, Nina Kadakia, Gary Kalgaonkar, William Martin, Mariya Gazumyan, Pedro Sobers, and Jim LaRocque of Wyeth Research for contribution to the NR project, and would like to thank Richard Harrison of Wyeth Research for critical review of the chapter.

References

1. Perrin F (1926) Polarisation de la lumière de fluorescence. Vie moyenne des molécules dans l'état excite. J Phys Radium 7:390–401
2. Jameson DM (2001) The seminal contributions of Gregorio Weber in modern fluorescence spectroscopy. In: New trends in fluorescence spectroscopy. Springer, Heidelberg, pp 35–53
3. Jameson DM, Sawyer WH (1995) Fluorescence anisotropy applied to biomolecular interactions. Methods Enzymol 246:283–300
4. Checovich WJ, Bolger RE, Burke T (1995) Fluorescence polarization - a new tool for cell and molecular biology. Nature 375:141–144
5. Terpetschnig E, Szmacinski H, Lakowicz JR (1997) Long-lifetime metal-ligand complexes as probes in biophysics and clinical chemistry. Methods Enzymol 278:295–321
6. Hill JJ, Royer CA (1997) Fluorescence approaches to study of protein-nucleic acid complexation. Methods Enzymol 278:390–416
7. Kakehi K, Oda Y, Kinoshita M (2001) Fluorescence polarization: analysis of carbohydrate-protein interactions. Anal Biochem 297:111–116
8. Lakowicz JR (1999) Fluorescence anisotropy. In: Lakowicz JR (ed) Principals of fluorescence spectroscopy, 2nd edn. Kluwer Academic/Plenum Publishers, New York, NY, pp 291–319
9. Perrin F (1929) La fluorescence des solutions. Induction moléculaires. Polarisation et durée d'émission. Photochimie. Ann Phys 10 (12):169–275
10. Perrin F (1931) Fluorescence. Durée élémentaire d'émission lumineuse. Conférences d'Actualités Scientifiques et Industrielles XXII, 2–41
11. Lakowicz JR (1999) Introduction to Fluorescence. In: Lakowicz JR (ed) Principals of fluorescence spectroscopy, 2nd edn. Kulwer Academic/Plenum Publishers, New York, NY, pp 1–23
12. Cantor CR, Schimmel PR (1980) Biophysical chemistry. Part II: Techniques for the study of biological structure and function. W. H. Freeman, Oxford, pp 454–465
13. Lakowicz JR (1999) Time-dependent anisotropy decays. In: Lakowicz JR (ed) Principals of fluorescence spectroscopy, 2nd edn. Kulwer Academic/Plenum Publishers, New York, NY, pp 321–345
14. Mackman N (2004) Role of tissue factor in homeostasis, thrombosis and vascular development. Arterioscler Thromb Vasc Biol 24:1015–1022
15. Shirk RA, Vlasuk GP (2007) Inhibitors of Factor VIIa/Tissue Factor. Arterioscler Thromb Vasc Biol 27:1895–1900
16. Dennis MS, Eigenbrot C, Skelton NJ, Ultsch MH, Santell L, Dwyer MA, O'Connell MP, Lazarus RA (2000) Peptide exosite inhibitors of factor VIIa as anticoagulants. Nature 404:465–470
17. Huang X (2003) Fluorescence polarization competition assay: the range of resolvable inhibitor potency is limited by the affinity of the fluorescent ligand. J Biomol Screen 8:34–38
18. Huang X (2003) Equilibrium competition binding assay: inhibition mechanism from a single dose response. J Theor Biol 225:369–376
19. Turconi S, Shea K, Ashman S, Fantom K, Earnshaw DL, Bingham RP, Haupts UM, Brown MJB, Pope A (2001) Real experiences of uHTS: a prototypic 1536-well fluorescence anisotropy-based uHTS screen and application of well-level quality control procedures. J Biomol Screen 6:275–290

20. Wu G, Yuan Y, Hodge CN (2003) Determining appropriate substrate conversion for enzymatic assays in high-throughput screening. J Biomol Screen 8:694–700
21. Unpublished results
22. Lakowicz JR, Gryczynski I, Gryczynski Z, Danielsen E (1992) Time-resolved fluorescence intensity and anisotropy decays of 2,5-diphenyloxazole by two-photon excitation and frequency-domain fluorometry. J Phys Chem 96:3000–3006

Chapter 8

Time-Resolved Fluorescence Assays

Chen-Ting Ma and Eduard A. Sergienko

Abstract

Fluorescence-based detection techniques are popular in high throughput screening due to sensitivity and cost-effectiveness. Four commonly used techniques exist, each with distinct characteristics. Fluorescence intensity assays are the simplest to run, but suffer the most from signal interference. Fluorescence polarization assays show less interference from the compounds or the instrument, but require a design that results in change of fluorophore-containing moiety size and usually have narrow assay signal window. Fluorescence resonance energy transfer (FRET) is commonly used for detecting protein-protein interactions and is constrained not by the sizes of binding partners, but rather by the distance between fluorophores. Time-resolved fluorescence resonance energy transfer (TR-FRET), an advanced modification of FRET approach utilizes special fluorophores with long-lived fluorescence and earns its place near the top of fluorescent techniques list by its performance and robustness, characterized by larger assay window and minimized compound spectral interference. TR-FRET technology can be applied in biochemical or cell-based in vitro assays with ease. It is commonly used to detect modulation of protein-protein interactions and in detection of products of biochemical reactions and cellular activities.

Key words TR-FRET, Time-resolved fluorescence resonance energy transfer, Protein-protein interaction, Enzyme activity assay, Product detection

1 Introduction

In modern drug discovery, high throughput screening (HTS) of hundreds of thousands of compounds occur routinely against targets of interest, and an important aim has been to develop HTS-ready assays that are inexpensive, simple, and robust, yielding minimal false positives/negatives. Fluorescence-based techniques are very popular among HTS assays due to ease of use and high sensitivity. They encompass a large group of diverse approaches. Fluorescence intensity assays rely on generation of fluorescent molecular species (fluorophores) from nonfluorescent species (known as fluorogenes) in the course of the assay. Fluorophores absorb at excitation wavelength and then emit light at a higher wavelength; the difference in wavelength or frequency between excitation and emission spectra is known as Stokes shift.

William P. Janzen (ed.), *High Throughput Screening: Methods and Protocols*, Methods in Molecular Biology, vol. 1439,
DOI 10.1007/978-1-4939-3673-1_8,

The minimal concentration of a fluorophore in the assay is defined by it brightness; one needs to overcome stray light generated in the detection instrument by light reflection, scattering, or bleed-through between excitation and emission channels. The higher the Stokes shift is the larger separation between the excitation and emission channels could be achieved and, therefore, the smaller potential effect of these optical artifacts would be. While still in everyday use, fluorescence intensity assays are the most prone among fluorescent assays to optical interference suffering from signal interference by colored and fluorescent compounds, as well as from instrument-generated noise, such as light scatter in the emission channel or bleed-through from the excitation light.

Another popular HTS format is fluorescence polarization (FP) that is typically utilized to assess binding in biological systems (*see* Chapter 3). These assays are usually very inexpensive requiring only a low-molecular weight fluorescently labeled tracer (e.g. small-molecule ligand or peptide with molecular weight usually below 5 kDa) and a purified receptor, but require instruments with ability to generate highly polarized light and to measure the intensity of the polarized and depolarized lights. The signal obtained in the FP assays is based upon the ratio of polarized and depolarized light intensity values and correlates with the change in rotational speed of the tracer molecular movement that in its turn correlates with degree of its binding to the receptor molecule. A large difference in molecular sizes between the tracer and the receptor are required to generate a usable assay window. Therefore protein-protein interactions, where both binding partners are of comparable size, cannot be measured with this technique. In another common type of FP-based applications, a fluorophore is modified during the course of an assay to result in a significant size change of fluorophore-containing molecule; the change in molecular weight is then assessed through fluorescence polarization signal. Generation of small molecule products, e.g., nucleotides or phosphorylated peptides, could be assessed through the use of competition with a fluorescently labeled analog of the product from its complex with a large molecule, e.g., a specific antibody or a resin with affinity to phosphate groups. As in any fluorescent assay, the brightness of fluorophore that correlates with the efficiency of light absorption and emission defines the concentrations of assay components; the brighter the fluorophore is the lower the concentrations of the tracer, and indirectly of the receptor as well, could be used in the assay. Although FP assays are characterized with inherently low signal to background ratios (S/B), they are able to compensate for this apparent deficiency by relying on ratiometric readout that overcomes minor instrument-associated noise and signal variations generated by liquid dispense variations. At the same time, FP assays commonly relying on low concentrations of fluorophores are acutely sensitive toward compound optical interference and light

scattering caused by precipitation/aggregation; hits identified in FP assays commonly need reconfirmation in an orthogonal format, e.g., another ratiometric assay modality, such as FRET or TR-FRET.

Fluorescence resonance energy transfer (FRET) and time-resolved fluorescence resonance energy transfer (TR-FRET) assays offer an alternative homogenous format that accounts for and largely bypasses background fluorescence from assay buffer and reagents. The concept of the FRET assay, first introduced by Förster in 1959, is based on the quantum phenomenon where a fluorescent donor molecule absorbs light and instead of emitting light, nonradiatively transfers energy to a proximal fluorescent acceptor molecule with excitation frequency matching that of the donor emission. In turn, the acceptor emits at a wavelength specific to this fluorophore [1], and the signal measured in both acceptor and donor emission channels is utilized to calculate FRET signal, also referred to as FRET ratio. FRET signal normally does not depend on the molecular weight of the fluorophores, as long as the two fluorophores could come in close proximity. Distance diminishes energy transfer efficiency to the sixth power, resulting in working distances in the 10–100 Å range, making FRET an ideal technique for intramolecular and intermolecular interactions [1].

FRET assays are usually based on common high-quantum yield fluorophores such as small-molecule fluorescent dyes or fluorescent proteins. Selection of fluorophores for pairing in a FRET assay is guided by their spectral properties. The main requirement is that emission spectrum of the donor fluorophore overlaps with the excitation spectrum of the acceptor molecule. The degree of overlap is directly proportional to the resonance energy transfer that can be achieved. At the same time, excitation spectra of the donor and acceptor should be significantly different; a large overlap between the excitation spectra will result in a larger fluorescence signal component independent of the proximity distance between the two moieties, i.e., the assay background signal. Most common small-molecule fluorophores, such as derivatives of fluorescein, rhodamine, or proprietary dyes as well as fluorescent proteins have low Stokes shifts and very broad spectra resulting in high background values and therefore, low signal to background ratio.

A modification of a FRET assay, sometimes referred to as quenching resonance energy transfer (QRET), utilizes a quenching molecule instead of an acceptor and can achieve slightly higher S/B values than standard FRET assays. Due to the described drawbacks, FRET assays are usually utilized as a last resort when no other approaches are available; in most assays, transformation into a TR-FRET format is possible and would commonly result in superior sensitivity and assay robustness.

Commercially available rare earth lanthanides such as Terbium Tb^{3+} or Europium Eu^{3+} bound to a chelate or cryptate organic

molecule are most common donors used in TR-FRET assays. They provide bright fluorophores with lifetimes 1–2 ms, allowing for a delay of 50–150 μs between the excitation and measurement of the emission signal, thus the time-resolved part [2–4]. This delay ensures that background fluorescence characterized with nsec and μsec lifetimes is largely decayed. Another advantage over FRET assays is lanthanide's narrow peaks in fluorescence emission spectra that provide basis for additional significant boost in S/B by selection of appropriate narrow-band excitation and emission filters. Ratiometric readout of acceptor emission and donor emission can minimize the impact of liquid-handler and plate reader errors by normalizing fluorescence output against donor emission. In addition to calculating TR-FRET signal, fluorescence detected in the donor emission channel is commonly used to detect compounds that optically interfere with the assay, thus, reducing the false positive rate [5].

TR-FRET assay has been in use for the last two decades, with applications involving detection of protein and small-molecule moieties, protein-protein interactions, assembly of cell-surface receptors, enzymatic assays, as well as biomarker detection [1–6]. We exemplify in this chapter the assay development and optimization process for TR-FRET assays detecting both protein-protein interactions and determining enzyme activity (*see* **Note 1**). For the former, we have chosen to illustrate the assay optimization process for binding of SUMO to SUMO-Interaction-Motif (SIM) containing peptide [7–9], and cullin neddylation, specifically tailored to be sensitive to Ubc12 enzyme activity, for the latter [10, 11].

2 Materials

Prepare all solutions using ultrapure water (prepared by purifying deionized water to attain resistivity greater than 18.0 MΩ cm at 25 °C) and analytical grade reagents. Prepare all reagents at room temperature and store as indicated. Diligently follow all waste disposal regulations when disposing waste materials.

1. 1 M HEPES pH 7.5 and pH 7.8: Add 150 ml water to glass beaker. Weigh 47.7 g HEPES and add to beaker. Dissolve HEPES powder and pH to 7.5 or 7.8 in separate beakers with concentrated NaOH. Add water to bring volume up to 200 ml. Pass through 0.22 μm filtration unit. Store at 4 °C.
2. 1 M DTT: Add 7.5 ml water to glass beaker. Weigh 1.54 g dithiothreitol (DTT) and add to beaker. Dissolve DTT powder and add water to bring volume up to 10 ml. Do not use pH meter. Pass through 0.22 μm filtration unit. Freeze in aliquots and store at −20 °C.

3. 10 % Tween 20: Add 9 ml water to 15 ml disposable conical tube. Snip off the tip of 1 ml pipette tip and use the truncated tip to transfer 1 ml of Tween 20 detergent to conical tube. Aspirate and dispense several times to clear Tween 20 from the tip. Pass the solution through a 0.22 μm syringe filter into a new 15 ml conical tube. Store at 4 °C for no more than 2 months.
4. Tb-anti-GST and Tb-anti-FLAG: Store frozen aliquots at −80 °C. Store thawed aliquot on ice and flash freeze the remaining amount at end of assay day.
5. GST-SUMO3: Store frozen aliquots at −80 °C. Store thawed aliquot on ice and flash-freeze the remaining amount at end of assay day.
6. Fluorescein-peptide (f-S2): Sequence: Fluorescein-(carboxy-aminohexanoic acid linker)-KGDVIDLTIE. Weigh 1 mg f-S2 powder and add to 1.6 ml Eppendorf tube. Add appropriate amount of DMSO to resuspend at 1 mM concentration, and mix by vortexing. Store at −80 °C in smaller aliquots. Store thawed aliquot at room temperature and flash freeze the remaining amount at end of assay day.
7. 3 M NaCl: Weigh 35.1 g NaCl and add to beaker. Dissolve NaCl powder and add water to bring volume up to 200 ml. Pass through 0.22 μm filtration unit. Store at 4 °C.
8. 0.5 M TCEP.
9. 1 M $MgCl_2$: Add 75 ml water to glass beaker. Weigh 20.3 g $MgCl_2$ hexahydrate and add to beaker. Dissolve $MgCl_2$ powder and add water to bring volume up to 100 ml. Pass through 0.22 μm filtration unit. Store at 4 °C.
10. Ubc12.
11. Fluorescein-labeled Nedd8 (fluo-Nedd8).
12. His-tagged NAE1: (recombinant expression) E1-enzyme for neddylation cascade.
13. FLAG-tagged SCF (FLAG-SCF): (recombinant expression) Cullin complex.
14. SUMO-SIM Assay Buffer: Mix 600 μl of 1 M HEPES, pH 7.5, 12 μl of 1 M DTT solution, 6 μl of 10 % Tween 20 solution, and 11.38 ml water in a 15 ml disposable conical tube, followed by thorough mixing by vortexing or serological pipette. Prepare this Assay Buffer fresh for every assay day.
15. 4 nM Tb-anti-GST solution: Dilute 2.2 μl of 3700 nM Tb-anti-GST solution in 2 ml Assay Buffer in 2 ml Eppendorf tube. Mix by pipetting.
16. 40 nM diluted GST-SUMO3: Dilute 2.7 μl of 14.6 μM GST-SUMO3 solution in 1000 μl Assay Buffer in a 1.6 ml Eppendorf tube. Mix by pipetting.

17. Cullin neddylation Assay Buffer: Mix 300 μl of 1 M HEPES, pH 7.8, 200 μl of 3 M NaCl solution, 12 μl of 1 M $MgCl_2$ solution, 24 μl of 0.5 M TCEP solution, 6 μl of 10 % Tween 20 solution, and 11.46 ml water in a 15 ml disposable conical tube, followed by thorough mixing by vortexing or serological pipette. Prepare this Assay Buffer fresh for every assay day.
18. 2 nM Tb-anti-FLAG and 20 nM Ubc12 mixed solution: Dilute 10.3 μl of 171 nM Tb-anti-FLAG solution and 11.3 μl of 3120 nM Ubc12 solution in 859 μl of Assay Buffer.
19. 1 μM diluted FLAG-SCF solution: Dilute 2.2 μl of 215 μM FLAG-SCF solution in 237.8 μl of Tb-anti-FLAG/Ubc12 mixed solution.
20. 5 mM ATP solution: Dilute 110 μl of 40 mM ATP solution in 770 μl of Assay Buffer.
21. Activated NAE1 is prepared by preincubation of NAE with Nedd8 and ATP. The solution contains 2 μM NAE1, 4 μM fluo-Nedd8 and 5 mM ATP. Dilute 1.2 μl of 790 μM fluo-Nedd8 solution and 24 μl of 20 μM NAE1 solution in 215 μl of 5 mM ATP solution.
22. 1536-well white polystyrene, HiBase, flat-bottom, square well assay plate.
23. Agilent Bravo Automated Liquid Handling Platform.
24. P30 and P10 pipette tips in 384-well racks.
25. 384-well, deepwell, polypropylene plate.
26. VIAFLO electronic multichannel pipette.
27. PHERAstar plate reader or other TR-FRET compatible reader.

3 Methods

Carry out all procedures at room temperature unless otherwise specified.

3.1 SUMO to SIM Containing Peptide Protein-Protein Interaction Screen

1. Transfer 18 μl of 4 nM Tb-anti-GST solution to eight adjacent wells each in two adjacent columns in a new 384-well intermediate polypropylene plate (*see* **Note 2**).
2. Transfer 11 μl of 40 nM diluted GST-SUMO3 to eight adjacent wells in a column in a new 384-well intermediate polypropylene plate. Prepare parallel column without GST-SUMO3, i.e., only containing 11 μl of Assay Buffer.
3. Prepare 36 μM diluted f-S2 peptide solution by diluting 3.6 μl of 1 mM f-S2 stock in 96.4 μl Assay Buffer in well A1 of new intermediate 384-well polypropylene plate. Perform threefold serial dilutions to reach the following concentrations: 9, 3, 1, 0.33, 0.11, 0.037, 0.012, and 0 μM. If twofold serial dilutions were performed, more concentrations and wells should be

tested to achieve the same approximate range of concentrations. Take half of the volume of all the wells with VIAFLO multichannel electronic pipettor and transfer to adjacent column. Wrap the intermediate plate, plus lid, in aluminum foil to avoid photo-bleaching.

4. Spin down the f-S2 peptide, the GST-SUMO3, and the Tb-anti-GST intermediate plates at 182 × *g* for 1 min. Use the Bravo liquid handler and two columns of unused P30 tips to aspirate 13 μl from the Tb-anti-GST plate and dispense 3 μl into quadruplicate wells in the 1536-well assay plate (*see* **Note 3**). With new P10 tips, aspirate 7 μl from the GST-SUMO3 plate and dispense 1.5 μl into quadruplicate wells in the 1536-well assay plate.

   Spin down the lidded assay plate. Incubate for 60 min.

5. With new P10 tips, aspirate 7 μl from the f-S2 plate and dispense 1.5 μl into quadruplicate wells in the 1536-well assay plate. Spin down the lidded assay plate. Incubate for 60 more minutes.

6. Read immediately on the PHERAstar plate reader with TR-FRET optical module (ex337/em520/em490) with delay of 100 μs and integration time of 200 μs. Seal the plate to prevent evaporation if additional reads at later times are desired.

7. Start the data analysis by plotting ratiometric data (FI 520/FI 490) of acceptor and donor channels. Perform background subtraction by subtracting no-GST-SUMO3 control data from GST-SUMO3 data for each f-S2 concentration (Fig. 1a). Fit the background-subtracted data to the Hill equation. If the Hill coefficient is 1 ± 0.2, use Michaelis-Menten equation instead. Remember to include a constant offset term in the equation if background subtraction does not move the starting data point to a corrected TR-FRET ratio of nearly 0.

8. Continue data analysis by calculating S/B for every f-S2 concentration. This is done by dividing the ratiometric data of GST-SUMO3-containing sample data by no-GST-SUMO3 sample data. Most successful TR-FRET assays require an assay window or S/B of 2.0 or higher (Fig. 1b). The f-S2 concentration with highest S/B should be chosen for subsequent assays and optimizations, in this case 1 μM was chosen. This concentration is usually within twofold of the EC50 value calculated in **step 7**.

9. Repeat **steps 2** through **8** for the titration of Tb-anti-GST while holding f-S2 at 1 μM (shown in Fig. 1b) (*see* **Note 4**). (Optional) Repeat **steps 2** through **8** for titration of GST-SUMO3 while holding f-S2 at 1 μM and Tb-anti-GST at optimal concentration. While anti-GST antibodies usually show high picomolar affinity, Tb-anti-His would require more His-SUMO3 due to poorer binding affinity.

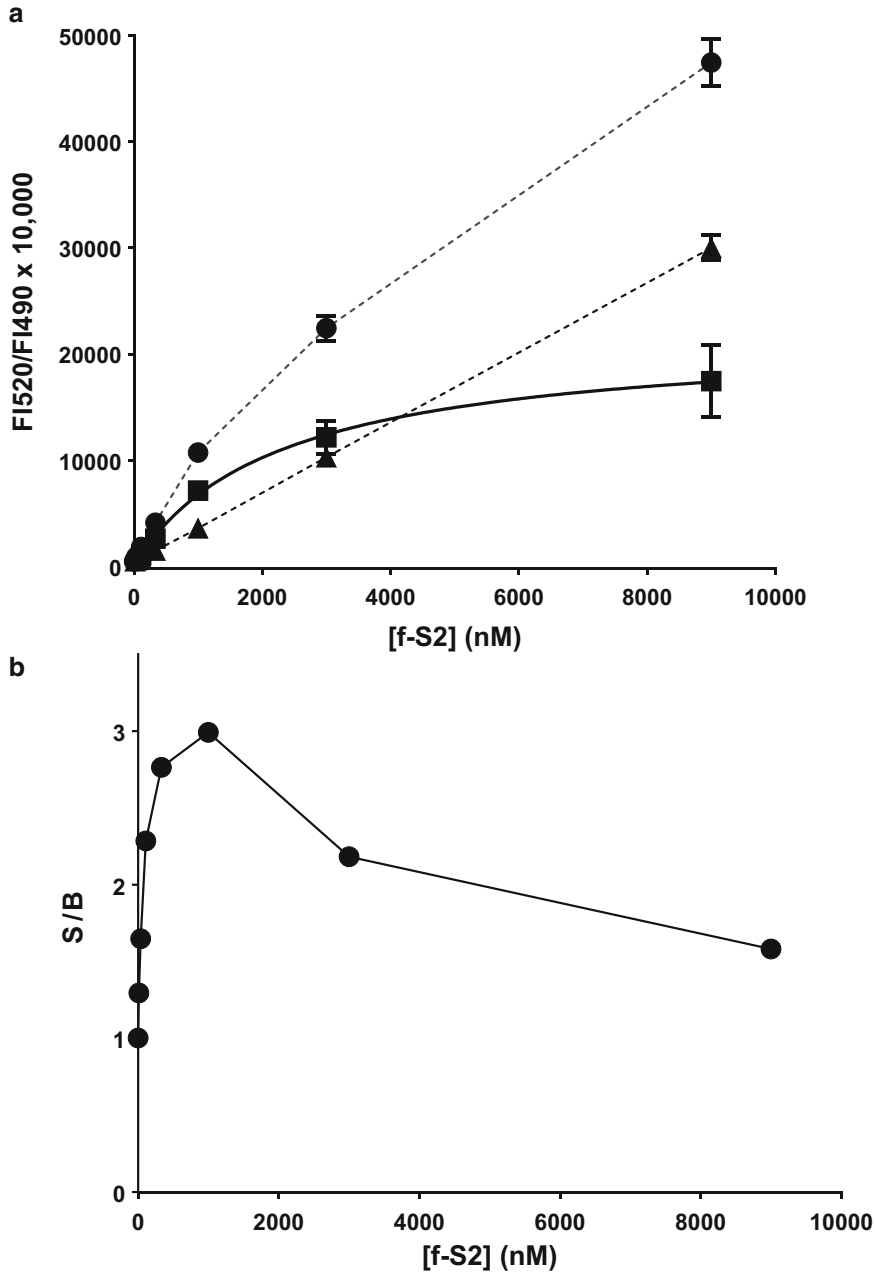

Fig. 1 (**a**) Sample titration of fluorescent peptide. Changes in ratiometric TR-FRET signal, with multiplier of 10,000 applied, are plotted against fluorescein-S2 peptide concentration. No-enzyme background (▲) is subtracted from GST-SUMO3 signal (●), and the background-subtracted value (■) is fitted to Hill equation. Assay window is 22,000 ± 1100, Hill coefficient 0.98 ± 0.057, and EC50 2300 ± 290 nM. (**b**) Sample Signal/Background plot. GST-SUMO3 signal is divided by no-enzyme background to yield Signal/Background (S/B) ratio, presented in line plot. Maximum value is observed at 1 μM of f-S2 peptide.

3.2 Cullin Neddylation Enzymatic Assay

1. Transfer all 240 µl of 1 µM diluted FLAG-SCF solution to well A1 of new intermediate polypropylene plate and perform twofold serial dilutions of 120 µl horizontally (A2, A3, etc.) to achieve 2, 1, 0.5, 0.25, 0.125, 0.0625, 0.03125, and 0 µM FLAG-SCF, using Tb-anti-FLAG/Ubc12 mixed solution to achieve constant Tb-anti-FLAG and Ubc12 concentrations. Then populate the seven rows beneath the first row with 14 µl of each SCF concentration so that a matrix of 8 × 8 is available. Wait 60 min with foil wrap to prevent photobleaching. This is the SCF plate.
2. Transfer all 240 µl of the activated NAE1 solution to well A1 of a new intermediate polypropylene plate and perform twofold serial dilutions of 120 µl vertically (B1, C1, etc.) to achieve 4, 2, 1, 0.5, 0.25, 0.125, 0.06125, 0 µM fluo-Nedd8, using 5 mM ATP solution to achieve constant ATP concentration. Then populate the seven columns to the right of the first column with 14 µl of each fluo-Nedd8 concentration so that a matrix of 8 × 8 is available. Wait 60 min with foil wrap to prevent photobleaching. This is the fluo-Nedd8 plate (*see* **Note 5**).
3. Spin down the fluo-Nedd8 and the SCF intermediate plates at 182 × *g* for 1 min. Use Bravo liquid handler and eight columns of unused P10 tips to aspirate 9 µl from the fluo-Nedd8 plate and dispense 2 µl into quadruplicate wells in the 1536-well assay plate. Repeat with the SCF plate (*see* **Note 6**). Spin down the lidded assay plate.
4. Immediately after spin, read on the PHERAstar plate reader with TR-FRET optical module (ex337/em520/em490) with delay of 100 µs and integration time of 200 µs. Use kinetic mode with 5 min intervals and 120 min total time course.
5. Start the data analysis by plotting ratiometric data (FI 520/FI 490) of acceptor and donor channels. Look for linear regions of the progress curve, in this case closer to 1 h, and calculate the slope for each well. This is proportional to the enzymatic steady-state rate and can be used directly without converting to specific activity or turnover number. Plot fluo-Nedd8 on the *x*-axis. Perform background subtraction by subtracting no-SCF control data from all other data for each fluo-Nedd8 concentration and fit the data to Hill equation (Fig. 2a). If Hill coefficient is 1 ± 0.2, a simple Michaelis-Menten equation would be sufficient. If too much of the protein binding to the Terbium donor is added, in this case FLAG-SCF complex, the "hook effect" may be observed (*see* **Note 7**), represented by a negative linear slope in the plotting equation (Fig. 2b). Choose optimal SCF and fluo-Nedd8 concentrations based on assay window and relative EC50 values (*see* **Note 8**).

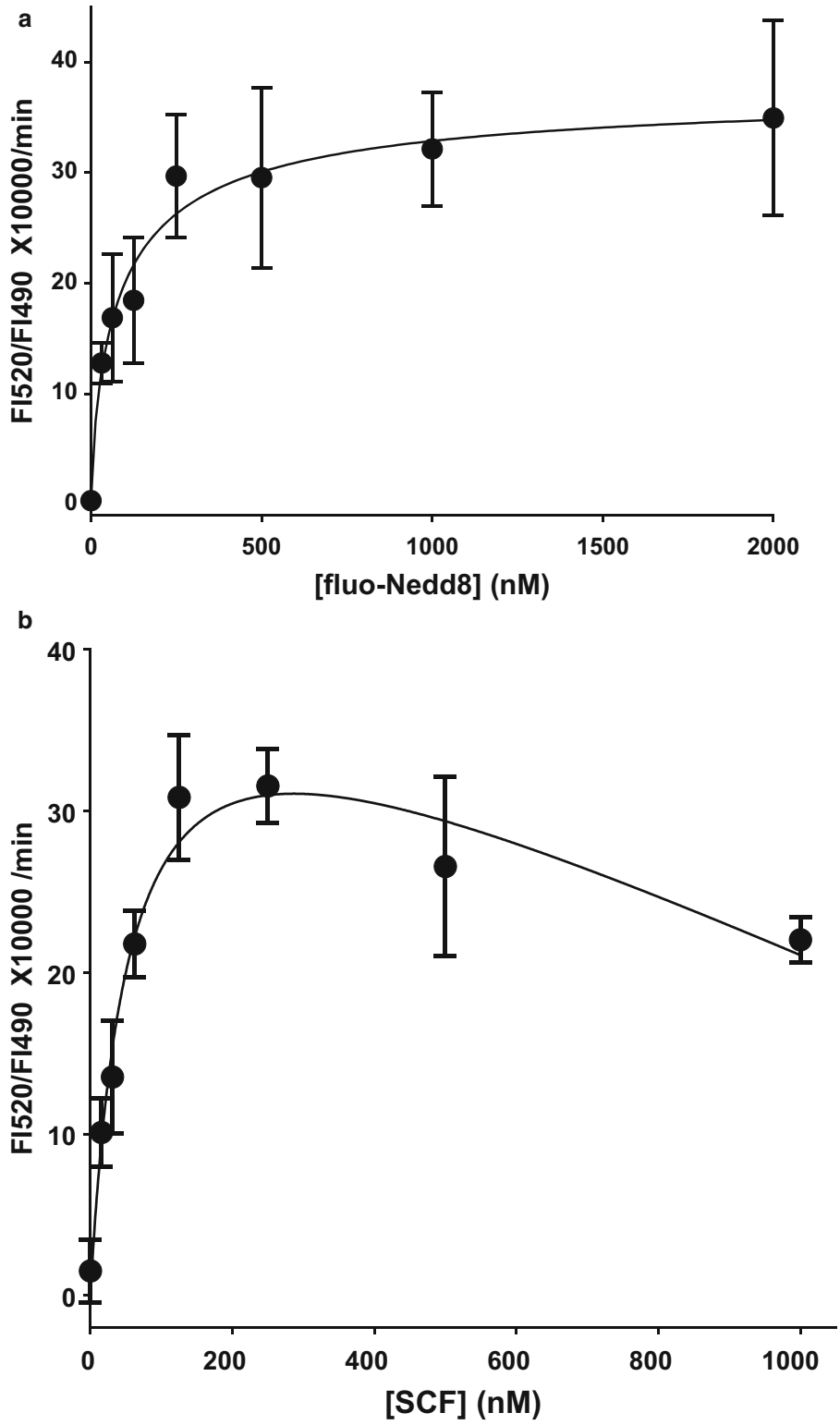

Fig. 2 (**a**) Sample matrix titration of fluo-Nedd8 and cullin complex (FLAG-SCF). Enzymatic rate in terms of ratiometric TR-FRET signal change per unit time, with multiplier of 10,000 applied, are plotted against fluo-Nedd8 concentration. No-SCF background is already subtracted from all data sets, and the background-subtracted value is fitted to Hill equation. Only the 125 nM SCF dataset is shown. Assay window is 37 $\pm$ 5.9,

6. Repeat **steps 2** through **5** for titration of Tb-anti-FLAG and NAE1 while holding FLAG-SCF at 125 nM and fluo-Nedd8 at 180 nM (shown in Fig. 2a, b) (*see* **Note 8**).

4 Notes

1. Many examples of binding assays exploring protein-protein interactions through TR-FRET detection can be found in the PubChem Bioassay section (PubChem AIDs 602429, 631, 2152, etc.). There are also many examples of enzymatic assays utilizing TR-FRET detection of substrate disappearance or product formation in the PubChem Bioassay section (PubChem AIDs 485273, 651699, 588664, etc.).
2. If there are unused wells remaining after dilution, intermediate plates and assay plates can be reused. One or two empty columns should serve as a sufficient spacer to reduce cross-contamination.
3. The 4× GST-SUMO solution, the 2× Tb-anti-GST solution, and the 4× f-S2 solution are mixed and thus diluted, so the final concentrations of protein and peptide reagents in the assay well are less than the concentrations described in Subheading 3.
4. Sometimes, lanthanide labeling efficiency of the anti-GST/His-label antibody can vary and excessive donor antibody may result in higher background values. Thus, the optimal amount of the antibody should be determined experimentally; it could be less than 2 nM final concentration.
5. Although, NAE1 concentration is halved each time a serial dilution occurs; the high ATP and NAE1 concentrations, and the pre-incubation will pre-load NAE1 with fluo-Nedd8 in the first 1-2 min after mixing. The rate-determining step of the overall reaction is controlled by the E2 enzyme Ubc12.
6. The 2× fluo-Nedd8 solution and the 2× SCF solution are mixed and thus diluted, so the final concentrations of protein and peptide reagents in the assay well are ½ the concentrations described in Subheading 3.
7. See PerkinElmer online resource guide for detailed explanation of the Hook effect: http://www.perkinelmer.com/hk/Resources/TechnicalResources/ApplicationSupportKnowledgebase/AlphaLISA-AlphaScreen-no-washassays/hook-effect.xhtml

Fig. 2 (continued) Hill coefficient 0.77 ± 0.27, and EC50 88 ± 41 nM. (**b**) Sample Matrix Titration focusing on SCF. Enzymatic rate in terms of ratiometric TR-FRET signal change per unit time, with multiplier of 10,000 applied, are plotted against FLAG-SCF concentration. The dataset is fitted to Michaelis-Menten equation with negative slope for donor dilution effects. Only the 250 nM fluo-Nedd8 dataset is shown. Assay window is 44 ± 0.008; slope is −0.021 ± 0.00072; and EC50 is 55 ± 0.27 nM

8. No more than 10 % of the substrate should be consumed to maintain steady-state condition. Thus, when the assay window is too small, for example at time = 0 and the end of the linear region of progress curve, an increase in the lowest substrate concentration within the assay would allow more product conversion and thus a larger assay window. Usually, the EC50 or K_m is chosen as the appropriate concentration for substrate concentration in enzymatic activity assays, but twofold EC50 is also acceptable for maximizing the enzymatic rate or assay window. Take into consideration that the EC50 for one substrate may change with the concentration of the second substrate.

Acknowledgments

This work was supported by NIH Roadmap Initiatives grants U54HG003916 and U54HG005033. The protein-protein interactions protocol has been developed in a collaborative project with Dr. Yuan Chen (City of Hope). The enzymatic activity protocol has been developed in collaboration with Dr. Matt Petroski (Sanford-Burnham-Prebys MDI).

References

1. Cardullo RA (2013) Theoretical principles and practical considerations for fluorescence resonance energy transfer microscopy. Methods Cell Biol 114:441–456
2. Carlson CB, Horton RA, Vogel KW (2009) A toolbox approach to high-throughput TR-FRET-based SUMOylation and DeSUMOylation assays. Assay Drug Dev Technol 7 (4):348–355
3. Degorce F et al (2009) HTRF: a technology tailored for drug discovery - a review of theoretical aspects and recent applications. Curr Chem Genomics 3:22–32
4. Zhang WG, Shor B, Yu K (2006) Identification and characterization of a constitutively T-loop phosphorylated and active recombinant S6K1: expression, purification, and enzymatic studies in a high capacity non-radioactive TR-FRET Lance assay. Protein Expr Purif 46(2):414–420
5. Madiraju C et al (2012) TR-FRET-based high-throughput screening assay for identification of UBC13 inhibitors. J Biomol Screen 17 (2):163–176
6. Fernandez-Duenas V et al (2012) Fluorescence resonance energy transfer-based technologies in the study of protein-protein interactions at the cell surface. Methods 57 (4):467–472
7. Alontaga AY et al (2015) Design of high-throughput screening assays and identification of a SUMO1-specific small molecule chemotype targeting the SUMO-interacting motif-binding surface. ACS Comb Sci 17 (4):239–246
8. Namanja AT et al (2012) Insights into high affinity small ubiquitin-like modifier (SUMO) recognition by SUMO-interacting motifs (SIMs) revealed by a combination of NMR and peptide array analysis. J Biol Chem 287 (5):3231–3240
9. Song J et al (2005) Small ubiquitin-like modifier (SUMO) recognition of a SUMO binding motif: a reversal of the bound orientation. J Biol Chem 280(48):40122–40129
10. Petroski MD (2010) Mechanism-based neddylation inhibitor. Chem Biol 17(1):6–8
11. Toth JI et al (2012) A gatekeeper residue for NEDD8-activating enzyme inhibition by MLN4924. Cell Rep 1(4):309–316

Chapter 9

Protein Kinase Selectivity Profiling Using Microfluid Mobility Shift Assays

Peter Drueckes

Abstract

Biochemical selectivity profiling is an integral part of early drug development. Typically compounds from optimization phase are regularly tested for off-target activities within or across target families. This article presents workflow and critical aspects of biochemical protein kinase profiling based on microfluidic mobility shift assays.

Key words Kinase, Selectivity profiling, Microfluidic mobility shift assay, Compound preparation

1 Introduction

Protein kinases belong to the most important families of pharmaceutical targets. However, it took several scientific break-through, from the discovery of protein phosphorylation as regulatory mechanism [1, 2], to become a highly investigated class of drug targets. Despite initial doubts about the general "druggability" of this target class [3], several inhibitors had been described [4] and helped to better understand the roles and functions of kinases. Finally, the clinical success and subsequent approval of Gleevec (imatinib) in 2001 demonstrated protein kinases as valid drug targets. By now, 28 small-molecule protein kinase inhibitors have been approved by the FDA and many more have entered clinical studies [3, 5].

One hallmark of protein kinases as target family is that they share a highly conserved binding site for ATP. While this provides a well-defined pocket that can be targeted and explored by medicinal chemistry, the high degree of structural similarity between different family members also raises concerns about the selectivity of inhibitors and thus, the safety of drug candidates. This question is addressed throughout the development of kinase inhibitors and starts early in the drug development process, typically by testing

William P. Janzen (ed.), *High Throughput Screening: Methods and Protocols*, Methods in Molecular Biology, vol. 1439,
DOI 10.1007/978-1-4939-3673-1_9,

candidate compounds in panels of biochemical kinase assays. The size, composition, and assay technology of this selectivity testing can vary largely depending on the purpose, resources available, and stage in drug discovery. Many of these assays are also available as service by CROs, offering additional options and flexibility for groups with limited internal resources [6].

Biochemical kinase profiling became a quasi-standard within the pharmaceutical industry. Still, it needs to be clear that, as it is only one part of integrated drug discovery efforts, the value of profiling data has to be seen in the context of other information, such as data from cellular assays and pharmacokinetics.

Hand in hand with the growing interest in protein kinases, the number and variety of available tools and assay technologies to study kinases have increased. To provide a comprehensive overview of the available methods is out of scope for this article. However, several excellent reviews have been published on the topic [7, 8].

While, most available assay technologies can be used for profiling, some technologies are better suited for profiling, depending on assay conditions and reagent or reader requirements. Profiling usually involves parallel testing the same compounds in several assays, typically using different kinases. The objective for running those assays is to provide data that are able to guide the medicinal chemistry efforts by predicting cellular potency and selectivity. While it is not possible to simulate the full complexity of a cellular environment in single biochemical readouts, relevant cellular assays can be used as guidance during assay development and optimization.

Features expected from any assay technology and particularly required for profiling are robustness and flexibility with regard to assay conditions. Profiling assays can run for extended periods and are expected to deliver comparable results over time. For monitoring purpose, it is recommended to run reference compounds for each assay to control plate-to-plate variability and trends over time. Setting up kinase panels for compound profiling requires sufficient flexibility with regard to the assay conditions to allow biologically relevant assays and at the same time keep overall similar and defined conditions that allow comparison and interpretation of the results from different assays. Therefore, the number of specific reagents needed for individual assays (e.g., antibodies) should be minimized. A much discussed topic is the choice of the ATP concentration. A widely applied approach is to adjust the ATP concentration in each assay to the individual apparent K_M of the enzyme under the chosen conditions. This leads to standardized assay sensitivity toward inhibitors across all assays. Alternatively, the preference maybe to run all assays at rather high ATP concentrations in order to simulate competition closer to the estimated ATP concentration in cells. However, some assay technologies have limitations with regard to the tolerated ATP concentration.

Different preferences and different prerequisites lead to different compromises and setups, and the chosen conditions must be taken into account when interpreting the results.

Aspects of kinase profiling not covered in the article are for example potency and selectivity assessment with regard to different kinase conformations, as well as "kinetic profiling" also looking at on- and off-rates of inhibitors [3, 9, 10].

We have chosen to use a microfluidic mobility shift technology, originally developed by Caliper technologies [11] (now part of PerkinElmer). Two types of readers are available in our profiling laboratory: the LC3000, a stand-alone reader with plate stackers and environmental controls, and the EZ-reader II, a smaller desktop instrument for single plates integrated in small lab automation systems.

The basic assay principle of this technology is based on the separation of phosphorylated and unphosphorylated peptides in an electric field due to their charge difference (more precisely charge over mass z/m difference) introduced by the kinase. Typically, kinase reactions are performed in regular 384 well microplates. This can be done with multiple plates on any automated liquid handling system. Kinase reactions are stopped and transferred to the reader (endpoint determination), or run continuously with the plate in the reader and repeated sampling (kinetic mode). The separation and detection are done in a microfluidic chip with 4 or 12 sippers (Fig. 1). For sampling, the plate is placed underneath the chip and lifted up until the sippers are submerged in the assay solution in the plate wells. A small volume (in the nanoliter range) is taken up by the sippers and transported into the flow cell of the chip. The transport and separation of molecules of

Fig. 1 Image of a 12-sipper Labchip

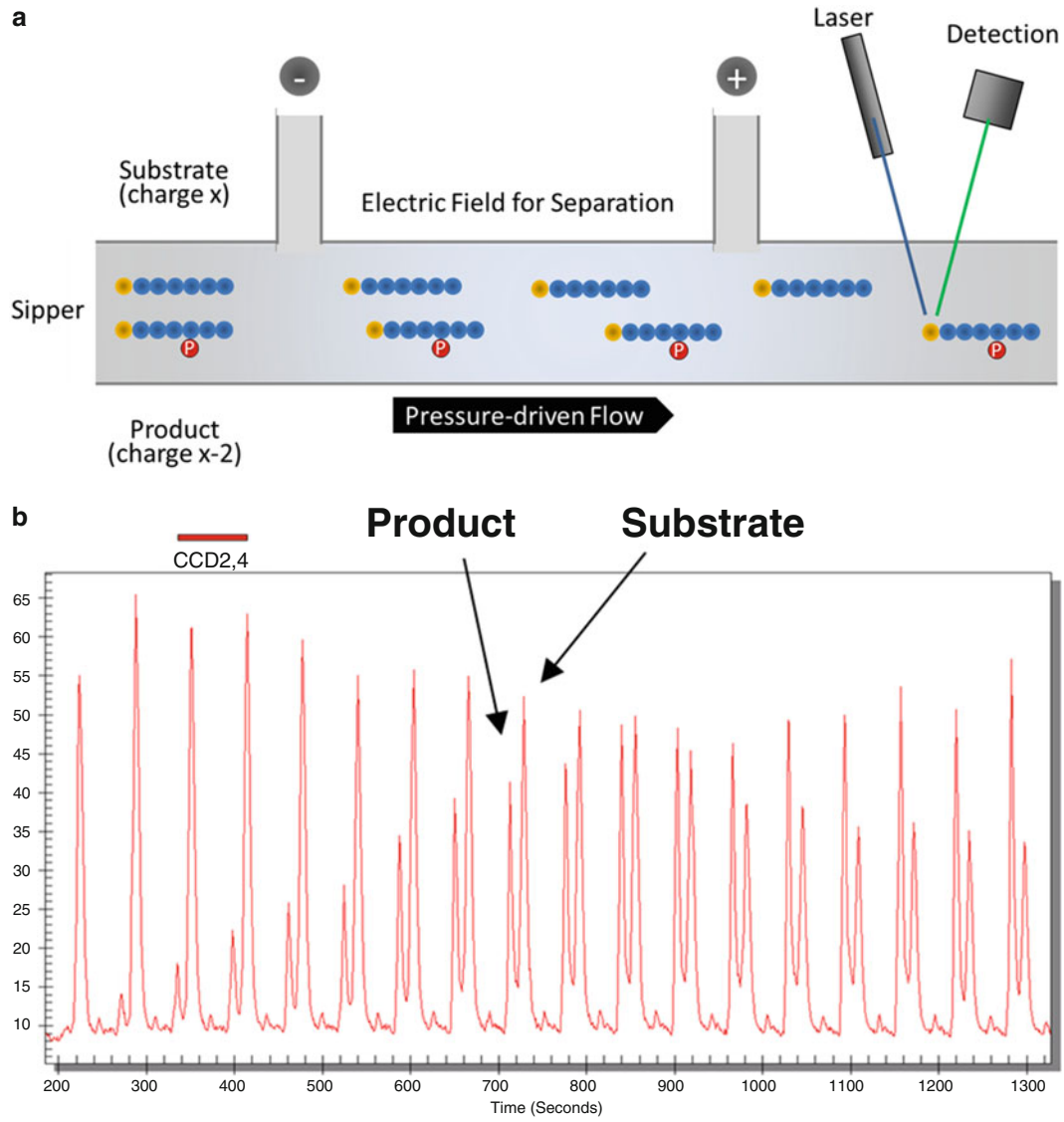

Fig. 2 (**a**) Illustration of flow, separation, and detection of fluorescently labeled peptides in a microfluidic channel. Peptide substrates (*blue*) carrying a fluorescent label (*yellow*) are transported through the microfluidic system by constant flow. An electric field is applied to one part of the capillaries separating molecules with different charge/mass ratios, e.g., phosphorylated vs. unphosphorylated peptides. Each peptide is detected by laser- or LED-induced fluorescence. (**b**) Image of the detection output of repeated sampling from a kinase reaction (kinetic mode) showing the increase of the product peak (*left peak*) and decrease of the substrate peak (*right peak*)

different z/m ratios is achieved by a combination of continuous flow and electric field. The peptides used for kinase assays typically carry a fluorescent tag and their migration is monitored by laser excitation. For each well, the intensities of product peak (phospho peptide) and substrate peak (unphosphorylated peptide) are

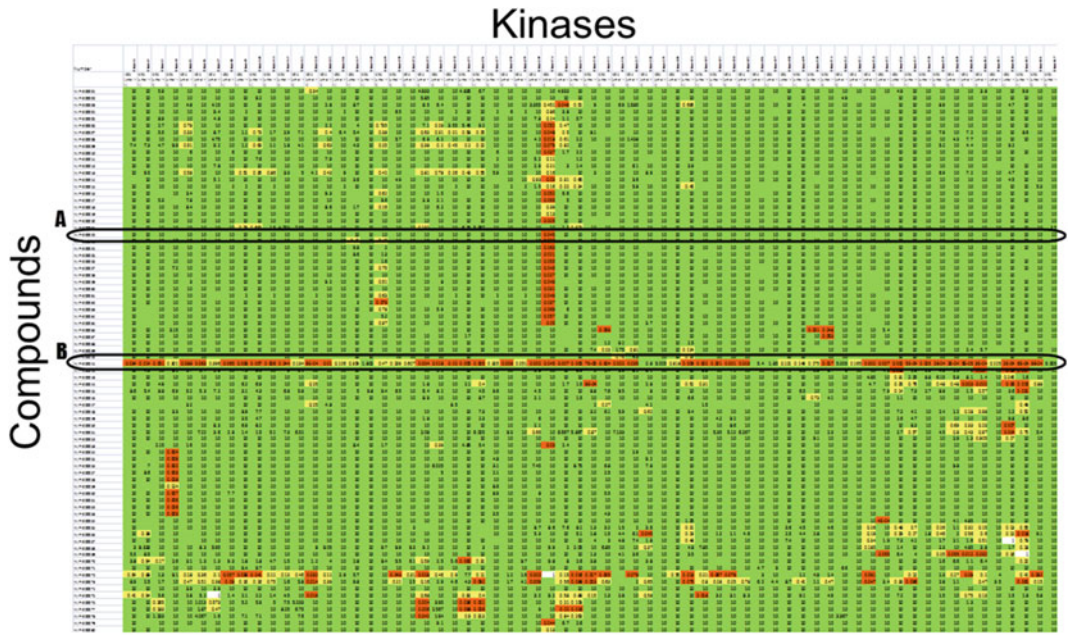

Fig. 3 Example for a heat map visualization showing examples for specific inhibitors (**a**) and promiscuous inhibitors (**b**). IC_{50} values representing high potency are colored in *red*, IC_{50} values representing low or no potency and colored in *green*

determined. The turnover of the enzymatic kinase reaction is expressed as product-sum ratio ($p/(p + s)$) (Fig. 2a, b) [12].

We found the microfluidic mobility shift technology well suited for large-scale profiling of kinase inhibitors. The main advantages of the used method are the robustness of this assay, achieved by the separation and ratiometric quantitation of product and substrate, the fact that no further reagents are needed and the possibility of running continuous kinetic measurements. On the other hand, one drawback of the method is the limitation to peptide substrates that may not be available or feasible for each kinase.

Larger data sets as generated from testing many compounds across broad kinase panels can be visualized as so called "heat maps." Assay data are organized in tables assay ID vs. compound ID with color coded potency data. This visualization supports, e.g., the identification of specific (A) vs. promiscuous inhibitors (B) (Fig. 3).

Continued running of compounds across enzymatic panels under defined assay conditions quickly generates consistent, large data sets that can serve as valuable source for data mining. Several groups have published in-silico approaches trying to identify general principles for the explanation and better prediction of kinase inhibitor selectivity [13–15].

2 Materials

1. Kinases: Many kinases can be obtained from commercial sources. They can carry tags for affinity purification, however, it is preferred to use proteins with cleaved tags in order to avoid potential interference with, e.g., activity or activation. Some kinases with special features, e.g., a defined phosphorylation state were prepared in-house.
2. Substrates: Substrate peptides were usually ordered as custom synthesis from external vendors with either Fluorescein isothiocyanate (FITC) or 5-Carboxyfluorescein (5FAM) dye, joined via an aminohexanoic (Ahx) linker to the N- or C-terminus of the peptide. Some substrates may require additional modifications, such as phospho-amino acids for "pre-phosphorylation." Peptides containing cysteine or methionine are sensitive to oxidation and therefore impurities. Those amino acids may be substituted on a case by case basis, if no impact on biological activity is apparent (*see* **Notes 1**–**3**).
3. Compounds: Compounds were usually received as 10 mM stock solutions in DMSO. Test solutions were prepared by serial dilutions of the stocks in 90 % DMSO to cover the desired concentration range (*see* **Note 4**). Compounds were typically tested as 8-point dilutions with 10 μM as highest tested concentration. 50 nl of the prediluted compound solutions were transferred to the corresponding wells of the empty assay plate prior to addition of assay solutions using an Echo 555 (Labcyte).
4. Assay buffer: 50 mM HEPES, pH 7.5, 1 mM DTT, 0.02 % Tween 20, 0.02 % BSA, 10 mM beta-glycerophosphate, 10 μM sodium orthovanadate. The concentrations for the kinase, ATP, and peptide substrate, as well as for $MgCl_2$ and $MnCl_2$ were adjusted to conditions optimal for the individual kinase. ATP concentrations were adjusted to the apparent K_M for ATP for the respective kinase. Assay concentrations for the peptide substrate were adjusted to the apparent K_M for the substrate peptide for the respective kinase if lower than 2 μM or set to 2 μM as the maximal arbitrary concentrations.
5. 2× enzyme mix: 2× assay concentration of kinase in 50 mM HEPES, pH 7.5, 1 mM DTT, 0.02 % Tween 20, 0.02 % BSA, 10 mM beta-glycerophosphate, 10 μM sodium orthovanadate.
6. 2× substrate mix: 2× assay concentration of peptide, ATP, and $MgCl_2$/$MnCl_2$ in 50 mM HEPES, pH 7.5, 1 mM DTT, 0.02 % Tween 20, 0.02 % BSA, 10 mM beta-glycerophosphate, 10 μM sodium orthovanadate.

7. Stop buffer: 100 mM HEPES pH 7.5, 5 % DMSO, 10 mM EDTA, and 0.015 % Brij 35.
8. Run Buffer: 100 mM HEPES pH 7.5, 5 % DMSO, 10 mM EDTA, and 0.015 % Brij 35, 0.1 % PerkinElmer coating reagent CR-3, 50 μM PerkinElmer coating reagent CR-8. Typically, 200 ml of running buffer was prepared and supplied in the appropriate reservoir of the reader for circulation in the chip and system.
9. Wash Buffer: 0.001 % Pluronic F68 and 10 % Isopropanol in Milli-Q water.
10. Plates: Assays are performed in black low volume 384 well plates. Compound dilutions were done in V-bottom 96-well polypropylene plates. 384-well polypropylene plates were used for compound master plates.
11. Reader and chips: Plates with terminated kinase reactions were read in either a Labchip 3000 system or in an EZ-reader II. Both instruments were loaded with a Labchip 12-sipper chip allowing the analysis of 12 samples in parallel. Individual separation protocols were developed for each substrate peptide and optimized for the best combination of peak resolution and reading time (*see* **Notes 1**–**3**).
12. Automation: All assays and protocols can be done also manually; however, the majority of profiling assays are done on automated liquid handling systems. A typical setup consists of a 16-channel Nanodrop express (Innovadyne) for contact-free reagent dispensing, an incubator STX40ICBT (Liconic Instruments), and a Twister II robotic arm (Perkin Elmer).

3 Methods

1. Compound Preparation: All containers used for handling compounds including matrix tubes and plates were barcoded and registered in internal databases to allow status tracking at any time. Compounds were typically received as 10 mM stock solutions in 100 % DMSO in 1.4 ml Matrix tubes. Tubes were stored at 2 °C or at −20 °C for longer storage.
   (a) Pre-dilution plates: Four 96-well polypropylene plates were used to prepare serial dilutions of the test compounds. Each plate contained ten test compounds on the plate positions A1-A10, one standard compound at A11, and one DMSO control at A12. Rows B to H were used to prepare serial dilutions of the test compounds in 90 % (v/v) DMSO, by applying either a semi-log or 1:5 dilution depending on the desired concentration range.

(b) Master plates: 100 μl of all individual compound solutions including standard compound and controls of the 4 "pre-dilution plates" were transferred into one 384 "master plate." The final layout of the plate contains 8-point serial dilutions for 40 test compounds in the columns 1–20, four 8-point serial dilutions reference compounds in the columns 21 and 22, and DMSO controls in the columns 23 and 24. The DMSO controls in the last two columns are used for high and low controls of the assay.

(c) Assay plates: Identical "assay plates" were prepared by dispensing 50 nl of compound solutions from the "master plates" into empty 384-well "assay plates" with an Echo 555 workstation. Other volumes may be dispensed for different concentration ranges. Typically, one assay plate is prepared for each enzyme/assay in the panel and one kinase is run per plate. Assay plates with pre-dispensed compound solutions are considered "ready-to-use," however, can be stored over night at 4 °C if sealed or lidded. Each plate is used for one kinase assay.

2. Manual Assays: The manual procedure is used for assay development and small campaigns with a limited number of targets. Pipetting steps are performed manually with electronic hand pipettes. Incubations for endpoint determinations were performed in an incubator at 30 °C and plates subsequently transferred to a PerkinElmer LC3000 for reading. For kinetic measurements, plates were incubated in the PerkinElmer LC3000 workstation. Kinase reactions were prepared in 384 standard volume plates by the following sequence:

   (a) 0.1 μl Compound.

   (b) 9 μl 2× peptide/ATP solution.

   (c) 9 μl 2× enzyme solution.

   (d) Incubate for 60 min at 30 °C.

   (e) 70 μl stop/run buffer.

3. Automated Assays: The automated procedure is used for in-vitro kinase panel profiling with higher throughput. Compared to the manual procedure, the pipetting volumes were reduced by 50 % or modified according to automation requirements. Incubation time and temperature were kept identical. Liquid handling and incubation steps were done on a PerkinElmer Staccato workstation equipped with an Innovadyne Nanodrop Express. Between pipetting steps, tips were cleaned in wash cycles using wash buffer. Plates with terminated kinase reactions were transferred to the PerkinElmer LC3000

workstations for reading. Kinase reactions were prepared in 384 low volume plates by the following sequence:

(a) 0.05 µl Compound.

(b) +4.5 µl 2× peptide/ATP solution.

(c) +4.5 µl 2× enzyme solution.

(d) Incubate for 60 min at 30 °C.

(e) +16 µl stop/run buffer.

4. Assay Development: A typical assay development consists of several steps and helps to define and optimize assay parameters such as enzyme concentration, substrate concentrations for ATP and peptide, and buffer composition. For automated testing of compound solutions, it is also advisable to test for DMSO tolerance and protein stability over time. Some assay parameters are kept constant, if possible, for reasons of automation and comparability. In our setup, those are for example, reaction time and temperature, buffer pH, detergent. It should, however, always be kept in mind that compromising on important biological parameters should be avoided in order to maintain biological relevance.

   Except for the titration of Mg/Mn, all assays during assay development are typically done manually in kinetic mode. This ensures the linearity of the reaction and is particularly relevant with regard to stability and Michaelis-Menten kinetics.

   (a) Enzyme Titration: To determine the necessary enzyme concentration for further experiments, a serial dilution of the kinase is done in a standard buffer containing 0.5 mM ATP and 10 mM $MgCl_2$. This is usually done as manual assay in kinetic mode. The aim is to use the lowest possible enzyme concentration as it determines the theoretical sensitivity of the assay. A reasonable starting point for further experiments is the enzyme concentration achieving 10–20 % turnover in 60 min.

   (b) Mg/Mn Titration: Protein kinases depend on the presence on bivalent cations for the coordination of ATP. Therefore, kinase assays usually contain either Mg^{2+} or Mn^{2+} or a mixture of both. The best concentration for a given kinase is determined by running assays with a 2-dimensional dilution of $MgCl_2$ vs. $MnCl_2$ at 0–10 mM (Fig. 4). Whenever possible, the preference should be given to $MgCl_2$ alone for physiological reasons.

   (c) K_M Determinations: Once the final buffer conditions have been defined, the apparent Michaelis-Menten constants for the substrates are determined under those conditions. First, a twofold serial dilution of ATP is tested at 2 µM constant peptide concentration and the ATP concentration

		1	2	3	4	5	6	7	8	9	10	11	12	13	14	15	16
	$MgCl_2$ mM →	0	1	2	3	4	5	6	7	8	9	10	12	14	16	18	20
A	$MnCl_2$ mM ↓ 0	3	5	16	24	32	35	36	36	34	32	30	24	20	16	13	11
B	1	5	24	53	65	64	63	65	65	60	57	53	48	39	32	24	21
C	2	16	54	69	70	69	65	66	65	64	62	58	46	46	42	36	34
D	3	49	73	69	62	59	55	54	52	49	46	43	38	35	31	29	27
E	4	72	73	67	52	49	47	48	48	43	40	38	35	30	32	30	28
F	5	56	61	70	58	45	40	39	36	32	32	32	31	29	30	27	26
G	6	37	59	77	65	55	46	49	51	47	45	44	41	35	36	37	32
H	7	64	68	53	42	37	34	33	36	35	31	32	32	29	33	31	31
I	8	42	50	38	35	33	32	32	33	31	31	33	33	34	34	34	34
J	9	30	35	32	30	30	30	33	32	34	33	33	34	33	34	33	34
K	10	23	25	27	27	30	31	31	32	32	34	34	34	35	36	36	38
L	12	21	21	24	25	27	29	29	35	32	34	36	37	37	38	41	39
M	14	18	22	22	22	26	25	30	34	35	35	33	37	40	40	42	40
N	16	18	22	24	26	28	27	29	31	30	31	34	37	41	43	43	37
O	18	16	18	23	23	25	30	29	33	34	32	34	37	40	42	39	40
P	20	19	22	23	26	26	29	30	34	35	33	35	38	40	42	39	42

Fig. 4 Two-dimensional Titration of $MgCl_2$ vs. $MnCl_2$. Increasing concentrations of $MgCl_2$ and $MnCl_2$ and pipetted into the columns and rows of a 384-well micro plate generating mixtures of different Mg/Mn ratios. Buffer, ATP, peptide substrate, and kinase are added to start the kinase reaction. After 60 min incubation at 30 °C, the reactions are stopped and the plate analyzed in the reader. Enzymatic activity at the respective conditions is shown as percent turnover

is determined leading to half-maximal activity. Second, a twofold serial dilution of the peptide is tested at the previously determined K_M for ATP. Both titrations are done in kinetic mode to ensure the linearity of kinase reaction over time under the chosen conditions (Fig. 5). It should be noted that the analysis of the peptide titration is more difficult, since using variable concentrations of the labeled peptide leads also to variable peak sizes for substrate and product in the detection.

(d) DMSO Sensitivity: Once the assay conditions have been defined, the kinase reaction is tested under increasing concentration of DMSO (Fig. 6). This test is again performed in kinetic mode, to ensure that the enzyme reaction is stable over time at the desired DMSO concentration. A high sensitivity of an assay to DMSO can limit the maximal compound concentration that can be tested.

5. Data Analysis.

(a) Kinetic Data: Product-sum-ratios from different time points were exported from the reader software and imported to GraphPad Prism (Version 6.04; GraphPad software). Kinetics for, e.g., different enzyme or substrate concentrations were analyzed by linear regression. Obtained slopes are used as read-out for enzyme activity. Apparent K_M values for substrates were determined by plotting slopes vs. substrate concentration and analyzed in GraphPad Prism by nonlinear regression using the equation (Eq. 1):

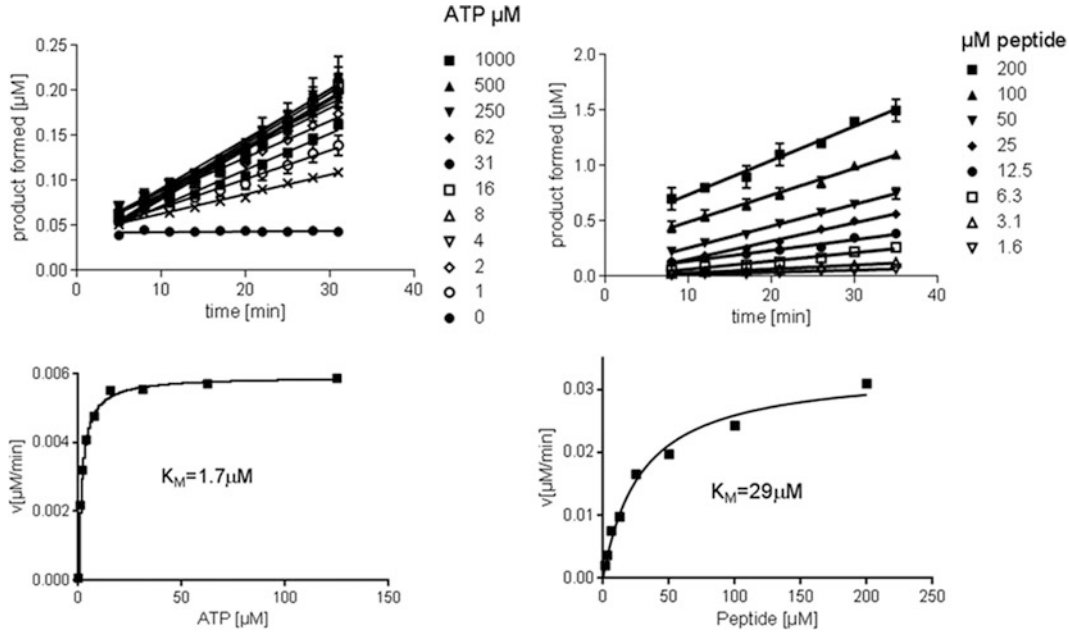

Fig. 5 Example for the determination of the apparent K_M values for ATP and peptide. *Upper panel* shows the linear kinetics of kinase reactions at different substrate concentrations (*left*: ATP, *right*: peptide). The *lower panel* shows the nonlinear fitting of the resulting slopes and the resulting K_M values

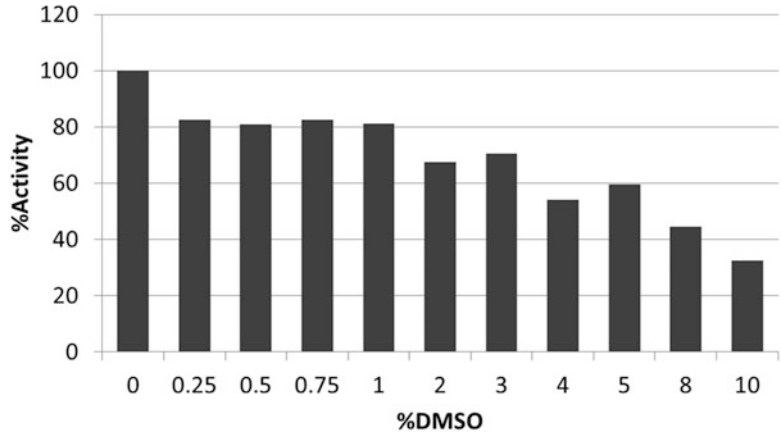

Fig. 6 Example for the determination of the DMSO sensitivity. Different DMSO concentrations are tested in kinetic mode and the slopes are determined. %Activity at different DMSO concentrations is calculated relative to 0% DMSO set to 100% Activity

$$V = V_{\max}\tilde{n}[S]/([S] + K_M) \quad (1)$$

(b) IC_{50} determination of kinase inhibitors: Product-sum-ratios from endpoint determinations were exported from

the reader software and converted to percent inhibition using the high and low controls as reference (Eq. 2).

$$\%\text{inh} = -100 \times \left(\text{PSR}_{\text{sample}} - \text{PSR}_{\text{LC}}\right)/\left(\text{PSR}_{\text{HC}} - \text{PSR}_{\text{LC}}\right) \quad (2)$$

PSR: product-sum ratio $p/(p + s)$.

LC: low control.

HC: high control.

IC_{50} values were calculated, using the standard Novartis in-house assay data analysis software (Helios software application, Novartis Institutes for BioMedical Research, unpublished) using the methods described by Normolle, Formenko et al., Sebaugh, Kelly et al., and Kahm et al. [16–20] (*see* **Notes 5** and **6**).

c. Assay quality and consistency was monitored by calculating Z' as plate-based quality parameter [21] and reference inhibitors on each plate (Fig. 7a, b) (*see* **Note 7**). Z' values were calculated according to Eq. 3:

$$Z' = 1 - \left(3 \times \left(\text{SD}_{\text{HC}} + \text{SD}_{\text{LC}}\right)/\left(\text{MEAN}_{\text{HC}} - \text{MEAN}_{\text{LC}}\right)\right) \quad (3)$$

SD: standard deviation.

MEAN: arithmetic mean.

LC: low control.

HC: high control.

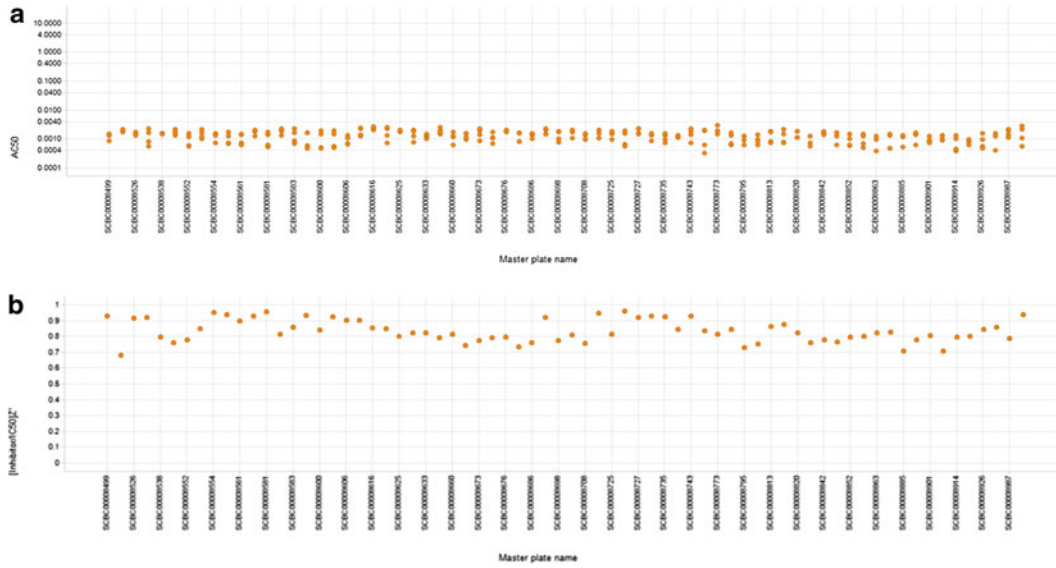

Fig. 7 Example for QC monitoring of assay plates from one kinase assay. The data are taken from a period of about 4 months. Panel (**a**) shows IC_{50} values of the reference compound staurosporine across several assay plates. Panel (**b**) shows the Z'-values for the same plates

4 Notes

1. It is advisable to order the labeled substrate peptides HPLC purified at the highest possible purity, e.g., ≥90 %. Problems can arise, if even small contaminants of 10 % or less that also carry the fluorescent label co-migrate with the product peak. If it is not possible to separate those two peaks by adapting the separation conditions, this will have a negative impact on the minimal turnover, necessary for robust determination of the product peak.
2. Since the separation of substrate and product (unphosphorylated vs. phosphorylated peptide) is controlled by the z/m ratio, size and net charge of the substrate peptides should be considered during substrate design. Smaller peptides are preferable over large ones and good net-charges for the substrate are close to plus one or zero.
3. Multiple phosphorylation sites should be avoided, since this could lead to more than one substrate peak and interfere with the analysis.
4. Compound preparation has a big impact on assay quality. It is recommended to perform all compound dilutions in 90–100 % DMSO in order to avoid precipitations in intermediate DMSO/water mixtures. Dispensing of compounds directly from DMSO solutions might require low-volume dispensing technologies, such as the Labcyte Echo or the Hamilton Hummingbird, to keep the final DMSO concentration within the determined DMSO tolerance of the assay. 100 % DMSO solutions are prone to water uptake and require additional measures such as environmental controls or lidded containers. Use of 90 % DMSO limits further uptake of water and provides a stable condition for compound dilutions.
5. The specific details of all assays are captured in an in-house assay registration database, linking the reported results to the applied assay conditions and allowing a better interpretation and understanding of the data.
6. Single point vs. IC50: Since potencies of individual inhibitors often vary between different kinases, compounds are usually tested as dose-responses (yielding IC_{50} values for each compound) to allow better comparison than percent inhibition at a single concentration (Fig. 8). For large sets of compounds, it can be more economically to pretest at a single concentration (e.g., 10 μM) and retest only active compounds as dose response.

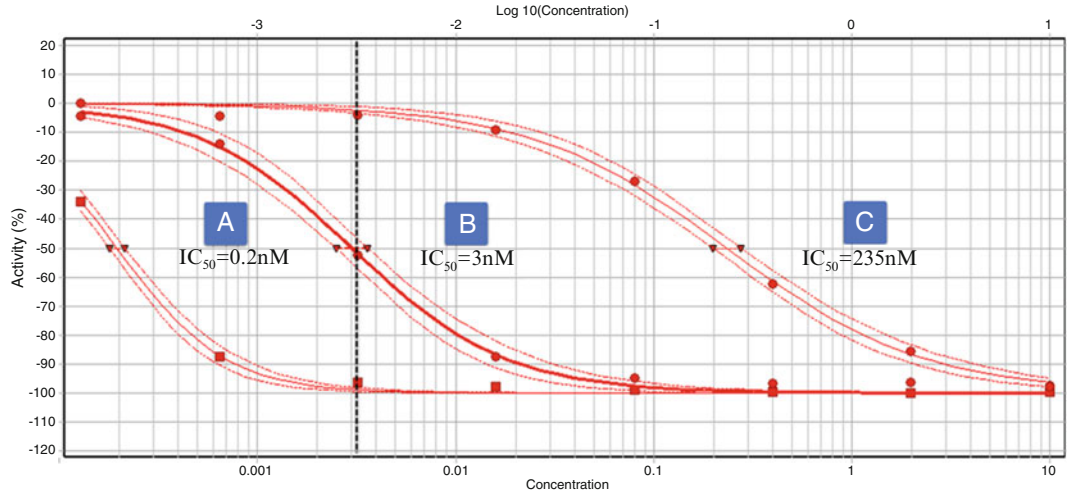

Fig. 8 Fitted dose–response curves for staurosporine tested with three different kinases, with IC_{50} values of 0.2, 3, and 235 nM. The respective %-inhibition values for single point testing at, e.g., 3 nM were −96, −53, and −4 %. Single point testing at 100 nM or higher would not have distinguished between kinase A and B

7. High and low controls: High controls (maximal enzymatic activity) contain typically all assay reagents as in the other wells, but only DMSO instead of a compound solution. Negative controls (no enzymatic activity) can be achieved by omitting the kinase. However, we prefer to use all reagents including kinase with pre-dispensed EDTA stop solution.

Acknowledgment

I would like to thank Shin Numao and Patrik Roethlisberger for their helpful input to the manuscript. I would like to thank Joerg Trappe for suggesting and encouraging the drafting of this manuscript.

References

1. Fischer EH, Krebs EG (1955) Conversion of phosphorylase b to phosphorylase a in muscle extracts. J Biol Chem 216:121–132
2. Krebs EG, Kent AB, Fischer EH (1958) The muscle phosphorylase b kinase reaction. J Biol Chem 231:73–83
3. Klebl B, Müller G, Hamacher M (2011) Protein kinases as drug targets. Methods and principles in medicinal chemistry, vol 49. Wiley, New York, NY
4. Cohen P (2002) Protein kinases - the major drug targets of the twenty-first century? Nat Rev Drug Discov 1:309–315
5. Wu P, Nielsen ET, Clausen MH (2015) FDA-approved small-molecule kinase inhibitors. Trends Pharmacol Sci 36(7):422–439
6. Comley J (2013) Outsourced kinase profiling services - adding value to in-house kinase programmes. Drug Discov World Fall 2013:26–45
7. Ma H, Deacon S, Horiuchi K (2008) The challenge of selecting protein kinase assays for lead discovery optimization. Exp Opin Drug Discov 3(6):607–621
8. Li H (2009) Review of biochemical assays for protein kinase drug discovery. Trends Bio/Pharmaceutical Ind 5(1):24–32

9. Chène P (2008) Challenges in design of biochemical assays for the identification of small molecules to target multiple conformations of protein kinases. Drug Discov Today 13(11/12):522–529
10. Heedmann B, Klumpp M (2015) Screening for inhibitors of kinase autophosphorylation. In: Janzen WP (ed) High throughput screening: methods and protocols, 3rd edn. Springer, New York, NY
11. Cohen CB, Chin-Dixon E, Jeong S, Nikiforov TT (1999) A microchip-based enzyme assay for protein kinase A. Anal Biochem 273:89–97
12. Perrin D, Frémaux C, Shutes A (2010) Capillary microfluidic electrophoretic mobility shift assays: application to enzymatic assays in drug discovery. Exp Opin Drug Discov 5(1):51–61
13. Miletti F, Hermann JC (2012) Targeted kinase selectivity from kinase profiling data. Med Chem Lett 3:383–386
14. Niijima S, Shiraishi A, Okuno Y (2012) Dissecting kinase profiling data to predict activity and understand cross-reactivity of kinase inhibitors. J Chem Inf Model 52:901–912
15. Jacoby E, Tresadern G, Bembenek S, Wroblowski B, Buyck C, Neef J-M, Rassokhin D, Poncelet A, Hunt J, van Vlijmen H (2015) Extending kinome coverage by analysis of kinase inhibitor broad profiling data. Drug Discov Today 20(6):652–658
16. Normolle DP (1993) An algorithm for robust non-linear analysis of radioimmunoassay and other bioassays. Stat Med 12:2025–2042
17. Formenko I, Durst M, Balaban D (2006) Robust Regression for high-throughput screening. Comput Methods Programs Biomed 82:31–37
18. Sebaugh JL (2011) Guidelines for accurate EC50/IC50 estimation. Pharm Stat 10:128–134. doi:10.1002/pst.426, http://onlinelibrary.wiley.com/doi/10.1002/pst.426/pdf
19. Kelly C, Rice J (1990) Monotone smoothing with application to dose-response curves and the assessment of synergism. Biometrics 46(4):1071–1085
20. Kahm M, Hasenbrink G, Lichtenberg-Frate H, Ludwig J, Kschischo M (2010) grofit: fitting biological growth curves with R. J Stat Softw 33(7):1–21
21. Zhang JH, Chung TDY, Oldenburg KR (1999) A simple statistical parameter for use in evaluation and validation of high throughput screening assays. J Biomol Screen 4:67–73

Chapter 10

Screening for Inhibitors of Kinase Autophosphorylation

Bianca Heedmann and Martin Klumpp

Abstract

Autophosphorylation of kinases influences their conformational state and can also regulate enzymatic activity. Recently, this has become an area of interest for drug discovery. Using Alk2 as an example, we present two protocols — one based on phosphate-binding Alphascreen beads, the other on coupled luminescence measurements of ADP formation — that can be used to screen for inhibitors of autophosphorylation.

Key words Kinase, Autoactivation, Autophosphorylation, Alphascreen, Luminescence, ADP-Glo, Alk2, Assay development, High-throughput screening

1 Introduction

Kinases are one of the most prominent target classes in modern drug discovery and numerous assay formats to measure their activity and screen for their inhibitors have been described [1, 2]. The main components of these assays typically are the kinase itself, ATP as the phosphate donor and a second substrate (protein, peptide, or low-molecular weight metabolite) that acts as phosphate acceptor. A special situation arises when kinase autophosphorylation, which often is a critical regulatory mechanism and therefore of therapeutic relevance, needs to be investigated because the target then assumes the roles of enzyme and substrate simultaneously, thus complicating the development of sensitive and meaningful screening assays.

Although the search for inhibitors of kinase-catalyzed protein phosphorylation has become routine [3], the autoactivation of kinases only recently started to be explored as a possible target of drug discovery efforts [4, 5], despite being studied in academia since decades [6, 7]. A major driving force for considering kinase autoactivation as an intervention point for the treatment of disease seems to be the quest for selectivity [8]. Whereas the active conformations of different kinases have similarly structured catalytic sites, their inactive conformations show much more variability and

William P. Janzen (ed.), *High Throughput Screening: Methods and Protocols*, Methods in Molecular Biology, vol. 1439,
DOI 10.1007/978-1-4939-3673-1_10,

thus represent a higher chance to achieve specificity over other kinases [9]. Therefore, rather than just complicating assay development and screening [10], the auto-activation of therapeutically relevant kinases offers specific and novel opportunities for drug discovery. As classical enzyme activity assays are biased toward identifying inhibitors of active kinase conformations, alternative approaches need to be explored. Here, we describe two assay protocols that we have used to measure autophosphorylation of Alk2 [11, 12] as well as inhibition thereof.

The protocol we present in Subheading 3.1 is based on direct detection of phosphorylated Alk2 with an Alphascreen readout. In Alphascreen [13] assays, light-induced release of singlet oxygen from so-called donor beads can trigger chemiluminescence at a shorter wavelength if appropriate acceptor beads are in close proximity (<~200 nm). As the distance constraints are less strict than the Förster radius that limits time-resolved fluorescence energy transfer (TR-FRET) assay setups, where typical radii are in the range of 4–6 nm, Alphascreen assays are not restricted to small peptide substrates in the same way as TR-FRET [14] or fluorescence polarization [15] assays, and therefore can be applied to intact proteins. For measurements of kinase activity, biotinylated substrates bind to streptavidin-coated donor beads while so-called phosphobeads coated with Lewis metal ions [16] that recognize phosphate groups on the substrate protein are used as acceptor beads. In principle, any protein that can be immobilized on the donor beads, including the enzymatically active kinase itself, can serve as the phosphate acceptor and this opens the possibility to measure autophosphorylation. Moreover, unlike approaches that use an antibody for detecting the autophosphorylated kinase [5], the protocol presented in Subheading 3.1 is not restricted to a specific target but should be transferable to other kinases that undergo autophosphorylation.

While this approach is a valuable tool for screening LMW compounds at a fixed concentration of kinase (at least once assay conditions have been thoroughly optimized, e.g., by recording time courses at different enzyme concentration), it can be challenging to use this assay format for rapid characterization of unknown enzyme samples. The main reason is the so-called hook effect [17], which results in decreasing Alphascreen signal at high kinase concentrations (Fig. 1). In addition, the dual role of Alk2 as substrate and enzyme in this setup makes it impossible to run the assay with an excess of substrate over enzyme, which is the basis for the assumptions made in applying the Michaelis-Menten and Briggs-Haldane equations [18].

There are several mechanisms through which Alk2 autophosphorylation activity can be inhibited — on the one hand direct inhibition of the activated kinase (exemplified by the reference inhibitor LDN-193189 [19], Fig. 2a) and on the other hand a

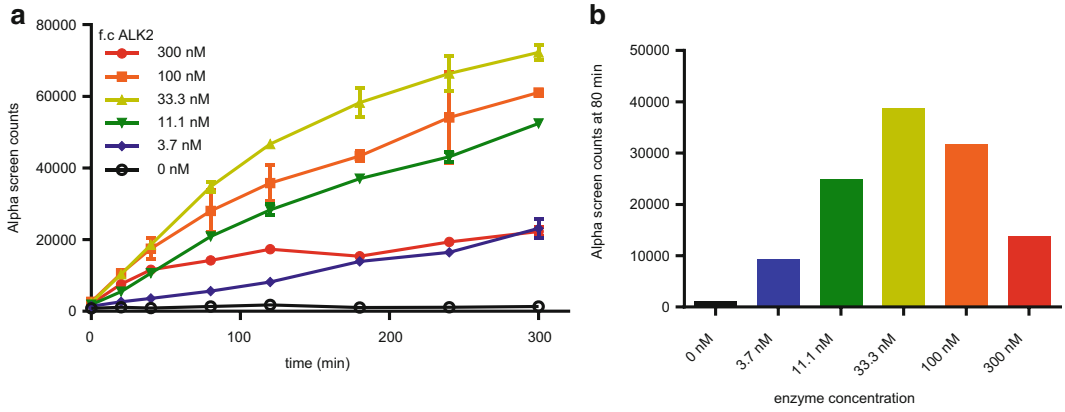

Fig. 1 Measuring autophosphorylation of Alk2 with an Alphascreen readout. (**a**) The indicated concentrations of biotinylated Alk2 (aa 172–499) were incubated with 3 μM ATP for the indicated time, after which the reaction was stopped by addition of staurosporine. Following addition of acceptor and donor beads as described, phosphorylation was determined by measuring chemiluminescence on an appropriate reader with Alphascreen option (*see* **Note 10**). (**b**) The signal measured after 80 min of enzyme reaction is plotted as a function of kinase concentration and clearly passes a maximum, indicating the typical "hook effect" [17]

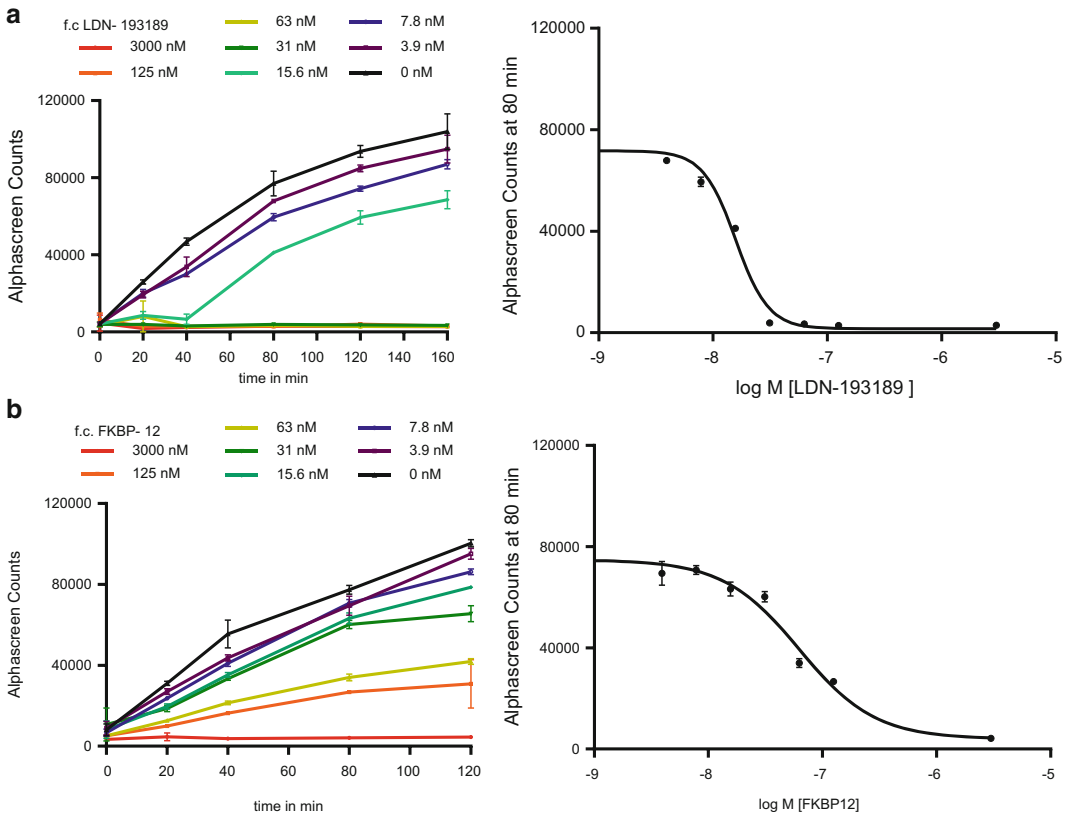

Fig. 2 Inhibition of Alk2 autophosphorylation by different mechanisms. (**a**) Alk2 autophosphorylation in the presence of the LMW inhibitor LDN-193189 [19] was measured by Alphascreen over time as described (*left*); and the signal measured after 80 min was plotted as a function inhibitor concentration (*right*). (**b**) Alk2 autophosphorylation in the presence of the allosteric regulator FKBP12 [20] was measured by Alphascreen over time as described (*left*); and the signal measured after 80 min was plotted as a function inhibitor concentration (*right*)

shielding of the not-yet active kinase from becoming phosphorylated (exemplified by the physiological regulator FKBP12 [20], Fig. 2b). The IC_{50} values measured for unknown compounds may reflect one or the other of these phenomena, or an aggregate of both. Note that the time courses at intermediate concentrations of the LMW inhibitor LDN-193189, which do not completely suppress enzyme activity, reveal a clear "lag phase," presumably reflecting a gradual acceleration as autoactivation progresses. On the other hand, above a certain compound level, the activity is suppressed completely instead of gradually leveling off. Together, this translates into a very steep transition of the dose-response curves (hill slope around -3) and presumably reflects a bimolecular autophosphorylation reaction, in which different Alk2 molecules act as enzyme and as substrate. Filtering of HTS hits based on the slope of the dose-response curve must therefore be applied with great caution. In contrast, FKBP12 inhibits Alk2 much more gradually (hill slope around -1.5).

Like any other readout, Alphascreen is affected by compound interference. Therefore, we recommend measuring enzyme activity or inhibition in several different assay formats as a basis for sound decisions. As an alternative readout for following the autophosphorylation reaction as well as its inhibition, we present in Subheading 3.2 a protocol for luminescence-based measurements of ADP formation in a coupled enzyme assay [21]. Whereas the rate of signal increase clearly depends on the amount of Alk2 (Fig. 3a), enzyme activity is not significantly influenced by addition of the known Alk2 substrate [22] Smad1 (Fig. 3b). This demonstrates that the reaction setup, which is not constrained to any particular kinase or substrate, primarily measures autophosphorylation and therefore is suitable as an orthogonal assay to the Alphascreen-based protocol. Whereas compounds that inhibit in only one of the assays are likely to be readout artifacts, those that show up in both readouts have a high probability of being true inhibitors of the enzyme reaction (Fig. 4).

2 Materials

1. Alk2: The experiments and protocols presented here used recombinant, purified Alk2 (amino acids 172–499, corresponding to the GS-rich region and the kinase domain, which together are also known as the cytoplasmic domain [23]). For the autophosphorylation assay, the protein had been biotinylated in vivo using an Avi-tag [24] attached to the C-terminus (*see* **Note 1**). Protein identity and phosphorylation state were verified by Liquid Chromatography coupled to Mass Spectrometry (LC-MS, *see* **Note 2**).

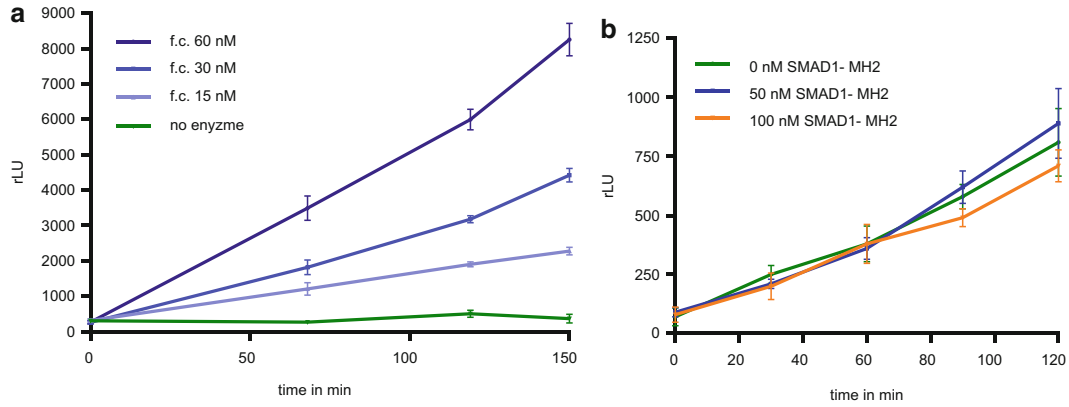

Fig. 3 Measuring substrate-independent ADP formation catalyzed by Alk2 with an ADP-Glo readout. In white 384-well plates (*see* **Note 4**), the conversion of 3 μM ATP to ADP was measured with the help of the luminescence-based ADP-Glo assay [21] in a reaction volume of 7 μl. The reaction was stopped by adding 4 μl ADP-Glo Reagent. After incubation of 40 min at room temperature, 8 μl of Kinase Detection Reagent was added and after an additional incubation of 25 min at room temperature luminescence was measured as described (*see* **Note 10**). (**a**) ADP formation by the indicated concentrations of Alk2 was followed over time. (**b**) ADP formation by 30 nM Alk2 was followed over time in the presence or absence of different concentrations of Smad1's MH2 domain, which is a physiological substrate of Alk2 [22]

2. Autophosphorylation assay reaction buffer: 25 mM Tris–HCl, pH 7.2, 10 mM $MgCl_2$, 3 mM $MnCl_2$, 0.02 % Tween 20 and 0.5 mM DTT, which was added freshly. For removal of dust and precipitates, the buffer was filtrated with 0.22 μM filters before use.
3. Autophosphorylation assay stop buffer: 80 μM staurosporine in 10 mM Tris–HCl pH 7.0, 100 mM NaCl, 0.1 % Tween 20.
4. ADP formation assay reaction buffer: 25 mM Tris–HCl at pH 7.2, 10 mM $MgCl_2$, 3 mM $MnCl_2$, 0.02 % [v/v] Tween 20 and 0.5 mM DTT, which was added freshly. For removal of dust and precipitates, the buffer was filtrated with 0.22 μM filters before use.
5. PhosphoSensor Acceptor Beads (PerkinElmer No. 6760147) and Streptavidin Donor Beads (Perkin Elmer No. 6760007B) were obtained as part the PhosphoSensor Detection Kit (Perkin Elmer Cat. No. 6760307D/M/R).
6. ADP-Glo reagent and the Kinase Detection reagent were obtained as part of the ADP-Glo™ Kinase Assay (Promega Cat. No. V9103).

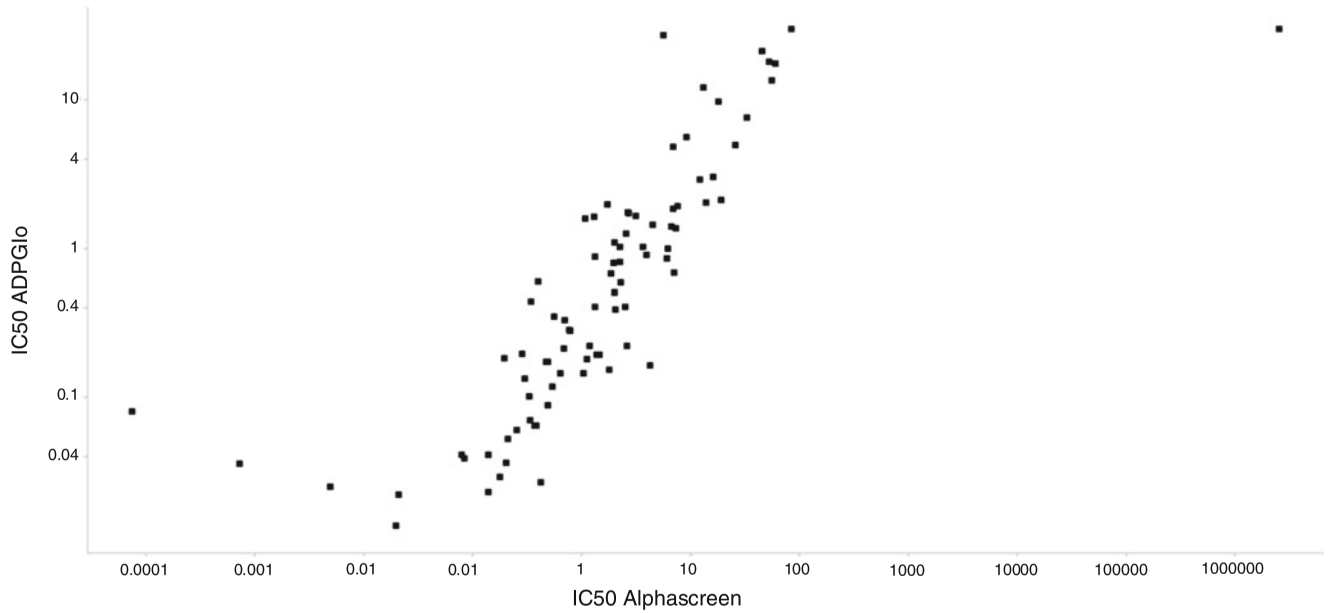

Fig. 4 Correlation of orthogonal assays for autophosphorylation. In order to compare the two assay formats described, and to explore the correlation between them, a small collection of reference compounds was tested in dose-response mode both with the Alphascreen-based Alk2 Autophosphorylation assay and the ADP-Glo luminescence assay measuring ADP formation; the resulting IC_{50} values for each compound are plotted on logarithmic scales as a function of each other. The inhibitors originated from cellular assays and in-silico approaches and had been confirmed to bind Alk2 based on its stabilization against thermal denaturation as measured by Differential Scanning Fluorimetry [30]. With few exceptions (mostly representing extrapolated IC_{50} values outside the tested concentration range), potency in both formats was comparable

3 Methods

3.1 Alk2 Autophosphorylation Assay

1. Preincubate 100 nl (*see* **Note 3**) of 2 mM LMW (low-molecular weight) compound (dissolved in 90 % DMSO) or serial dilutions thereof in white 384-well microtiter plates (*see* **Note 4**) with 3 µl (*see* **Note 5**) of 60 nM Alk2 (*see* **Note 6**) autophosphorylation assay reaction buffer for 10 min at room temperature.
2. Start the autophosphorylation reaction by adding 3 µl of 6 µM ATP in reaction buffer and incubate at room temperature for 120 min.
3. Stop the autophosphorylation reaction by adding 2 µl of stop buffer (*see* **Note 7**).
4. Initiate detection of autophosphorylated Alk2 by adding 3 µl of a pre-mix containing 148 µg/ml PhosphoSensor Acceptor Beads (*see* **Note 8**) and 74 µg/ml Streptavidin Donor Beads in stop buffer and incubate at room temperature in the dark (*see* **Note 9**) for 4 h.
5. Measure (chemi)luminescence on an appropriate Alphascreen-compatible reader (*see* **Note 10**).

This corresponds to concentrations of 30 nM Alk2 and 3 µM ATP during the 120 min enzymatic reaction.

3.2 Alk2 ADP Formation Assay

1. Preincubate 50 nl (*see* **Note 3**) of 2 mM test compound (dissolved in 90 % DMSO) or serial dilutions thereof in white 1536-well microtiter plates (*see* **Note 4**) with 1.6 µl (*see* **Note 5**) of 20 nM (*see* **Note 6**) Alk2 in ADP formation assay reaction buffer.
2. Start the autophosphorylation reaction by adding 1.6 µl of 10 mM ATP in reaction buffer and incubate for 60 min at room temperature.
3. Stop the enzyme reaction by adding 2 µl ADP-Glo reagent and incubate at room temperature for 30 min.
4. Initiate detection by adding 4 µl Kinase Detection reagent (diluted by a factor of 2.3) and incubate for 30 min at room temperature.
5. Measure luminescence on an appropriate reader (*see* **Note 10**) with the emission filter LUM WL = 400–700 nm with a T_{min} of 65 %, a top mirror dedicated for luminescence measurements and a measurement time of 0.1 s.

This corresponds to concentrations of 10 nM Alk2 and 3 µM ATP during the 60 min enzymatic reaction.

4 Notes

1. Although the assay principle does not depend on how the kinase is bound to the donor beads, the extremely high affinity of the biotin-streptavidin interaction makes it relatively resistant to false-positive hits from compound interference (biotin or its analogs of course do show an effect but can be easily recognized). We therefore prefer site-specific biotinylation of the kinase [24] to immobilizing a GST fusion on GSH-coated beads [25] when screening unknown compounds.
2. Measuring self-activation of kinases by means of autophosphorylation inherently necessitates that the original, non-phosphorylated material is not completely inactive but shows some basal kinase activity. This may result from an inherent equilibrium between conformations with different activity that shifts under the influence of (auto)phosphorylation. Such a mechanism has been described for Alk2 [26] and is compatible with both "cis" and "trans" autophosphorylation [27, 28]. Alternatively, the basal kinase activity may reflect trace amounts of phosphorylated kinase molecules that act as "seeds" for triggering a cascade of activation between different molecules, which implies that phosphorylation has to happen in "trans." In any case, we advise to check the phosphorylation state of the enzyme material to be used in the autophosphorylation assay by determining its exact molecular mass by LC-MS. Ideally, samples should be compared before and after incubation with ATP to verify enzymatic activity.
3. Transfer of compound stock solutions in DMSO can be performed with the help of a sub-microliter liquid handling system such as the Hummingbird (Genomic Solutions) or the Echo Liquid Handler (Labcyte) to avoid the need for intermediate dilution plates. If the latter have to be used, e.g., due to lack of appropriate equipment, compound solubility has to be closely monitored to avoid precipitation at intermediate DMSO levels.
4. The protocols described in this manuscript represent the most miniaturized variants of the respective screening assays that we have applied, and in our hands produced Z' [29] values of 0.5 or higher. For measurements in other plate formats, volumes can be increased proportionally.
5. Dispensing of reagents into microtiter plates can be accomplished using solenoid dispensers such as the Synquad (Cartesian Technologies) or dispensers based on SMLD microvalves such as the Certus (Gyger) or Preddator (Redd and Whyte). For dispensing in 384-well and larger formats, the Multidrop Combi Reagent Dispenser (Thermo Scientific) or manual pipetting are also an option.

6. All enzyme concentrations are nominal, i.e., based on the total protein concentration as measured in the respective batch of purified protein. Due to batch-to-batch variations with regard to specific enzyme activity, they need to be fine-tuned for each individual batch.
7. The metal chelate coating of the acceptor beads may be sensitive to EDTA, which is commonly used as a stop reagent for kinase assays. Therefore, known kinase inhibitors are preferable for stopping the enzyme reaction. If no LMW inhibitor is available, EDTA concentrations need to be carefully optimized so that a useable assay window is maintained.
8. The phosphate-binding acceptor beads are coated with a metal chelate, which binds phosphate groups rather indiscriminately [16]. While this makes the assay protocol generic for different kinases, it also confers vulnerability to interference by other phosphate-containing assay components. For example, the amount of nucleotides that can be added to the assay may be limited and needs to be carefully titrated. To some extent, this limitation can be overcome by increasing the concentration of acceptor beads. In order to maintain an appropriate ratio of donor to acceptor beads, this necessitates cross-wise titration of both bead types. What cannot be compensated in this way, however, is the high concentration of phosphate in PBS (phosphate-buffered saline) or similar buffers which have to be avoided as the high concentrations of free phosphate otherwise would compete off the phosphorylated reaction product.
9. The Alphascreen reagents used in the autophosphorylation protocol, in particular the donor beads, are sensitive to light. Therefore, avoid repeat measurements and keep stock solutions in nontransparent vessels (or wrap them using aluminum foil) and incubate assay plates in the dark. If necessary, perform the experiments under monochromatic (green or yellow) light. Further information on the properties of the various reagents is available in the vendor manual.
10. Several vendors provide readers suitable for measurements of chemiluminescence with (Alphascreen) or without stimulation by light. Examples are the BMG Pherastar, the PerkinElmer Envision, or the TECAN Infinite readers. Note that luminescence readings are not absolute values but just relative numbers as they depend on reader geometry and filter setup.

Acknowledgments

We highly appreciate the supply of recombinant Alk2 and its substrate Smad1-MH2 by Sonia Faut and Myriam Duckely as well as protein characterization through LC-MS by Peggy Lefeuvre and

Francis Bitsch. The support from Geoffrey Cutler in implementing the miniaturized ADP formation assay on an automated screening system was also very helpful. The whole Alk2 project team is acknowledged for input and stimulating discussions. Last but not least, we would like to thank Joerg Trappe for suggesting and encouraging the drafting of this manuscript.

References

1. Klumpp M, Boettcher A, Becker D, Meder G, Blank J, Leder L, Forstner M, Ottl J, Mayr LM (2006) Readout technologies for highly miniaturized kinase assays applicable to high-throughput screening in a 1536-well format. J Biomol Screen 11(6):617–633. doi:10.1177/1087057106288444
2. Drueckes P (2016) Protein kinase selectivity profiling using microfluidic mobility shift assays. In: Janzen WP (ed) High throughput screening: methods and protocols, 3rd edn. Methods Mol Biol 1439
3. Cohen P, Alessi DR (2013) Kinase drug discovery—what's next in the field? ACS Chem Biol 8(1):96–104. doi:10.1021/cb300610s
4. Newbatt Y, Hardcastle A, McAndrew PC, Strover JA, Mirza A, Morgan GJ, Burke R, Davies FE, Collins I, van Montfort RL (2013) Identification of autophosphorylation inhibitors of the inositol-requiring enzyme 1 alpha (IRE1alpha) by high-throughput screening using a DELFIA assay. J Biomol Screen 18(3):298–308. doi:10.1177/1087057112 465647
5. Liu Z, Galemmo RA Jr, Fraser KB, Moehle MS, Sen S, Volpicelli-Daley LA, DeLucas LJ, Ross LJ, Valiyaveettil J, Moukha-Chafiq O, Pathak AK, Ananthan S, Kezar H, White EL, Gupta V, Maddry JA, Suto MJ, West AB (2014) Unique functional and structural properties of the LRRK2 ATP-binding pocket. J Biol Chem 289:32937–32951. doi:10.1074/jbc.M114.602318
6. Wang JH, Stull JT, Huang TS, Krebs EG (1976) A study on the autoactivation of rabbit muscle phosphorylase kinase. J Biol Chem 251 (15):4521–4527
7. Nakayama GR, Parandoosh Z (1999) An immunoassay for assessment of receptor tyrosine kinase autophosphorylation. J Immunol Methods 225(1–2):67–74
8. Deacon SW, Beeser A, Fukui JA, Rennefahrt UE, Myers C, Chernoff J, Peterson JR (2008) An isoform-selective, small-molecule inhibitor targets the autoregulatory mechanism of p21-activated kinase. Chem Biol 15(4):322–331. doi:10.1016/j.chembiol.2008.03.005
9. Fabbro D, Cowan-Jacob SW, Mobitz H, Martiny-Baron G (2012) Targeting cancer with small-molecular-weight kinase inhibitors. Methods Mol Biol 795:1–34. doi:10.1007/978-1-61779-337-0_1
10. Ohmi N, Wingfield JM, Yazawa H, Inagaki O (2000) Development of a homogeneous time-resolved fluorescence assay for high throughput screening to identify Lck inhibitors: comparison with scintillation proximity assay and streptavidin-coated plate assay. J Biomol Screen 5(6):463–470
11. Zimmerman CM, Mathews LS (1996) Activin receptors: cellular signalling by receptor serine kinases. Biochem Soc Symp 62:25–38
12. Huse M, Muir TW, Xu L, Chen YG, Kuriyan J, Massague J (2001) The TGF beta receptor activation process: an inhibitor- to substrate-binding switch. Mol Cell 8(3):671–682
13. Eglen RM, Reisine T, Roby P, Rouleau N, Illy C, Bosse R, Bielefeld M (2008) The use of AlphaScreen technology in HTS: current status. Curr Chem Genomics 1:2–10. doi:10.2174/1875397300801010002
14. Pope AJ (1999) Introduction LANCEtrade mark vs. HTRF(R) technologies (or vice versa). J Biomol Screen 4(6):301–302
15. Seethala R (2000) Fluorescence polarization competition immunoassay for tyrosine kinases. Methods 22(1):61–70. doi:10.1006/meth.2000.1037
16. Delom F, Chevet E (2006) Phosphoprotein analysis: from proteins to proteomes. Proteome Sci 4:15. doi:10.1186/1477-5956-4-15
17. Fernando SA, Wilson GS (1992) Studies of the 'hook' effect in the one-step sandwich immunoassay. J Immunol Methods 151(1–2):47–66
18. Briggs GE, Haldane JB (1925) A note on the kinetics of enzyme action. Biochem J 19 (2):338–339
19. Hong CC, Yu PB (2009) Applications of small molecule BMP inhibitors in physiology and disease. Cytokine Growth Factor Rev 20 (5–6):409–418. doi:10.1016/j.cytogfr.2009.10.021

20. Chen YG, Liu F, Massague J (1997) Mechanism of TGFbeta receptor inhibition by FKBP12. EMBO J 16(13):3866–3876. doi:10.1093/emboj/16.13.3866
21. Zegzouti H, Zdanovskaia M, Hsiao K, Goueli SA (2009) ADP-Glo: a bioluminescent and homogeneous ADP monitoring assay for kinases. Assay Drug Dev Technol 7 (6):560–572. doi:10.1089/adt.2009.0222
22. Macias-Silva M, Hoodless PA, Tang SJ, Buchwald M, Wrana JL (1998) Specific activation of Smad1 signaling pathways by the BMP7 type I receptor, ALK2. J Biol Chem 273 (40):25628–25636
23. Huse M, Chen YG, Massague J, Kuriyan J (1999) Crystal structure of the cytoplasmic domain of the type I TGF beta receptor in complex with FKBP12. Cell 96(3):425–436
24. Leder L (2015) Site-specific protein labeling in the pharmaceutical industry: experiences from novartis drug discovery. Methods Mol Biol 1266:7–27. doi:10.1007/978-1-4939-2272-7_2
25. Bouchecareilh M, Caruso ME, Roby P, Parent S, Rouleau N, Taouji S, Pluquet O, Bosse R, Moenner M, Chevet E (2010) AlphaScreen-based characterization of the bifunctional kinase/RNase IRE1alpha: a novel and atypical drug target. J Biomol Screen 15(4):406–417. doi:10.1177/1087057110363823
26. Huse M, Kuriyan J (2002) The conformational plasticity of protein kinases. Cell 109 (3):275–282
27. Iwasaki Y, Nishiyama H, Suzuki K, Koizumi S (1997) Sequential cis/trans autophosphorylation in TrkB tyrosine kinase. Biochemistry 36 (9):2694–2700. doi:10.1021/bi962057x
28. Schwarz JK, Lovly CM, Piwnica-Worms H (2003) Regulation of the Chk2 protein kinase by oligomerization-mediated cis- and trans-phosphorylation. Mol Cancer Res 1(8): 598–609
29. Zhang JH, Chung TD, Oldenburg KR (1999) A simple statistical parameter for use in evaluation and validation of high throughput screening assays. J Biomol Screen 4(2):67–73
30. Senisterra G, Chau I, Vedadi M (2012) Thermal denaturation assays in chemical biology. Assay Drug Dev Technol 10(2):128–136. doi:10.1089/adt.2011.0390

Chapter 11

A Fluorescence-Based High-Throughput Screening Assay to Identify Growth Inhibitors of the Pathogenic Fungus *Aspergillus fumigatus*

Thomas M. Smith, Daryl L. Richie, and Jianshi Tao

Abstract

Due to the advancements in modern medicine that have resulted in an increased number of immunocompromised individuals, the incidences and the associated mortality of invasive aspergillosis have continued to rise over the past three decades despite appropriate treatment. As a result, invasive aspergillosis has emerged as a leading cause of infection-related mortality in immunocompromised individuals. Utilizing the resazurin to resorufin conversion fluorescence readout to monitor cell viability, herein, we outline a high-throughput screening method amenable to profiling a large pharmaceutical library against the clinically relevant but less frequently screened fungal pathogen *Aspergillus fumigatus*. This enables the user to conduct high-throughput screening using a disease-relevant fungal growth assay and identify novel antifungal chemotypes as drug leads.

Key words *Aspergillus fumigatus*, Fungus, Antifungal, Resazurin, High-throughput screening (HTS)

1 Introduction

Aspergillus fumigatus is a ubiquitous saprophytic fungus that propagates itself by releasing conidia into the atmosphere after physical disturbance of its environment [6, 7]. The unavoidable inhalation of conidia is without consequence in most healthy individuals due to clearance by innate immune responses. However, *A. fumigatus* is capable of causing a variety of diseases including life-threatening invasive infection in people with various health problems [3, 8, 9]. Severe neutropenia is the predominate risk factor for developing invasive aspergillosis with hematopoietic stem cell transplant and solid organ transplant recipients at greatest risk [4, 9]. However, the patient population considered at risk for invasive aspergillosis continues to expand due to the increasing use of aggressive and intensive chemotherapeutic regimens [2, 4, 5].

William P. Janzen (ed.), *High Throughput Screening: Methods and Protocols*, Methods in Molecular Biology, vol. 1439,
DOI 10.1007/978-1-4939-3673-1_11,

Currently, the generally accepted first-line therapy for invasive aspergillosis is voriconazole due to better tolerability and improved survival in comparison with amphotericin B [10]. With the limited treatment options the mortality rate associated with invasive aspergillosis remains unacceptably high, reflecting the need for novel chemical matter with new mechanisms of action [1]. To maximize the opportunity to identify such inhibitors, we outline a high-throughput assay amenable to screening upwards of a million compounds against the clinically relevant mold pathogen *A. fumigatus*. By running a phenotypic assay for compounds that directly affect the growth of a disease-associated organism, one will increase the probability of finding both novel chemical matter for lead development and identifying targets of interest. In use as part of an antifungal effort at the Novartis Institutes for BioMedical Research, this miniaturized high-throughput assay enabled the screening of the entire Novartis low-molecular-weight compound collection (~1.4 million wells) against *A. fumigatus* to identify novel inhibitory chemotypes with desired antifungal spectrum.

1.1 Assay Overview

The fungal cell growth assay was developed by using high-density 1536 well (1536w) plates and incorporating a fluorescence-based readout using the reduction of resazurin to resorufin [11]. The "resazurin reduction test" has historically been used to monitor microbial contamination of milk [12], and has since been developed into sensitive bioassays for assessing cell viability and cytotoxicity in a number of cell types including bacteria, yeast, protozoa, and cultured mammalian and piscine cells [13–16]. In these assays, resazurin (blue and nonfluorescent) is reduced to resorufin (pink and highly fluorescent) in metabolically active cells, and the fluorescence has been shown to be proportional to the number of viable cells in a population [13]. Since the use of resazurin for monitoring fungal growth has been described and validated for *Aspergillus species*, including *A. nidulans* and *A. fumigatus*, and in small-scale screening for antifungal compounds [17–19], herein we provide the user with a 1536w plate-based format assay, giving the flexibility for easily screening upwards of a million compounds for inhibitor identification. An overview of the assay details is shown in Fig. 1.

2 Materials

2.1 Scientific Equipment

1. Heraeus Incubator BB6220, Thermo Fisher Scientific (Waltham, MA, USA).
2. Sorvall RC-4 Centrifuge, Thermo Fisher Scientific (Waltham, MA, USA).

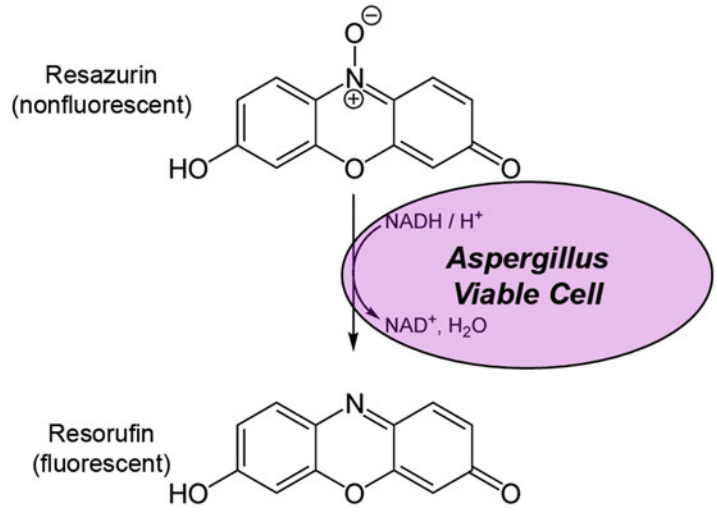

Fig. 1 Schematic of the resazurin-based *Aspergillus fumigatus* growth assay. Resazurin (*blue* and nonfluorescent) is reduced to resorufin (*pink* and highly fluorescent) during oxidation-reduction reactions in the living *Aspergillus* cells. In the optimized growth assay, there is a direct correlation between the reduction of resazurin and the quantity/proliferation of living cells

3. Flexdrop IV Liquid handler, Perkin Elmer, Inc. (Waltham, MA, USA).
4. EnVision 2102 Multilabel Reader, Perkin Elmer, Inc. (Waltham, MA, USA).

2.2 Reagents

1. RPMI-1640 growth media preparation: Powdered RPMI-1640 with glutamine and phenol red without bicarbonate is buffered with 0.165 mol/L 3-[N-morpholino] propanesulfonic acid (MOPS). Weigh 10.4 g of powdered RPMI-1640 and dissolve in 900 ml of distilled water. Add 34.53 g of MOPS (0.165 mol/L) and stir until dissolved. While stirring adjust pH to 7.0 at 25 °C using sodium hydroxide pellets and bring media up to a final volume of 1 L (*see* **Note 1**). Filter sterilize and store at 4 °C until use.
2. Amphotericin B preparation: Amphotericin B stock solution is used as an aqueous stock at 250 μg/ml or 20× the concentration used during the screening assay. The control solution is stored frozen at −20 °C, and with protection from air and light, the product remains active for 5 years. On the day of screening, a working stock solution is prepared by 20-fold dilution into RPMI-1640 growth media to a final concentration of 12.5 μg/ml.
3. Resazurin preparation: Resazurin is prepared as a sterile 300 mM or 3750× stock solution, 75 mg/ml, in RPMI-1640

and stored at 4 °C, protected from light. The stock solution is added to RPMI-1640 growth media as described in the high-throughput screening protocol.

3 Methods

3.1 Preparation of Aspergillus fumigatus Seed Stocks for Storage

1. Using an inoculum loop, streak *Aspergillus fumigatus* (ATCC MYA-3627) culture onto a Potato dextrose agar (PDA) slant (Becton Dickinson #297241) and incubate at 35 °C until adequate sporulation is obtained (2–5 days, *see* **Note 2**).
2. Harvest the conidia by adding 5 ml of sterile distilled water to the surface of the slant and lightly brushing the surface with a sterile swab.
3. Use a transfer pipette and filter the conidial suspension through autoclaved miracloth into a 50 ml conical tube to remove hyphal debris.
4. Centrifuge the conidial suspension to pellet the conidia and decant the water. To wash, resuspend the pellet into 5 ml of fresh sterile water, vortex, and repeat the centrifugation. Repeat for a total of three washes.
5. Following the final wash, resuspend the conidia in a 10 % glycerol solution, aliquot 50–100 μl into cryovials, and store at −80 °C until use. Use these as seed cultures to inoculate subcultures for the preparation of larger batches of conidia for high-throughput screening.

3.2 Preparation of Conidial Working Stock for High-Throughput Screening

1. Thaw the seed stock vials of *A. fumigatus* ATCC MYA-3627 at room temperature and subculture onto PDA slants. Incubate at 35 °C until adequate sporulation is obtained (2–5 days, *see* **Note 2**).
2. Harvest the conidia by adding 5 ml of sterile distilled water to the surface of the slant and lightly brushing the surface with a sterile swab.
3. Use a transfer pipette and filter the conidial suspension through autoclaved miracloth into a 50 ml conical tube to remove hyphal debris.
4. Centrifuge the conidial suspension to pellet the conidia and decant the water. To wash, resuspend into 5 ml of fresh sterile water, vortex, and repeat the centrifugation. Repeat for a total of three washes (*see* **Note 3**).
5. Following the final wash, the conidia are resuspended in 5 ml sterile distilled water and the conidia counted using a hemocytometer. The working conidial suspension is kept at a stock concentration of 10^6 conidia/ml at 4 °C until use.

Conidia were in stasis in water at 4 °C and diluted into room-temperature RPMI-1640 media just prior to use, so that screening was carried out at a final concentration of 10^5 conidia/ml (*see* **Note 4**).

3.3 High-Throughput Screening Protocol in 1536w Format

1. Obtain 1536w plates with compounds of interest in DMSO pre-plated to the desired concentration as assay-ready plates (*see* **Note 5**).
2. Preparation of active control [low-growth-activity baseline controls; RPMI media + conidia + amphotericin B (*see* **Note 6**)]:
3. To room-temperature RPMI-1640 media, dilute amphotericin B 20-fold to a final concentration of 12.5 μg/ml.
4. Dilute resazurin 3750-fold to the solution to a final concentration of 80 μM.
5. Add conidia to a final density of 10^5/ml (*see* **Note 7**).
6. Mix thoroughly and add to a dispensing bottle on the Flexdrop liquid handler (for active control columns 47–48).
7. The bottle is swirled routinely throughout the dispense (*see* **Note 8**).
8. Preparation of neutral control [high-growth-activity controls; RPMI medium + conidia] and samples for compound testing:
9. To room-temperature RPMI-1640 media, dilute resazurin to a final concentration of 80 μM.
10. Add conidia to a final density of 10^5/ml.
11. Mix thoroughly and add to dispensing bottle on the Flexdrop (for columns 1–44: sample columns; neutral control columns 45–46 contain DMSO only, not compounds).
12. Once bottles are attached, prime each bottle, load plates, and start dispensing 8 μl/well to Greiner 1536w black assay-ready compound plates.
13. After reagents have been dispensed, manually lid and centrifuge the plates at room temperature for 1 min at 600 rpm in a Sorvall RC-4 centrifuge.
14. Place lidded plates into a loading rack in a 35 °C humidified Heraeus Incubator BB6220.
15. Incubate overnight for 14–16 h (ensure log phase growth, *see* **Note 9**).
16. Read on EnVision plate reader, fluorescence at 544 nm excitation and 590 nm emission (*see* **Note 10**).

Using the above conditions, we were able to screen a total of ~1.49 million wells of the Novartis compound libraries at 40 μM compound concentration over a period of 14 days, with a median Z' for the entire HTS of 0.66.

4 Notes

1. Sodium hydroxide pellets were used in place of the suggested 1 mol/L sodium hydroxide solution. We found that the use of the sodium hydroxide pellets allowed us to more efficiently obtain the desired pH.
2. Harvesting the conidia on day 2 while they are less hydrophobic results in easier manipulation of conidia for suspension. Additionally, extended incubation times can result in decreased germination rates.
3. To avoid premature germination of the conidia it is important to complete all washes to remove residual nutrients present in the preparation.
4. In our hands, assay variation was not observed with working stocks stored at 4 °C in sterile distilled water up to 4 weeks. However, it is recommended to determine conidial germination rates/viability of the working stocks before screening as follows: Resuspend conidia assay medium at a final concentration of 1×10^5–5×10^5 in a 50 ml conical and vortex for 15 s. Add 200 μl of the conidial suspension to wells A1–A3 in a 96-well flat-bottom plate and incubate at 35 °C, since higher temperatures or increased conidial densities have been shown to be associated with lower germination rates in *Aspergillus* [20]. After 6–7 h of incubation, calculate the percent germination over time for 100 conidia analyzed microscopically in triplicate. A conidium is scored as germinated if the length of the extended germ tube is equal to or greater than the length of the initial conidium. Score the percent germination every hour until at least a 90 % germination rate is observed.
5. DMSO tolerance was evaluated up to 4 % concentration in the assay and found to be acceptable for screening, although we found that the time to reach stationary phase was delayed as the DMSO concentration increased. We recommend for the user to evaluate DMSO concentrations as appropriate in the initial growth assessment assay depending upon their final choice in the assay.
6. For control inhibitor compounds during HTS, the user can choose from several well-characterized antifungal agents (see Table 1). In our screen, we choose amphotericin B to be included as the active control, at a final inhibitory concentration of 12.5 μg/ml (13 μM).
7. The growth inhibition assay was initially tested in 1536w plate formats at two dilutions (10^5, 10^6 conidia/ml). We found that the growth kinetics at 10^6 conidia/ml were too rapid to be feasible for HTS and higher inoculum concentrations could give an adequate resazurin reduction signal despite significant

Table 1
Reference compound EC_{50} values for 1536w *Aspergillus fumigatus* assay

Compound	EC_{50} (μM)
Amphotericin B	3.8
Caspofungin	0.018
Ketoconazole	27.1
Nystatin	0.99

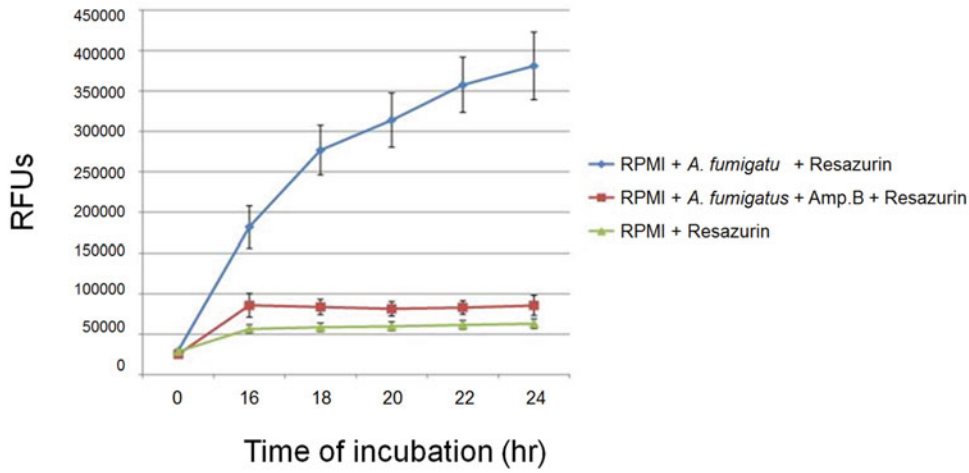

Fig. 2 *Aspergillus fumigatus* growth rates in 1536w plate format. The growth rate of *A. fumigatus* in RPMI media is measured by monitoring resazurin reduction fluorescence (Ex 544 nm, Em 590 nm) over time (*blue circles*). *A. fumigatus* incubated with 12.5 μg/ml of the inhibitor amphotericin B (*red squares*) show minimal growth during this time period. Similarly, RPMI media without added cells shows minimal change in fluorescence over the time period of the assay (*green triangles*)

growth inhibition. This resulted in an uncoupling of growth stage from resazurin conversion to resorufin (544 nm excitation and 590 nm emission). Compounds that may encompass similar mechanisms to echinocandins where germination occurs but significant growth inhibition results in small, rounds, compact hyphal forms could be overlooked as inactive against *A. fumigatus*. Hence all screening was carried out with conidial concentrations of 10^5 conidia/ml.

8. We have found that the conidial culture tends to settle during the time it takes to dispense stacks of plates; thus we routinely swirl the bottle to maintain a good suspension while the Flex-Drop is dispensing conidia to wells.
9. A typical growth curve of *A. fumigatus* is shown in Fig. 2. During screening, plates were read between 14 and 16 h which gave a good window between control wells.

10. One initial concern that arose due to the fluorescence-based nature of the assay was the potential for significant interference from fluorescent compounds. Specifically, what percent of the hits were due to compound interference with the fluorescent readout. To examine this, *Aspergillus* plates were incubated overnight in RPMI-1640 and 80 μM resazurin under the same growth conditions used to run the assay. The conditioned media and *A. fumigatus* conidia were then transferred to a fresh set of compound containing plates, and the fluorescence determined as before. We found that few of our hits identified at 40 μM compound (~1.6 %; data not shown) were found to be causing fluorescent interference in the growth assay.

Acknowledgements

We would like to thank the *Aspergillus fumigatus* inhibitor project team including Neil Ryder, Kathryn Thompson, Roger Fujimoto, Joseph Drumm, and Dominic Hoepfner for scientific input and advice during the screen. We would like to thank Heidi Faw for safety considerations regarding *Aspergillus* handling. We would like to thank Alejandra Raimondi for initial assay development work. We would like to thank Melissa Grippo for compound purity testing by LC-MS.

References

1. Lin S, Schranz J, Teutsch S (2001) Aspergillosis case-fatality rate: systematic review of the literature. Clin Infect Dis 32(3):358–366
2. McNeil M, Nash S, Hajjeh R, Phelan M, Conn L, Plikaytis B, Warnock D (2001) Trends in mortality due to invasive mycotic diseases in the United States, 1980–1997. Clin Infect Dis 33(5):641–647
3. Zmeili O, Soubani A (2007) Pulmonary aspergillosis: a clinical update. QJM 100 (6):317–334
4. Morgan J, Wannemuehler K, Marr K, Hadley S, Kontoyiannis D, Walsh T, Fridkin S, Pappas P, Warnock D (2005) Incidence of invasive aspergillosis following hematopoietic stem cell and solid organ transplantation: interim results of a prospective multicenter surveillance program. Med Mycol 43(1):S49–S58
5. Wilson L, Reyes C, Stolpman M, Speckman J, Allen K, Beney J (2002) The direct cost and incidence of systemic fungal infections. Value Health 5(1):26–34
6. Hospenthal D, Kwon-Chung K, Bennett J (1998) Concentrations of airborne Aspergillus compared to the incidence of invasive aspergillosis: lack of correlation. Med Mycol 36 (3):165–168
7. Goodley J, Clayton Y, Hay R (1994) Environmental sampling for aspergilli during building construction on a hospital site. J Hosp Infect 26(1):27–35
8. Brakhage J (2006) Molecular determinates of virulence in Aspegillus fumigatus. In: Heitman J (ed) Molecular principles of fungal pathogenesis. ASM Press, Washington, DC
9. Latgé J (1999) Aspergillus fumigatus and aspergillosis. Clin Microbiol Rev 12 (2):310–350
10. Herbrecht R, Denning D, Patterson T, Bennett J, Greene R, Oestmann J, Kern W, Marr K, Ribaud P, Lortholary O, Sylvester R, Rubin R, Wingard J, Stark P, Durand C, Caillot D, Thiel E, Chandrasekar P, Hodges M, Schlamm H, Troke P, Bd P (2002) Voriconazole versus amphotericin B for primary therapy of invasive aspergillosis. N Engl J Med 347(6):408–415
11. Rampersad S (2012) Multiple applications of Alamar Blue as an indicator of metabolic

function and cellular health in cell viability bioassays. Sensors 12(9):12347–12360

12. Pesch K, Simmert U (1929) Combined assays for lactose and galactose by enzymatic reactions. Milchw Forsch 8:551
13. Stoddart M (2011) Cell viability assays: introduction. Methods Mol Biol 740:1–6
14. O'Brien J, Wilson I, Orton T, Pognan F (2000) Investigation of the Alamar Blue (resazurin) fluorescent dye for the assessment of mammalian cell cytotoxicity. Eur J Biochem 267(17):5421–5426
15. Ahmed S, Jr RG, Walsh J (1994) A new rapid and simple non-radioactive assay to monitor and determine the proliferation of lymphocytes: an alternative to [3H]thymidine incorporation assay. J Immunol Methods 170 (2):211–224
16. Fai P, Grant A (2009) A rapid resazurin bioassay for assessing the toxicity of fungicides. Chemosphere 74(9):1165–1170
17. Monteiro M, Mdl C, Cantizani J, Moreno C, Tormo J, Mellado E, Lucas JD, Asensio F, Valiante V, Brakhage A, Latgé J, Genilloud O, Vicente F (2012) A new approach to drug discovery: high-throughput screening of microbial natural extracts against Aspergillus fumigatus using resazurin. J Biomol Screen 17 (4):542–549
18. Mania D, Hilpert K, Ruden S, Fischer R, Takeshita N (2010) Screening for antifungal peptides and their modes of action in Aspergillus nidulans. Appl Environ Microbiol 76(21): 7102–7108
19. Yamaguchi H, Uchida K, Nagino K, Matsunaga T (2002) Usefulness of a colorimetric method for testing antifungal drug susceptibilities of Aspergillus species to voriconazole. J Infect Chemother 8(4):374–377
20. Araujo R, Rodrigues A (2004) Variability of germinative potential among pathogenic species of Aspergillus. J Clin Microbiol 42(9):4335–4337

Chapter 12

Mycobacterium tuberculosis High-Throughput Screening

E. Lucile White, Nichole A. Tower, and Lynn Rasmussen

Abstract

High-throughput screening is a valuable way to identify hit compounds that combined with a robust medicinal chemistry program could lead to the identification of new antibiotics. Here, we discuss our method for screening large compound libraries with virulent *Mycobacterium tuberculosis*, possibly one of the more difficult bacteria to use because of its slow growth and assignment to Biosafety Level-3 by the CDC and NIH. The principles illuminated here, however, are relevant to the execution of most bacteria high-throughput screens.

Key words *Mycobacterium tuberculosis*, Mtb, H37Rv, Tuberculosis, TB, High-throughput screening, HTS, Antitubercular, Antibacterial, Antimicrobial, Antibiotics

1 Introduction

Notwithstanding recent improvements in either the prevention or treatment of tuberculosis (TB), its resurgence has led to an intensified effort in the development of treatments for *Mycobacterium tuberculosis (*Mtb). The global burden for TBTuberculosis (TB), according to the World Health Organization (WHO) in 2010, accounted for 8.5–9.2 million new cases and 1.2–1.5 million deaths (including deaths from TB among HIV-positive people) [1]. thus making TB the second leading cause of death from an infectious disease worldwide (after HIV, which caused an estimated 1.8 million deaths in 2008) [2]. The renewed interest in this disease has impacted not only the diagnostics and therapeutics areas but also the tools and technologies used to develop therapeutics. Aided by technologies such as high-throughput screening (HTS) and medicinal chemistry, rapid evaluation of potential antimicrobials has increased dramatically. It is especially desirable to identify new types of TB drugs acting on novel drug targets with no cross-resistance to existing drugs or interfering interactions with antiretrovirals.

William P. Janzen (ed.), *High Throughput Screening: Methods and Protocols*, Methods in Molecular Biology, vol. 1439,
DOI 10.1007/978-1-4939-3673-1_12,

The Southern Research High Throughput Screening Center team has screened >1.2 million compounds in single-dose screens and 70,000 compounds in dose-response in an in vitro assay against Mtb H37Rv adapted from the microdilution alamarBlue (AB) broth assay originally reported by Collins and Franzblau [3]. This method has been established as our standard operating procedure for end point determination and enumeration of potential inhibitory compounds against Mtb H37Rv since 2004 [4–6]. Recently, we have improved the assay by using Promega's BacTiter-Glo™ Microbial Cell Viability (BTG) end point reagent.

Laboratory manipulations with Mtb require meticulous attention to detail and all the parameters involved due to the pathogenicity of the organism (*see* **Note 1**) but also due to the sensitivity in growth of the organism. The screening assay as described here is robust and reproduces consistently if variables in the assay are accounted for and controlled. Subheading 3 contains three main parts, i.e., preparation of the components, execution of the Mtb assay, and execution of a counter-screen in mammalian cells. The discussion in Subheading 4 details some of the problems encountered and solutions.

2 Materials (*See* Note 2)

2.1 Media/Broth and Agar Plates (See Note 3)

1. 10× ADC (albumin, dextrose, catalase) (*see* **Note 4**): Weigh out 25 g BSA, 10 g glucose, and 0.015 g catalase. Bring the total volume up to 500 mL with Milli-Q water and dissolve dry components. Filter sterilize through a 0.2 μm 500 mL filter flask. Store at 4 °C up to 1 week.
2. 5 % Tween 80 solution: In a 100 mL glass flask with a stir bar, weigh out 0.5 g Tween 80. Bring total volume to 10 mL with Milli-Q water and dissolve, with heat if necessary.
3. 20 % Glycerol solution: In a 100 mL glass flask with a stir bar, weigh out 2 g of glycerol. Bring total volume to 10 mL with Milli-Q water and dissolve, with heat if necessary.
4. 7H9 Media/broth: Weigh 4.7 g Middlebrook 7H9 broth base into a 2 L glass flask with a stir bar. Add 880 mL of Milli-Q water and stir on a stir plate to dissolve. Add 10 mL of Tween 80 solution and 10 mL of glycerol solution. Autoclave the 7H9 solution for 20 min at 121 °C. The media will appear slightly cloudy at this time but will clear up as it cools. Allow the 7H9 solution to cool until it has reached room temperature.
5. H9 Media/broth: Add 100 mL of the 10× ADC solution (**item 1**) to the 7H9 solution. Filter through a 0.2 μm 1 L filter flask.

6. 7H11 agar plates: In a 2 L flask, dissolve 21 g of 7H11 agar base in 890 mL Milli-Q water. In a 100 mL glass flask, weigh out 2 g of glycerol. Add approximately 10 mL Milli-Q water and dissolve, with heat if necessary. Add back to broth base. Autoclave for 20 min at 121 °C. Allow the 7H11 to cool to 55 °C and add 100 mL Middlebrook OADC (oleic, albumin, dextrose, catalase) and mix. Aliquot 30 mL of 7H11 agar into sterile Petri plates carefully to prevent air bubbles from forming. Let the plates cool to room temperature and allow the plates to remain at room temperature overnight to dry and to check for contamination. Store plates for long term at 4 °C inverted in a sealed plastic bag up to 1 month.
7. Tryptic soy agar (TSA) plates: Weigh 40 g of dehydrated media (TSA) and bring up to 1 L with Milli-Q water. Autoclave at 121 °C for 20 min. Allow to cool to 45–50 °C. Dispense 30 mL into sterile Petri dishes carefully to prevent air bubbles from forming. Let the plates cool to room temperature. Allow the plates to remain at room temperature overnight to dry and to check for contamination. Store plates for long term at 4 °C inverted in a sealed plastic bag for up to 1 month.

2.2 alamarBlue Assay

1. 18.2 % Tween 80 solution: Weigh 18.17 g Tween 80 into a 200 mL glass flask. Dilute the Tween 80 with 100 mL of Milli-Q water. Autoclave at 121 °C for 20 min. 18.2 % Tween 80 may be kept for up to 2 months.

2.3 Mammalian Cell Cytotoxicity Assay

1. Cryopreservation media: 95 % Heat-inactivated FBS and 5 % DMSO.

2.4 Equipment

Where two pieces of equipment are indicated, one is located in the BSL-2 laboratory and one in the BSL-3.

1. Beckman Coulter Biomek FX.
2. Two—Thermo Matrix WellMates, with standard bore cassette.
3. Two—Incubators in which the humidity level can be controlled to 95 % or higher.
4. Two—PerkinElmer EnVision Multilabel Plate Readers.

3 Methods

Carry out all procedures at room temperature unless specified otherwise. In order to maintain sterility, all preparations should be carried out in a biological safety cabinet (BSC).

3.1 Stock Mtb H37Rv Preparation

All work with Mtb H37Rv occurs in a certified biological safety cabinet (BSC) within a BSL-3 laboratory (*see* **Note 5**).

3.1.1 Subculture Growth

1. Inoculate 5 mL of 7H9 media in a screw cap 50 mL conical tube with 0.2 mL of thawed Mtb H37Rv (ATCC 27294) from American Type Culture Collection. Loosely screw conical cap back on and cover cap with parafilm to allow for adequate gas exchange while preventing evaporation during incubation.
2. Incubate the subculture in a ~90 % humidified incubator at 37 °C without CO_2. Gently swirl the culture daily to mix the media.
3. Monitor the growth for turbidity. Take OD_{615} of subculture (pipette 66 μL of culture into Corning 384-well black clear bottom plate and read absorbance on EnVision using 615 nm filter.)
4. After about 7–8 days, the OD_{615} should be approximately 0.2 OD or a #1 on the McFarland turbidity standard.

3.1.2 Preparation of Stock Mtb H37Rv

1. Inoculate 30 mL of 7H9 with 1.5 mL (5 %) of the subculture in a 250 mL vented cap flask. The total volume may be adjusted depending on the amount of the stock desired considering that only 1/2 to 2/3 of the final volume will be collected.
2. Incubate flask in humidified incubator at 37 °C without CO_2. Swirl the culture daily to mix. Monitor the growth for turbidity.
3. Take OD_{615} of the subculture (pipette 66 μL of culture into Corning 384-well black clear bottom plate and read absorbance on EnVision using 615 nm filter).
4. After about 2–3 weeks, the OD_{615} should be approximately 0.6–0.8 (4–8 × 10^7 CFU/mL) or a #3–4 on the McFarland turbidity scale.
5. Streak out the culture from each flask onto a TSA plate to check for bacterial contaminants (*see* **Note 6**) before the cultures are combined.
6. Incubate overnight at 37 °C without CO_2 and check the plates for any growth.
7. If the cultures do not show any sign of contamination based on the TSA plates, combine the cultures and allow them to sit at ambient temperature for an hour.
8. Large clumps of bacteria will settle to the bottom of the flask. Remove the top 1/2 to 2/3 of the culture into a fresh flask or conical tube. Aliquot 1 mL of the culture into 2 mL cryovials and freeze at −80 °C.
9. Streak the pooled culture that remains onto TSA plates and incubate overnight at 37 °C without CO_2 to check for contamination.

3.1.3 Stock Titration

1. After at least 24 h, thaw three of the frozen aliquots. Do not combine aliquots.
2. Create a 1:10 dilution of each aliquot in 7H9 media.
3. Continue 1:2 serial dilution for ten dilutions.
4. Plate 100 μL of each dilution onto the 7H11 agar plates.
5. Place plates in polyethylene plastic bags (2 plates/bag).
6. Secure loosely and incubate inverted in a humidified incubator at 37 °C without CO_2 for ~21 days and monitor for colony growth and contamination.
7. Count the colonies after 21–28 days. Accurate counts can be made in the range of 30–300 colonies per plate.
8. Determine the average CFU/mL of the triplicate aliquots.

3.2 Mtb Microtiter Plate Assay

3.2.1 Media Preparation

1. Prepare 7H9 media at least 24 h prior to compound and Mtb H37Rv addition. (Media may be prepared up to a week in advance and stored at 4 °C.) The amount of 7H9 media needed is ~36 mL per microtiter plate (*see* **Note** 7), i.e., 12 mL for the addition of the bacteria and 24 mL for preparation of the compounds.
2. Place 10 mL of prepared media in a 50 mL conical and incubate in a humidified incubator overnight at 37 °C without CO_2. Check for contamination in the media by turbidity.

3.2.2 Compound Addition to Assay and Control Microtiter Plates

1. Compound addition occurs in a BSL-2 laboratory in a BSC. Barcoded assay plates containing the compounds are prepared the day that the bacteria will be added to the plates.
2. Test compounds which are in 100 % DMSO are diluted with 7H9 media at twice the screening concentration. DMSO is maintained at a constant 2 % concentration. The screening concentration is dependent upon the composition of the compound library and the resources to follow up on hits. For chemically diverse libraries, we have used 10 μg/mL and 10 μM.
3. Control compound stocks are 2.5 mg/mL amikacin and 10 mg/mL ethambutol dissolved in sterile Milli-Q water. Add DMSO to a final concentration of 2 %. Aliquots are frozen at −80 °C for single use (*see* **Note 8**).
4. The Biomek FX is used to add 25 μL of test compound, control compound, or media to each well of the 384-microtiter plate (Fig. 1). It usually takes 4–41/2 h to add compounds and controls to 100 microtiter plates.

3.2.3 Control Plates

1. Each assay run contains one plate of uninoculated medium, two plates of Mtb inoculated medium, and two other plates containing ethambutol or amikacin at their approximate MIC and 20 times the MIC.

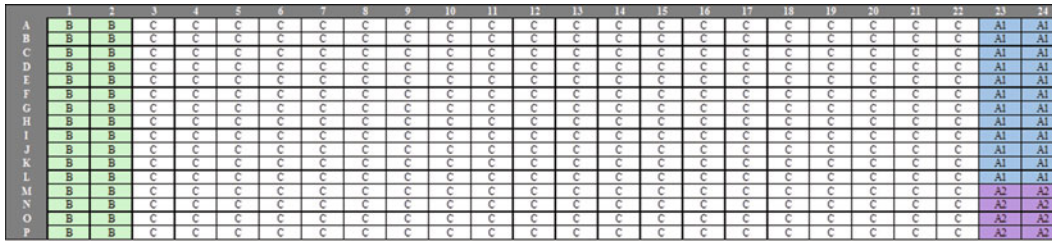

Fig. 1 The layout of the 384-well microtiter plate used in the *Mycobacterium tuberculosis* assay. B contains only media, 1 % DMSO, and Mtb H37Rv and serves as the 100 % growth control. Amikacin is included in the positive control wells in every assay plate at two concentrations. The high concentration, 2.5 μg/mL, completely inhibits Mtb growth and is used instead of uninoculated medium as background (A1). The low concentration of amikacin, 0.13 μg/mL, is the approximate MIC (A2) and is used to monitor assay performance. The test compounds (C) are in the remaining 320 wells

2. Media-only microtiter plate contains media used in the compound addition and plating of the bacteria (uninoculated). This plate is used to ensure media sterility at all stages of the assay. Read the absorbance at 615 nm on the Perkin Elmer EnVision.
3. The growth control/coefficient of variation (CV) plates contain Mtb H37Rv in media plus 1 % DMSO in all 384 wells.
4. The ethambutol control plate is included to confirm that a contaminating organism is not present after incubation since mycobacteria are susceptible to ethambutol but most other organisms are not. Columns 1 and 2 contain 1 % DMSO in 7H9 media and columns 23 and 24 contain Mtb H37Rv in media plus 1 % DMSO. The remaining 320 wells are equally divided between 0.5 and 10 μg/mL ethambutol.
5. The amikacin control plate is included to measure the consistent response of the mycobacterium to a known inhibitor throughout the multiple runs of a screening campaign. Columns 1 and 2 contain 1 % DMSO in 7H9 media and columns 23 and 24 contain Mtb H37Rv in media plus 1 % DMSO. The remaining 320 wells are equally divided between 0.13 and 2.5 μg/mL amikacin in media plus 1 % DMSO.

3.2.4 Mtb H37Rv Addition

1. Transport assay plates into the BSL-3 facility for addition of the mycobacterium.
2. Inside a BSC, thaw frozen stocks of H37Rv, pipette to mix, and inoculate the 7H9 media with a final in well dilution of 1–2 $\times$ 10^5 CFU/mL (*see* **Note 9**).
3. Place the inoculated media on a stir plate and allow the media to mix.
4. Carefully place the sterile WellMate cassette on the WellMate Dispenser. Make sure to keep the tips and tubing ends sterile.

Prime the WellMate by pumping uninoculated 7H9 media through the WellMate cassette and allow to sit in the lines for 1–2 min. Dispense an additional 5–10 mL through the lines.

5. Dispense 50 μL of uninoculated 7H9 media to one blank 384-well plate. This will be the control plate to monitor contamination and a negative end point control.
6. Dispense 25 μL of uninoculated 7H9 media to one empty 384-well plate. Observe any tips that may not be dispensing accurately.
7. Dispense 25 μL of diluted Mtb H37Rv (Subheading 3.2.4, **step 2**) to the CV plate. This will act as your CV plate to check WellMate dispensing for plating the bacteria and for the end point addition at the beginning of the run. Visually check that the WellMate dispensed into the center of each well.
8. Continue to dispense the diluted Mtb H37Rv to every well of the assay plates (test compounds plus ethambutol and amikacin control plates) using the Matrix WellMate.
9. After dispensing to ten plates (*see* **Note 10**), tap the sides of the plates to flatten the meniscus and knock any droplets of media on the sides into the assay wells and transfer the plates to the incubator.
10. Dispense 25 μL of uninoculated 7H9 media to a second empty 384-well plate. Observe any tips that may not be dispensing accurately.
11. Dispense 25 μL of diluted Mtb H37Rv (Subheading 3.2.4, **step 2**) to the CV plate. This will act as your CV plate to check that the WellMate is still dispensing accurately at the end of the run.
12. Incubate plates, stacked 2–3 high, in humidified incubator at 37 °C without CO_2 for 7 days.

It takes a single experienced operator ~1.5 h to execute a 100 plate run.

3.2.5 alamarBlue End Point Addition

1. Calculate the amount of alamarBlue needed for the run (4 mL for 384-well test plates).
2. Combine two parts of alamarBlue to 1.5 parts of 18.2 % Tween 80 (*see* **Note 11**).
3. Set up a new sterile WellMate cassette head on the dispenser and prime it with the alamarBlue/18.2 % Tween 80 solution.
4. Remove the assay plates from the incubator.
5. Starting with one of the Mtb CV plates, add 9 μL of the alamarBlue/18.2 % Tween 80 solution to every well.

6. Visually check the CV plate for dispensing to the center of each well.
7. Continue to add the solution to the assay plates. If all of the dispense steps have gone smoothly, then alamarBlue is added to the second CV plate at the end. If there has been a dispense issue either when the bacteria or end point reagent was added, then the second CV plate is moved to that place in the line. Tap the sides of the plates to flatten the meniscus and knock any droplets on the sides of the wells into the assay wells.
8. Incubate plates (stacked 2–3 high) in humidified incubator for 1 day at 37 °C without CO_2.
9. After 24 h, check that the bacteria control wells have turned pink (*see* **Note 12**).
10. Seal the plates with the aluminum foil seals. Bottom read the plates on the Perkin Elmer EnVision plate reader using the fluorescence setting with a 535 nm excitation and a 590 nm emission. If the bottom read is not an available option, then seal the plates with clear seals and top read (*see* **Note 13**).

3.2.6 Alternate End Point—BacTiter Glo™ End Point Addition (See Note 14)

1. Calculate the amount of BacTiter Glo™ needed for run (12 mL for 384-well plate) (*see* **Note 15**).
2. Equilibrate the two BacTiter Glo™ reagents to room temperature (*see* **Note 16**).
3. Mix the BacTiter reagent bottles as instructed by the manufacturer and combine in a flask. Protect the container from light by wrapping the container with foil.
4. Remove the media only plate and check that there is no turbidity in the media or indication of contamination.
5. Remove one Mtb CV plate from the incubator and allow it to equilibrate to room temperature.
6. Add 25 µL of BacTiter Glo™ to the Mtb CV plate.
7. After 10 min, seal the plate with a clear top seal.
8. Monitor the signal of the CV plate using the Perkin Elmer EnVision on the standard luminescence setting at 0.1-s-integration time. Read the plate every 5 min until the maximum signal is achieved and the signal begins to drop.
9. Based on the time to reach the maximum signal, calculate the timing from the WellMate dispense to the EnVision read to determine the number of plates that may be batched together in one dispense before the plates need to be read to capture the maximum signal.

10. Equilibrate the compound plates to room temperature and dispense 25 μL of BacTiter Glo™ to the assay plates, seal, incubate at room temperature, and read as in **step 8**.

3.2.7 Dose-Response Assay

Hits are picked from the original compound plates and screened in a dose-response assay using a stacked-plate method wherein each compound dilution is inter-plate rather than intra-plate [4]. Compounds screened in dose-response are tested in 10 twofold dilutions.

3.2.8 Preparation of Mammalian Cell Stocks

Using mammalian cells from frozen stocks facilitates the mammalian cell cytotoxicity assay by dissociating compound preparation from cell production.

1. Harvest Vero cells using TrypLE Express.
2. Collect the Vero cells in a 50 mL conical tube and centrifuge at 340*g* for 10 min.
3. Resuspend the cells in 20 mL c-MEM and determine cell concentration.
4. Centrifuge the cells at 340*g* for 10 min.
5. Resuspend the cells in cryopreservation media at 1.2×10^7 cells/mL.
6. Aliquot 1 mL of cells into the 2 mL cryovials.
7. Rate freeze the cells at 1 °C/min and then transfer to liquid N_2 for long-term storage.

3.2.9 Mammalian Cell Cytotoxicity Assay (See Note 17)

1. Hit compounds from the single-dose Mtb screen are screened using a stacked-plate method using the same 10 twofold dilutions as the Mtb assay.
2. 5 μL of compounds in c-MEM + 1.25 % DMSO are added at 5× concentration to columns 3–22 of each Corning 384-well assay plate.
3. Columns 1 and 2 contain 5 μL of c-MEM + 1.25 % DMSO and columns 23 and 24 contain 5 μL of 500 μM hyamine in c-MEM + 1.25 % DMSO.
4. Determine the amount of media (c-MEM) required for the assay assuming 36 mL per plate.
5. To the required volume of MEM add heat-inactivated FBS (final concentration 10 %) and P/S (final concentration 1 %). Mix.
6. Thaw the required number of aliquots of Vero cells rapidly in warm water.
7. Wash the cells by diluting in c-MEM and centrifuge at 340*g* for 10 min. Remove the supernatant.

8. Resuspend the cells in c-MEM and count using Trypan blue exclusion to determine cell viability.
9. Adjust to 125,000 cells/mL with c-MEM in a flask.
10. Stir on a stir plate for 5 min.
11. Prime the Wellmate with c-MEM + 1.25 % DMSO.
12. Plate 5 μL/well into two CV plates. Carefully place the cassette lines into the stirring cells. Prime the lines with cells and plate 20 μL/well into all columns of the CV plates. Ensure that there are no dispense problems. Continue dispensing 20 μL of cells to the assay plates containing 5 μL of compound.
13. Incubate at 37 °C and 5 % CO_2 with ~90 % humidity for 72 h.
14. Calculate the amount of CellTiter Glo™ needed for the run (12 mL for one 384-well plate).
15. Equilibrate the two CellTiter Glo™ reagents to room temperature.
16. Follow the manufacturer's instructions for mixing the CellTiter Glo™ reagents and combine into a flask (this method follows the manufacturer's instructions using a 1:1 end point addition). Protect the container from light by wrapping the container with foil.
17. Bring the CV plates to room temperature.
18. Add 25 μL of CellTiter Glo to the plates.
19. After 10 min, read the plates on the Perkin Elmer EnVision using the standard luminescence setting at 0.1-s integration time.
20. Ensure that there is not a dispense issue with the cassette head. If there is not, proceed with the compound assay plates.
21. Equilibrate the assay plates to room temperature.
22. Dispense 25 μL of CellTiter Glo to 10 of the assay plates.
23. Incubate at room temperature for 10 min.
24. Read on the Perkin Elmer EnVision as above.
25. Continue the process in groups of ten plates.

3.3 Data Analysis

1. Data from the microtiter plates is exported outside of the BSL-3 from the Perkin Elmer EnVision as individual .csv files named by the plate barcode. The data files are imported into IDBS Activity Base for data analysis and association with compound ID.
2. Results for each well are expressed as percent inhibition (% Inhibition) calculated as: 100 × ((Median Cell Ctrl-High Dose Ctrl Drug) − (Test well-High Dose Ctrl Drug))/(Median Cell Ctrl-High Dose Ctrl Drug).

3. Thirty-two control wells containing Mtb only and 24 wells containing Mtb and 2.5 μg/mL amikacin are included on each assay plate and are used to calculate Z' value [7] for each plate.
4. Any compound with an inhibition of ≥90 % is defined as a hit in the single-dose screen.
5. The dose-response data is analyzed using a four-parameter logistic fit (Excel Fit equation 205) with the maximum and minimum locked at 100 and 0. From these curves, Mtb IC_{90} and IC_{50} values can be calculated and CC_{50} values for Vero cell cytotoxicity.

During the course of a screening campaign, the median values for the Mtb control wells, 2.5 μg/mL amikacin, 0.13 μg/mL amikacin, and Z' value are graphed for each individual plate. This information on plate-to-plate and batch-to-batch variability is used to identify problems in the assay.

4 Notes

1. Mtb has been classified as a biosafety level 3 (BSL-3) agent by the Centers for Disease Control (CDC) and should be handled accordingly. We recently published a paper on the general safety procedures we use for HTS in containment [8]. Although the CDC has established some general rules for the handling of BSL-3 agents, each institution's biosafety committee will establish its own rules under these guidelines for handling a specific agent in its BSL-3 facility. Consequently, we have not provided details related to the regulatory and safety handling of this pathogen and refer the reader to this publication for general details and their institutional biosafety committee for detailed guidance.

   For efficiency, all work such as preparing the end point reagents that does not involve Mtb is performed at BSL2.
2. Table 1 contains information on the sourcing of materials that we have used successfully in HTS campaigns since, in our experience, the source for all of these components may be critical for a reproducible and robust HTS. If other sources are used they should be evaluated for their effect on the growth of H37Rv and their effect on the efficacy of know Mtb inhibitors. In either case, reagents should be purchased from one lot in sufficient quantity to execute the entire HTS campaign.
3. Other media/broths can be used to grow mycobacteria. Another common broth is 7H12 which is 7H9 broth supplemented with 0.1 % casitone, 5.6 μg/mL palmitate, 0.5 % bovine serum albumin, and 4 μg/mL catalase. These media

Table 1
Sources for materials used in successful HTS campaigns

Product	Manufacturer	Catalog number
7H11 agar base	Difco	283810
alamarBlue	Life Technologies	DAL1100
Amikacin sulfate	Sigma-Aldrich	A1774
BacTiter Glo	Promega	G8233
Bovine serum albumin	Sigma-Aldrich	A7638
CellTiter Glo	Promega	G7573
DMSO	Sigma-Aldrich	8418
Eagle's minimal essential media (MEM)	American Type Culture Collection (ATCC)	30-2003
Ethambutol dihydrochloride	Sigma-Aldrich	E4630
Fetal bovine serum (FBS)	Life Technologies	16140-063
Glucose	Sigma-Aldrich	G7528
Glycerol	Fisher Scientific	BP229-4
Middlebrook 7H9 broth base	Difco	271310
Middlebrook OADC	Fisher Scientific	211886
Mycobacterium tuberculosis H37Rv	ATCC	27294
Penicillin/streptomycin	Life Technologies	15140-122
Sodium chloride	Fisher Scientific	S271
TrypleE Express	Life Technologies	12604013
Tryptic soy agar (TSA)	Sigma-Aldrich	22091
Tween 80	Sigma-Aldrich	P1754
Vero cells	ATCC	CCL-81

formulations along with others were empirically determined to be best suited to growing mycobacterium in vitro many decades before current drug discovery initiatives began [9, 10]. Unfortunately, their composition can have a devastating effect on the drug discovery process [11].

4. Alternatively, Middlebrook 10 % ADC enrichment can be purchased form Becton Dickinson. The quality of the bacteria stock and the assay both rely on consistency in the media and the components that make up the media. The 10× ADC solution is a critical component in the media and dramatic variation in assay performance may be attributed to this component. There are differences from lot to lot in commercially purchased ADC, so our preference was to control this up front by

generating our own. In this reagent, the BSA has proven to be the most critical feature. Begin by testing a lot of BSA prior to purchasing and upon confirmation of consistent data then purchase sufficient amount of that lot of BSA for all future studies. The 10× ADC and media may be made up to a week in advance but fluctuations in performance have been noted after storage for a week. Additionally, it should be noted that Tween 80 will produce inconsistent results as the component ages. Therefore, replace the Tween 80 if a colorimetric change from pale yellow to dark yellow/orange is detected. Autoclaving the various media solutions in a container at least two times the volume of the media is also recommended not only to ensure that media is not lost to "boiling over" but also to ensure that media reaches a high enough temperature throughout to ensure a sterile culture.

5. The quality of the stock of Mtb is critical to ensuring reproducible and consistent results during screening. Again media preparation is key to this process. Due to the length of time required to generate the bulk culture, incubation in an upright humidified incubator is preferential to a water bath shaker due to the increased potential for contamination from a heated water bath. Furthermore, the propensity for Mtb to aggregate increases even with slow rotation in a shaker. Setting up the cultures in vented flasks substantially larger than the volume of the bulk culture allows adequate aeration and gently swirling the culture daily allows for adequate mixing of the media. Once the stock culture has been created and frozen, randomly selected vials are used to test for sterility and to calculate the stock Mtb concentration.
6. Mtb grows poorly on TSA which supports the growth of most potential contaminating microorganisms.
7. An experienced operator can easily run 100 plates in one run. However, we suggest that smaller batches, i.e., 50 plate batches, should be run until everyone is comfortable with work in the BSL-3.
8. These stocks are not stable for extended lengths of time. New stocks should be made periodically.
9. Due to the length of time for Mtb culturing and potential variability from one culture to the next, frozen stocks are used in the screen. This decreases the potential for any variants in batches of a large screening campaign which may not be evident until the end of the screen. The total 384-well assay volume for each well is 50 μL which provides adequate media to sustain the culture. The volume also decreases the edge effect from dehydration of the outer wells over the 7–8-day incubation period.

10. Handling the plates in batches of ten is somewhat arbitrary and depends on whether there is a single operator or additional people to move plates from the hood to the incubator. Groups of plates are moved into the incubator as the run proceeds in order to make space in the BSC. Media and bacteria are at room temperature but are not affected the same way as mammalian cells by exposure to room temperature and no added CO_2.
11. The 18.2 % Tween 80 solution and alamarBlue, 1.5:2 solution, are critical. As previously noted, fluctuations may occur due to the Tween 80 over time and alter the permeability of the bacteria to the alamarBlue.
12. The conversion from blue to pink may fluctuate depending on the length of time the plates are outside of the incubator during the addition of the alamarBlue mixture.
13. The Perkin Elmer EnVision will read fluorescence intensity, produced from alamarBlue, either from the top or bottom of the plate. However, the signal is more robust if the plates are sealed with an aluminum foil seal and read from the bottom.
14. BacTiter Glo™ end point reagent provides a simple mix, plate, and read luminescence end point. This reagent has several advantages over the alternative alamarBlue end point. The first is a shortened assay length, 7 days versus 8 days. The second is the decreased number of steps that the plates are handled by the screener. This decreases the potential to introduce contamination into an already lengthy assay and increases the safety of the procedure for the screener. Table 2 contains a comparison of EC_{50}, EC_{90}, and MIC values of known inhibitors of Mtb.

Table 2
Comparison of EC_{50}, EC_{90}, and MIC values of know inhibitors of TB

	AlamarBlue (AB)			Bac Titer-Glo (BTG)		
Compound	EC_{50} (μg/mL)	EC_{90} (μg/mL)	MIC (μg/mL)	EC_{50} (μg/mL)	EC_{90} (μg/mL)	MIC (μg/mL)
Rifampicin	0.02	0.02	0.16	0.02	0.03	0.04
Pyrimethamine	25.09	28.00	100.00	24.27	46.37	100.00
Isoniazid	0.19	>5.00	NA	0.13	0.20	0.31
Ethambutol	3.45	>200.00	NA	1.50	1.64	6.25
Cycloserine	24.76	28.01	100.00	23.55	26.38	100.00
Amikacin	0.12	0.14	0.16	0.07	0.12	0.16

15. This method will add 25 μL/well of BacTiter Glo™ across the plate. This is a modification from the manufacturer's instructions to accommodate the allowable volume per well in a 384-well plate.
16. It is important for this reagent that both the plates and the BacTiter Glo™ reagent are at room temperature to decrease temperature-based fluctuations in the data.
17. Normally, hits from the antimicrobial HTS are also evaluated in a mammalian cell cytotoxicity screen to ensure that the compounds are not cytotoxic to all cells. Historically, the cell line (Vero) most frequently used has been a kidney epithelial cell line derived from an African green monkey. We have also used THP and HepG-2 cells which may be more physiologically relevant.

References

1. International statistical classification of diseases and related health problems, 10th revision (ICD-10), 2nd edn. World Health Organization, Geneva, 2007
2. Global Health Observatory Data Repository (2015) World Health Organization, Geneva, Switzerland. http://apps.who.int/ghodata. Accessed July 2015
3. Collins LA, Franzblau SG (1997) Microplate alamar Blue assay versus BACTEC 460 system for high-throughput screening of compounds against *Mycobacterium tuberculosis* and *Mycobacterium avium*. Antimicrob Agents Chemother 41:1004–1009
4. Ananthan S, Faaleolea ER et al (2009) High throughput screening for inhibitors of mycobacterium tuberculosis H37Rv. Tuberculosis 89:334–353
5. Maddry JA, Ananthan S (2009) Antituberculosis activity of the molecular libraries screening center network library. Tuberculosis 89:354–363
6. Reynolds RC, Ananthan S et al (2012) High throughput screening of a library based on kinase inhibitor scaffolds against *Mycobacterium tuberculosis* H37Rv. Tuberculosis 92:72–83
7. Zhang J-H, Chung TDY et al (1999) A Simple Statistical Parameter for Use in Evaluation and Validation of High Throughput Screening Assays. J Biomol Screening 67–73
8. Rasmussen L, Tigabu B et al (2015) Adapting high-throughput screening methods and assays for biocontainment laboratories. Assay Drug Dev Technol 13:44–54
9. Youmans GP (1946) A method for the determination of the culture cycle and the growth rate of virulent human type tubercle bacilli. J Bacteriol 51(6):703–710
10. Sattler TH, Youmans GP (1948) The effect of "Tween 80", bovine albumin, glycerol, and glucose on the growth of mycobacterium tuberculosis var. hominis (H37Rv). J Bacteriol 56(2):235–243
11. Pethe K, Sequeira PC et al (2010) A chemical genetic screen in *Mycobacterium tuberculosis* identifies carbon-source-dependent growth inhibitors devoid of *in vivo* efficacy. Nat Commun 1(5):1–8. doi:10.1038/ncomms1060

Chapter 13

Identification of State-Dependent Blockers for Voltage-Gated Calcium Channels Using a FLIPR-Based Assay

Alberto di Silvio, JeanFrancois Rolland, and Michela Stucchi

Abstract

The FLIPR (Fluorescent Imaging Plate Reader) system has been extensively used in the early stages of drug discovery for the identification of small molecules as a starting point for drug development, and for the pharmacological characterization of compounds. The main application of the system has been the measurement of intracellular Ca^{2+} signals using fluorescent calcium indicators.

This chapter describes the application of a protocol for the study and characterization of state-dependent blockers of Voltage-Gated Calcium Channels (VGCC) on the $FLIPR^{TETRA}$.

The cell line suitable for the application of the protocol, and described hereafter, co-expresses the human CaV1.2 channel and the human inward rectifier K^+ channel Kir2.3. The presence of Kir2.3 allows the modulation of the plasma membrane potential and consequently of the state of the CaV1.2 channel by changing the extracellular K^+ concentration. In this way, CaV1.2 activity can be measured at different membrane voltages, corresponding to either the resting or partial inactivated state, by loading the cells with a calcium probe in extracellular low or high potassium buffer.

Key words State-dependent blockers, Voltage-gated calcium channel, Calcium fluorescent dye, FLIPR

1 Introduction

Ion channels belong to a large family of proteins that form pores in cellular membranes allowing the passage of ions down their electrochemical gradient. They react to membrane potential changes (voltage-gated), mechanical stress (mechano-sensitive), and/or chemical signals (ligand-gated) [1–3].

The "gold standard" technique for the study of voltage-gated channels is electrophysiology (patch clamp). The development of the patch clamp technique [4], which was acknowledged by the 1991 Nobel Prize in Physiology and Medicine, led to a great improvement in ion channel function understanding and pharmacology. However, the application of manual patch clamp to the screening of large

William P. Janzen (ed.), *High Throughput Screening: Methods and Protocols*, Methods in Molecular Biology, vol. 1439,
DOI 10.1007/978-1-4939-3673-1_13,

compound collections has been hampered by the intrinsic low throughput nature of the technique. Moreover, traditional electrophysiology is labor-intensive and requires very sophisticated skills. To overcome these limitations, over the last 15 years, different automated electrophysiology instruments with improved throughput have been developed [5]. However, although the throughput has been increased, the high cost associated with these automated systems is not compatible with the testing of a hefty number of chemical compounds. Hence, alternate techniques are needed to perform a primary selection of a more reasonable number of compounds to enter the "electrophysiological funnel."

Many efforts have been made to develop surrogate techniques that could allow the screening of ion channels against a larger number of compounds. These technologies fall in two main categories: nonfunctional (i.e., ligand binding assays and liquid chromatography mass spectrometry) or functional assays (i.e., flux and fluorescence assays) [6].

Fluorescence-based assays have become the most commonly used in high throughput screening for ion channel drug identification. In particular, fluorescent indicators allowing the measurement of the increase of cytosolic calcium concentrations are used for the study of voltage-gated calcium channels.

Voltage-gated calcium channels open in response to membrane depolarization allowing calcium to enter the cells. They mediate various cell functions such as contraction, neurotransmitter release, and signal transduction [7]. In fluorescence-based assays, the activation of these channels is triggered by the application of a buffer containing a high potassium concentration, thus inducing a depolarization. However, a major issue when measuring the activity of voltage-gated ion channels using a fluorescence indicator is represented by the absence of control of the plasma membrane potential. A smart approach to circumvent this limit was developed for the first time approximately 10 years ago [8]. The method employs the coexpression of a voltage-gated channel together with an inward rectifying potassium channel (Kir). The Kir channel keeps the cells hyperpolarized by shifting the plasma membrane potential close to the equilibrium potential for potassium (i.e., around −80 mV) when incubated in physiological extracellular solution. Under this condition, any increase in extracellular potassium concentration will change the ionic equilibrium and lead to a depolarization (Fig. 1). Different extracellular potassium concentrations are used to modulate the membrane potential and promote the conformational changes of the channel (from a closed/resting to a partial inactivated and to an open/conducting state).

In this chapter, we will describe how to set up a fluorescent-based assay protocol suitable for the identification of state-dependent blockers of a voltage-gated calcium channel (CaV1.2) on the FLIPR^{TETRA}.

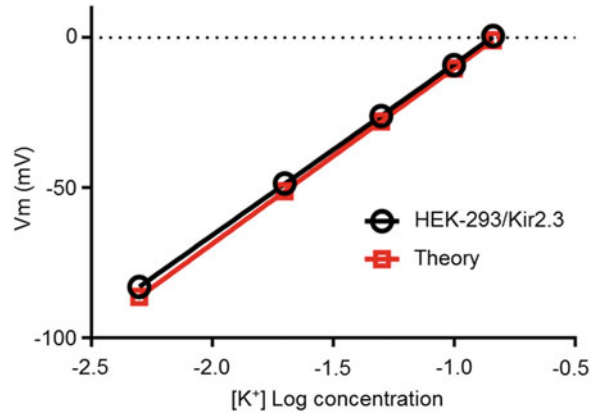

Fig. 1 Experimental and theoretical linear relationships between the extracellular potassium concentration and the plasma membrane potential of the HEK-293/Kir2.3 cell line. The *black* and *red symbols* represent the measured membrane potential obtained in current-clamp experiments (average ± SEM; $n = 4$) and the theoretical values calculated with the Goldman-Hodgkin-Katz equation, respectively

2 Materials

2.1 Cell Line and Culture Medium

1. Human embryonic kidney 293 (HEK-293) cells stably co-express the α1c, α2δ1, and β3 subunits of the human L-type CaV1.2 together with the K^+ inward rectifier channel Kir2.3.
2. Cells are cultured in EMEM Minimum Essential Medium Eagle with Earl's salts Balanced Salt Solution supplemented with 10 % fetal bovine serum, 2 mM L-glutamine, 1 % of penicillin/streptomycin, 0.2 mg/mL of G418, 2.5 μg/mL of zeocin, and 5 μg/mL of hygromycin B for selection.

2.2 Reagents and Buffers

1. "K0-Na150-Ca2" buffer: 150 mM NaCl, 2 mM $CaCl_2$, 10 mM glucose, 10 mM Hepes, pH 7.4 (*see* **Note 1**). For 1 L solution, add 200 mL of ultrapure water (prepared by purifying deionized water to reach a resistivity of at least 18 MΩ cm at 25 °C) to a 1 L graduated glass beaker. Add 8.76 g NaCl, 2.38 g Hepes, 0.29 g $CaCl_2 \times 2H_2O$, and 294.04 g glucose. Add ultrapure water to a volume of 900 mL. Mix with a magnetic stir bar and adjust the pH to 7.4 with 5 M NaOH. Transfer to a 1 L graduated cylinder and make up to 1 L with ultrapure water. Do not autoclave. Filter with a 0.22 μm filter membrane and store at 4 °C (*see* **Note 2**).
2. "K150-Na0-Ca2" buffer: 150 mM KCl, 2 mM $CaCl_2$, 10 mM glucose, 10 mM Hepes, pH 7.4 (*see* **Note 1**). For 1 L solution, add 200 mL of ultrapure water (prepared by purifying

deionized water to reach a resistivity of at least 18 MΩ cm at 25 °C) to a 1 L graduated glass beaker. Add 11.18 g KCl, 2.38 g Hepes, 0.29 g $CaCl_2 \times 2H_2O$, and 294.04 g glucose. Add ultrapure water to a volume of 900 mL. Mix with a magnetic stir bar and adjust the pH to 7.4 with 5 M NaOH. Transfer to a 1 L graduated cylinder and make up to 1 L with ultrapure water. Do not autoclave. Filter with a 0.22 μm filter membrane and store at 4 °C (*see* **Note 2**).

3. Assay buffer for resting state: 146 mM NaCl, 4 mM KCl, 2 mM $CaCl_2$, 10 mM glucose, 10 mM Hepes, pH 7.4, obtained by combining the required amount of "K0-Na150-Ca2" and "K150-Na0-Ca2" buffers so that the final osmolarity on the cells is not altered. To prepare 1 L of a 4 mM K^+ assay buffer mix 26.7 mL of "K150-Na0-Ca2" with 973.3 mL of "K0-Na150-Ca2."
4. Assay buffer for partial inactivated state: 125 mM NaCl, 25 mM KCl (or *X* mM KCl, *X* to be calculated according to **Note 3**), 2 mM $CaCl_2$, 10 mM glucose, 10 mM Hepes, pH 7.4, obtained by combining the required amount of "K0-Na150-Ca2" and "K150-Na0-Ca2" buffers so that the final osmolarity on the cells is not altered. For instance, to prepare 1 L of a 25 mM K^+ assay buffer, mix 166.7 mL of "K150-Na0-Ca2" with 833 mL of "K0-Na150-Ca2."
5. Assay buffer for target activation: "K150-Na0-Ca2" buffer.
6. Fluo-8 No Wash (Fluo-8 NW) Ca^{2+}-sensitive dye: thaw all the kit components at room temperature before use. Resuspend the lyophilized Fluo-8 NW dye in 200 μL DMSO into the vial and mix them thoroughly by pipetting up and down extensively. To prepare 100 mL of working solution (*see* **Note 4**), add 5 mL of pluronic-F127 component to 95 mL of the proper assay buffer and 100 μL of dye. Mix well. Pluronic-F127 helps to improve dye solubility. The dye solution can be prepared few hours in advance and kept at room temperature in the dark (or under sodium light, the dye is light sensitive) until usage. Best performance is achieved with freshly prepared dye solution, although dye can be used several hours after dilution in assay buffer (at room temperature and protected from light). Other fluorescent calcium dyes, such as Fluo-4 AM, Fluo-4 NW, and others could be used following the manufacturer indication (*see* **Note 5**).
7. Reference blocker, isradipine: prepare 10 mM stock solution in 100 % DMSO by dissolving 10 mg of powder in 2.69 mL of DMSO. Prepare aliquots, protect from light, and store at −20 °C.

3 Methods

1. Twenty-four hours prior to the experiment, wash cells with PBS and detach them from the tissue culture flask by trypsinization (enzyme-free dissociation buffer might be used instead).
2. Count the cells and resuspend them in growth medium without antibiotics at the required number of cells per volume. Usually 10,000–15,000 cells are seeded in 25 μL volume per well in a 384-well poly-D-lysine-coated plate (*see* **Note 6**).
3. Store the plate in an incubator (37 °C, 5 % CO_2).
4. Twenty-four hours after seeding, carefully remove the culture medium by flicking the cell plate or with the help of a cell washer. Make sure the wells are dry and the medium has been completely removed to avoid poor loading due to dye hydrolysis by the serum.
5. Add 20 μL/well of Fluo-8 NW working solution to the cell monolayer by using a multidrop dispenser or a multichannel electronic pipette. Make sure to keep the cell monolayer undamaged while adding the dye. The dye solution has been prepared in the appropriate buffer for studying the target in either its resting (assay buffer for resting state) or partially inactivated state (assay buffer for partial inactivated state). The proper K^+ concentration to be used to produce the half inactivation of the target is determined by running a test plate (*see* **Note 3**).
6. Incubate the cells for about 1 h at room temperature (*see* **Note 7**). During incubation, the dye uptake by the cell and its de-esterification in the cytoplasm occur.
7. Prepare the test compound plate to be used for injection on the cells loaded with the dye (*see* **Note 8**). Depending on the aim of the experiment, compounds can either be analyzed at a single or at several different concentrations (dose-response curve, DRC) in single or replicate points. Compounds will be prepared at a stock concentration which allows then to reach the desired final well concentration once injected by the $FLIPR^{TETRA}$ on the cell plate. For instance, to prepare the DRC plate for isradipine and/or test compounds, use a 96-well polypropylene plate as support. For a 10-point DRC with 10 μM as top compound concentration and half logarithmic dilution steps, start diluting 2 μL of a 10 mM stock solution into 8 μL of DMSO. Hence, compounds are 2 mM concentrated. Then, serially move 3.2 μL into 6.8 μL of DMSO until all the ten concentrations to be tested are obtained. To each compound and concentration, add 265 μL of proper assay buffer (for resting or for partial inactivated state) in order to produce the 5× concentrated working solutions in 2.5 % DMSO. Mix well and transfer into a 384-well polypropylene

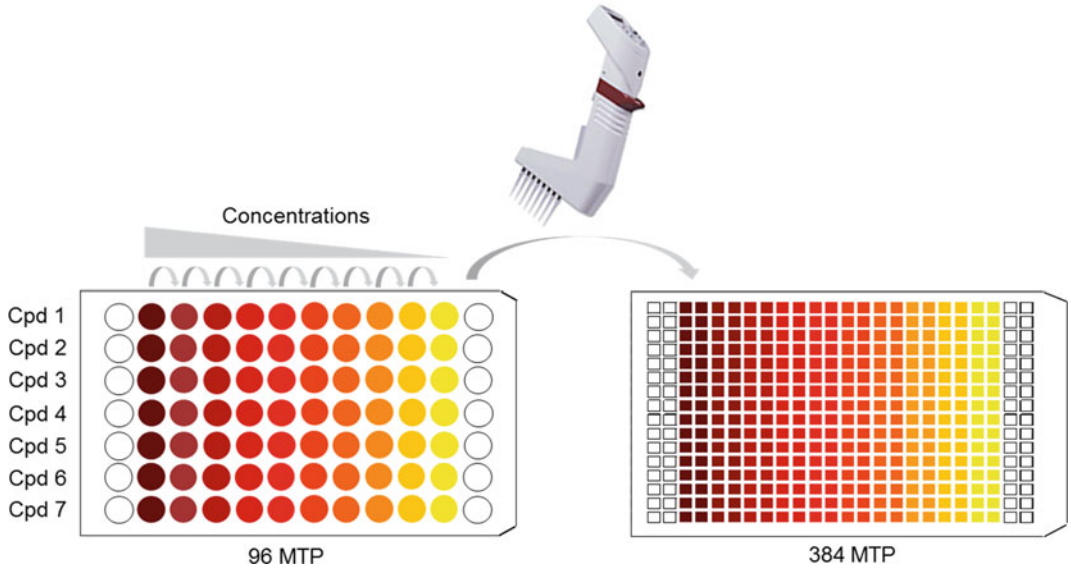

Fig. 2 Scheme of test compound plate preparation. Test compound dose-response curves are first prepared in 100 % DMSO in a 96-well polypropylene plate. After dilution in the suitable assay buffer, all the compounds/concentrations are transferred into a 384-well polypropylene plate thus obtaining quadruplicate data points

plate (V bottom), with the help of a multichannel pipettor or a 96-pipettor head. In this way, a quadruplicate data point can be obtained for each compound and concentration (Fig. 2). Run this procedure with any compound that needs to be tested, adjusting the volumes according to the stock concentrations and to the concentration range you want to test. It is recommended to prepare the compound plate under sodium yellow light to protect any photosensitive compound from light. Make sure to include on the compound plate the appropriate negative and positive controls.

8. Prepare the activator plate by filling a 384-well polypropylene plate (V bottom) with the assay buffer for target activation.
9. On the FLIPR^{TETRA}, read the basal RFU values of the assay plate with the excitation/emission pair 470_495 nm LEDs (for Fluo-8 NW excitation) and 515_575 nm emission filters (*see* **Note 9**). Adjust the FLIPR^{TETRA} settings in order to have basal fluorescence counts around 5000–10,000 RFUs. If the FLIPR^{TETRA} is equipped with an EMCCD camera, start from a basal fluorescence around 500–1000 RFUs.
10. Define the dedicated protocol on FLIPR^{TETRA}:
    (a) Assign the plate to position: the assay plate to the "read position," compound plate to the "source plate 2," and the activator plate to the "source plate 3." The "load tips position" can be used to put a reservoir with a 50 % DMSO/water solution for washing tips after compound injection.

(b) First injection: 5 μL of the 5× concentrated compounds, incubate for 5–10 min and record the emitted fluorescence. Make the FLIPR acquire samples every 1 s during the first minute after injection and every 2–5 s in the remaining minutes before KCl (assay buffer for target activation) addition. This helps to better define the kinetic shape immediately after compound injection.

(c) Wash tips first with water, then with a 50 % DMSO/water solution in the reservoir and last with water again.

(d) Second injection: 25 μL of assay buffer for target activation (75 mM KCl final in well and isotonic with Na^+) to activate the target. Measure the emitted fluorescence for two additional minutes and again acquire samples every 1 s during the first minute after injection and every 2–5 s in the remaining minute. This helps to better define the target activation kinetic immediately after its onset. Wash tips with water.

11. For data analysis: compute the response value by considering the delta between the Max RFU value after the second injection and the RFU mean immediately before the second injection. Divide this delta by the basal value which is measured at the first time point of the kinetic ($\Delta F/F0$) (Fig. 3).

12. Use a software like Graphpad or Genedata to draw the dose-response curve and to calculate the IC_{50} (Fig. 4).

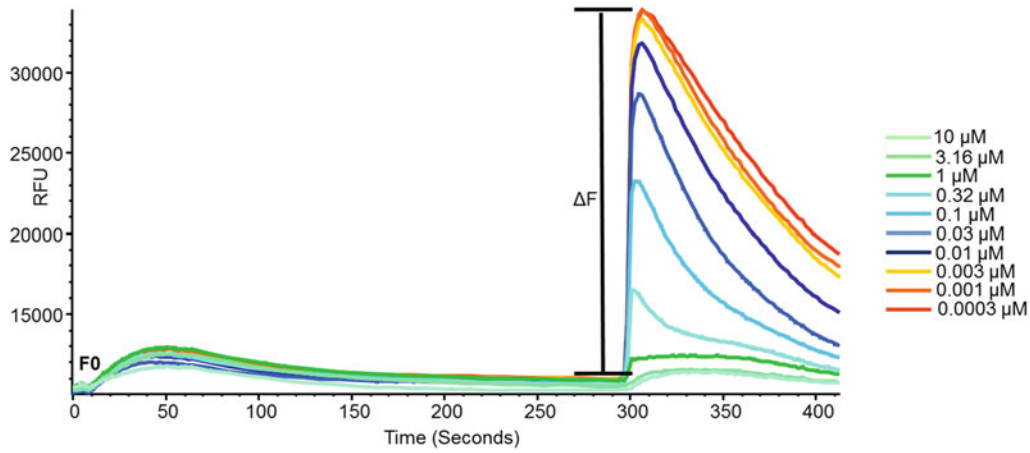

Fig. 3 Kinetic traces recorded by the FLIPR^{TETRA} and response value computation. Calcium responses in the presence of different isradipine concentrations were monitored on the FLIPR^{TETRA} in HEK-293 cells stably transfected with the CaV1.2 together with Kir2.3. The compounds injection occurs few seconds after the beginning of the measurement. After the desired incubation time (usually 3–5 min), the target activation buffer (75 mM KCl, final in the wells) is added to the cells and the emitted fluorescence is recorded for additional 110″–120″. The response value is computed as $\Delta F/F0$ where ΔF is the difference between the maximum peak recorded after target activation and the fluorescence measured at the few time points before activation buffer injection. $F0$ is the fluorescence recorded at the first time point

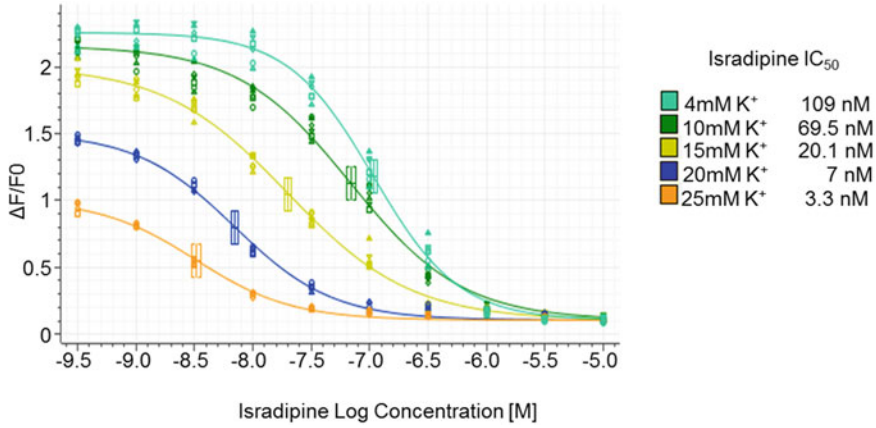

Fig. 4 Isradipine dose-response curve in different K^+ concentrations. Calcium responses were monitored on the FLIPR^{TETRA} in HEK-293 cells stably transfected with the CaV1.2 together with Kir2.3. Cells were loaded at RT with Fluo-8 NW solubilized in buffer containing different KCl concentrations (4–10–15–20–25 mM). Five minutes after the addition of the CaV 1.2 blocker isradipine in the proper K^+ buffer (4–10–15–20–25 mM), channels were activated with the activation buffer (75 mM K^+, final in the wells)

4 Notes

1. Magnesium is not included in the buffers, in order to avoid the possible inhibition of Kir2.3 channel (*see* Ref. 9).
2. Alternatively, the "K0-Na150-Ca2" and "K150-Na0-Ca2" buffers can be prepared starting from salts stock concentrations (i.e., 4 M NaCl, 3 M KCl, 1 M $CaCl_2$, 1 M glucose, and 1 M Hepes all prepared in ultrapure water). For instance, to obtain 1 L of "K0-Na150-Ca2," add 37.5 mL of 4 M NaCl, 2 mL of 1 M $CaCl_2$, 10 mL of 1 M glucose, and 10 mL of 1 M Hepes to 900 mL of water in a beaker and adjust the pH to 7.4 with 5 M NaOH. Transfer to a 1 L graduated cylinder and make up to 1 L with water. Filter with a 0.22 μm filter membrane, do not autoclave, and store at 4 °C.
3. To determine the proper K^+ concentration of the assay buffer for the half inactivation, an "inactivation curve" should be tested before starting the experiment. To do that, incubate cells with Fluo-8 NW dye made up in assay buffers containing KCl at different concentrations (1, 4, 10, 15, 20, 25, 30, and 50 mM, all concentrations must be isotonic with NaCl). Activate the target on the FLIPR^{TETRA} by injecting 75 mM K^+ buffer (assay buffer for target activation), compute the response values as described in Subheading 3, and draw a dose-response curve with the help of a software like Graphpad or Genedata. The KCl concentration yielding a half response with respect to the 1–4 mM KCl condition is the one that should be used to assay the target in its half inactivated state (Fig. 5).

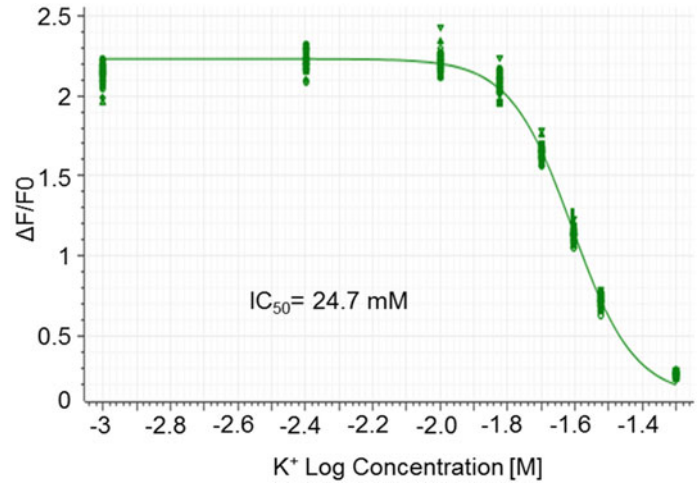

Fig. 5 K^+ inactivation curve. Calcium responses were monitored on the FLIPR^{TETRA} in HEK-293 cells stably transfected with the CaV1.2 together with Kir2.3. Cells were loaded at RT with Fluo-8 NW solubilized in buffer containing different KCl concentrations (1–4–10–15–20–25–30–50 mM, isotonic with Na^+). The target was activated by the injection of the activation buffer. The K^+ concentration giving the half inactivation of the channel is retrieved by considering the max kinetic peak after KCl injection, computing it as $\Delta F/F0$ (Fig. 3) and drawing a dose-response curve with a suitable software (such as Graphpad or Genedata). The calculated "IC_{50}" value is the K^+ concentration to be used to assay the target in its half inactivated state

4. Usually, the protocol suggested for the preparation of the dye working solution by the manufacturer can be tailored by reducing the final dye concentration without losing sensitivity. It is considered good practice to compare the different dye solutions by checking the assay performance and quality in the different conditions. Further, when preparing a large batch of dye solution to be used for a huge number of plates, it is important to verify the dye stability over time.
5. With cell lines different from HEK-293 and/or with other Ca^{2+}-sensitive dyes (such as Fluo-4 AM), it might be necessary to add probenecid (0.5–5 mM) to block the anionic pumps, endogenously expressed in the cells, that would extrude the dye from the cytoplasm.
6. Poly-D-lysine-coated plates can be either purchased or prepared by the operator according to the following procedure:
   (a) Starting from a 1 mg/mL stock solution, dilute the poly-D lysine to 50 μg/mL in sterile H_2O.
   (b) Add 25 μL/well of the diluted solution to a 384 MTP.
   (c) Incubate for 30′ at 37 °C or overnight at room temperature.

(d) Discharge the poly-D lysine solution, and rinse twice with 50 μL/well of sterile PBS to carefully remove any trace of residual poly-D-lysine since it can affect cell viability.

(e) Dry the plate by placing it open under a laminar flux hood.

7. The incubation with the Fluo-8 NW dye can be carried out at either room temperature or 37 °C. The advantage of the incubation at RT is the reduction of possible plate effects due to temperature drift across the plate that may occur when the assay plate is taken out from the 37 °C incubator before the reading on the FLIPR^{TETRA}. It is advisable to test both experimental conditions and check which one gives the best assay quality, especially with those dyes with which the 37 °C incubation is recommended (Fluo-4 AM).
8. The preparation of the compound plate might take considerable time; therefore, make sure to have it ready in due time (i.e., prepare it in DMSO before dye loading and dilute it in buffer during dye loading—it is recommended to add the buffer right before the injection on the cells).
9. These settings are chosen when using calcium-sensitive dyes such as Fluo-4 NW, Fluo-4 AM, or Fluo-8 NW. Different calcium indicators can require different LEDs/filters pairs since excitation and emission wavelength might change.

References

1. Moreau A, Gosselin-Badaroudine P, Chahine M (2014) Biophysics, pathophysiology, and pharmacology of ion channel gating pores. Front Pharmacol 5:1–19
2. Sukharev S, Sachs F (2012) Molecular force transduction by ion channels: diversity and unifying principles. J Cell Sci 125:3075–3083
3. Auerbach A (2013) The energy and work of a ligand-gated ion channel. J Mol Biol 425: 1461–1475
4. Neher E, Sakmann B (1976) Single-channel currents recorded from membrane of denervated frog muscle fibres. Nature 260:799–802
5. Farre C, Fertig N (2012) HTS techniques for patch clamp-based ion channel screening—advances and economy. Expert Opin Drug Discov 7:515–524
6. McManus OB (2014) HTS assays for developing the molecular pharmacology of ion channels. Curr Opin Pharmacol 15:91–96
7. Catteral WA, Perez-Reyes E, Snutch TP et al (2005) International union of pharmacology. XLVIII. Nomenclature and structure-function relationships of voltage-gated calcium channels. Pharmacol Rev 57:411–425
8. Xia M, Iredy JP, Koblan KS et al (2004) State-dependent inhibition of L-type calcium channels: cell-based assay in high-throughput format. Anal Biochem 327:74–81
9. Matsuda H (1991) Magnesium gating of the inwardly rectifying K^+ channel. Annu Rev Physiol 53:289–298

Chapter 14

A Luciferase Reporter Gene System for High-Throughput Screening of γ-Globin Gene Activators

Wensheng Xie, Robert Silvers, Michael Ouellette, Zining Wu, Quinn Lu, Hu Li, Kathleen Gallagher, Kathy Johnson, and Monica Montoute

Abstract

Luciferase reporter gene assays have long been used for drug discovery due to their high sensitivity and robust signal. A dual reporter gene system contains a gene of interest and a control gene to monitor non-specific effects on gene expression. In our dual luciferase reporter gene system, a synthetic promoter of γ-globin gene was constructed immediately upstream of the firefly luciferase gene, followed downstream by a synthetic β-globin gene promoter in front of the *Renilla* luciferase gene. A stable cell line with the dual reporter gene was cloned and used for all assay development and HTS work. Due to the low activity of the control *Renilla* luciferase, only the firefly luciferase activity was further optimized for HTS. Several critical factors, such as cell density, serum concentration, and miniaturization, were optimized using tool compounds to achieve maximum robustness and sensitivity. Using the optimized reporter assay, the HTS campaign was successfully completed and approximately 1000 hits were identified. In this chapter, we also describe strategies to triage hits that non-specifically interfere with firefly luciferase.

Key words Cell-based assay, Dual luciferase reporter gene assay, Firefly luciferase, *Renilla* luciferase, High-throughput screening, Hit triage

1 Introduction

Cell-based assays have long been recognized as a promising strategy in drug discovery. This is due to the fact that cell-based assays better mimic the physiological contexts and represent more relevant mechanisms than cell-free systems [1]. Cell-based reporter gene systems are an attractive option to study gene regulation and other cellular responses [1–3]. Early reporter gene systems, such as chloramphenicol acetyltransferase (CAT), alkaline phosphatase (AP), and β-galactosidase (β-gal), used colorimetric detection assays. Other reporter genes, such as green fluorescent protein (GFP), use fluorescence as the detection signal. These detection systems are less robust, insensitive, and can be prone to background interference. Bioluminescence reporter genes, on the other hand, have

William P. Janzen (ed.), *High Throughput Screening: Methods and Protocols*, Methods in Molecular Biology, vol. 1439,
DOI 10.1007/978-1-4939-3673-1_14,

several favorable features: they are very robust and sensitive, have no endogenous activity, show stable enzyme activity and signal, utilize a simple assay protocol, and have relatively low cytotoxicity. Several common luminescence reporter genes are firefly luciferase, *Renilla* luciferase, aequorin, and *Gaussia* [2]. These reporter gene products have different features and hence usages as reviewed in ref. [2]. Firefly luciferase has been engineered to be stable and have robust activity [4]. Its activity requires luciferin, ATP, and Mg^{2+} [5]. *Renilla* luciferase catalyzes the oxidative decarboxylation of coelenterazine in the presence of dissolved oxygen to produce blue light [6–8]. The reaction of *Renilla* luciferase does not require cofactors such as ATP or Mg^{2+}. The different conditions of these two enzymes enable the possibility to measure their activities sequentially, as described in the protocol section.

One important application of a reporter gene system is to study promoter activity of a target gene, as well as factors regulating the promoter activity [1, 8, 9]. A relatively simple single gene reporter system can be designed in which the promoter and/or other regulatory elements of a target gene are constructed to control the expression of the reporter luciferase. The reporter gene DNA constructs are then delivered into mammalian cells. As a result, the luciferase reporter activity can reflect the promoter activity. Stable cell lines harboring the reporter gene are preferred for assay development and high-throughput screening (HTS) because they typically have consistent and homogenous activity. However, it can be time consuming to generate stable cell lines. To allow for quicker analysis, transient transfection of selected cells with the reporter gene DNA can be employed.

Though very sensitive and robust, a single luciferase reporter gene system may be prone to some general non-specific effects on gene expression. A dual reporter gene system allows measurement of expression of the gene of interest and expression of a control gene in the same cell context. Through normalizing with the control gene activity, a number of non-specific effects can be excluded, such as transfection efficiency, general gene regulation, and cytotoxicity. The dual reporter genes can be in two separate DNA constructs and delivered into cells via co-transfection, or the two reporter gene cassettes can be tandemly configured in a single construct. Firefly luciferase and *Renilla* luciferase are commonly employed to build a dual reporter system [10, 11]. This is mainly because they use different substrates and their activities can be measured sequentially. Despite these favorable features, dual reporter gene systems may not be amenable to HTS. The sequential measurement of two luciferases is more labor and time intensive, and can potentially increase assay variability. When testing hundreds of thousands or millions of compounds in an HTS, it is advantageous to reduce the number of assay steps to as few as possible. A risk–benefit analysis must be conducted to decide whether to use a

dual or single reporter gene system for HTS. The former is labor intensive and more costly up front, but screening data can be normalized to eliminate several undesired effects. The latter is a simpler process, but results have to be carefully managed through a triage system to eliminate false positives. No matter which assay format is used, there will be non-specific interference, resulting in false positive hits. For example, it has been reported that chemical compounds can modulate cytoplasmic levels of firefly luciferase in a manner not specific to the target of interest [9, 12–15]. In the report of Auld et al. [16, 17], luciferase inhibitors appeared to be reporter gene activators due to their abilities to bind and stabilize the enzyme. This underscores the importance of validating HTS hits with strategic triage assays to confirm on target specificity.

Our team aims to increase γ-globin gene expression to replace malfunctioned β-globin in sickle cell patients. One of our strategies is to use a reporter gene assay to identify γ-globin gene activators. In this chapter, we describe our gamma-globin activator HTS work as an example to illustrate a firefly luciferase reporter assay development, optimization, HTS process, and hit triage. Our dual luciferase reporter gene construct contains a synthetic promoter sequence of the human γ-globin gene placed directly upstream of a firefly luciferase gene, followed downstream by a β-globin gene promoter sequence and *Renilla* luciferase as a control gene. F-36P cells were electroporated with the constructs to generate a stable cell line (the stable cell line generation is not described here). The firefly luciferase assay alone was optimized for HTS based on the fact that the *Renilla* luciferase had very low activity, rendering it unsuitable for data normalization. Additionally, the dual luciferase measurement was labor intensive and not practical for HTS. Instead, we performed a triage assay after HTS to exclude false positives.

In brief, the methods described below include four major parts:

1. Dual luciferase activity measurement.
2. Firefly luciferase assay optimization for HTS.
3. HTS campaign and outcomes.
4. Confirmation of HTS hits and triage assays.

2 Materials

1. F-36P stable cell line harboring the dual reporter gene system was maintained in complete culture medium, RPMI-1640 with 20 % FBS and supplements (1 % GlutaMax, 10 ng/mL recombinant human GM-CSF, 1 mM sodium pyruvate).
2. The supplement recombinant human GM-CSF, was reconstituted from lyophilized protein to 0.1 mg/mL in sterile PBS. Aliquots were stored at −80 °C and freeze-thaws were limited.

3. Hemin as a tool compound, its stock solution was prepared in DMSO at 10 mM or as needed.
4. Hydroxyurea as a tool compound, the stock solution was prepared in DMSO at 100 mM or as needed.
5. A known luciferase binding small molecule, prepared in house.
6. Dimethyl sulfoxide.
7. Dual-Glo® Luciferase Assay System (Promega Corp.).
8. Renilla-Glo® Luciferase Assay System (Promega Corp.).
9. Steady-Glo® Luciferase Assay System (Promega Corp.).
10. Non-lysis assay substrate D-Luciferin, prepare 5 mM D-Luciferin stock solution in RPMI-1640. Mix well and use fresh.
11. HERAcell® 240 CO_2 tissue culture incubator (Thermo Fisher Scientific, Inc.).
12. Vi-CELL® Cell Viability Analyzer (Beckman Coulter, Inc.).
13. Echo® Liquid Handler (Labcyte, Inc.).
14. Multidrop™ Combi Reagent Dispenser (Thermo Fisher Scientific, Inc.).
15. Multidrop™ standard dispensing cassette (Thermo Fisher Scientific, Inc.).
16. Multidrop™ metal tip small tube cassette (Thermo Fisher Scientific, Inc.).
17. 384-well compound plate for compound preparation.
18. 384-well cell culture regular volume plate
19. 384-well cell culture small volume plate.
20. 1536-well cell culture plate with lid.
21. EnVision® Multilabel Plate Reader (PerkinElmer).
22. ViewLux® uHTS Microplate Imager (PerkinElmer).

3 Methods

3.1 Dual-Glo® Luciferase Activity Measurement

Our original plan for HTS was to measure γ-globin promoter-controlled firefly luciferase and β-globin promoter element-controlled *Renilla* luciferase. Utilizing electroporation, we transfected F-36P cells with the dual reporter gene plasmid (as shown in Fig. 1) and performed stable monoclonal selection. We analyzed F-36P monoclones with Dual-Glo® Luciferase Assay System. In this section, we describe the procedures to measure the firefly and *Renilla* luciferase activity in a 384-well plate format. These data provided initial information to select the monoclonal stable cell lines as well as the final HTS assay format.

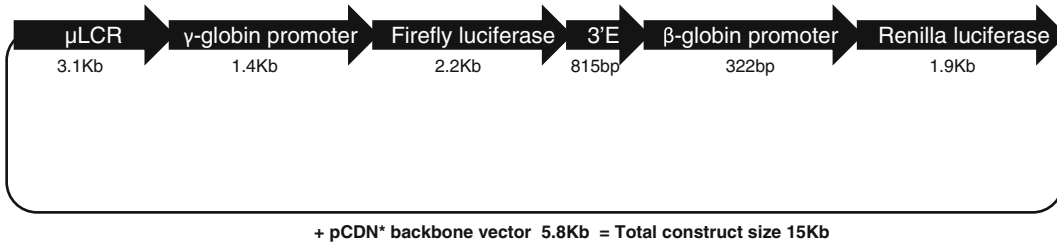

Fig. 1 Schematic of the dual luciferase reporter gene construct

3.1.1 Compound Plate Preparation and Cell Treatment

1. In a 384-well compound plate, add stock tool compound solutions in DMSO to column 1 or 13, then perform threefold serial dilutions in DMSO to sequential columns, skipping column 6 and 18, for a total 11 doses (*see* **Note 1**).
2. Use an Echo® to transfer 133 nL from the prepared compound source plate to a 384-well cell culture large volume plate.
3. Transfer freshly cultured F-36P cells from the selected monoclone to a 50 mL conical tube, centrifuge at 300 x *g* for 5 min (*see* **Note 2**).
4. Remove medium and resuspend cells in 10 mL of RPMI-1640 with 10 % FBS and supplements (*see* **Note 3**).
5. Count cell density and viability using a Vi-CELL®.
6. Dilute cells to 2.5×10^5 cells/mL in RPMI-1640 with 10 % FBS and supplements.
7. Sterilize a standard dispensing cassette attached to a Multidrop™ Combi by soaking the lines with 70 % ethanol or isopropanol for 10 min. Rinse with sterile PBS or assay medium (*see* **Note 4**).
8. Prime and dispense the cell solution at 40 μL/well to the assay plate stamped with compounds.
9. Allow plates to rest at room temperature for 30 min.
10. Incubate plates in an incubator at 37 °C with 5 % CO_2 for 72 h (*see* **Notes 5** and **6**).

3.1.2 Dual-Glo Luciferase Activity Detection

1. After incubation, remove assay plates from the incubator to equilibrate to room temperature for 30 min. This reduces variation caused by uneven temperature of plates.
2. According to the Dual-Glo® Luciferase Assay System manual, prepare firefly luciferase reagent by combining one bottle of Dual-Glo® Luciferase Buffer with one bottle of lyophilized Dual-Glo® Luciferase Substrate and mix well (*see* **Note 7**).
3. Using the Multidrop™ Combi and a standard dispensing cassette, add 20 μL/well of prepared firefly luciferase substrate

solution and incubate at room temperature in the dark for 20 min.

4. Read luminescence with the EnVision® Multilabel Plate Reader within 45 min (*see* **Note 8**).
5. Prepare Dual-Glo® *Renilla* luciferase reagent by diluting the Dual-Glo® Stop and Glo® Substrate 1:100 with Dual-Glo® Stop and Glo® Buffer and mix well (*see* **Note 9**).
6. Using the Multidrop™ Combi and a separate standard dispensing cassette, add 20 μL/well of Dual-Glo® *Renilla* luciferase solution and incubate at room temperature in the dark for 20 min. Read luminescence on EnVision®.
7. For *Renilla* luciferase activity measurement alone, replace the Dual-Glo® Luciferase Assay System with the Renilla-Glo® Luciferase Assay System and follow the manual accordingly.

Figure 2 shows the results of dual luciferase activity measurement with one representative F-36P clone. Figure 2a is the firefly luciferase activity signal after 72 h hemin treatment, while Fig. 2b shows the residual firefly luciferase signal after quenching (without addition of *Renilla* luciferase substrate). The data clearly demonstrate that γ-globin promoter-controlled firefly luciferase activity (Fig. 2a) is very high, resulting in significant residual signal almost equivalent to the *Renilla* luciferase levels alone, as shown in Fig. 2c. This situation was true for all of the clones we analyzed. Due to the substantial residual signal remaining from the firefly luciferase after quenching, normalization with *Renilla* luciferase activity became less advantageous. In addition, extra steps to measure the *Renilla* luciferase activity would be more labor intensive and increase probability of errors during the HTS process. Therefore, we decided to forgo the dual reporter assay and focus on the firefly luciferase activity.

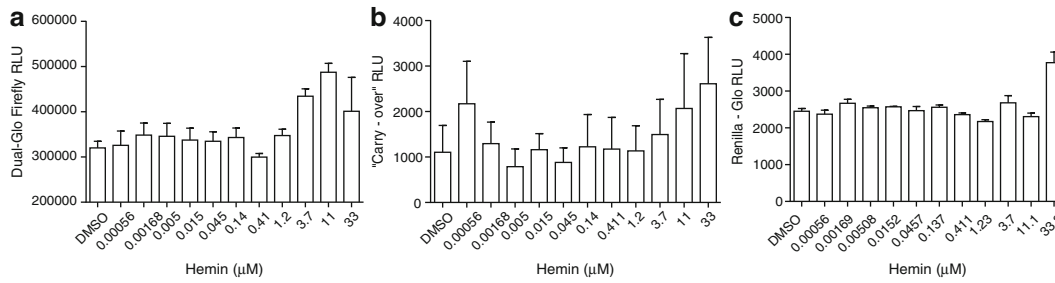

Fig. 2 Dual luciferase activity measurement in 384-well plates. (**a**) Firefly luciferase signal prior to the quenching step; (**b**) residual firefly luciferase signal after quench step, but without *Renilla* luciferase substrate; (**c**) *Renilla* luciferase signal alone measured with a *Renilla*-Glo® analysis system

3.2 Firefly Luciferase Reporter Assay Development for HTS

It is known that γ-globin has very low expression in adult blood cells. Our main goal to achieve therapeutic benefit is an up-regulation of γ-globin to at least 120–150 % vs. baseline (100 %). As indicated in the above section, our tool compounds showed mild activation with a modest signal window (signal/background around 2). To increase the robustness for HTS, we used tool compounds to identify conditions that would maximize the assay window and minimize variability. For a cell-based assay, several factors are in the scope of optimization, such as cell density, serum concentration, cell passage number, DMSO tolerance, and compound treatment time. In addition, we often prepare large supplies of frozen cells that can ensure a sufficient amount of cells with consistent activity throughout the entirety of the HTS. In the following section, we describe the optimization of a few factors leading up to HTS. Based on the results from Subheading 3.1 which was performed in 384-well large volume plates, we began to miniaturize the assay by titrating several conditions in 384-well small volume plates, and then ultimately transferred the assay to 1536-well plate for final optimization and validation.

3.2.1 Cell Density Titration in 384-Well Plates

1. Using an Echo®, stamp 33 nL of compounds to 384-well small volume plates.
2. Prepare cell solution as described from **steps 3** to **5** in Subheading 3.1.1.
3. Dilute cells in RPMI-1640 with 10 % FBS and supplements to desired cell densities: 5×10^5, 2.5×10^5, and 1.25×10^5 cells/mL.
4. Using a Multidrop™ Combi with a metal tip small tube cassette, dispense 10 μL/well of cell solution to a 384-well plate previously stamped with compounds.
5. Incubate plates for 72 h in a tissue culture incubator at 37 °C with 5 % CO_2.
6. After incubation, let plates equilibrate at room temperature for 30 min.
7. Prepare Steady-Glo® Luciferase Assay System according to the manufacturer's instructions.
8. Using a separate cassette, dispense 5 μL/well of reconstituted Steady-Glo® reagent.
9. Incubate for 20 min at room temperature in the dark. Read luminescence signal with EnVision®.

3.2.2 Serum Titration in 384-Well Plates

1. Similarly to **steps 3–5** in Subheading 3.1.1, reconstitute cells to desired cell density (5×10^5 cells/mL) in RPMI-1640 with all of the supplements but no serum.
2. Add serum to different concentrations: 10 %, 5 %, 2.5 %, and 1.25 %.

3. Dispense cell solutions at 10 μL/well to 384-well culture plates stamped with tool compounds.
4. Perform the treatment and detection as described in Subheading 3.2.1.

3.2.3 DMSO Titration in 1536-Well Plates

After the cell density and serum titration in 384-well small volume plates, we transferred the assay to 1536-well plates. The volume of cells dispensed to each well was halved (from 10 to 5 μL) in 1536-well plates to test cell density and serum based on the data from 384-well plates. The data were very consistent between 384-well and 1536-well plates. Our next step was to test DMSO tolerance and frozen cell activity in 1536-well format.

1. Using an Echo®, transfer 15 nL of tool compounds to 1536-well culture plates.
2. Transfer freshly cultured F-36P cells to conical tubes. Centrifuge cells and resuspend to 5×10^5 cells/mL in RPMI-1640 with 5 % FBS and all supplements.
3. Add DMSO to cell solutions to concentrations of 0 %, 0.2 %, 0.45 %, 0.7 %, 1.2 %, and 1.7 %.
4. Using a Multidrop™ Combi with a sterilized small tube cassette, dispense cell solutions at 5 μL/well to 1536-well plates stamped with tool compounds. Together with the DMSO introduced by compound solutions, the final DMSO levels were 0.3 %, 0.5 %, 0.75 %, 1 %, 1.5 %, and 2 %.
5. Incubate the plates for 72 h in a tissue culture incubator at 37 °C with 5 % CO_2.
6. After incubation, bring plates out, remove the lids from the plates, and allow plates to equilibrate to room temperature for 30 min.
7. Prepare Steady-Glo® Luciferase Assay System according to the manufacturer's instructions.
8. Using a Multidrop™ Combi with a small tube cassette attached, dispense 3 μL/well of reconstituted Steady-Glo® at medium dispensing speed (*see* **Note 10**).
9. Incubate for 20 min at room temperature in the dark. Read luminescence signal with EnVision®.

3.2.4 Comparison of Freshly Cultured Cells with Cryopreserved Cells in 1536-Well Plates

1. Using an Echo®, transfer 15 nL compounds to 1536-well culture plates.
2. Quickly thaw cryopreserved cells in a 37 °C water bath.
3. Wash cells once with RPMI-1640 containing 5 % FBS and supplements (*see* **Note 11**).
4. Reconstitute cells in the same medium, count cell density and viability using a Vi-CELL®.

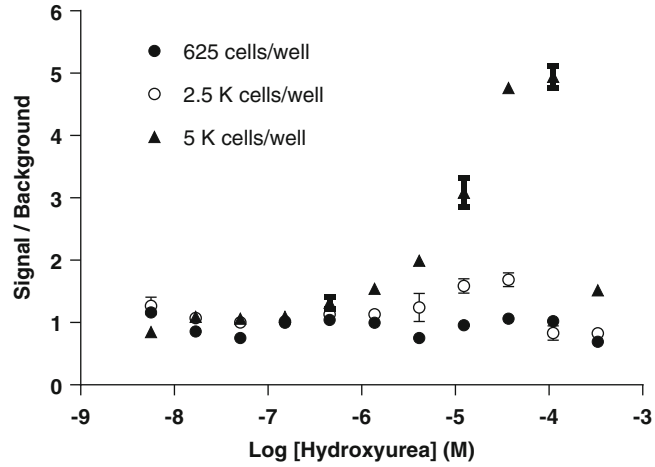

Fig. 3 Cell density titration testing firefly luciferase activity in 384-well plates. Cells were resuspended to three densities, then plated at 10 μL/well, and treated for 3 days before the measurement of firefly luciferase activity

5. Dilute cells to 5×10^5 cells/mL in the same medium.
6. With similar steps as described in **steps 3–5** in Subheading 3.1.1, prepare fresh cell solution at 5×10^5 cells/mL in RPMI-1640 with 5 % FBS and all supplements.
7. Dispense both cell solutions to 1536-well plates stamped with tool compounds.
8. Perform the treatment and detection as described in the previous section.

Cell density affects signal window, sensitivity, and cytotoxicity tolerance. Figure 3 shows that the tool compound hydroxyurea had a greater signal/background with the highest cell density (5 K cells/mL). As a result, we selected the cell density of 5×10^5 cells/mL (5 K cells/10 μL/well for the 384-well plate format, 2.5 K cells/5 μL/well for the 1536-well plate format).

Serum affects cell viability, proliferation, and biological signaling pathways. It may also affect the binding affinity of compounds and reduce hit identification. As a result of these conflicting outcomes, the amount of serum to use becomes a balance between these aspects. In Fig. 4, hemin shows a higher response with lower serum concentrations, while hydroxyurea has a higher response with higher serum concentrations. Although not tested, we assume that serum proteins bound to hemin and reduced its potency. For hydroxyurea, higher serum concentrations ensured cell viability and possibly cell proliferation, resulting in higher activity. Based on the responses of these two tool compounds, we selected 5 % FBS as our final serum concentration to balance the serum effects.

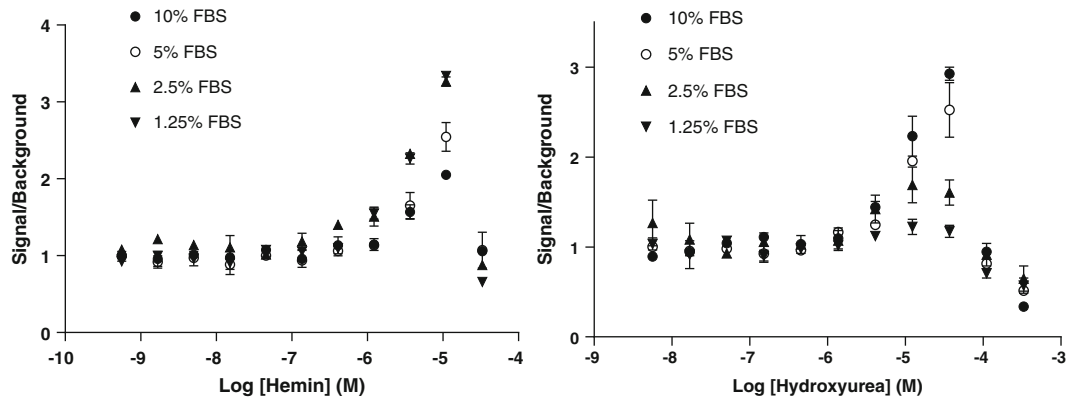

Fig. 4 Titration of serum concentration with tool compound treatment in 384-well plates. Cells were resuspended in medium with different concentrations of FBS, plated, and treated for 3 days before the measurement of firefly luciferase activity

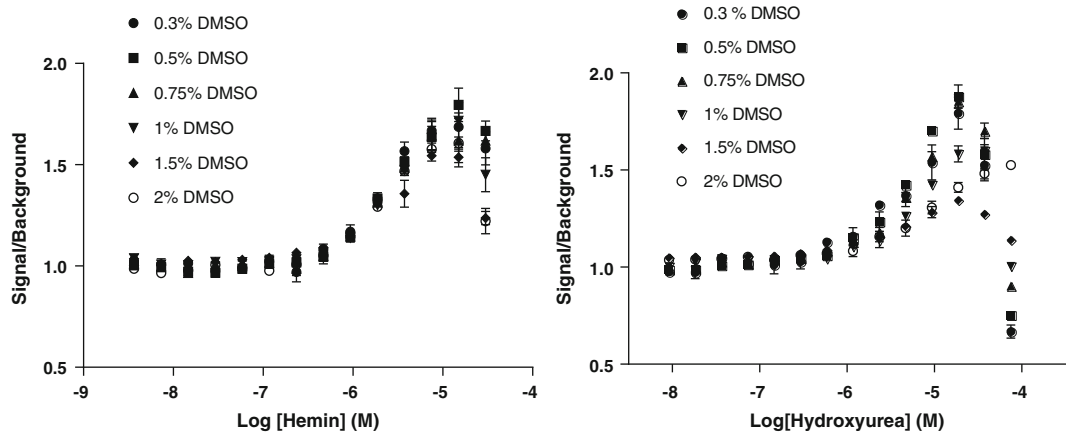

Fig. 5 Titration of DMSO concentration in 1536-well plates. The final DMSO concentrations (shown in the figure) were from compound source (0.3 %) and additional DMSO to cell solutions. Cells were plated and treated for 3 days before the measurement of firefly luciferase activity

A DMSO titration was performed to determine assay tolerance to solvent. Our compound library is dissolved in neat DMSO to 1 mM concentration and introduces 0.5–2 % DMSO to our assays depending on the final compound concentration. Figure 5 shows that DMSO levels greater than or equal to 1 % had a negative effect on the signal/background. Therefore, we chose to limit DMSO to 0.5 % in this assay.

One may have noticed that data from Fig. 5 had lower signal/background when compared with Fig. 4. This might be due to the cell passage effect since the cells used for DMSO titration had high passage numbers (around 22 passages). In addition, we noticed that cells that were scaled up for cryopreservation in large flasks

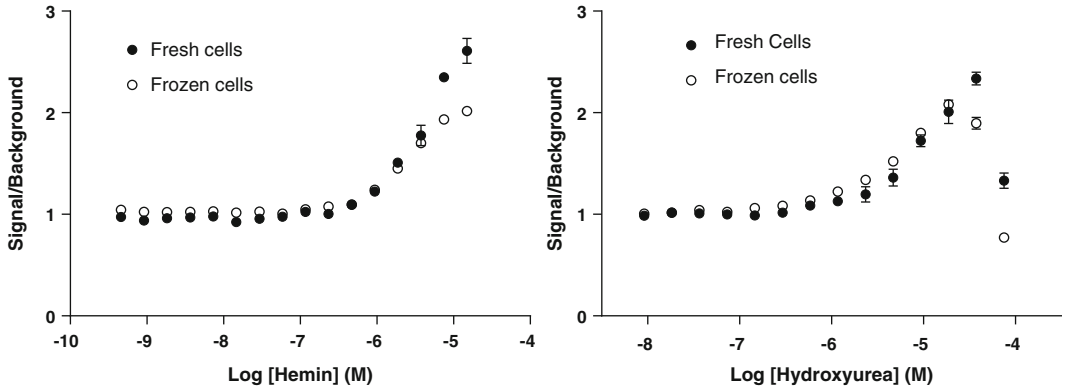

Fig. 6 Comparison of tool compound responses with frozen cells and freshly cultured cells. Cell solutions were prepared from cryopreserved cells or freshly cultured cells, plated, and treated for 3 days before the measurement of firefly luciferase activity

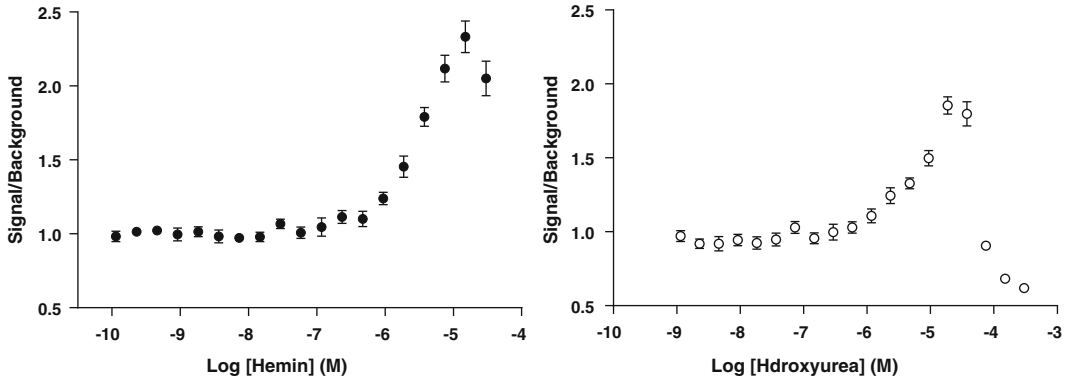

Fig. 7 Tool compound responses with frozen cells under final HTS assay conditions in 1536-well plate format

(3 L) had lower responses to tool compounds. Ultimately, we had success generating fit for purpose frozen cell batches using earlier passage cells (the process to scale up began from an earlier stock at passage 11).

Several batches of frozen cells were prepared and their responses in the assay were compared to freshly maintained cells at similar passage numbers. Figure 6 demonstrates that frozen cells had comparable tool compound responses as fresh cells. All of the HTS batches were similarly validated with tool compounds. With the final optimized 1536-well assay conditions (2.5 K cells/5 μL/well, 5 % FBS, 72 h treatment, 0.5 % DMSO), we tested the tool compounds to validate a frozen batch of cells. Figure 7 shows that both hemin and hydroxyurea had expected dose–response curves. Hemin had a higher and less variable signal/background, as well as a high signal plateau which is ideal for a high control. Therefore, we used hemin at the plateau concentration (15 μM) as

the high control for the HTS. With these finalized conditions, we tested assay performance with a 10 K compound validation set. The data demonstrate acceptable robustness (S/B around 3, Z' around 0.6, *see* **Note 12**) and coefficient of variation less than 10 %. The hit cut-off value was set at 145 % with the control DMSO set at 100 % (*see* more discussion in Subheading 3.4).

3.3 HTS Campaign and Outcomes

We performed the HTS with the optimized and validated firefly luciferase assay in 1536-well format. The screening library, consisting of approximately 1.8 million diverse small molecules, was screened one time at 5 μM. To accommodate the 3 day treatment, our campaign was scheduled for cell plating on Monday, Tuesday, and Friday while detection and plate reading occurred on Thursday, Friday, and Monday. The protocol below is an example of a 200 plate run, a typical daily batch size in our facility.

3.3.1 Compound Stamping

Using an Echo®, transfer 25 nL of 1 mM compound stock solution to 1536-well plates. Columns 11 and 12 had DMSO only; columns 35 and 36 were left empty (*see* **Note 13**). Seal plates and store at 4 °C until ready for use. Plates should be equilibrated to room temperature prior to adding cells.

3.3.2 Cell Plating and Treatment

1. Quickly thaw frozen cells in a 37 °C water bath, then transfer cells to 50 mL conical tubes.
2. Slowly add RPMI-1640 with 5 % FBS and all supplements at a ratio of around 10 mL of medium per 1 mL thawed cells. Gently pipette up and down to mix.
3. Centrifuge at 200 × *g* for 4 min.
4. Remove supernatant and add about the same amount of culture media. Gently pipette up and down to break up cell pellet and reduce cell aggregation (*see* **Note 14**).
5. Further dilute cells with media to achieve a cell concentration of approximately 1–2 × 10^6 cells/mL and mix thoroughly.
6. Count cell density and viability using a Vi-CELL®.
7. Dilute cells to 5 × 10^5 cells/mL into a sterile container (a glass bottle). Calculate the amount of cell solutions required for plating. Always keep at least 200 mL of dead volume. For two hundred 1536-well plates, approximately 1.75 L cell solution would be required.
8. Transfer 99 mL of cell solution to another container and add the high-control hemin to achieve a final concentration of 15 μM at 0.5 % DMSO.
9. Using a Multidrop™ Combi with a small tube cassette, dispense 5 μL/well of cell solution prepared in **step** 7 to 1536-well plates stamped with compounds (prepared in Subheading 3.3.1), skipping columns 35 and 36 (*see* **Note 15**).

10. Using another small tube cassette, dispense 5 μL/well of cell solution with the high control (prepared in **step 8**) to columns 35 and 36.
11. Place lids on microtiter plates, centrifuge plates at 200 × *g* for 1 min in a table top centrifuge.
12. Allow plates to rest at room temperature for 30 min.
13. Place plates in a 37 °C, 5 % CO_2 incubator for 72 h.

3.3.3 *Firefly Luciferase Detection*

1. After 72 h treatment, remove plates from the incubator and remove lids and equilibrate at room temperature for 30 min.
2. Prepare 1 L of Steady-Glo® substrate solution following the manufacturer's instructions.
3. Using a Multidrop™ Combi with a small tube cassette, dispense 3 μL/well of Steady-Glo substrate solution using medium dispensing speed.
4. Centrifuge the plates at 200 × *g* for 1 min in a table top centrifuge.
5. Incubate for at least 10 min at room temperature, shielded from light.
6. Read luminescence signal with a ViewLux® (*see* **Note 16**).

Figure 8a is a flow chart showing the HTS process. Among a total of 1350 plates screened, only a few plates had failed *Z′* values (below 0.4). Figure 8b shows the assay performance (the inset) and

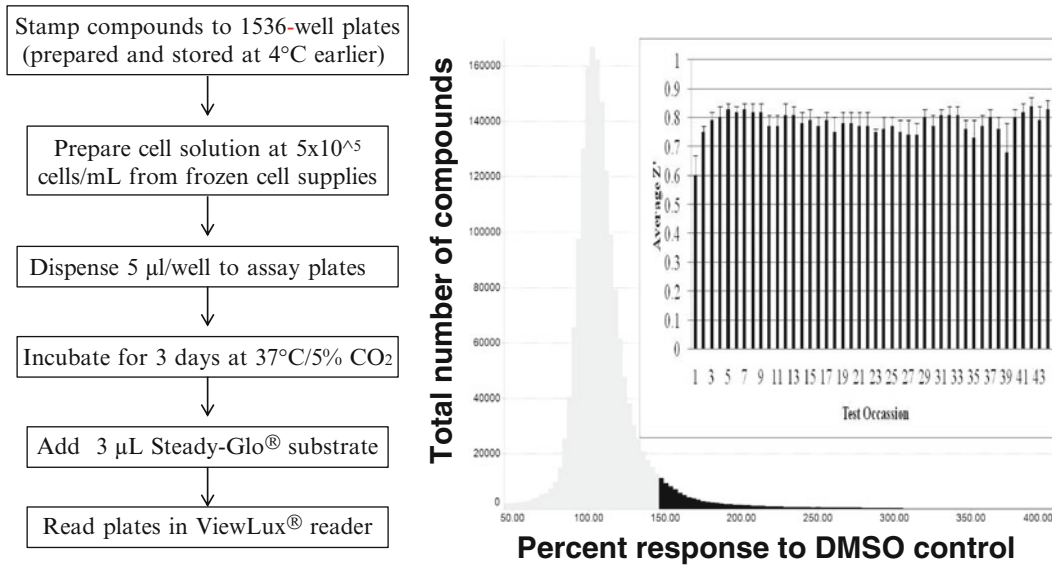

Fig. 8 HTS process flow chart (*left panel*), hit distribution (*right panel*), and assay performance (*inset*). For the hit distribution, the black area highlighted the hits with responses above 145 %. In the inset graph, each bar represents the average of *Z′* value from a batch of 32 plates

the distribution of hits. With the cut-off value of 145 %, approximately 31,000 compounds were identified (the dark area in Fig. 8b) and followed up with our triage assay as described below.

3.4 Confirmation of HTS Hits with Triage Assays

As discussed in Subheading 1, some firefly luciferase inhibitors can appear to be activators in cell-based firefly luciferase reporter gene assays. It is therefore very important to have an effective triage strategy to eliminate these false positives. We used a non-lysis substrate system (no detergent) to test the HTS hits, and then compare the activity with the lysis substrate (Steady-Glo) activity to identify potential false positives. Our rationale is that firefly luciferase binders stabilize the enzyme and increase the protein concentration [1–6]. In the Steady-Glo® substrate system, the strong detergent used to lyse cells would dissociate the inhibitor and the enzyme, resulting in higher activity. In the non-lysis substrate system which has no detergent, the luciferase-inhibitor complex would remain intact, rendering the enzyme incapable of turning over the luciferin substrate. Compounds active in the lysis format, but inactive in the non-lysis format would be considered false positives. We tested our hypothesis with the validation set (diverse set of 10 K compounds) as well as a known luciferase binders. Data demonstrated that both systems were necessary to select true hits.

Compounds, including the validation set of 10,000 compounds and HTS hits of 31,000 compounds, were tested at 5 μM. The validation set was run in triplicate (standard process for HTS validation), while the HTS hits were tested in duplicate.

3.4.1 Cell Lysis System with Steady-Glo

The Steady-Glo® Luciferase Assay System (with lysis) was performed the same as described in Subheading 3.3.

3.4.2 Non-Lysis Substrate System Activity Measurement

1. Compound preparation and cell treatment were the same as in Subheadings 3.3.1 and 3.3.2.
2. Following treatment, remove plates from the incubator and equilibrate without lids at room temperature for 30 min.
3. Prepare 0.266 mM D-Luciferin solution by diluting the 5 mM D-Luciferin stock solution (*see* Subheading 2) in room temperature RPMI-1640.
4. Using a Multidrop™ Combi with a small tube cassette, dispense 3 μL/well of 0.266 mM D-Luciferin. The final D-Luciferin substrate concentration was at 0.1 mM (*see* **Note 17**).
5. Centrifuge plates at 200 × *g* for 1 min in a table top centrifuge.
6. Incubate for at least 10 min at room temperature, shielded from light.
7. Read plates on a ViewLux® (*see* **Note 18**).

3.4.3 Full Dose Curve Confirmation

1. Compounds active in both lysis and non-lysis systems were further analyzed in full dose curves in duplicate. Cells were treated with compounds at top concentration of 50 μM, three-fold serial dilutions to 11 points (*see* **Note 1**).
2. The firefly luciferase activity detection was performed in both lysis and non-lysis substrate systems, as described above.

Figure 9 shows the activities of two tool compounds in both the lysis and non-lysis substrate systems. Data clearly showed that hemin, a biologically relevant γ-globin activator, was active in both systems but the luciferase binder was only active in the lysis

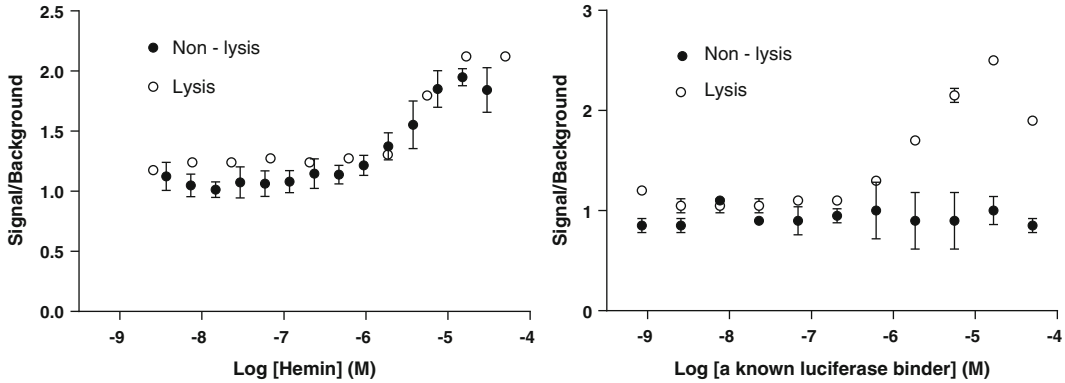

Fig. 9 Comparison of two tool compounds in the lysis and non-lysis substrate systems

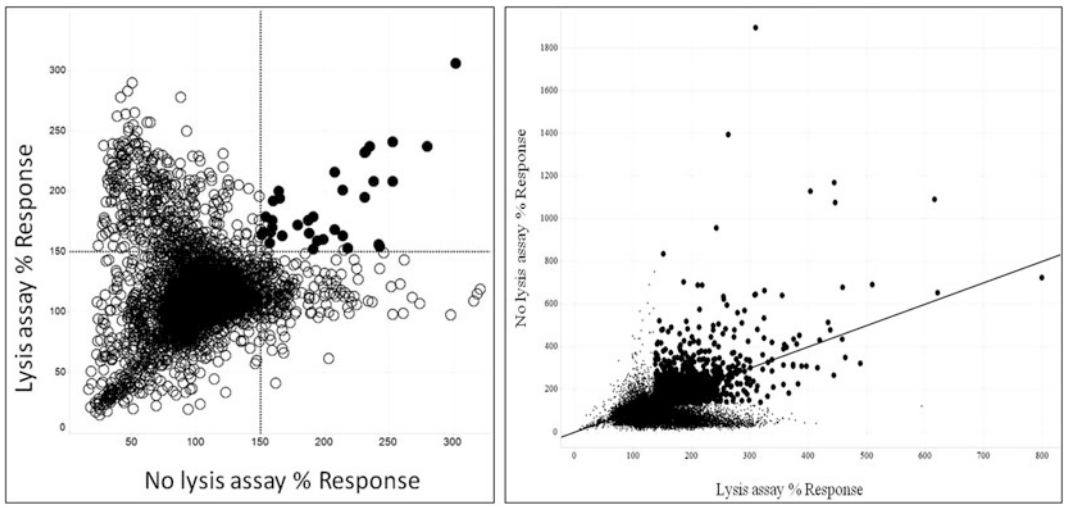

Fig. 10 Comparison of lysis and non-lysis substrate systems. *Left panel*: validation set compounds were analyzed in triplicate and averaged in each symbol. The *open circles* were inactive compounds, or only active in one system. *Solid circles* were compounds active in both systems. *Right panel*: HTS hits were analyzed in duplicate and averaged. *Large, closed circles* were active in both systems (>138 % response) while *small, open circles* were inactive or only active in one system

substrate system. The validation set analysis (Fig. 10, left panel) also supported the observation. The hit rates for the lysis and non-lysis assay formats were 6 % and 3 %, respectively, while the hit rate for compounds active in both assay formats was 0.4 %. The hit rates for each system were unusually high, indicating non-specific hits for both systems. The hit rate for actives in both systems was 0.4 %, which was in a reasonable range for HTS. Taken together, data indicated that both assay formats would be essential for HTS hit triage.

Approximately 31,000 HTS hits went through the triage process in duplicate. As shown in Fig. 10, right panel, a large part of HTS hits were either inactive or only active in one assay. Approximately 1660 compounds were active in both systems. These 1660 compounds were further confirmed in full dose curve analysis with both luciferase detection systems. In our dose curve analysis, most compounds showed bell-shaped dose curves which complicated the determination of hit confirmation. Our strategy was to select compounds with two consecutive doses showing a response above 140 %. With this selection, 1072 compounds were confirmed in both systems in dose responses.

In summary, this chapter describes the development and strategy for a firefly luciferase reporter gene HTS to identify γ-globin gene activators. We started from characterization of cell clones, selection of the assay format and optimization, and then HTS process and hit triage. We used tool compounds for assay optimization, a validation set to assess assay robustness, hit rate, and hit triage strategy. From this example, we learned several invaluable points for future utilization of reporter gene systems in drug discovery (*see* **Note 19**).

4 Notes

1. A typical 384-well compound source plate contains compounds in DMSO at desired concentrations. Column 6 has DMSO as the basal control; column 18 has the high-control compound. The top concentrations can be decided based on the potency reported in literature, or determined with initial experiments. The compound dose curve should cover a broad range which is typically obtained with threefold serial dilution for 11 doses. Under some circumstances, twofold serial dilutions with 20 or more doses can be used to determine more accurate dose response. The Labcyte Echo® Liquid Handler was used to transfer compounds to the destination plate wells. The amount to be transferred was calculated based on the volume of cell solution to generate the desired final concentrations.
2. Transient expression of a reporter gene in cells can be used for assay development and screening. One should be aware that

different batches of transfection may have different expression level, resulting in variation of reporter gene activity. Therfore, it is recommended to prepare sufficient cells from a few large batches to reduce variation. Alternatively, as in our system, a monoclonal stable cell line can be generated. After the transfection and monoclonal preparation, we obtained a few clones for characterization. We used tool compounds to test their responses to select a suitable clone for assay development and HTS. We used freshly cultured cells at early passages for assay development. Meanwhile, we prepared frozen cells of characterized cells at early passages to ensure cell supply.

3. Different cell lines use different culture medium. Our culture medium for F-36P cells was RPMI-1640 with 20 % FBS and supplements (1 % GlutaMax, 1 mM sodium pyruvate and 10 ng/mL recombinant GM-CSF). The assay medium was initially RPMI-1640 with 10 % FBS and supplements, then optimized to RPMI-1640 with 5 % FBS and supplements. FBS from different sources can have significant effects on some targets and should be tested.
4. Multidrop™ Combi Reagent Dispensers and cassettes were used to dispense solutions to 384-well and 1536-well plates. To dispense cell solutions, the cassettes can be disinfected by soaking the tubes in 70 % ethanol and priming several times with 70 % ethanol. Seperate cassettes are used for different solutions. To dispense small volume (below 15 μL), use small tube cassettes. To dispense large volume (at or above 20 μL), use standard cassettes.
5. Compound treatment time is a critical parameter to evaluate during assay optimization. It is related to the target biology pathway and cytotoxicity. For our target, we intensively optimized the treatment time with other assays which were not described in this chapter. We selected the treatment time based on the optimal response and minimal cytotoxicity.
6. Wells on the edges of microtiter plates, particularly for 1536-well plates, have more evaporation after a long period of incubation at 37 °C, generating significant differences of assay signal (edge effects). Special efforts can be applied to reduce edge effects. Besides adding enough H_2O to the reservoir, minimizing incubator door opening is helpful. Letting plates stand at room temperature for 30 min after cell addition can also reduce edge effects. During the HTS campaign with a large number of plates, we stacked 3–4 plates and placed wet paper towels under the bottom plates.
7. Follow the kit instructions. Bring kit components to room temperature prior to preparation. The buffer may be stored at room temperature. However, the substrate should be kept at −80 °C. Reconstituted Steady-Glo® may be frozen at −80 °C and reused one or two times.

8. An EnVision® luminescence reading protocol should be optimized following the manufacturer's optimization wizard. Luminescence signal is stable for a couple of hours, but should be read as soon as possible.
9. To measure the remaining firefly signal after quenching, the Stop and Glo® solution was added to the cells without *Renilla* substrate. We initially had variable and low signal of *Renilla* luciferase activity with the Dual-Glo® luciferase activity measurement. The variation was suspected to come from the interference of residual signal from the firefly luciferase. Hence, we decided to measure the residual signal after the quench but without *Renilla* luciferase substrate. We also used a *Renilla*-Glo® kit to measure the *Renilla* luciferase activity alone. The data from Fig. 2b and c demonstrated this possibility.
10. Do not cover the plates with lids after addition of Steady-Glo®. We found that liquid in some plates wicked up onto the lid, causing cross contamination and increased variation. Instead of putting a lid, stack plates on top of each other and place an empty plate on the top. Using the medium dispensing speed setting with the Multidrop Combi rather than a high speed setting can reduce foaming and bubbles.
11. We typically prepare cryopreserved cells in 90 % FBS and 10 % DMSO at cell density of 10–20 million cells/mL. Cells can be washed once with a ratio of 10 mL medium to 1 mL cell solution.
12. Refer to [18] for detailed explanations of a few statistical parameters commonly used in HTS assays.

    Z' values are used to indicate assay robustness features. It is calculated as below:

    $Z' = 1 - 3x$[(Standard deviation of high control + Standard deviation of low control)/(average of high signal − average of low signal)].

    A screening assay should always include a high control and a low control with pharmacologically relevant tool compounds. The controls are important to determine pharmacological responses, assay performance, and the cut-off value. However, for an activator assay, if no relevant tool compound is available, the high control can be omitted since the activation can be measured in relation to the basal level (DMSO control).
13. A typical 1536-well plate has the low control in columns 11 and 12 and the high control in columns 35 and 36. The high-control compounds can be transferred with an Echo® Liquid Handler to the wells. Alternatively, the compound can be added directly to an aliquot of cell solution to reach the desired concentration. The cell solution with the high-control compound is then dispensed to the wells. The latter option may have lower variation.

14. Cell aggregation significantly affects variation, particularly for adherent cells. Adherent cells should be well dissociated. Cell solutions should be gently but thoroughly pipetted up and down to reduce aggregation.
15. Use a sterile magnetic stir bar to keep cells in suspension during the long dispensing process for several hundreds of plates. It may be necessary to replace the dispensing cassette after a hundred of plates, particularly if there is a sign of clogging.
16. EnVision® Multilabel Plate Readers typically have greater sensitivity than the ViewLux Microplate Imager. We chose to use EnVision® to read luminescence signal during assay development. For HTS, due to the required increased throughput, ViewLux® Microplate Imagers are preferred due to faster read time relative to EnVision®. The ViewLux® read protocol should be optimized with a full plate with high signal for flatfield correction, well location, binning, speed, etc.
17. For the non-lysis system, the substrate D-Luciferin was reconstituted in RPMI-1640 without detergent. D-Luciferin is permeable to intact cells to interact with free luciferase. The concentration of D-Luciferin in the non-lysis system was titrated. The conditions used in this chapter had the optimal signal/background. Steady-Glo® Luciferase Assay System uses detergents to lyse cells which can dissociate compounds binding with luciferase as well.
18. In the non-lysis system, the signal is lower than the Steady-Glo® Luciferase Assay System. The exposure time for plate reading with ViewLux® may need to be increased.
19. From this reporter gene HTS, a few points are worthy of further discussion. One has to be aware that reporter gene assays are subject to many known or unknown mechanisms of modulation. It is very critical to understand what liabilities may be present in the system and have a triage strategy to eliminate false positives. In our case, the non-lysis system effectively identified luciferase binders. It is also important to realize that the reporter gene assay system may not closely recapitulate in vivo biology, particularly if the cell line used is not representative of the cell type(s) involved in the disease state. It is necessary to use more biologically relevant (and often lower throughput) secondary assays to confirm the triaged hits. Indeed, the majority of the hits did not show expected response in assays with physiologically relevant primary cells. This indicates the importance of developing HTS assays with more physiologically relevant cell systems. Newer technologies, such as genome editing, can build reporter genes in primary cells or disease relevant cells. With the advancement of new technologies, we hope to continue to leverage the power of luciferase reporter systems in drug discovery.

Acknowledgments

We thank our colleagues at the Department of Sample Management Technologies for library compound handling and dispensing. We also thank Andrew Benowitz, Ricardo Macarron, Jeff Gross, and Gordon McIntyre for their supervision and leadership.

References

1. Michelini E, Cevenini L, Mezzanotte L, Coppa A, Roda A (2010) Cell-based assays: fuelling drug discovery. Anal Bioanal Chem 398:227–238. doi:10.1007/s00216-010-3933-z
2. Miraglia LJ, King FJ, Damoiseaux R (2011) Seeing the light: luminescent reporter gene assays. Comb Chem High Throughput Screen 14:648–657, BSP/CCHTS/E-Pub/00172 [pii]
3. Yun C, Dasgupta R (2014) Luciferase reporter assay in Drosophila and mammalian tissue culture cells. Curr Protoc Chem Biol 6:7–23. doi:10.1002/9780470559277.ch130149
4. Koksharov MI, Ugarova NN (2012) Approaches to engineer stability of beetle luciferases. Comput Struct Biotechnol J 2: e201209004. doi:10.5936/csbj.201209004, CSBJ-2-e201209004 [pii]
5. da Pinto SL, Esteves da Silva JC (2012) Firefly chemiluminescence and bioluminescence: efficient generation of excited states. Chemphyschem 13:2257–2262. doi:10.1002/cphc.201200195
6. Lorenz WW, McCann RO, Longiaru M, Cormier MJ (1991) Isolation and expression of a cDNA encoding Renilla reniformis luciferase. Proc Natl Acad Sci U S A 88:4438–4442
7. Lorenz WW, Cormier MJ, O'Kane DJ, Hua D, Escher AA, Szalay AA (1996) Expression of the Renilla reniformis luciferase gene in mammalian cells. J Biolumin Chemilumin 11:31–37. doi:10.1002/(SICI)1099-1271(199601)11:1<31::AID-BIO398>3.0.CO;2-M
8. Shifera AS, Hardin JA (2010) Factors modulating expression of Renilla luciferase from control plasmids used in luciferase reporter gene assays. Anal Biochem 396:167–172. doi:10.1016/j.ab.2009.09.043, S0003-2697(09)00679-4 [pii]
9. Thorne N, Inglese J, Auld DS (2010) Illuminating insights into firefly luciferase and other bioluminescent reporters used in chemical biology. Chem Biol 17:646–657. doi:10.1016/j.chembiol.2010.05.012, S1074-5521(10)00197-3 [pii]
10. Stables J, Scott S, Brown S, Roelant C, Burns D, Lee MG, Rees S (1999) Development of a dual glow-signal firefly and Renilla luciferase assay reagent for the analysis of G-protein coupled receptor signalling. J Recept Signal Transduct Res 19:395–410. doi:10.3109/10799899909036660
11. Parsons SJ, Rhodes SA, Connor HE, Rees S, Brown J, Giles H (2000) Use of a dual firefly and Renilla luciferase reporter gene assay to simultaneously determine drug selectivity at human corticotrophin releasing hormone 1 and 2 receptors. Anal Biochem 281:187–192. doi:10.1006/abio.2000.4570, S0003-2697(00)94570-6 [pii]
12. Braeuning A (2015) Firefly luciferase inhibition: a widely neglected problem. Arch Toxicol 89:141–142. doi:10.1007/s00204-014-1423-3
13. Leitao JM, Esteves da Silva JC (2010) Firefly luciferase inhibition. J Photochem Photobiol B 101:1–8. doi:10.1016/j.jphotobiol.2010.06.015, S1011-1344(10)00155-7 [pii]
14. Thorne N, Auld DS, Inglese J (2010) Apparent activity in high-throughput screening: origins of compound-dependent assay interference. Curr Opin Chem Biol 14:315–324. doi:10.1016/j.cbpa.2010.03.020, S1367-5931(10)00046-3 [pii]
15. Thorne N, Shen M, Lea WA, Simeonov A, Lovell S, Auld DS, Inglese J (2012) Firefly luciferase in chemical biology: a compendium of inhibitors, mechanistic evaluation of chemotypes, and suggested use as a reporter. Chem Biol 19:1060–1072. doi:10.1016/j.chembiol.2012.07.015, S1074-5521(12)00268-2 [pii]
16. Auld DS, Thorne N, Nguyen DT, Inglese J (2008) A specific mechanism for nonspecific activation in reporter-gene assays. ACS Chem Biol 3:463–470. doi:10.1021/cb8000793
17. Auld DS, Southall NT, Jadhav A, Johnson RL, Diller DJ, Simeonov A, Austin CP, Inglese J (2008) Characterization of chemical libraries for luciferase inhibitory activity. J Med Chem 51:2372–2386. doi:10.1021/jm701302v
18. Iversen PW, Beck B, Chen YF, Dere W, Devanarayan V, Eastwood BJ, Farmen MW, Iturria SJ, Montrose C, Moore RA, Weidner JR, Sittampalam GS (2004) HTS assay validation. NBK83783 [bookaccession]

Chapter 15

A High-Throughput Flow Cytometry Assay for Identification of Inhibitors of 3′,5′-Cyclic Adenosine Monophosphate Efflux

Dominique Perez, Peter C. Simons, Yelena Smagley, Larry A. Sklar, and Alexandre Chigaev

Abstract

Assays to identify small molecule inhibitors of cell transporters have long been used to develop potential therapies for reversing drug resistance in cancer cells. In flow cytometry, these approaches rely on the use of fluorescent substrates of transporters. Compounds which prevent the loss of cell fluorescence have typically been pursued as inhibitors of specific transporters, but further drug development has been largely unsuccessful. One possible reason for this low success rate could be a substantial overlap in substrate specificities and functions between transporters of different families. Additionally, the fluorescent substrates are often synthetic dyes that exhibit promiscuity among transporters as well. Here, we describe an assay in which a fluorescent analog of a natural metabolite, 3′,5′-cyclic adenosine monophosphate (F-cAMP), is actively effluxed by malignant leukemia cells. The F-cAMP is loaded into the cell cytoplasm using a procedure based on the osmotic lysis of pinocytic vesicles. The flow cytometric analysis of the fluorescence retained in F-cAMP-loaded cells incubated with various compounds can subsequently identify inhibitors of cyclic AMP efflux (ICE).

Key words Cyclic AMP, Fluorescent substrates, High-throughput flow cytometry, Efflux inhibitors, ABC transporters

1 Introduction

ATP-binding cassette (ABC) transporters are often associated with multidrug resistance in relapsed cancers. ABC transporters are also implicated in the initiation and progression of metastatic malignancies due to their increased expression in cancer stem cells [1, 2]. As a result, the development of novel approaches to study ABC transporter activity to identify small molecule modulators or inhibitors is vital for translation to cancer therapy. Previously, high-throughput assays for transporter inhibition have relied upon the use of inside-out vesicles containing specific transporters, or of cancer cell lines which have been induced or engineered to acquire

William P. Janzen (ed.), *High Throughput Screening: Methods and Protocols*, Methods in Molecular Biology, vol. 1439,
DOI 10.1007/978-1-4939-3673-1_15,

drug resistance [3–6]. In both cases, these approaches have been largely dependent on measuring the intracellular fluorescence of synthetic substrates remaining in cells after exposure to compounds. While several small molecules identified in this manner were capable of reducing the multidrug resistance of cancer cells in vivo, few of these molecules have been successful in clinical trials [4, 7, 8]. This may be due in part to the limitations of these transporter efflux assays.

Often, synthetic fluorescent dyes known to be substrates of a particular transporter are used as probes to screen for hit compounds. A major limitation of this technique is the considerable similarity in cell transporter structures, and therefore substrates are capable of being effluxed by a multitude of transporters [9]. Thus, the inhibitory compounds identified in these assays fail to exhibit specificity toward the originally investigated transporter. Other attempts at measuring efflux of cellular metabolites have used radioactive conjugates of substrates to evaluate changes in intracellular concentrations. However, this results in lower throughput data collection [10]. The approach described here differs from earlier methods because it uses a fluorescent conjugate of a natural metabolite of cell membrane transporters, 3′,5′-cyclic adenosine monophosphate (cAMP), and measures its efflux from cells through unmodulated, endogenously expressed transport proteins, allowing for thousands of samples to be measured in a short period of time.

The cAMP signaling pathway has been a focus of cancer research due to its relationship to multiple intracellular signaling components and, specifically, to programmed cell death, apoptosis. Existing evidence indicates aberrant cAMP regulation in malignant cells in comparison to normal, healthy cells [11]. It has long been known that increased concentration of intracellular cAMP is capable of triggering cell death in certain cancer cells [12]. Typically, such research has relied upon modulation of the major cAMP-synthesizing enzymes adenylate cyclases (AC) or of the phosphodiesterases (PDEs) that hydrolyze cAMP to increase cytosolic cAMP and reduce cancer cell survival [11, 13]. Until recently, an additional step of the cAMP signaling pathway that could be targeted for drug discovery was overlooked: cAMP efflux by ABC transporters. The approach described here utilizes high-throughput flow cytometry for measurement of the efflux of a fluorescent cAMP analog (F-cAMP, Fig. 1) from leukemic cells. This assay assesses the ability of cells to efflux cAMP through their endogenously expressed transporters rather than through analysis of the activity of specific protein targets. It thus allows the measurement of the inherent efflux potential of a cancer cell.

As a proof of this concept, we demonstrate the accumulation and release of F-cAMP with flow cytometry (Fig. 2). We present here the results of a high-throughput screen (HTS) for the

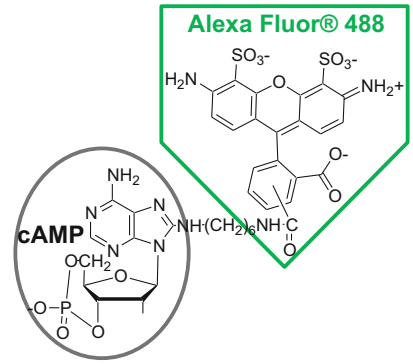

Fig. 1 Structure of the fluorescent cAMP analog (F-cAMP) used in this assay, Alexa Fluor®488 8-(6-aminohexyl) aminoadenosine 3′,5′-cyclicmonophosphate, bis(triethylammonium) salt

identification of ICE from two libraries: the SPECTRUM Collection (2320 compounds—60 % drugs, 25 % natural products, 15 % bioactive components) and the Prestwick Chemical Library (~1200 previously FDA-approved drugs). The acute myelogenic leukemia (AML) cell line U937 was screened according to the methods described in this chapter, and the cells were incubated with compounds overnight (~18 h; Figs. 3 and 4). From this screen, 51 hits were identified as having F-cAMP fluorescence $\geq$ 2 standard deviations above the plate mean negative control values (Fig. 4). These hits were validated by testing the compound F-cAMP efflux inhibition in eight-point dose–responses ranging from 60 μM to 9 nM (Fig. 5a). For this validation, the F-cAMP mean or median fluorescence intensity (MFI) values were normalized based on F-cAMP fluorescence at time = 0. The dose–response curves were fit with sigmoidal curves, and those compounds which exhibited EC_{50} values < 30 μM and had well-behaved sigmoidal dose–response curves were selected for further validation (Fig. 5b). This yielded eight compounds of interest (artemisinin, parthenolide, patulin, quinalizarin, harmalol, pyrithione zinc, clioquinol, and cryptotanshinone). Bioinformatics analysis of the compound structures allowed for the identification of three additional related small molecules: artesunate, artemether, and dihydroartemisinin. The 11 compounds of interest were tested in dose–response in flow cytometric apoptosis and cell cycle secondary assays to measure the effects of ICE on U937 cell vitality after overnight incubation (Fig. 6). Additional CellTiter-Glo® viability measurements found that six of the hit compounds (artesunate, dihydroartemisinin, clioquinol, cryptotanshinone, parthenolide, and patulin) were selectively inhibitory to leukemia cells at EC_{50} concentrations

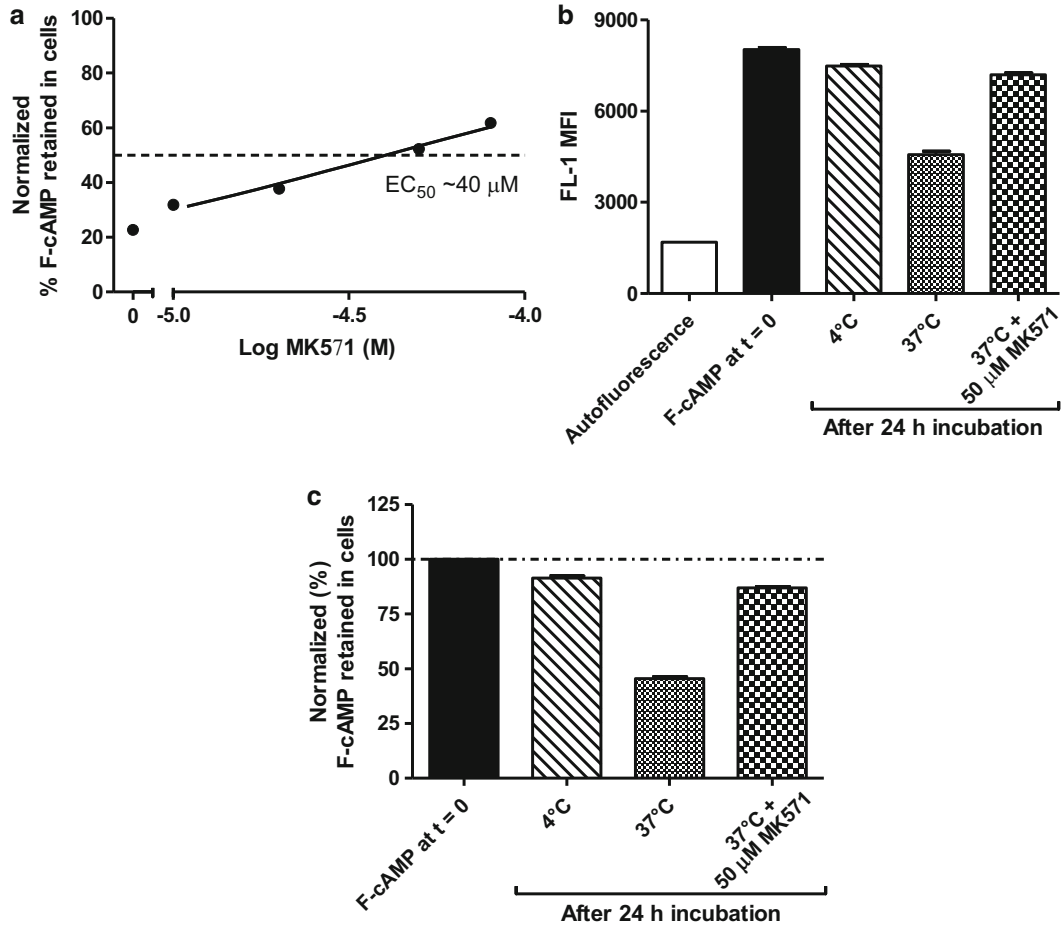

Fig. 2 Cell line MK571 optimization and determination of cell F-cAMP efflux ability. (**a**) Example of MK571 optimization assay results. Data shown were obtained using the acute myeloid leukemia (AML) cell line U937 loaded with F-cAMP and incubated overnight (~16 h) in appropriate concentrations of positive control MK571. Data were fit with a sigmoidal dose–response formula, and constrained with top = 100 and bottom = 0 to determine the EC_{50} of inhibition by MK571 . (**b**) Determination of ability of AML cell line MV411 to efflux F-cAMP. Data shown are raw FL-1 MFI values collected from control and treated samples. (**c**) Normalized data for the assay data shown in (**b**). Cell line autofluorescence was subtracted from sample MFI's and normalized such that F-cAMP MFI at time 0 = 100 %. These data indicate that MV411 cells lose ~8.5 % of F-cAMP through passive leakage (4 °C) and ~45 % by active efflux (37 °C). The positive control with MK571 limited F-cAMP loss to 13 %. Error bars in (**b**) and (**c**) indicate the data mean ± standard error of the mean (SEM) from three independent experiments

much lower than those determined for healthy human primary blood mononuclear cells (PBMCs; data not shown). Subsequent testing of the hit compounds to determine mechanisms of action confirmed that the molecules work by modulation of the cAMP pathway and induce programmed cell death. Thus, the utility of the F-cAMP efflux assay approach to identify ICE for leukemia therapeutics has been validated.

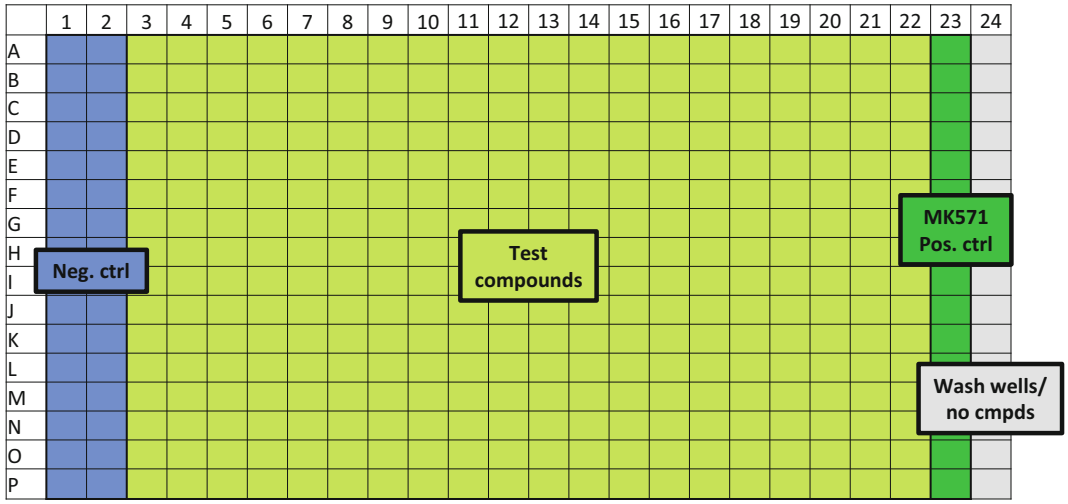

Fig. 3 Sample configuration for a 384-well compound mother plate, as described in **Note 15**. Solubilized reagents are added to the plate at a minimum volume of 6 μL. Test compounds may be used in a single-point or dose–response manner. This plate incorporates both negative (compound solvent) and positive (MK571) controls so that normalized ability to efflux F-cAMP and Z' values can be determined for each plate. If reagent availability is limited, fewer wells per plate may be used for positive controls

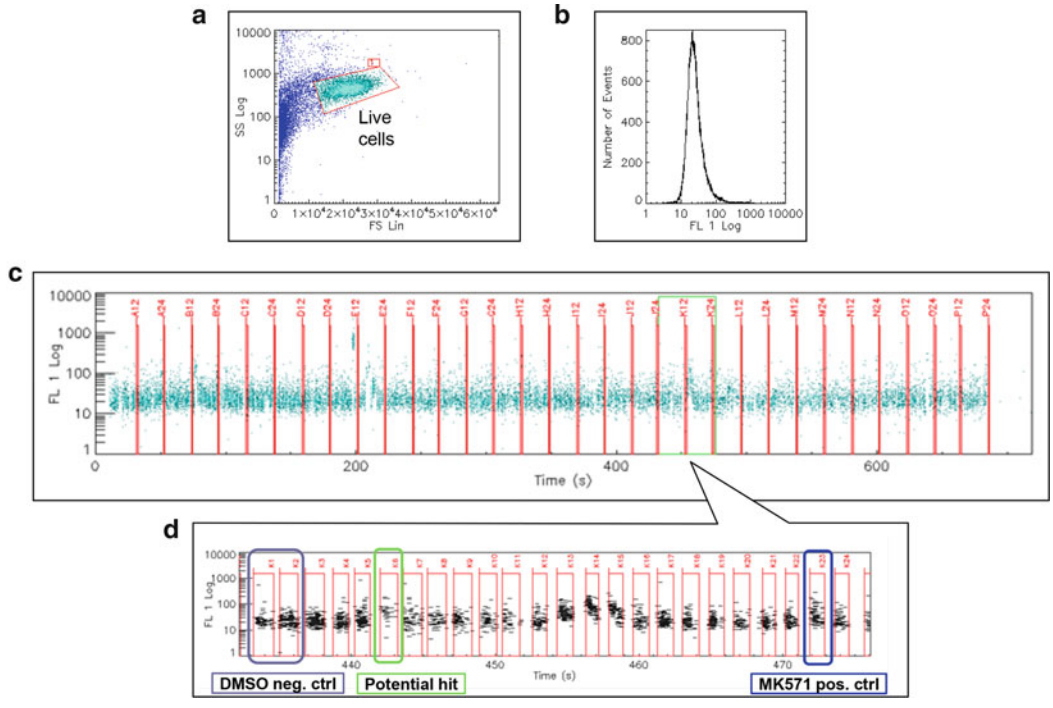

Fig. 4 Sample data from a 384-well F-cAMP efflux assay plate collected as in Subheading 3.3, **step 9**. Data were analyzed with HyperView software (IntelliCyt, Albuquerque, NM, USA) and time-gated to define data from each well. (**a**) FSC vs SSC plot with gate around untreated ("live") cells. (**b**) FL1-H histogram. (**c**) Time vs FL1-H plot from one 384-well plate. (**d**) A magnified row from the time vs FL-1H plot in (**c**), indicating controls and the potential hit compound clioquinol

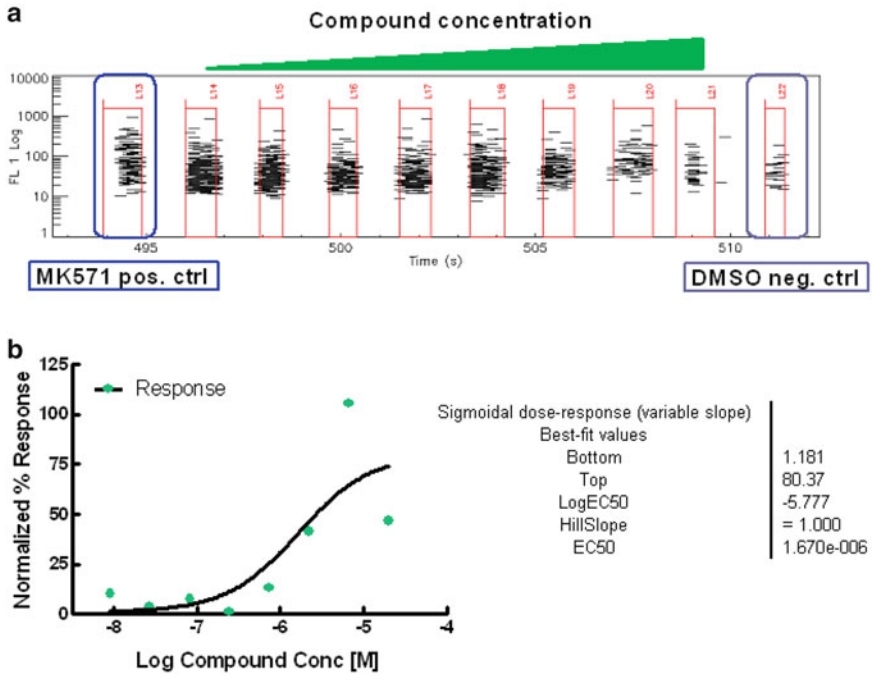

Fig. 5 Sample data from hit compound dose–response validation. (**a**) Magnified time vs FL1-H plot for an F-cAMP efflux 8-point dose–response for the hit compound of interest, clioquinol, including negative and positive controls. (**b**) Graph of normalized response for the data shown in (**a**). Sample FL1-H MFI were normalized such that F-cAMP fluorescence at the time of compound addition (time = 0) = 100 %. Data were fit by sigmoidal curves with Hill slope = 1 and top < 250. Graph, fit, and EC_{50} determination were done with GraphPad Prism 5.01 software (GraphPad Software, Inc., La Jolla, CA, USA)

2 Materials

All solutions should be prepared following proper aseptic techniques. Dispose of waste materials according to appropriate regulations. All fluid component handling and storage is done in polypropylene tubes: 1.7 mL microcentrifuge, 15 mL conical, 50 mL conical. Cells are grown and incubated in a humidified 37 °C, 5 % CO_2 incubator unless otherwise specified.

2.1 Components for Fluorescent Cyclic AMP Loading

1. 50 mL NF-RPMI: RPMI-1640, 5 mg/L phenol red, 2 mM L-glutamine, 100 U/mL penicillin, 100 μg/mL streptomycin, 10 mM HEPES. No fetal bovine serum (FBS).
2. 50 mL cRPMI: RPMI-1640, phenol red, 2 mM L-glutamine, 100 U/mL penicillin, 100 μg/mL streptomycin, 10 mM HEPES, and 10 % heat-inactivated fetal bovine serum (FBS; *see* **Note 1**).

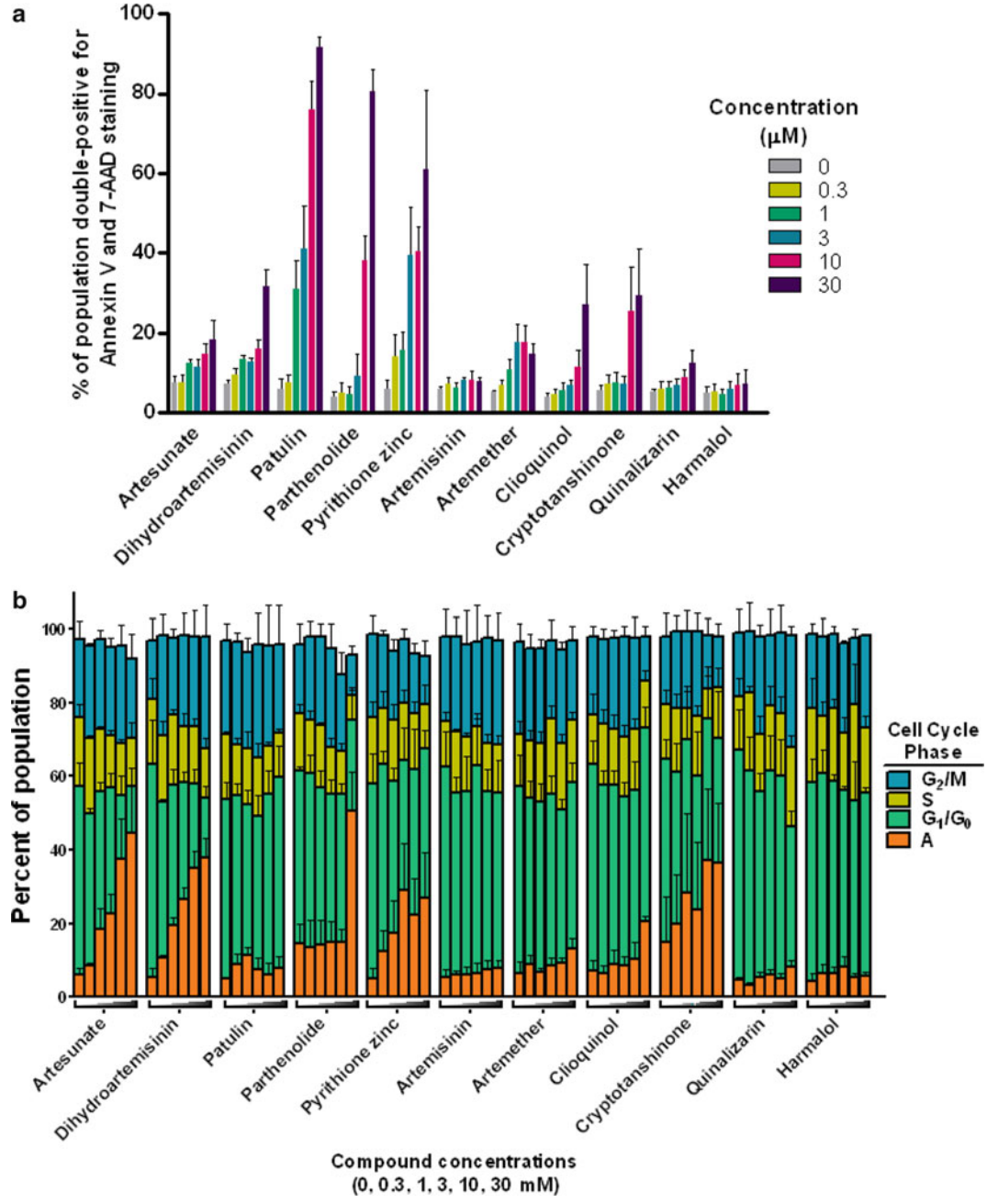

Fig. 6 Impact of ICE hit compounds, after overnight incubation, on U937 leukemia cell vitality in flow cytometric secondary assays. (**a**) Dose-dependent effects of the identified ICE on apoptosis. Bars indicate the percentages of cell populations which stained double-positive with Annexin V-PE and 7-AAD, indicating that late apoptotic events had occurred. (**b**) Effects of ICE on U937 cell cycle. The bars indicate the percentages of the cell population in each phase of the cell cycle, as determined by propidium iodide (PI) DNA staining. The gating was done on PI histograms as follows: G_1/G_0: DNA $= 2n$, S: $2n <$ DNA $< 4n$, G_2/M: DNA $= 4n$, Apoptosis (A): DNA $< 2n$. Error bars in both graphs indicate the data mean $\pm$ SEM from three independent experiments

3. Fluorescent cAMP analog (F-cAMP), Alexa Fluor®488 8-(6-aminohexyl) aminoadenosine 3′,5′-cyclicmonophosphate, bis(triethylammonium) salt (*see* Fig. 1 and **Note 2**).
4. *Hyper*tonic solution: 10 % w/v polyethylene glycol (PEG), 500 mM sucrose in NF-RPMI. 0.1 g poly(ethylene glycol) (PEG) 1000, 0.17 g sucrose, 0.9 mL NF-RPMI. In a 15 mL conical tube, add 0.9 mL NF-RPMI, then weigh and add 0.1 g PEG and mix thoroughly by vortexing (*see* **Note 3**).
5. In a sterile tissue culture hood, push the hypertonic solution through a 3–10 mL syringe fitted with a 0.2 μm nylon membrane filter (Pall Corporation) and transfer into a sterile 1.7 mL microcentrifuge tube.
6. *Hypo*tonic solution: 40 % purified, deionized water, 60 % cRPMI. Add 1 mL sterile water to 1.5 mL cRPMI in microcentrifuge tube. Mix by light vortexing. Filter-sterilize as in Subheading 2.1, **item 5**.
7. Cells known to efflux cAMP, 1–2 × 10^7 in a 50 mL conical polypropylene tube (*see* **Note 4**).
8. 1.7 mL microcentrifuge tube.
9. Centrifuge(s) with capacity for 50 mL conical and 1.7 mL microcentrifuge tubes.
10. T-75 tissue culture flask for F-cAMP-loaded cell equilibration.

2.2 cAMP Efflux Assay Components

1. 1 mL untreated cells (no F-cAMP loaded) at ≥4 × 10^5/mL for autofluorescence testing.
2. F-cAMP-loaded cells from Subheading 2.1.
3. Sterile 12-well cell culture plate with lid (or other means of covering for incubation).
4. 20 mL cRPMI.
5. ≥60 μL 30 mM MK571 positive control, solubilized in dimethyl sulfoxide (DMSO).
6. ≥80 μL DMSO.
7. Flow cytometer with 488 nm laser, 530/30 bandpass optical filter (or similar), and multiwell plate auto-sampling capabilities. This assumes the use of an Alexa Fluor(r) 488-conjugated cAMP. If the F-cAMP that you use involves another fluorophore, use an appropriate flow cytometer configuration.
8. Fifteen sample tubes for flow cytometer.

2.3 High-Throughput Screening Components

1. 1 mL untreated cells (no F-cAMP loaded) at ≥4 × 10^5/mL for autofluorescence testing.
2. F-cAMP-loaded cells from Subheading 2.1.

3. Multiwell plates, preferably 384-well, for compound mother plates and the high-throughput F-cAMP efflux assay (*see* **Note 5**).
4. Compound mother plates: 384 well plates which contain positive and negative controls, as well as compounds of interest to be tested in the high-throughput F-cAMP efflux assay.
5. ≥110 μL 10 mM MK571 positive control per compound mother plate.
6. ≥225 μL DMSO negative control per compound mother plate.
7. Proper seals (e.g., DMSO resistant adhesive foil microplate seals) and storage equipment, such as desiccators and/or −20 °C freezer, for the compound mother plates (*see* **Note 6**).
8. Liquid dispensing equipment: this can either be an automated system or multichannel pipettors capable of delivering 5 μL volumes to wells in 384-well plates (*see* **Note 7**).
9. 100 nL pintool or analogous compound transfer equipment (*see* **Note 8**).
10. 384-Well plate lids or seals for the assay plates (*see* **Note 9**).
11. Multiwell plate vortexer.
12. Flow cytometer with 488 nm laser, 530/30 bandpass optical filter (or similar), and multiwell plate auto-sampling capabilities (*see* Subheading 2.2, **step 7**).
13. Software which can resolve data from individual wells after high-throughput flow cytometry analysis.

3 Methods

3.1 Loading F-cAMP into Cells

1. Centrifuge cells at 160 × g_{max} for 10 min and remove supernatant.
2. Wash/remove serum from cell medium: Resuspend cells in 1 mL NF-RPMI with slow pipetting, add an additional 19 mL NF-RPMI, gently mix, and centrifuge for 10 min. Discard supernatant.
3. While cells are centrifuging, prepare the F-cAMP loading solution. In a microcentrifuge tube, add 200 μL *hyper*tonic solution and 10 μL of 5 mM F-cAMP (250 μM final).
4. Again resuspend the cells in 1 mL NF-RPMI with slow pipetting and transfer to a 1.7 mL microcentrifuge tube.
5. Centrifuge the cells at ~120 × g_{max} for 2 min and remove the supernatant.
6. Gently resuspend the cells in the 210 μL of F-cAMP loading solution (*see* Subheading 3.1, **step 3**).

7. Incubate the cells with F-cAMP loading solution at room temperature for 10 min, with gentle mixing by hand or light vortexing 1–2 s ~120 × g_{max} every 3 min during this incubation (*see* **Note 10**).
8. Centrifuge the cells ~120 × g_{max} for 2 min, remove the supernatant, and resuspend the cells in 1 mL of *hypo*tonic solution.
9. Incubate the cells in *hypo*tonic solution for 2 min at room temperature, with gentle mixing at 1 min.
10. Centrifuge the cells ~120 × g_{max} for 2 min, remove the supernatant, and gently resuspend the cells in 1 mL of cRPMI.
11. Transfer the 1 mL of resuspended cells to a T-75 tissue culture flask containing 24 mL cRPMI and gently mix. If 10^7 cells were used for the F-cAMP loading, then this gives a final concentration of 4×10^5 cells/mL.
12. Place the T-75 flask in the incubator to allow the F-cAMP-loaded cells to recover for 30–120 min (*see* **Note 11**).

3.2 Optimization of F-cAMP Efflux Positive Control and Determining Cell F-cAMP Efflux Ability

This protocol will allow for optimization of the F-cAMP efflux assay and conditions. This step should be performed before the high-throughput F-cAMP efflux assay is attempted. Once the positive control and incubation time(s) are determined for a particular cell line, this step may be skipped.

1. Add 500 μL cRPMI to each well of a 12-well tissue culture plate, then add 500 μL of F-cAMP-loaded cells to all wells and mix by gentle pipetting (final concentration = 2×10^5 cells/mL). Save two 1 mL samples of F-cAMP-loaded cells for control purposes, to be used in Subheading 3.2, **steps 5–8**.
2. Add DMSO and 30 mM MK571 to the wells (Table 1) for $n = 2$ for each concentration tested and mix by gentle pipetting (*see* **Notes 12** and **13**). Do not exceed a final concentration of 1 % DMSO per sample, as this can be toxic to cells.

Table 1
Volumes of MK571 and DMSO added to each 1 mL well containing F-cAMP-loaded cells to give final DMSO concentration = 1 %

Final conc. MK571 (μM)	30 mM MK571 (μL)	DMSO added (μL)
0	–	10.0
10	1.0	9.0
25	2.5	7.5
50	5.0	5.0
75	7.5	2.5
100	10.0	–

3. Incubate the lidded tissue culture plate overnight (16–24 h) under normal cell culture conditions (*see* **Note 14**).
4. *Run control samples immediately after the plate is placed in the incubator, to collect fluorescence data to be used for normalization of the treated samples (time = 0 MFI).*
5. Run untreated, non-F-cAMP-loaded cells on the flow cytometer, using the 488 nm laser for excitation and collecting fluorescence data with a 530/30 bandpass optical filter. Collect ≥ 3000 events. Create an FSC vs SSC density plot and set a "live cell" gate on the major population of the cells. Then, create an FL-1 channel histogram based on the live cell gate. Data from this untreated sample will provide the baseline/autofluorescence of the cell line.
6. Run a 1 mL sample of the F-cAMP-loaded cells through the flow cytometer with the same settings and parameters detailed in Subheading 3.2, **step 5**. Ensure that the FL-1 channel histogram does not go off scale; adjust settings so that the entirety of the histogram is visible (*see* **Note 15**). This sample will serve as the "100 % F-cAMP fluorescence" control for time = 0 of the assay.
7. Place the remaining 1 mL sample of F-cAMP-loaded cells at 4 °C for the duration of the MK571 optimization plate incubation time.
8. After incubation, run the 4 °C-incubated F-cAMP-loaded cell sample in the flow cytometer under the same settings used in Subheading 3.2, **step 5**. This will provide a measurement for the F-cAMP "passive efflux" ability of the cell line (*see* **Note 16**).
9. Gently mix the contents of each well in the MK571 optimization plate by pipetting, collect individual samples, and interrogate with the flow cytometer (*see* **Note 17**). Set a gated event count limit for each sample of ≥ 1000 events.
10. To process the F-cAMP efflux data, use MFI values from data collected in Subheading 3.2, **steps 5–8**.
11. Subtract the autofluorescence MFI value (Subheading 3.2, **step 5**) from the MFIs of all of the F-cAMP-loaded samples, including the F-cAMP fluorescence control collected at time = 0 (Subheading 3.2, **step 6**).
12. Divide the MFIs from each sample by the MFI collected from the 100 % F-cAMP fluorescence/ time = 0 control (Subheading 3.2, **step 6**). This will indicate the percentage of F-cAMP remaining within the cells under each condition.
13. Fit the MK571 dose–response data with a variable slope sigmoidal dose–response equation constrained with "bottom" equal to 0 and "top" equal to 100 (fluorescence at initial staining). This will determine the EC_{50} of MK571 for cAMP

efflux inhibition. Example data from an overnight MK571 optimization assay with U937 cells are shown in Fig. 2a.

14. Once an optimal MK571 concentration is determined for a particular cell type, the assay described here may be used to determine the efflux ability of F-cAMP-loaded samples at other iterations or incubation times. Example data from an assay to determine the MV411 leukemia cell line cAMP efflux ability is shown in Fig. 2b. The MV411 F-cAMP efflux assay data normalized according to Subheading 3.2, **steps 11** and **12** is shown in Fig. 2c.

3.3 High-Throughput F-cAMP Efflux Assay

The following protocol is designed for a 384-well high-throughput assay (*see* **Note 18**). For information on modifications which may be done to conduct the assay in 96-well plates (*see* **Note 19**). If no adjustments were made to the protocol completed in Subheading 3.1 (25 mL F-cAMP-loaded cells at 4×10^5 cells/mL), then this protocol will allow for the creation of 10, 384-well assay plates.

1. Create a compound mother plate with solubilized compounds at 100× final assay concentration. Dedicate wells for negative control (compound solvent) and positive control (MK571; *see* **Notes 20** and **21** and Fig. 3 for example plate map). Alternatively, an acoustic dispenser may be used to deliver compounds directly to assay plates in Subheading 3.3, **step 3**, and if so, the creation of separate compound mother plates is not necessary.
2. Dispense 5 μL cRPMI to all wells of the 384-well assay plates with a liquid handler or multichannel pipettor.
3. With a 384-well pintool (or other similar liquid transfer equipment), transfer 100 nL from the compound mother plates to the assay plates (*see* **Note 8**).
4. Dispense 5 μL F-cAMP-loaded cells to the negative and positive control, and compound-treated wells in the assay plates (*see* **Note 21**). If the added cells were originally at a density of 4×10^5/mL, then this provides a final cell density of 2×10^5/mL, or 2000 cells/10 μL final volume well. Save two, 1 mL aliquots of excess F-cAMP-loaded cells for flow cytometer optimization and fluorescence testing.
5. Seal the assay plates and store upside down in the incubator for desired incubation time (*see* **Note 9**).
6. Conduct cytometer optimization and fluorescence testing according to Subheading 3.2, **steps 5–7**.
7. After assay plate incubation, run the 4 °C-incubated F-cAMP-loaded cell "passive efflux" sample as in Subheading 3.2, **step 8**.

8. Vortex (2000 rpm) each F-cAMP efflux assay plate 15 s before running samples through the high-throughput flow cytometer (*see* **Note 22**). Add an FL-1 vs time density plot to the cytometer collection parameters to allow for well data separation during analysis.
9. Use high-throughput flow cytometry analysis software to identify cells and FL-1 MFI from individual wells (*see* Fig. 4 for example data).
10. To analyze well/compound data, exclude samples with <50 events. Normalize data according to Subheading 3.2, **steps 11** and **12** (*see* **Note 23**). Calculate the Z' values for each plate for quality control purposes. Assay plates which indicate a Z' factor of ≥0.3 should be considered acceptable [14]. Hit compounds may be determined per the user's preference. We identified hits as samples with MFI values ≥2 standard deviations above the plate mean negative control values.
11. To further validate sample data and decrease the number of false-positive hits, compounds were assayed in a high-throughput dose–response assay. Plates were set up as in the HTS, with the exception that the plate formats contained 10-well dose–responses for each hit compound, at final concentrations ranging from 30 μM to 4 nM.

4 Notes

1. If the cells used in this assay are typically cultured in another medium, please substitute that medium for all instances of cRPMI in this protocol.
2. Other fluorescently-conjugated cAMP may be utilized, but fluorophores conjugated to cAMP at sites which do not mimic the molecule shown in Fig. 1 have not yet been validated nor tested for this assay.
3. Dissolving PEG 1000 in NF-RPMI may be somewhat difficult. Continue vortexing and tilting tube back and forth. If the PEG still does not readily enter solution, wait a few hours or overnight for the flakes to dissolve. Otherwise, placing the tube in a 37 °C water bath for 5–15 min may help.
4. We have tested F-cAMP loading in leukemia cell lines, at numbers up to 18×10^6 under the conditions described in this method. For adherent or other cell types, it would be best to optimize the assay starting at 10^7 cells and gradually testing other cell counts and F-cAMP concentrations to suit your needs. If the assay volumes and/or cell densities that you require are higher than those described in this protocol, adjust

the component volumes and cell numbers loaded with F-cAMP accordingly (*see* **Note 19**).

5. You will need at least 10, 384-well plates for the cAMP assay, and a number of plates to create compound mother plates. The high-throughput F-cAMP efflux assay protocol described here is for a small assay volume (10 μL). It would be best to have small volume flat-welled plates or conical wells for these assay plates. In our experience, this assay has worked with both polystyrene and polypropylene multiwell plates.

   The compound mother plates need to have the same well format as the assay plates (e.g., 384 wells). The compound mother plates should have well structures optimized for the transfer of small volumes of reagents. We found that wells with conical bottoms were optimal for our 100 nL compound transfers by pintool.

6. The compound mother plates may be saved and reused if stored properly. The plates should be foil-sealed, preferably after being flushed with nitrogen gas to remove excess oxygen and moisture from the wells. The plates can be stored at −20 °C (typically best for long-term compound storage, avoiding several freeze-thaws) or in a climate-controlled, low humidity, high-nitrogen desiccator. Plates stored in a desiccator may be stable for up to 3 months, depending on the properties of individual compounds.

7. Take note of the "dead volume" specifications of your liquid dispensing equipment. When following the described protocol, ensure that the volumes of the reagents used are adjusted to meet these minimum requirements before beginning the high-throughput F-cAMP efflux assay.

8. The wells in this assay will have a final volume of 10 μL F-cAMP-loaded cells in culture medium. A compound delivery of 100 nL will result in a DMSO concentration below 1 %. If a 100 nL pintool or equivalent is unavailable, then intermediate compound dilution plates will need to be prepared to allow for 1 μL volumes to be transferred to assay wells while maintaining DMSO at ≤1 %.

   To prepare intermediate compound dilution plates, stock from the compound mother plates is diluted 1:10 in culture medium. This is accomplished in additional 384-well plates, by combining 9 μL of culture medium with 1 μL of the well contents from the compound mother plates. Mix well contents thoroughly by pipetting or plate vortexer before making 1 μL transfers from the intermediate compound dilution plates into the assay plates (Subheading 3.3, **step 3**).

9. Depending on the optimal culturing conditions for the cell line tested, the assay plates may be incubated with fitted lids or

sealed with gas-permeable, solid polymer, or foil seals. Take into consideration that the assay plates will contain small volumes (10.1 μL final), and incubation with lids or gas-permeable seals may result in some evaporation of well volumes, especially on the edges of the assay plates. We found that leukemia cell line responses to the F-cAMP efflux assay were best when non-permeable seals were used on the assay plates. Gas permeable plate covers seemed to decrease cell viability, as evidenced in population shifts on flow cytometer FSC vs SSC density plots when plates were analyzed after incubation.

10. We have not tested the sensitivity of F-cAMP-loaded cells incubated and equilibrated in full-light conditions. We recommend incubating the cells in the dark to minimize the potential for ambient light to reduce treated cell MFI's.
11. It is possible for the cells to be used in the efflux assay immediately, but because the plasma membranes have been subjected to stress from the osmotic lysis of pinocytic vesicles in the F-cAMP loading procedure, it would be beneficial to allow the membrane integrity to be regained before proceeding. This step allows the cells to recuperate before testing with compounds. Different cell lines will recover at different rates. Check the cells with a light microscope to determine whether the cells appear healthy and rounded before advancing to the efflux assay.
12. MK571 is a known inhibitor of ABC C-family transporters (also known as multidrug resistance proteins), and it is often used as a positive control for cAMP efflux. The concentrations tested here are used to generate a dose–response curve to determine the EC_{50} of MK571 cAMP efflux inhibition. Alternative concentrations may also be tested. With U937 cells, we determined an MK571 EC_{50} of ~40 μM, and used a final concentration of 100 μM in our HTS assays to ensure effective cAMP efflux inhibition (Fig. 2a).
13. Because this optimization step does not require many F-cAMP-loaded cells, multiple plates, MK571 concentrations, and incubation times may be tested as well.
14. The MK571 optimization incubation time should match the incubation time in which the HTS assay will be conducted. We have performed this assay at various times from 16 to 48 h. Please note, however, that cells which do not actively efflux cAMP well, or incubation time that is too short may not produce data with significant effects or dose-dependent efflux inhibition by MK571. Incubation times which are too long (~48 h) could lead to increased levels of apoptosis, depending on the sensitivity to the cells to high concentrations of MK571.

15. If the FL-1 channel cytometer settings had to be adjusted in this step, run the untreated, non-loaded cells (Subheading 3.2, **step 5**) again to ensure proper assessment of the cell line autofluorescence for the assay readings.
16. For some cell lines, incubation at 4 °C can cause apoptosis, and this is evident in shifting of the population on the FSC vs SSC plot. Only use data from events which fall within the "live cell" gate created with the untreated/ autofluorescence cells.
17. All or partial aliquots of the wells may be collected during this step. If only a few hundred microliters of each well are sampled, this allows for the remainder of the plate to continue to be incubated, allowing for aliquots to be collected at multiple time points.
18. All plate setup and compound handling for HTS can be done in ambient conditions outside of a tissue culture hood.
19. Considerations for completing the high-throughput F-cAMP efflux assay in 96-well plates:
    (a) The compound mother plates and assay plates should have the same well configurations, to ease compound transfer.
    (b) Assays conducted in 96-well plates typically require higher minimum volumes per well for samples to be collected by high-throughput flow cytometry. These minimum volumes are contingent on the geometry of the plate wells, of course, but it can be expected that the wells would require $\geq$50 μL final volumes.
    (c) While the volume per well can vary from the 10 μL final volume described in this protocol, it is ideal to maintain final well concentrations of $\leq$1 % DMSO and $>2 \times 10^5$ cells/mL.
20. In this step, any number of compound mother plates may be created for use with the ten assay plates. Therefore, individual compound mother plates may be used multiple times to increase the sample size tested per compound, or each assay plate may be tested with different compound mother plates. For our tests to identify "inhibitors of cAMP efflux", our compound mother plates consisted of 6 μL final volume per well. There were 10 mM DMSO-solubilized compounds in all wells in columns 3–22, the negative control was in columns 1–2, and the positive control was in column 23 of the 384-well plate (Fig. 3). Alternatively, if compounds of interest are already known, the compound mother plate can be made to test the compounds in dose–response, with negative controls in columns 1 and 13, and dose series in columns 2–10 and 12–22. The MK571 positive control can be incorporated into the plate as a dose–response series, or as few wells in column 23 at a static concentration.

21. For example, if the compound mother plates were set up as shown in Fig. 3, F-cAMP-loaded cells would be added to all wells in columns 1–23 of the assay plates. Because column 24 would not have any compound or cells added, these wells would serve as "wash" wells.
22. In our assay, we used flow cytometers configured with HyperCyt® autosampling systems (IntelliCyt), with peristaltic pump speeds at 15 rpm, and aspiration for 1 s/well (up times between wells could be set from 300–500 ms). This allowed for approximately 2 μL (~400 cells) to be sampled from each well.
23. In some instances, the positive and negative control data may indicate a gradient of MFI values dependent on well position on the plate. In such cases, it would help to normalize F-cAMP efflux for the samples on a per-row basis (e.g., using only the positive and negative control MFI values from Row H to normalize the Row H sample MFIs).

Acknowledgments

This work was supported by The Oxnard Foundation, University of New Mexico Clinical & Translational Science Center Pilot Award 1UL1RR031977, and New Mexico Cancer Nanotechnology Training Center grant R25CA153825.

References

1. Fletcher JI, Haber M, Henderson MJ, Norris MD (2010) ABC transporters in cancer: more than just drug efflux pumps. Nat Rev Cancer 10(2):147–156
2. Zinzi L et al (2014) ABC transporters in CSCs membranes as a novel target for treating tumor relapse. Front Pharmacol 5:163
3. Aronsen L, Orvoll E, Lysaa R, Ravna AW, Sager G (2014) Modulation of high affinity ATP-dependent cyclic nucleotide transporters by specific and non-specific cyclic nucleotide phosphodiesterase inhibitors. Eur J Pharmacol 745:249–253
4. Wu C-P, Calcagno AM, Ambudkar SV (2008) Reversal of ABC drug transporter-mediated multidrug resistance in cancer cells: evaluation of current strategies. Curr Mol Pharmacol 1 (2):93–105
5. Shiozawa K et al (2004) Reversal of breast cancer resistance protein (BCRP/ABCG2)-mediated drug resistance by novobiocin, a coumermycin antibiotic. Int J Cancer 108(1):146–151
6. Jekerle V et al (2006) In vitro and in vivo evaluation of WK-X-34, a novel inhibitor of P-glycoprotein and BCRP, using radio imaging techniques. Int J Cancer 119(2):414–422
7. Ozben T (2006) Mechanisms and strategies to overcome multiple drug resistance in cancer. FEBS Lett 580(12):2903–2909
8. Zarrin A, Mehdipour AR, Miri R (2010) Dihydropyridines and multidrug resistance: previous attempts, present state, and future trends. Chem Biol Drug Des 76(5):369–381
9. Nigam SK (2014) What do drug transporters really do? Nat Rev Drug Discov 14(1):29–44
10. Copsel S et al (2011) Multidrug resistance protein 4 (MRP4/ABCC4) regulates cAMP cellular levels and controls human leukemia cell proliferation and differentiation. J Biol Chem 286(9):6979–6988
11. Fajardo AM, Piazza GA, Tinsley HN (2014) The role of cyclic nucleotide signaling pathways in cancer: targets for prevention and treatment. Cancers (Basel) 6(1):436–458

12. Coffino P, Bourne HR, Tomkins GM (1975) Mechanism of lymphoma cell death induced by cyclic AMP. Am J Pathol 81:199–204
13. Dou A, Wang X (2010) Cyclic adenosine monophosphate signal pathway in targeted therapy of lymphoma. Chin Med J (Engl) 123(1):95–99
14. Zhang J, Chung T, Oldenburg K (1999) A simple statistical parameter for use in evaluation and validation of high throughput screening assays. J Biomol Screen 4(2):67–73

Chapter 16

High-Throughput Cell Toxicity Assays

David Murray, Lisa McWilliams, and Mark Wigglesworth

Abstract

Understanding compound-driven cell toxicity is vitally important for all drug discovery approaches. With high-throughput screening (HTS) being the key strategy to find hit and lead compounds for drug discovery projects in the pharmaceutical industry [1], an understanding of the cell toxicity profile of hit molecules from HTS activities is fundamentally important. Recently, there has been a resurgence of interest in phenotypic drug discovery and these cell-based assays are now being run in HTS labs on ever increasing numbers of compounds. As the use of cell assays increases the ability to measure toxicity of compounds on a large scale becomes increasingly important to ensure that false hits are not progressed and that compounds do not carry forward a toxic liability that may cause them to fail at later stages of a project. Here we describe methods employed in the AstraZeneca HTS laboratory to carry out very large scale cell toxicity screening.

Key words Toxicity, Cell-based assays, Phenotypic, High-throughput screening, HTS, Resazurin, Apoptosis

1 Introduction

With the increasing use of cell-based assays in high-throughput screening [2] the need to measure the toxicity of large numbers of compounds has grown. This is for two key reasons. The first is the desire to rule out false positives due to the killing of the cells rather than inhibiting the target or pathway of interest. The second is the objective of annotating compounds and compound series as to whether they appear to have a toxic liability. This enables project teams to make choices of what series to progress. It is also apparent from studies on historical projects that a key reason for failure of compounds in the clinic is toxicity [3] and to flag this as early as possible in drug discovery projects will enable the right decisions to be made to ensure that this liability is reduced and thereby improve the attrition rate. Within HTS at AstraZeneca, we carry out a variety of assays to measure the toxicity of compounds to ensure we have the most confidence in the data and that any compounds labeled as toxic really are toxic. We carry out initial screening using a

William P. Janzen (ed.), *High Throughput Screening: Methods and Protocols*, Methods in Molecular Biology, vol. 1439,
DOI 10.1007/978-1-4939-3673-1_16,

CellTiter-Blue® (also known as alamarBlue® or resazurin) cell viability assay. Resazurin is metabolized by viable cells to highly fluorescent resorufin and so any cell death will reduce this conversion compared to control. This is a well-published assay [4–7] that also has the advantages of being low cost and easily put onto laboratory automation being a single addition and read. It also gives us the ability to detect both toxic and cytostatic compounds, but does not distinguish between them. In order to provide further mechanistic information, we utilize a number of orthogonal assays which also confirm the toxicity of a compound [8]. The first orthogonal assay is a cell membrane integrity assay for which we use the CellTox™ Green reagent from Promega [9, 10]. This is again a single addition assay amenable to being run on automated platforms and is based on the principle that cells with compromised membranes cannot exclude the CellTox™ Green dye that then binds to the DNA in the cell and fluoresces. There are other membrane integrity assays available with many being based around release of lactate dehydrogenase (LDH) [11–13]. This orthogonal assay confirms that the compound is toxic and allows the separation of toxic and cytostatic compounds, in combination with the CellTiter-Blue® screening data. Where further detail is required on the mechanism of toxicity then we run a four-parameter apoptosis assay on a high-throughput flow cytometer, the Intellicyt iQue® Screener, although any flow cytometer can be used [14]. We use a kit supplied by Intellicyt but there are other kits from, for example, Promega, that can measure similar parameters using a standard plate reader (e.g. Promega ApoTox™ Glo assay, ApoLive Glo™ Multiplex assay, Mitochondrial ToxGlo™ assay, etc.). The four-parameter apoptosis assay measures caspase 3/7 activation, phosphatidylserine flipping via Annexin V binding, membrane integrity (live/dead cells), mitochondrial integrity, and total cell counts [14]. This gives a very comprehensive view of the mechanism of toxicity and allows comprehensive profiling of compounds.

In this chapter, we describe the methods for these assays. We describe their use with THP-1 cells which we use as a standard cell line for measuring toxicity across different compounds to allow comparisons to be made. Of course, we also measure toxicity in the actual cell types used in a particular assay and any of the methods described here can be used with most mammalian cells, both adherent or suspension cell lines, with the relevant assay optimizations. Adherent cells are more difficult to use in flow cytometry and have to be removed from the plate surface before being assayed (not described in these methods) or the aforementioned alternative plate-based techniques could be used.

In the materials and methods, we have described the use of the specific reagents and equipment we routinely use in our laboratory. The reader should note that alternative equivalent reagents and equipment should generate comparable data.

2 Materials

All reagents to be prepared in Type 1 ultrapure water (e.g. MilliQ water) unless indicated otherwise. Compounds to be dissolved in analytical grade dimethyl sulfoxide (DMSO) and kept at −20 °C. Follow all local safety rules and local rules when disposing of liquid mammalian waste and other waste products.

2.1 Cell Culture Components for All Three Toxicity Assays

1. Cell culture medium: RPMI-1640 medium with phenol red, 10 % v/v fetal calf serum, 200 mM L-Glutamine.
2. Cell plating medium: RPMI-1640 medium, phenol red free, 10 % v/v fetal calf serum, 200 mM L-Glutamine, 100 U/mL of Penicillin Streptomycin.
3. THP-1 monocytic cell line.
4. Dulbecco's Phosphate-Buffered Saline.
5. 1700 cm^2 roller bottles for large-scale cultures.
6. 4 mL sample cup for counting cell suspension density.
7. Vi-Cell XR Cell Viability analyzer (Beckman Coulter Ltd, High Wycombe, UK) (*see* **Note 1**).
8. 50 mL centrifuge tubes with flat caps.
9. 500 mL large-volume centrifuge tubes.
10. Multidrop™ Combi Reagent Dispenser with two different-sized cassettes used dependent on assay volumes dispensed; standard tube dispensing cassette, and small tube metal tip dispensing cassette (Fisher Thermo Scientific UK Ltd, Loughborough, UK).
11. 50 mL reagent reservoir.
12. Water bath.
13. Water bath treatment to stop algal and bacterial growth. We routinely use SigmaClean® but any equivalent reagent can be used.
14. 1, 10, 25, and 50 mL disposable Stripettes®.
15. Class 2 Biological Safety Cabinet.
16. Roller bottle incubator maintained at 37 °C in a 95 % humidified atmosphere of 5 % v/v CO_2/95 % v/v air set to 110 rpm (*see* **Note 2**).
17. Incubator maintained at 37 °C in a 95 % humidified atmosphere of 5 % v/v CO_2/95 % v/v air for plates.
18. Optical Microscope.
19. Centrifuge for tissue culture vessels and plates.

20. 70 % v/v ethanol solution: Prepare 100 mL using 30 mL 100 % ethanol to 70 mL distilled water.
21. 2 % Virkon® disinfectant cleaner. Add 2 mL Virkon® to 98 mL water. Any other suitable disinfectant can be used.

2.2 Assay Ready Plate Generation

1. Labcyte Echo® 555 instrument (Labcyte Europe, Dublin, Ireland).
2. Puromycin dihydrochloride used as inhibitor control compound. Dissolve in DMSO and store at −20 °C (*see* **Note 3**).
3. DMSO used as vehicle control.
4. 384-Well polypropylene v-bottom microtiter plates.

2.3 CellTiter-Blue® Components

1. CellTiter-Blue® Viability Reagent (Promega UK Ltd, Southampton, UK). To be stored at −20 °C unless diluted. Diluted stock to be prepared on the day of assay. Stable for ~7 h. Any source of resazurin can be used.
2. 384 assay: make 1:8 dilution of CellTiter-Blue® Viability reagent in assay dilution buffer (*see* **Note 4**).
3. 1536 assay: make 1:16 dilution of CellTiter-Blue® Viability reagent in assay dilution buffer (*see* **Note 4**).
4. Resorufin reagent. Dilute in assay dilution buffer to the empirically determined concentration and use on the day of preparation.
5. Assay dilution buffer: RPMI-1640 medium, phenol red free, 10 % v/v fetal calf serum, 200 mM L-Glutamine.
6. 384-Well solid black plates or 1536-well solid black plates with lids (*see* **Note 5**).
7. Plate seals.
8. Pipettes and pipette tips.
9. Fluorescence plate reader.
10. Puromycin dihydrochloride used as inhibitor control compound. Dissolve in DMSO and store at −20 °C (*see* **Note 3**).
11. DMSO used as vehicle control.

2.4 CellTox™ Green Components

1. CellTox™ Green Express Cytotoxicity Assay (Promega UK Ltd, Southampton, UK). Store at −20 °C. On day of assay dilute reagent 1:500 in assay dilution buffer to give a final dilution of 1:1000 in the assay plate.
2. Assay dilution buffer: RPMI-1640 medium, phenol red free, 10 % v/v fetal calf serum, 200 mM L-Glutamine.
3. 384-Well solid black plates with lids (*see* **Note 5**).
4. Plate seals.

5. Pipettes and pipette tips.
6. Fluorescence plate reader.
7. Puromycin dihydrochloride used as inhibitor control compound. Dissolve in DMSO and store at −20 °C.
8. DMSO used as a vehicle control.

2.5 Intellicyt MultiCyt 4-Plex Apoptosis Kit Components

1. Multicyt 4-Plex Apoptosis Screening kit (Intellicyt, Albuquerque, USA).
2. Assay dilution buffer: RPMI-1640 medium, phenol red free, 10 % v/v fetal calf serum, 200 mM L-Glutamine.
3. 384-Well polypropylene V-bottom plates with lids.
4. Puromycin dihydrochloride used as inhibitor control compound. Dissolve in DMSO and store at −20 °C (*see* **Note 3**).
5. DMSO vehicle control.
6. Intellicyt iQue® Screener HD high-throughput flow cytometer system (Intellicyt, Albuquerque, USA) or equivalent.

3 Methods

Three toxicity assays were used to evaluate cytotoxicity of AstraZeneca compound collections. Different assay formats were deployed for the level of throughput required for the specific assay. The CellTiter-Blue® assay was developed in both 1536 and 384 assay formats, CellTox™ Green and the Intellicyt Multicyt 4-plex Apoptosis assays in 384-well format only. To ensure that the data generated are as comparable as possible across assays and to simplify laboratory logistics all three employ the same generic protocols for the following:

1. Routine cell culture.
2. Cell culture preparation and cell plating.
3. Generation of assay ready compound plates.

All generic protocols will be described in the initial Methods sections.

3.1 Routine Cell Culture Method

All cell culture procedures performed in a biological safety cabinet whilst practising routine aseptic techniques.

For cell waste decontamination, waste is placed in 2 % Virkon® or equivalent for 15 min before putting to drain. Refer to local rules for waste disposal methods prior to cell culture work.

1. THP-1 cells were passaged every 2–3 days depending on the density of the cell suspension. Cells should not exceed 1.5×10^6 cells/mL in a growing culture; if so these cells should be discarded as assay response will be impaired.

2. Fill water bath to 5 cm deep with distilled water treated with SigmaClean® or equivalent. Pre-heat water to 37 °C.
3. Pre-warm cell culture medium by placing in the 37 °C water bath 20–30 min prior to use.
4. Collect growing cultures of THP-1 cells in 1700 cm^2 roller bottles from incubator, aseptically transfer the roller bottle(s) into the biological safety cabinet.
5. To obtain a viable cell count from the growing cell culture remove 1 mL of cell culture with a 1 mL Stripette® and dispense into a 4 mL sample cup. Determine viable cell number per mL using a Beckman Vi-cell XR cell viability cell analyzer or equivalent. Cells are not suitable for the assay if a growing culture density $>1.5 \times 10^6$ cells/mL has been reached.
6. Carefully pour 500 mL of cell culture medium into a new 1700 cm^2 roller bottle. Transfer required volume of THP-1 cell suspension from the growing culture for a starting growth density of 0.4×10^5 cells per mL. Cell cultures are then maintained at 37 °C in a 95 % humidified atmosphere of 5 % v/v CO_2/95 % v/v air in a roller bottle incubator set to 110 rpm.

3.2 Cell Culture Preparation and Cell Plating

All cell culture procedures performed in a biological safety cabinet whilst practising routine aseptic techniques.

For cell waste decontamination waste is placed in 2 % Virkon® or equivalent for 15 min before putting to drain. Refer to local rules for disposal methods prior to cell culture work.

1. Fill water bath to 5 cm deep with distilled water treated with SigmaClean® or equivalent reagent. Pre-heat water to 37 °C.
2. Warm cell culture and cell plating medium by placing in the 37 °C water bath 20–30 min prior to use.
3. Collect growing cultures of THP-1 cells in 1700 cm^2 roller bottles from roller bottle incubator. Aseptically transfer the roller bottle into the biological safety cabinet.
4. Pour cells into 500 mL centrifuge tube with plug seal cap. Spin tubes at $300 \times g$ for 3 min in a bench top centrifuge to pellet the cells.
5. Remove supernatant using 50 mL Stripette® being careful to not dislodge cell pellet. All waste to be placed into a 2 % Virkon® waste pot or another relevant decontamination route. Re-suspend cells in 200 mL Dulbecco's Phosphate-Buffered Saline. Spin tubes at $300 \times g$ for 3 min in a bench top centrifuge.
6. Remove Dulbecco's Phosphate-Buffered Saline using a 50 mL Stripette® being careful to not dislodge the cell pellet. All waste to be placed into a 2 % Virkon® waste pot.

7. Re-suspend cells in 30 mL cell plating medium and transfer to a sterile 50 mL centrifuge tube with flat cap.
8. To obtain a cell count remove 1 mL of cell culture with a 1 mL Stripette® and dispense into a 4 mL sample cup. Determine cell number per mL using a Beckman Vi-cell XR cell viability cell analyzer or equivalent. Cells are not suitable for the assay if a growing culture density $>1.5 \times 10^6$ cells/mL has been reached.
9. Dilute cells to the required density in cell plating medium for the chosen assay (a) CellTiter-Blue®, 250,000 cells/mL, (b) CellTox™ Green, 625,000 cells/mL, (c) 4-plex Apoptosis assay, 1 million cells/mL.
10. Set up Multidrop™ Combi by attaching appropriate-sized Multidrop™ cassette to dispense cells into assay plates. Standard volume cassette for dispense volumes ranging from 20 μL to >200 μL. Low-volume cassette for dispense volumes <20 μL.
11. Sterilize the Multidrop™ Combi cassettes before use with cells. Prime 20 mL of 70 % v/v ethanol through tubing leaving for 15 min followed by 20 mL of cell plating medium to rinse out 70 % v/v ethanol and coat the tubes before passing through cell suspension. All waste collected for disposal into 2 % Virkon®.
12. Transfer cell suspension using a Multidrop™ Combi on fast dispense speed setting to the relevant assay ready plate (a) 1536-well CellTiter-Blue®, 1000 cells per well in 4 μL medium, (b) 384-well CellTiter-Blue®, 10,000 cells per well in 40 μL medium, (c) 384-well CellTox™ Green, 12,500 cells per well in 20 μL medium, (d) 384-well 4-plex Apoptosis assay, 20,000 cells per well in 20 μL medium. Place a lid on each plate (*see* **Note 6**).
13. Incubate lidded assay plates at room temperature for 15 min to equilibrate temperature across the plate which will minimize edge effects before incubating at 37 °C in 5 % v/v CO_2/95 % v/v air in humidified incubator. For incubation times see relevant assays sections.

3.3 Preparation of Assay Ready Screening Plates (ARPs)

Preparation of compound plates for assay can be achieved in many different ways from manual handheld pipette through to fully automated systems, providing that the concentration of compound and vehicle are within acceptable limits. However, AstraZeneca deploys a system of assay ready plates for high-throughput and concentration response screening that utilizes automated compound storage alongside acoustic dispense, to ensure the highest quality and reproducibility possible [15]. Test compounds are retrieved from long-term automated storage in a climate-controlled

environment and plated into master-plates. Compounds are pre-dispensed in nanoliter volumes into assay plates prior to the addition of cells or reagents removing the need for pre-dilution steps of compounds dissolved in 100 % v/v DMSO (*see* **Note 7**). Assay ready plates are generated via acoustic dispensing from the master-plate stocks using a Labcyte Echo® 555 instrument or equivalent. All test compounds prepared in 100 % v/v DMSO at 10 mM unless otherwise stated.

1. For the 1536 primary screen transfer 20 nL of compound to each well of a 1536-well solid black plate giving a final DMSO concentration of 0.5 % v/v in the assay.
2. For concentration response screening the volume of compound transferred to each well is assay dependent (see below for volumes). Each compound is dispensed to create 10 point CR curves with a final compound concentration range between 100 μM and 5 nM. Backfill wells where necessary with the appropriate volume of DMSO to ensure a consistent final screening concentration of 1 % v/v DMSO.
3. 384-Well CellTiter-Blue®—400 nL compound; 40 μL of cell suspension added.
4. 384-Well CellTox™ Green—200 nL compound; 20 μL cells suspension.
5. 384-Well Apoptosis assay—200 nL compound; 20 μL cell suspension.
6. All ARP plates have specific wells assigned for assay controls. These control compounds enable analysis of interplate and intraplate variation and calculation of Z' values [16] plus they are also used for setting the normalization window. The positioning of these control compounds are dependent on the assay format used (*see* **Note 8**).
7. 384-Well assay format has 32 control wells in total, 16 wells assigned to each control.
8. Neutral control (DMSO)—A11, B11 to H11 then I12, J12 to P12.
9. Inhibitor control (puromycin)—I11, J11 to P11 then A12, B12 to H12.
10. 1536-Well assay format has 128 control wells, 64 wells assigned to each control.
11. Neutral control (DMSO)—A21, A22 to P21, and P22 then Q23, Q24 to AF23, and AF24.
12. Inhibitor control (puromycin)—A23, A24 to P23, and P24 then Q21, Q22 to AF21, and AF22.

3.4 Cytotoxicity Assays

When developing cytotoxicity/cell viability assays there are a number of parameters that need to be considered for overall assay performance and quality.

1. Relevant cell type.
2. Cell number per well.
3. Reagent concentration and volumes to be added including DMSO sensitivity.
4. Compound incubation times.
5. Linearity of response/signal and data is proportional to cell toxicity and cell number.

All the cytotoxicity/viability methods described here have been optimized using the chosen THP-1 monocytic cell line with 48 h compound exposure unless indicated otherwise. THP-1 is used as a reference cell line to allow compound comparisons to be made across projects. Assays on other cell types are carried out within our laboratory and the user needs to ensure that the assay is optimized for each cell type used for at least the five parameters listed above.

All of these assays are suitable for running on automated screening platforms found in high-throughput screening laboratories (*see* **Note 9**).

3.5 CellTiter-Blue® Method

CellTiter-Blue® (Promega registered trade name for alamarBlue® or resazurin) is a homogeneous fluorescent assay for measuring the viability of cells. Living cells are able to convert the redox dye, resazurin, to the highly fluorescent resorufin (Fig. 1). Non-viable cells lose metabolic capacity and do not generate resorufin. Whilst we have used CellTiter-Blue® any resazurin preparation can be used but the user must determine the dilution of reagent needed and any other experimental parameters.

This assay was developed in both 1536-well and 384-well assay formats and each format will be described within this section. 1536-Well format was deployed for high-throughput primary screening (*see* **Note 10**) and 384-well format for concentration response curves for further annotation of compounds.

1. Refer to generic protocols for cell culture and cell preparation and cell plating.
2. Incubate lidded assay plate(s) for 15 min at room temperature to equilibrate the plate temperature before transferring the lidded (*see* **Note 10**) plate(s) to 37 °C, in a 5 % v/v CO_2/95 % v/v air humidified incubator for 48 h.
3. After 48 h incubation with compound, prepare CellTiter-Blue® solution for the relevant assay format.

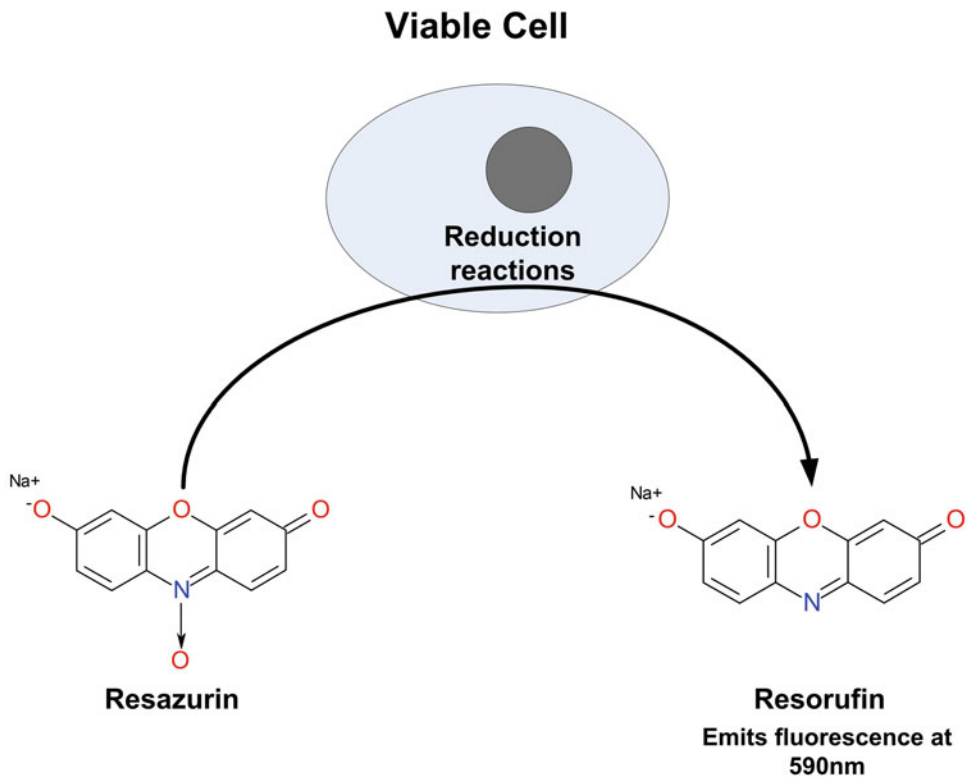

Fig. 1 Schematic diagram illustrating the principle of the CellTiter-Blue® cell viability/cell toxicity assay

4. 384 assay format: using a Multidrop™ Combi (small volume cassette used at fast speed setting) add 8 μL of diluted CellTiter-Blue® Viability reagent (*see* **Note 4**).
5. 1536 assay format: using a Multidrop™ Combi (small volume cassette used at fast speed setting), add 2 μL of diluted CellTiter-Blue® Viability reagent (*see* **Note 4**).
6. Incubate the assay plate(s) for a further 2 h at 37 °C, in a 5 % CO_2 v/v/95 % v/v air humidified incubator.
7. Centrifuge plate(s) at 300 × *g* in a bench top centrifuge for 1 min so cells settle to the bottom of the plate.
8. Read assay plate(s) on a fluorescence plate reader at λ_{ex} 540 nm ± 20 nm; λ_{em} 590 nm ± 20 nm (*see* **Note 11**).

3.6 Compound Fluorescence Quench Assay for CellTiter-Blue®

In order to help determine if compounds are false positives due to quenching of the fluorescence of resorufin we had duplicate copies of compound plates made and used the second copy to determine any quenching at the concentration response stage of screening. Resorufin was added to give equivalent measured fluorescence seen in the neutral control wells in the CellTiter-Blue® assay. If no quench is seen, there will be no significant change in detected

fluorescence across the range of compound concentrations. If quench is seen (indicated by a compound concentration-dependent decrease in fluorescence), this should be taken into account when assessing if a compound is toxic or not. Confirmation of toxicity in an orthogonal assay (CellTox™ Green or Intellicyt Multicyt 4-plex Apoptosis assay) will also help determine whether or not a compound is toxic. We carried out this assay in 384 plates only.

Refer to generic protocols for cell culture and cell preparation and cell plating.

1. Incubate lidded assay plate(s) for 15 min at room temperature to equilibrate the plate temperature before transferring the lidded plate(s) to 37 °C, in a 5 % v/v CO_2/95 % v/v air humidified incubator for 2 h to equilibrate temperature.
2. After 2 h incubation with compound prepare a resorufin solution at the empirically determined concentration.
3. 384 assay format: using a Multidrop™ Combi (low volume cassette used at fast speed setting) add 8 μL of resorufin.
4. Incubate the assay plate(s) for a further 2 h at 37 °C, in a 5 % CO_2 v/v/95 % v/v air humidified incubator (*see* **Note 12**).
5. Centrifuge plate(s) at 300 × *g* in a plate centrifuge for 1 min so cells settle to the bottom of the plate.
6. Read assay plate(s) on a fluorescence plate reader at λ_{ex} 540 nm ± 20 nm; λ_{em} 590 nm ± 20 nm.

3.7 CellTox™ Green Method

This assay detects changes in membrane integrity as a result of incubating THP-1 cells with potentially cytotoxic compound(s) leading to cell death. In this assay, a proprietary cyanine dye is used that is excluded from cells with an intact cell membrane. If a cell dies through a cytotoxic insult the membrane is compromised and DNA is released to which the dye binds. Once bound to DNA the dye fluoresces giving an increase in fluorescence proportional to cytotoxicity (*see* **Note 13**).

1. Refer to generic protocols for cell culture and cell preparation and cell plating.
2. Incubate lidded assay plate(s) for 15 min at room temperature to equilibrate the plate temperature before transferring lidded plate(s) to 37 °C, in a 5 % v/v CO2/95 % v/v air-humidified incubator for 48 h.
3. After 48 h incubation with compound equilibrate assay plates for 30 min at room temperature.
4. During this incubation prepare a 2× diluted stock of CellTox™ Green reagent in assay dilution buffer. Dispense 20 μL of CellTox™ Green reagent to each well using a Multidrop™

Combi with a standard volume Multidrop cassette on fast speed to give a final 1:1000 dilution.

5. Shake assay plate for 15 min on an orbital shaker shielded from light for optimal staining of cells.
6. Read assay plate(s) on a fluorescence plate reader at λ_{ex} 485 nm ± 20 nm; λ_{em} 535 nm ± 20 nm.

3.8 Intellicyt MultiCyt 4-plex Apoptosis Assay Method

This flow cytometry method was used to further annotate a selection of compounds that were identified as cytotoxic from the CellTiter-Blue® and CellTox™ Green screens. As shown in Fig. 2, compounds were tested against four different apoptosis endpoints (Caspase 3 and 7 activation, binding of annexin-V, membrane integrity, and mitochondrial depolarization) to ascertain the mechanism of toxicity (*see* **Note 14**). Although we used the Intellicyt iQue any flow cytometer can be used.

1. Refer to generic protocols for cell culture and cell preparation and cell plating.
2. Incubate lidded assay plate(s) for 15 min at room temperature to equilibrate the plate temperature before transferring lidded plate(s) to 37 °C, in a 5 % v/v CO_2/95 % v/v air-humidified incubator for 24 h (*see* **Note 15**).
3. Prepare the Intellicyt MultiCyt 4-plex Apoptosis kit (*see* **Note 16**). Thaw all kit reagents at room temperature. Once thawed, gently vortex tubes then centrifuge to bring all reagents to the bottom of the tube.
4. Add the following volumes of the kit reagents to make a 2× staining cocktail stock in cell plating media. Vortex staining cocktail before use. Volumes are for one 384-well plate.

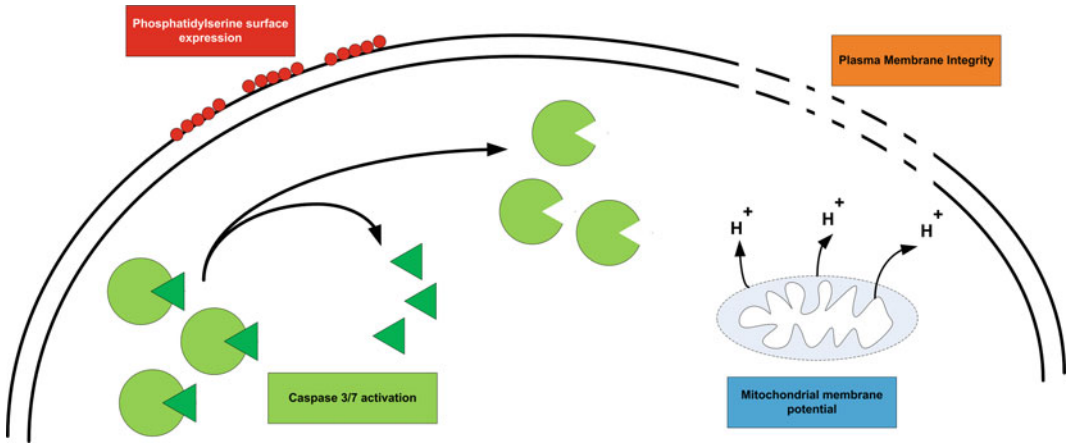

Fig. 2 Schematic diagram illustrating the four parameters of apoptosis measured in the Intellicyt MultiCyt 4-plex assay

(a) Culture media—7.1 mL.
(b) Caspase—16 μL.
(c) Annexin—8 μL.
(d) Viability—80 μL.
(e) Mitochondrial damage—8 μL.
(f) 10× buffer—800 μL.

5. Add 20 μL of 2× staining cocktail stock to each well of a 384-well plate. Shake plate vigorously to ensure thorough mixing. The plate shaker on the iQue® Screener HD was used for this step (15 s at 2800 rpm) but similar vigorous plate shakers will suffice.
6. Incubate assay plate for 1 h at 37 °C, in a 5 % v/v CO_2/95 % v/v air-humidified incubator.
7. Place plate on iQue® Screener HD and read. Refer to Intellicyt instruction manual for setting up the instrument and defining experiment with sample data. Intellicyt also supply pre-defined analysis templates for this assay that can be downloaded from their website. Other flow cytometers can be used.

3.9 Example Data

The figures in this section show some data from all three assays described in this chapter. All the data shown come from a primary screen of approximately 390,000 compounds and the follow-up concentration response assays and illustrate the type of data that can be achieved with these assays (Figs. 3, 4, and 5).

4 Notes

1. Any method of counting cells can be used. It is very important to assess the number of viable cells and not just an absolute cell count. Cultures with significant numbers of non-viable cells should be discarded.
2. THP-1 cells are grown in a roller bottle incubator set to 110 rpm. This enables the cell suspension to maintain a level of viability at ≥95 % over 40+ passages. THP-1 cells can also be grown in a static flask or bottle but this may affect the viability and the number of passages that can be achieved. Cells should be discarded if viability drops below 85 %.
3. Puromycin was used as the inhibitor control where it is added at 50 μM (approximately 50-fold above its IC_{50}) to ensure cell death. Any known cytotoxic compound can be used in place of puromycin such as staurosporine or menadione. Compounds can have different time courses of toxicity and this should be taken into account when choosing an inhibitor control compound. Choice of inhibitor control compound should not affect assay performance if it is used at the correct concentration and time.

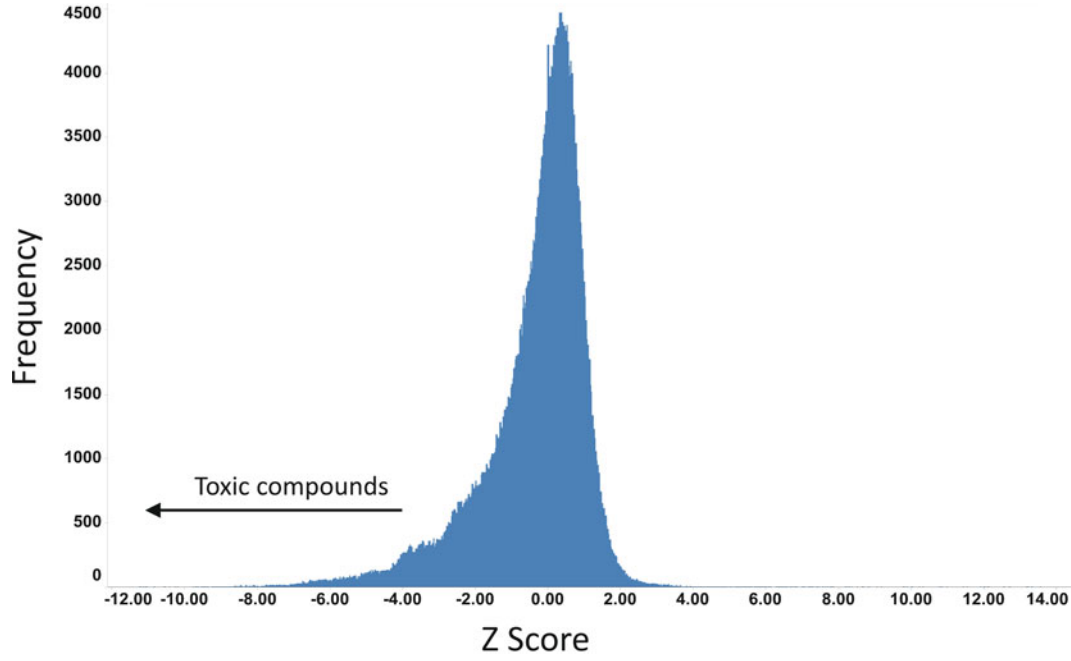

Fig. 3 Histogram of a primary screen of approximately 390,000 compounds tested at 50 μM in the CellTiter-Blue® assay against THP-1 cells. Activity of compounds is normalized using robust Z scores where a Z score of 1 indicates a compound with an activity 1 robust standard deviation from the median of all compound wells on a plate. Negative Z scores indicate an active compound in this assay. Approximately 4 % of compounds tested were found to be active in this assay. This is representative of other diversity sets from our experience

4. We have found that the CellTiter-Blue® reagent can be diluted much more than stated in the Promega assay protocol where they state that 20 μL of neat reagent be added to 100 μL of cell media in 96-well plates and 5 μL neat reagent to 25 μL of media in 384-well plates. This will be very assay dependent particularly on the cell type being used and will vary from laboratory to laboratory. The user must do the relevant checks to ensure any dilution used gives a robust, linear signal whilst allowing the reagent to go as far as possible.
5. If an adherent cell line is used black μClear plates with transparent well bottoms can be used.
6. Cells should be gently stirred with a sterile stirrer bar when plating to reduce plate to plate variability by maintaining a homogenous cell suspension.
7. Users should not see any difference between using assay ready plates and plates prepared using more conventional methods where a solution of compound is diluted stepwise prior to adding to the plate. It is important that the DMSO concentration is 1 % v/v or lower as DMSO in higher concentrations is potentially toxic.

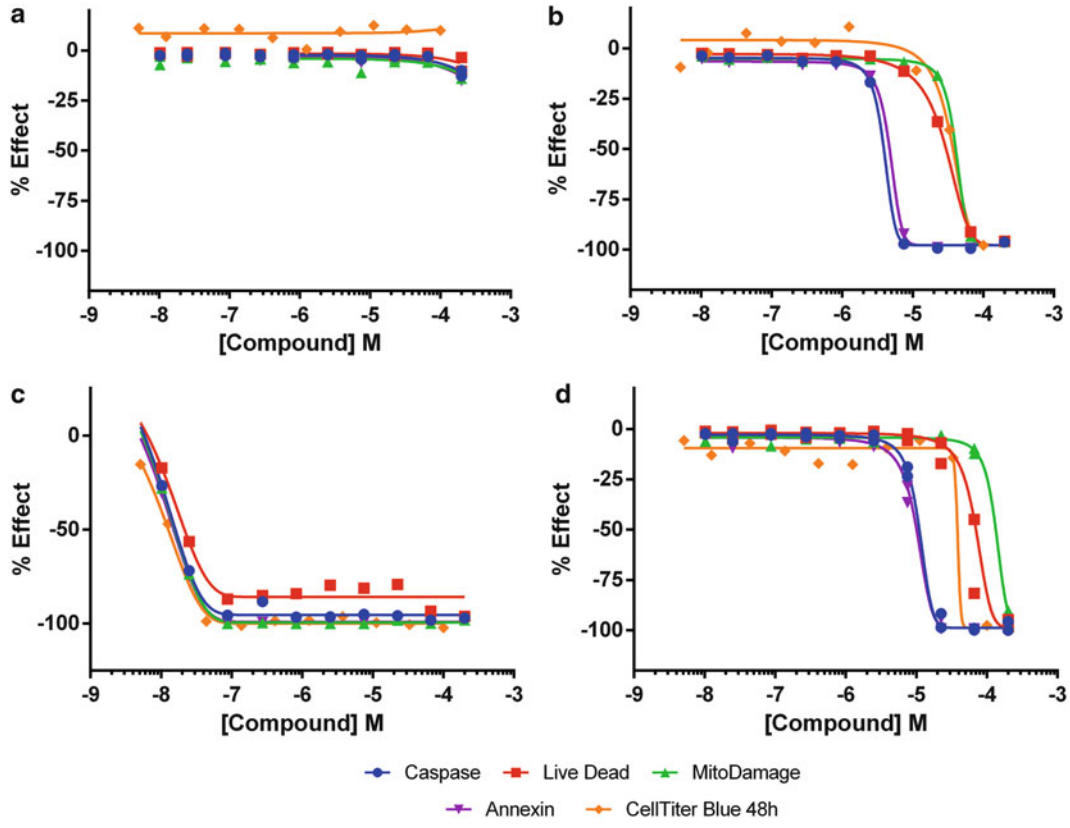

Fig. 4 Concentration responses for four representative compounds from the screen described in Fig. 3. The curves show the activity in the CellTiter-Blue® assay and the Intellicyt Multicyt 4-plex apoptosis assay. Graph **a** shows the confirmation of a non-toxic compound in all assay formats. Graphs **b**, **c** and **d** show compounds of varying toxicity confirmed in both assays. While very toxic compounds are often equipotent across assays (**c**), other compounds (**b**, **d**) show increased potency across early markers of toxicity (Capsase and Annexin)

8. It is important to consider carefully where to place control wells on the plates. It is quite common to see control wells placed on the outermost columns but this is not recommended as these wells will be affected by any edge effect which in turn will lead to incorrect normalization of the data. We place the control wells in the middle of the plate to minimize any effect of edge effects. Ideally controls could be dispersed across more of the plate but this is difficult to achieve with more traditional liquid handling equipment and adds complexity although we do employ such layouts for some concentration response screens.
9. In our laboratory we used Agilent Biocel automation platforms (Santa Clara, CA, USA) for the high-throughput assays. For lower throughput follow-up orthogonal assays we ran the assays at manual workstations with stackers on the plate readers.

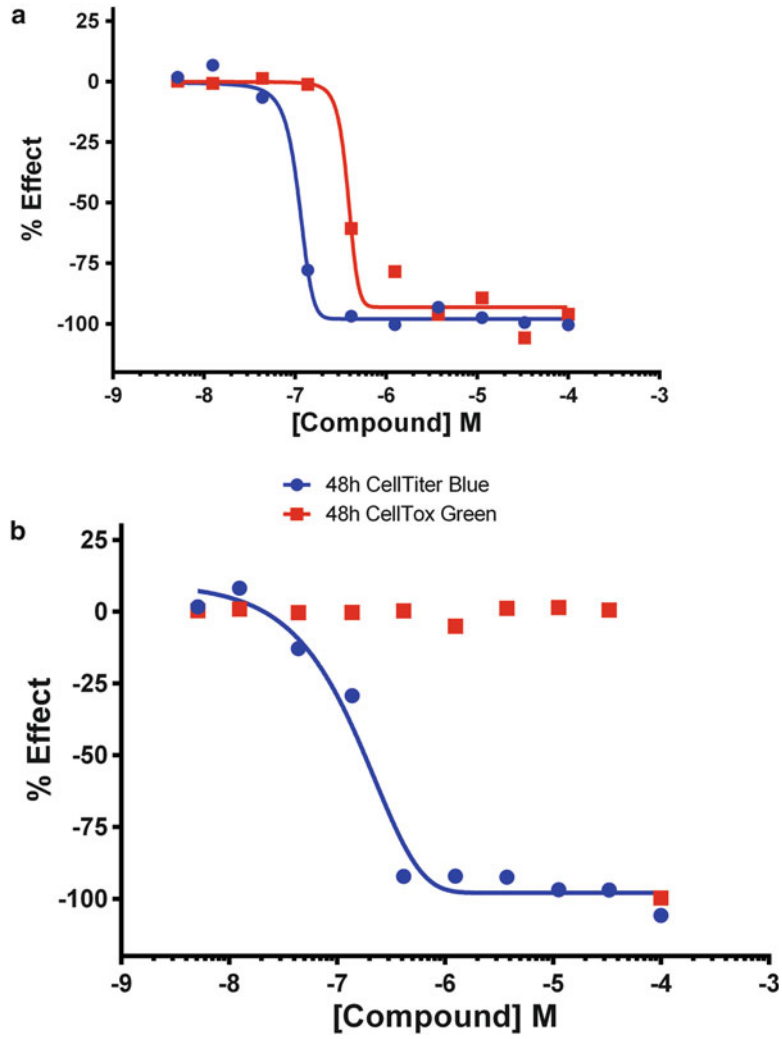

Fig. 5 Concentration responses for two active compounds from the screen described in Fig. 3. The curves show the activity in the CellTiter-Blue® and CellTox™ Green assays. Graph **a** shows a compound where the CellTox™ Green assay confirms the toxicity of the compound seen in the CellTiter-Blue® assay. Graph **b** shows a compound where it looks toxic in the CellTiter-Blue® assay but is inactive in the CellTox™ Green assay at all compound concentrations except for 100 μM. It is likely that the compound is cytostatic rather than toxic as no quench in the CellTiter-Blue® assay was detected (data not shown)

10. Due to the small volumes in a well of a 1536-plate users may well have problems with evaporation of the well contents over the extended incubation times employed in cytotoxicity assays despite the plates having lids placed on them. This evaporation will increase salt concentrations in the media causing cell death leading to potential false positive results. We have found that using an adhesive plate seal will minimize such evaporation. We have had success with both impermeable seals and gas-permeable hydrophobic seals. Alternatively we have excluded

the use of the outermost wells of the 1536 plates leaving them filled with just media. We have not seen these issues in 384-well plates. Allowing plates to sit at room temperature for 15 min can help reduce plate edge effects [17] although we have found this not to be the case with all assays. We have also found that edge effects can also be worse depending on how many plates are loaded into an incubator and counter-intuitively have found that often more plates loaded can lead to worse patterns and edge effects. We have not investigated this further but make this observation to help the reader investigate their own plate pattern issues.

11. Fluorescent compounds can be a problem in this assay as they will mask any change in fluorescence and be potential false negatives. To detect fluorescent compounds plates can be read before adding the CellTiter-Blue® reagent.
12. Once resorufin is added the plates could be read straight away but we decided to keep this assay consistent with the conditions employed in the CellTiter Blue® assay once the detection reagent is added.
13. Further details of the CellTox Green™ kit and assay principle can be found on the Promega website (https://www.promega.com/products/cell-health-and-metabolism/cytotoxicity-assays/real-time-cytotoxicity-assay/celltox-green-cytotoxicity-assay/?activeTab=1). Other types of membrane integrity assay are available and should be able to be substituted although we have not used any of them and cannot therefore make any recommendations.
14. There are other similar apoptosis assays commercially available with some assays requiring the use of a plate reader rather than a flow cytometer. These should be able to be substituted but we have not used any of them and so cannot therefore make any recommendations.
15. We found the optimal incubation time with compounds was 24 h in this assay. The Multicyt 4-plex Apoptosis kit measures early events in a cell starting to undergo apoptosis and a time course showed 24 and 48 h data to be equivalent for early markers of apoptosis across a number of compounds (data not shown). If using a 48 h incubation very toxic compounds can cause complete lysis of cells leading to clogging of the iQue® flow cytometer fluidics.
16. Intellicyt (http://www.intellicyt.com) provides comprehensive protocols with the MultiCyt kits and these should be used as the basis for setting up the assay. Intellicyt also provides analysis templates for their kits.

References

1. Macarron R et al (2011) Impact of high-throughput screening in biomedical research. Nat Rev Drug Discov 10:188–195
2. Mayr LM, Bojanic D (2009) Novel trends in high-throughput screening. Curr Opin Pharmacol 9:580–588
3. Cook D et al (2014) Lessons learned from the fate of AstraZeneca's drug pipeline: a five-dimensional framework. Nat Rev Drug Discov 13:419–431
4. O'Brien J et al (2000) Investigation of the Alamar Blue (resazurin) fluorescent dye for the assessment of mammalian cell cytotoxicity. Eur J Biochem 267:5421–5426
5. Hamid R et al (2004) Comparison of alamar blue and MTT assays for high through-put screening. Toxicol In Vitro 18(2004):703–710
6. Nakayama GR et al (1997) Assessment of the Alamar Blue assay for cellular growth and viability in vitro. J Immunol Methods 204:205–208
7. Slater K (2001) Cytotoxicity tests for high-throughput drug discovery. Curr Opin Biotechnol 12:70–74
8. Weyermann J et al (2005) A practical note on the use of cytotoxicity assays. Int J Pharm 288:369–376
9. Promega Corporation. CellTox™ Green Cytotoxicity Assay. https://www.promega.com/products/cell-health-and-metabolism/cytotoxicity-assays/real-time-cytotoxicity-assay/celltox-green-cytotoxicity-assay/?activeTab= 0. Accessed 1 July 2015
10. McDougal M et al (2010) Nucleic acid binding dyes and uses thereof. US Patent 2010/0233710 A1
11. Korzeniewski C, Callewaert DM (1983) An enzyme-release assay for natural cytotoxicity. J Immunol Methods 64:313–320
12. Lobner D (2000) Comparison of the LDH and MTT assays for quantifying cell death: validity for neuronal apoptosis? J Neurosci Methods 96:147–152
13. Fotakis G, Timbrell JA (2006) In vitro cytotoxicity assays: comparison of LDH, neutral red, MTT and protein assay in hepatoma cell lines following exposure to cadmium chloride. Toxicol Lett 160:171–177
14. Luu YK et al (2012) Profiling of toxicity and identification of distinct apoptosis profiles using a 384-well high-throughput flow cytometry screening platform. J Biomol Screen 17:806–812
15. Griffith D et al (2012) Implementation and development of an automated, ultra-high-capacity, acoustic, flexible dispensing platform for assay-ready plate delivery. J Lab Autom 17(5):348–358
16. Zhang J-H et al (1999) A simple statistical parameter for use in evaluation and validation of high throughput screening assays. J Biomol Screen 4:67–73
17. Lundholt BK et al (2003) A simple technique for reducing edge effect in cell-based assays. J Biomol Screen 8:566–570

Chapter 17

BRET: NanoLuc-Based Bioluminescence Resonance Energy Transfer Platform to Monitor Protein-Protein Interactions in Live Cells

Xiu-Lei Mo and Haian Fu

Abstract

Bioluminescence resonance energy transfer (BRET) is a prominent biophysical technology for monitoring molecular interactions, and has been widely used to study protein-protein interactions (PPI) in live cells. This technology requires proteins of interest to be associated with an energy donor (i.e., luciferase) and an acceptor (e.g., fluorescent protein) molecule. Upon interaction of the proteins of interest, the donor and acceptor will be brought into close proximity and energy transfer of chemical reaction-induced luminescence to its corresponding acceptor will result in an increased emission at an acceptor-defined wavelength, generating the BRET signal. We leverage the advantages of the superior optical properties of the NanoLuc® luciferase (NLuc) as a BRET donor coupled with Venus, a yellow fluorescent protein, as acceptor. We term this NLuc-based BRET platform "BRET^n". BRET^n has been demonstrated to have significantly improved assay performance, compared to previous BRET technologies, in terms of sensitivity and scalability. This chapter describes a step-by-step practical protocol for developing a BRET^n assay in a multi-well plate format to detect PPIs in live mammalian cells.

Key words Bioluminescence resonance energy transfer (BRET), Nanoluc luciferase (NLuc), Hippo signaling pathway, YAP-TEAD interaction, Ultra high-throughput screening (uHTS)

1 Introduction

Bioluminescence resonance energy transfer (BRET) is a naturally occurring phenomenon existing in some marine species such as *Aequorea*, where radiation-less transfer of energy is observed from an activated bioluminescent donor (e.g., photoprotein aequorin) to its associated green fluorescent protein (GFP). This natural physical process has been engineered to monitor direct molecular interactions, due to its stringent distance requirement ($\leq$10 nm) to allow efficient energy transfer [1–3]. In principle, the photons from the light-emitting donor can excite an acceptor fluorophore by resonance energy transfer if the donor and acceptor fluorophore are in close proximity with proper orientation and have appropriate

William P. Janzen (ed.), *High Throughput Screening: Methods and Protocols*, Methods in Molecular Biology, vol. 1439,
DOI 10.1007/978-1-4939-3673-1_17,

overlap between the donor emission and acceptor excitation spectra. Several versions of BRET have been reported by combining various donor and acceptor pairs [2–4]. Previously described BRET systems include BRET^1 and BRET^2, which use *Renilla* luciferase (RLuc) as BRET donors [4]. These systems have revolutionized the way we study PPIs, especially in live cells. Here we describe a working protocol of a Nanoluc luciferase (NLuc)-based BRET platform.

Nanoluc luciferase is a luminescent protein engineered from the luciferase of a luminous deep-sea shrimp, *Oplophorus gracilirostris* [5]. It has been shown that NLuc is the smallest (19 kDa) and brightest luciferase to date, with superior stability, glow-type luminescence, and narrow emission spectrum [5]. These improved properties of NLuc allowed us to generate a new BRET platform for PPI detection, termed BRET^n to stand for NanoLuc-based BRET. For the BRET^n PPI biosensor design, NLuc was used instead of the conventional RLuc as a BRET^n donor. Venus [6], a yellow fluorescent protein variant, serves as a BRET^n acceptor. The interaction of NLuc-fused protein X and Venus-fused protein Y brings the donor and acceptor into close proximity, leading to energy transfer of the luminescence signal from NLuc to Venus upon substrate, furimazine, and oxidation (Fig. 1). The emission signal of Venus can then be used as a measurement of BRET signal for detection of PPIs (Fig. 1).

The performance of BRET^n has been demonstrated as a PPI biosensor for pathway profiling and PPI modulator screening [7]. The improved properties of BRET^n enable miniaturization of the assay to a 1536-well plate uHTS format for large-scale screening. The following protocol describes a general step-by-step procedure for developing a BRET^n assay to monitor PPIs in live cells. The results of BRET^n assay development for monitoring the YAP-TEAD interaction [8–10], a key PPI involved in the Hippo signaling pathway, are presented as a case study. The Hippo signaling pathway plays a critical role in normal physiology, such as the control of organ size during development. Its dysregulation has

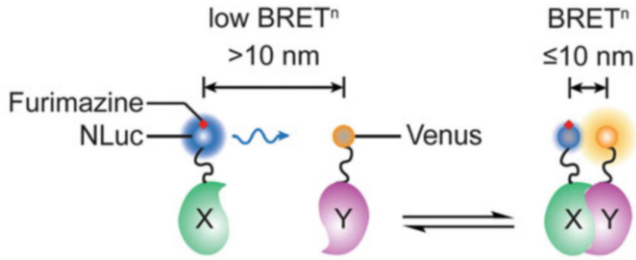

Fig. 1 Schematic illustration of BRET^n design. NLuc and Venus are genetically fused to the N-terminal end of each protein of interest, X and Y, respectively. BRET signal can be detected when NLuc and Venus are brought into close proximity upon interaction of protein X and Y

been associated with tumorigenesis in a range of cancer types [8–10]. Targeting the YAP-TEAD interaction has been suggested to be a promising strategy for treatment of YAP-addicted cancers [11, 12]. However, no specific YAP-TEAD small molecule inhibitors are currently available [11, 12]. In order to better understand the function of the YAP-TEAD interaction, a highly sensitive BRET^n assay for discovery of interaction disruptors has been designed and optimized. Small molecule chemical probes that disrupt the YAP-TEAD interaction will enable physiological studies and have potential for anti-cancer therapeutic development. Using the YAP-TEAD interaction as a model system, a detailed protocol for a BRET^n assay for monitoring PPIs in live cells is described. While this chapter uses YAP-TEAD as an example, the procedure described in this chapter can be readily adapted and applied to other molecular interactions.

2 Materials

2.1 Plasmids for NLuc-tagged TEAD2 and Venus-tagged YAP1 Construction (see Note 1)

1. Entry vector with TEAD2 in pDONR221.
2. pENTR/D-TOPO vector.
3. TOPO® Cloning kit.
4. Gateway pDEST26 Vector.
5. pFUW vector.

2.2 Other Reagents

1. Cell culture media: 1× Dulbecco's Modified Eagle Medium (DMEM) without phenol red indicator, supplemented with 4 mM L-glutamine, 4.5 g/L glucose, 1 mM sodium pyruvate, 100 U/mL penicillin, 100 mg/mL streptomycin, and 10 % fetal bovine serum.
2. Human Embryonic Kidney 293T (HEK293T) cells (*see* **Note 2**).
3. Polyethylenimine (PEI) transfection reagent stock solution (*see* **Note 2**): dissolve PEI (1 mg/mL) in deionized water at 80 °C with stirring. Adjust solution to pH 7.2 using 0.1 M HCl at room temperature. Filter-sterilize, aliquot, and store at −20 °C.
4. Nano-Glo® luciferase assay system (Promega, Madison, WI).
5. Plate (*see* **Note 3**): 1536-well solid bottom white plate and clear bottom black plate and 384-well polypropylene plate.
6. Plate reader for BRET signal measurements (*see* **Note 4**): for YAP-TEAD BRET^n assay development, BRET^n signal measurement was performed using 460 and 535 nm emission filters.

3 Methods

3.1 Plasmid Construction

NLuc-tagged TEAD2 and Venus-tagged YAP1 were constructed using Gateway® cloning system as described [7] (*see* **Note 1**). Entry vector with TEAD2 in pDONR221 was purchased. Entry vector with YAP1 was cloned into pENTR/D-TOPO vector using PCR and TOPO® Cloning kit. The NLuc coding sequence (Promega, Madison, WI), along with a linker (*see* **Note 1**), was inserted into the pDEST26 (Invitrogen) to generate Gateway®-based NLuc destination expression vector. The Venus coding sequence, along with a linker (*see* **Note 1**), was inserted into the pFUW vector (Emory University) to generate the Gateway®-based Venus destination expression vector. NLuc-TEAD2 and Venus-YAP1 expression plasmids were constructed by performing LR reactions between corresponding entry and destination vectors using LR Clonase™ II enzyme mix.

3.2 Plating Cells

HEK293T cells (2000 cells in 4 μl per well (*see* **Note 3**)) were dispensed into a 1536-well plate. Cells were plated side by side sequentially in both a solid bottom white plate and a clear bottom black plate (*see* **Note 3**). Plates were sealed with a gas permeable sealing membrane.

3.3 Transient Transfection

Below we describe a typical experiment where the donor and acceptor expression levels are varied by serial dilution of the amount of DNA to be transfected. This experimental setup will allow the acceptor to saturate the donor and provide a maximal BRET signal. A template design for a 384-well DNA plate format for orthogonal co-transfection is shown in Fig. 2 (*see* **Note 5**).

1. Serially dilute NLuc-TEAD2 and NLuc-empty plasmid to 0.2 and 0.1 ng/mL in dH_2O in sterile Eppendorf tube (*see* **Note 6**).
2. Dilute Venus-YAP1 and Venus-empty plasmid to 40 ng/μl with dH_2O in sterile Eppendorf tube. Then serially dilute Venus-YAP1 to 20 and 10 ng/μl, and Venus-empty to 20, 10, and 5 ng/mL using pcDNA (40 ng/μl) (*see* **Note 6**).

			pcDNA	Venus-YAP1			Venus-empty		
DNA amount (ng/well)			10	2.5	5	10	1.25	2.5	5
			1	2	3	4	5	6	7
dH_2O		A							
NLuc-TEAD2	0.025	B							
	0.05	C							
NLuc-empty	0.025	D							
	0.05	E							

Fig. 2 An example 384-well plate format for DNA transfection. Various amounts of NLuc and Venus plasmids were mixed orthogonally using multichannel pipette. The final DNA amount transfected into a single well of 1536-well cell plate is indicated

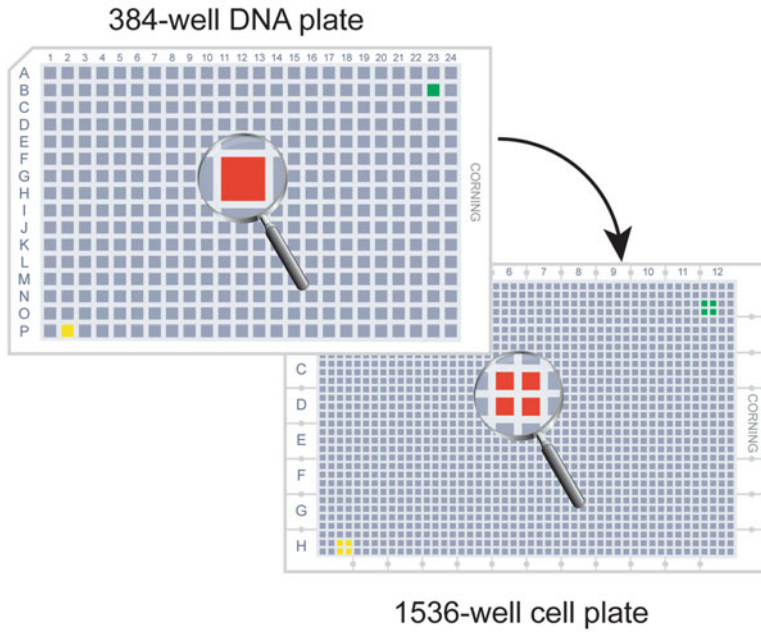

Fig. 3 Schematic illustration of forward in-well transfection from 384-well DNA plate into 1536-well cell plate in four replicates

3. Orthogonally mix 5 μl NLuc plasmids (0.1 and 0.2 ng/μl for both NLuc-TEAD2 and NLuc-empty) and 5 μl Venus plasmids (10, 20, and 40 ng/μl for Venus-YAP1 and 5, 10, and 20 ng/μl for Venus-empty) according to the format as shown in Fig. 2 in a 384-well plate.
4. Dilute PEI to 60 ng/μl in cell culture media (*see* **Note 2**).
5. Dispense 10 μl/well of the 60 ng/μl PEI dilution into the 384-well DNA plate to make the final ratio of PEI:DNA = 3:1.
6. Incubate the DNA:PEI mix at 25 °C for 20 min.
7. Perform forward in-well transfection using an automated liquid handler. Transfer 1 μl of DNA:PEI mix from 384-well plate into 1536-well plate in four replicates (Fig. 3). The final amount of DNA transfected into each 1536-well is indicated in Fig. 2. The 1536-well solid bottom white plate and clear bottom black plate are transfected side by side.
8. Incubate cells in CO_2 incubator at 37 °C for 2 days.

3.4 BRET^n Measurement

1. Load 1536-well clear bottom black plate into plate reader and detect fluorescence signal (FI) (excitation: 480 nm, emission: 535 nm) using microplate reader software.
2. Immediately prior to the BRET measurement, prepare furimazine (i.e., Nano-Glo® Luciferase Assay Substrate) by diluting the stock solution 1:100 in cell culture media (*see* **Note 7**).

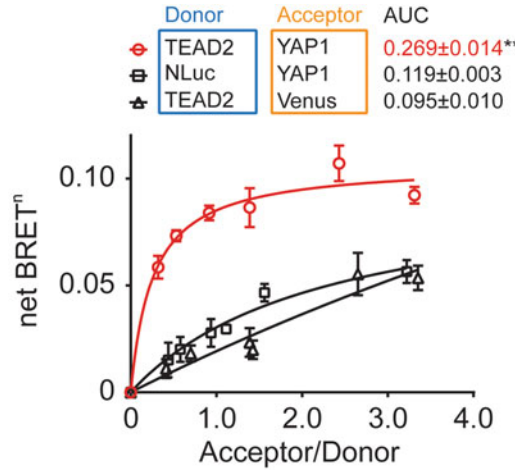

Fig. 4 BRET^n saturation curve of NLuc-TEAD2 and Venus-YAP1 interaction. The error bar represents the s.d. from four replicates. AUC values are presented as mean ± s.d. from three independent experiments

3. Dispense 1 μl of 1:100 diluted substrate directly into a 1536-well solid bottom white plate (cell culture media does not need to be changed) (*see* **Note 7**).
4. Load 1536-well solid bottom white plate into plate reader and take BRET^n reading by measuring luminescence at 460 ± 15 nm (I_{460}) and 535 ± 15 nm (I_{535}).

3.5 Data Analysis

1. The BRET^n signal can be determined by I_{535}/I_{460}.
2. The net BRET^n signal is calculated by subtracting out background BRET^n signal from cells transfected with donor plasmid only.
3. Calculate the net fluorescence intensity (FI) by subtracting out background fluorescence from cells transfected with pcDNA only.
4. Calculate the net I_{460} by subtracting out background luminescence from cells transfected only with pcDNA.
5. Calculate the acceptor/donor ratio by dividing the net FI by net I_{460}.
6. Using graphing software, plot the acceptor/donor ratio against the net BRET^n as in Fig. 4 (*see* **Note 8**). The data can then be fit with a nonlinear regression model.

4 Notes

1. BRET^n follows classical rules of energy transfer in that the energy transfer efficiency is inversely proportional to the sixth power of distance between two fluorophores, and is also

Table 1
Recommended cell culture condition and DNA transfection range for performing BRET^n assay in other multiple well plates

	Cell number (per well)	Cell culture volume (μl)	NLuc plasmid (ng/well)	Venus plasmid (ng/well)	1:100 diluted substrate (μl)
384-Well	8000	50	0.1–0.2	10–40	5
96-Well	30,000	200	0.5–1	50–200	20
48-Well[1]	60,000	500	1–2	100–400	50
24-Well[1]	150,000	1000	2–5	200–800	100
6-Well[1]	600,000	2000	10–20	500–3000	400

[1]Considering the limited supplies of solid bottom white and clear bottom black types of 48-, 24-, and 6-well plate, as well as the cost of luciferase substrate, it is more feasible to detach and transfer the cells into high-density plate on the day of BRET^n measurement

correlated with the orientation of two fluorophores. Therefore, it is advantageous to use peptide linkers, such as GGGGSGGGGS used in this study, between the NLuc/Venus tag and the proteins of interest to allow sufficient movement of the tags with less steric hindrance. Moreover, there are eight possible fusion combinations for each pair of proteins considering different tag placements at N- or C-terminus of the gene of interest. It is highly recommended to try all eight pairing combinations in order to achieve a maximized BRET^n dynamic window.

2. Other cell lines and transfection reagents can be used. We choose to use HEK293T and PEI as they yield high transfection efficiency and reproducibility at affordable cost. For cell lines other than HEK293T cells, the amount of DNA transfected and DNA/PEI ratio need to be optimized empirically.
3. Other types and formats of standard multiple well plates can be used with the method described above and the reagent amount suggested in Table 1. We use plates from Corning (Corning, NY). Other plate manufacturers may be acceptable but should be thoroughly tested prior to use.
4. We use the EnVision® Multilabel Reader (PerkinElmer) for our BRET^n assay. Other plate readers equipped with desired emission filters can be used. To collect BRET^n data, we use the Wallac EnVision Manager software (PerkinElmer). Wallac is able to automatically calculate the BRET^n signal from I_{460} and I_{535} channel, and export the data in a format that is compatible with Microsoft Excel.
5. Controls are essential to assess the success of the BRET^n assay. Negative controls, such as NLuc-TEAD and Venus, and NLuc

and Venus-YAP1, are necessary to rule out false-positive signals due to nonspecific energy transfer. Positive controls, such as the NLuc-Venus fusion protein, allow the researcher to define positive BRET signals.

6. The amount of NLuc and Venus plasmid used for transfection needs to be determined empirically based on the PPI pairs.
7. $BRET^n$ assay can also be performed with cell lysates, instead of live cell detection described in this study with appropriate modifications of protocol.
8. Conventionally, BRET data was quantified solely by calculating maximal BRET signal ($BRET_{max}$) based on nonlinear regression analysis, where $BRET_{50}$ was often neglected. In this scenario, in order to get precise $BRET_{max}$, the BRET saturation curve needs to reach plateau. We employed an area under the curve (AUC) analysis method to quantitatively compare the $BRET^n$ signal between PPI and controls, as AUC reflects both $BRET_{max}$ and $BRET_{50}$ for various PPIs [7].

Acknowledgments

We thank Dr. Kun-Liang Guan for providing YAP1, and Dr. Atsushi Miyawaki for providing Venus cDNA plasmid as cloning template. We would like to thank Drs. Jonathan Havel and Zenggang Li for their contributions in generating NLuc destination vector and Venus-YAP1 construct. We also thank Dr. Yuhong Du for her constructive inputs to make this assay work, and Dr. Margaret Johns for editing the text. This study is supported in part by National Cancer Institute to H.F. (NIH U01CA168449) and to the Winship Cancer Institute of Emory University (NIH 5P30CA138292).

References

1. Xu Y, Kanauchi A, von Arnim AG, Piston DW, Johnson CH (2003) Bioluminescence resonance energy transfer: monitoring protein-protein interactions in living cells. Methods Enzymol 360:289–301
2. Pfleger KDG, Eidne KA (2006) Illuminating insights into protein-protein interactions using bioluminescence resonance energy transfer (BRET). Nat Methods 3(3):165–174. doi:10.1038/Nmeth841
3. Xu Y, Piston DW, Johnson CH (1999) A bioluminescence resonance energy transfer (BRET) system: application to interacting circadian clock proteins. Proc Natl Acad Sci U S A 96(1):151–156
4. Couturier C, Deprez B (2012) Setting up a bioluminescence resonance energy transfer high throughput screening assay to search for protein/protein interaction inhibitors in mammalian cells. Front Endocrinol 3:1–13. doi:10.3389/fendo.2012.00100
5. Hall MP, Unch J, Binkowski BF, Valley MP, Butler BL, Wood MG, Otto P, Zimmerman K, Vidugiris G, Machleidt T, Robers MB, Benink HA, Eggers CT, Slater MR, Meisenheimer PL, Klaubert DH, Fan F, Encell LP, Wood KV (2012) Engineered luciferase reporter from a deep sea shrimp utilizing a novel imidazopyrazinone substrate. ACS Chem Biol 7(11):1848–1857. doi:10.1021/Cb3002478

6. Nagai T, Ibata K, Park ES, Kubota M, Mikoshiba K, Miyawaki A (2002) A variant of yellow fluorescent protein with fast and efficient maturation for cell-biological applications. Nat Biotechnol 20(1):87–90. doi:10.1038/nbt0102-87
7. Mo X-L, Luo Y, Ivanov AA, Su R, Havel JJ, Li Z, Khuri F, Du Y, Fu H (2015) Enabling systematic interrogation of protein-protein interactions in live cells with a versatile ultra-high throughput biosensor platform. J Mol Cell Biol. doi: 10.1093/jmcb/mjv064
8. Johnson R, Halder G (2014) The two faces of Hippo: targeting the Hippo pathway for regenerative medicine and cancer treatment. Nat Rev Drug Discov 13(1):63–79. doi:10.1038/nrd4161
9. Harvey KF, Zhang X, Thomas DM (2013) The Hippo pathway and human cancer. Nat Rev Cancer 13(4):246–257. doi:10.1038/nrc3458
10. Huang J, Wu S, Barrera J, Matthews K, Pan D (2005) The Hippo signaling pathway coordinately regulates cell proliferation and apoptosis by inactivating Yorkie, the *Drosophila* homolog of YAP. Cell 122(3):421–434. doi:10.1016/j.cell.2005.06.007
11. Zhang Z, Lin Z, Zhou Z, Shen HC, Yan SF, Mayweg AV, Xu Z, Qin N, Wong JC, Zhang Z, Rong Y, Fry DC, Hu T (2014) Structure-based design and synthesis of potent cyclic peptides inhibiting the YAP-TEAD protein-protein interaction. ACS Med Chem Lett 5(9):993–998. doi:10.1021/ml500160m
12. Liu-Chittenden Y, Huang B, Shim JS, Chen Q, Lee SJ, Anders RA, Liu JO, Pan D (2012) Genetic and pharmacological disruption of the TEAD-YAP complex suppresses the oncogenic activity of YAP. Genes Dev 26(12):1300–1305. doi:10.1101/gad.192856.112

Chapter 18

Application of Imaging-Based Assays in Microplate Formats for High-Content Screening

Adam I. Fogel, Scott E. Martin, and Samuel A. Hasson

Abstract

The use of multiparametric microscopy-based screens with automated analysis has enabled the large-scale study of biological phenomena that are currently not measurable by any other method. Collectively referred to as high-content screening (HCS), or high-content analysis (HCA), these methods rely on an expanding array of imaging hardware and software automation. Coupled with an ever-growing amount of diverse chemical matter and functional genomic tools, HCS has helped open the door to a new frontier of understanding cell biology through phenotype-driven screening. With the ability to interrogate biology on a cell-by-cell basis in highly parallel microplate-based platforms, the utility of HCS continues to grow as advancements are made in acquisition speed, model system complexity, data management, and analysis systems. This chapter uses an example of screening for genetic factors regulating mitochondrial quality control to exemplify the practical considerations in developing and executing high-content campaigns.

Key words High-content screening, High-content analysis, Automated microscopy, RNAi, siRNA, Functional genomics, Imaging assay, Assay development, Image analysis

1 Introduction

The emergence of cell-based screening strategies has extended the reach of discovery biology (small and large molecule) and enabled large-scale functional genomics with siRNA, shRNA, and now CRISPR/Cas9 platforms. Emphasis in cell-based screening has given way to phenotypic analyses, where the goal is to understand how exogenous agents change complex and interconnected pathway biology in a target agnostic manner. Since there are limits to the biology accessible through assays on purified components such as proteins and nucleic acids, the aim of phenotypic screening is twofold: (1) expand the assay context to capture non-canonical biological target-space, and (2) allow for observation of more physiologically relevant phenomena. The original implementations of high-throughput phenotypic screening relied upon bulk

William P. Janzen (ed.), *High Throughput Screening: Methods and Protocols*, Methods in Molecular Biology, vol. 1439,
DOI 10.1007/978-1-4939-3673-1_18,

Table 1
Typical types of measurements found in an HCA platform

Type of HCS readout	Examples of utility in screening assays
Cell morphology	Measuring toxicity of exogenous agents, changes in neurites outgrowth, chemotaxis, differentiation, polarity, cell cycle, and cellular stress
Rare event detection	Detecting non-obvious population dynamics or phenomena that a human viewer would easily overlook due to a low occurrence within hundreds or thousands of cells
Cell counting	Cell growth, division, and viability
Total fluorescence intensity	Measuring the expression of a target protein in a given cellular compartment. Also useful for detecting reporter quenching and compound fluorescence
Per cell fluorescence	Score for the fraction of cells positive or negative for fluorescence. Quantitate rescue or loss of fluorescently labeled proteins
Co-localization	Identify gain or loss of co-localization between labeled proteins
Protein translocation	Pathway activation and cell signaling events
Nuclear intensity	Cell cycle, live/dead analysis, mitotic index
Nuclear morphology	Genotoxicity, apoptosis

Many other HCS readouts are possible and the choice of which to use will depend on the biology being queried and the types of probes/reporter utilized

readouts such as well-level luminescence and fluorescence from reporter genes or measurement technologies (e.g. ELISA). Automated microscopy instrumentation paired with microplate platforms has ushered in an era of phenotypic screening that queries biological pathways on a subcellular, cellular, and cell-population level. These approaches are rooted in quantifying phenotypes exhibited by each individual cell within all or part of a well. When microplate-based imaging is combined with unbiased analysis tools and a multiparametric phenotypic assay, "high-content" screening (HCS) can be achieved. Also referred to as high-content analysis (HCA), the key concept is the ability to make multiple measurements (Table 1) on signals encoded in the raw images of cells (Table 2) to describe phenotypic alterations.

While relying on the tools of conventional microscopy such as fluorescence, phase contrast, and luminescence techniques, HCS has a strong emphasis on hardware and software automation and throughput. This chapter discusses the practical considerations in building assays for HCS and the types of analyses used to extract meaningful data from such highly parallel experiments. As examples of how HCS can be the basis of high-throughput biology, we describe siRNA screening for genetic modulators of Parkin translocation to damaged mitochondria (Fig. 1), and the subsequent autophagic clearance of these mitochondria. Mitochondria are a central hub of multiple biochemical and energetic processes and

Table 2
Classes of fluorescent and non-fluorescent labeling strategies utilized in HCA

HCS readout tool	Advantages	Disadvantages
Fluorescent protein (e.g. GFP, mCherry)	Can label specific proteins and monitor location and intensity (better at location than intensity)	Can suffer from poor dynamic range; high auto fluorescence in cells can interfere with signal. Requires overexpression to efficiently detect most fusion proteins
Nuclear stain (Hoechst—Live, DAPI, DRAQ5)	Robust label of nucleus which is essentially a required starting point for segmentation	Choose appropriately to match with other fluorescent tools
Cell imaging dyes (e.g., EdU stain, caspase stain, nuclear stain, live/dead stain)	Can capture a variety of cellular processes in living cells that can then be measured post-fixation	Difficult to multiplex and are sometimes very expensive
Live cell imaging dyes (e.g., mitotracker, lysotracker)	Detects certain subcellular structures in live cells without the need for genetic manipulation of cells	Autofluorescence and artifactual labeling of other structures; care must be taken to determine correct concentration and washing required. Some of these may survive fixation, others will not. Live imaging may limit throughput
Antibody staining	Label endogenous proteins; potential for significant signal amplification and thus a robust assay window	Requires high-quality immunofluorescence (IF) antibody; introduces much additional handling; almost always done with fixed samples
Brightfield/phase contrast imaging	Offers a simple, label-free method to identify cells and potentially describe features such as dense inclusions or vacuolization	A high degree of variability in white light microscopy between cells in a field can make analysis difficult. Light and dark features in widefield and phase images can be generated by many biological structures including debris making the differentiation of specific biological events more complicated

At a minimum, most HCS assays will label nuclei and a cytosolic component, so that these two basic areas in the cell may be segmented. Up to seven different channels are possible on modern HCA instruments, but three to four different probes is likely the most typical number

their health is a key factor in a variety of human pathologies [1, 2]. One autophagic pathway that maintains the fidelity of mitochondria is driven by the ubiquitin kinase PINK1 and the E3 ubiquitin ligase Parkin. Implicated in the etiology of familial Parkinson's disease [3, 4], the PINK1/Parkin-mediated mitochondrial quality control is triggered when a mitochondrion loses membrane

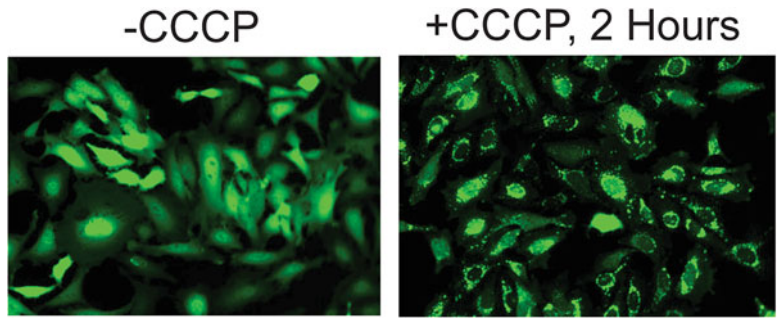

Fig. 1 Example of Parkin translocation phenotype after mitochondrial depolarization. HeLa cells expressing GFP-Parkin (*left panel*) were subjected to 10 μM CCCP treatment for 2 h to collapse mitochondrial membrane potential (*right panel*). This treatment induces a rapid translocation of the GFP-Parkin to the mitochondria in a characteristic punctate pattern. Note the loss of the strong GFP florescence from the nuclear region of the cell in many of the cells. Images were collected using widefield fluorescence imaging at 20× magnification

potential and accumulates PINK1 protein on the outer membrane [5]. The phosphorylation of ubiquitin by PINK1 (unknown at the time of our original study) triggers the recruitment of autophagic adaptor proteins to assemble around the damaged mitochondrion in a process greatly amplified by the concomitant activation and translocation of cytosolic Parkin [6–9]. Ultimately, damaged mitochondria are engulfed by autophagic machinery and shuttled to the lysosome for destruction in a process known as selective mitophagy. These pathway mechanics presented an excellent opportunity to illuminate genes involved in the recruitment of Parkin to depolarized mitochondrial bodies with genome-wide siRNA screening. To determine the factors involved in the pathway on a genomic scale, an assay was designed for HCS in 384-well plates based on earlier demonstrations of fluorescently labeled Parkin activation and recruitment to mitochondria by the PINK1 kinase [10, 11]. HCS presented the most direct and useful method to evaluate genetic modulators of the PINK1/Parkin-mediated mitophagy—not only was it able to identify genetic modifiers of translocation, but it could also account for unwanted pleiotropic effects on mitochondrial or cellular morphology which would go unnoticed in single-parameter screening. Specifically, the HCS assay we built [12] was able to:

1. Quantify the degree of Parkin translocation to damaged mitochondria on a per cell basis.
2. Allow for the measurement of mitochondrial clearance and mitophagy on a per cell basis.
3. Delimit specious gene knockdowns that would obscure translocation by altering cell morphology.

4. Identify gene knockdowns that would deplete or expand the population of mitochondria in a given cell and therefore appear to alter Parkin translocation dynamics.
5. Determine the toxicity of each gene knockdown by counting nuclei/cell number.

Beyond the example presented in this chapter, HCS has proven to be a powerful tool in the high-throughput arena. Chemical screening with HCS assays has been used to track the behavior of both cells [13–15] and model organisms [16, 17] exposed to bioactive compounds, and the unbiased prediction of compound mechanism-of-action is now possible with HCS [18–20]. More recently, HCS has been used to characterize approved drugs that can revert disease phenotypes [21]. Overall, the advantages of imaging-based HCS are manifold:

1. Leverage microscopy hardware to build assays with highly multiplexed readouts. Fluorescence microscopy is the most common implementation of HCS, and four to seven channels are typically available for the collection of phenotypic data.
2. HCS techniques offer the user a robust toolbox to identify, characterize, and compensate for (or filter out) off-target effects, reporter interference, and generally misleading activities that dominate chemical and functional phenotypic screens. Such activities are generally removed in time-consuming secondary screens in traditional HTS campaigns.
3. Assays based on subtle and intricate subcellular phenotypes are much more feasible in HCS because image analysis can integrate a multitude of measurements including texture, intensity, puncta, and spatial position relative to subcellular guideposts (e.g. nucleus, cytosol, organelles, cell membrane) to characterize a change in the biology of interest. HCS is especially well-suited to measure changes in cellular morphology (e.g. neurite outgrowth) or translocation of protein signaling components.
4. HCS enables the capture of rare events in cell populations that would otherwise be missed in homogeneous assay formats. This could be extremely important in experiments with limited penetrance (e.g., heterogeneous transfection or gene editing efficiency).
5. HCS allows for the characterization and subsequent clustering of subtle, complex, and multiparametric phenotypes that would not otherwise be possible [22]. This greatly enhances our ability to identify relationships between different screening reagents and even extends those inferences into cellular space (e.g., pathways).
6. Images can be reanalyzed in the future for additional characteristics.

1.1 General Considerations in HCS Assay Design and Execution

1.1.1 Start from Robust Biology in an Appropriate Model System

The conversion of a cellular phenotype observed in conventional microscopy into a high-content screening assay requires a number of considerations. As with any screening effort, the first criteria to be considered should be robustness of the effect—small effect sizes observed in low-throughput manual microscopy, while biologically intriguing, are often not a good starting point for an HCS assay. Events that require complex live-cell manipulations or hands-on intervention, such as targeted photobleaching and photoactivation, are non-starters. As with any high-throughput process, minimizing the number of reagent additions and avoiding reagent additions that must be synchronized in time with the imaging of wells is essential for HCS tractability. While it is hard to quantify the level of robustness required, a rather glib rule of thumb for basic HCS explorations is often, "if you can't see it, don't screen it." However, relying on one's eyes alone as the definitive judge of phenotypic change is limiting since image analysis tools focusing on intricate features such as texture, granularity, shape, and polarity are often able to find highly significant patterns that we are unable to perceive. A better guiding principle is really to understand how the biology connects to the chosen measurements as many measurements have no bearing on the particular question at hand.

Along with consideration of assay robustness, care must also be taken when choosing a model system to serve as the screening assay platform. When possible, one should always choose the most biologically relevant model system such as patient primary cells. However, not all cells are amenable to HCS workflows (e.g., loosely adherent, suspension, or relatively compact cells with hard-to-distinguish organelles) and may pose challenges in adapting to an automated microplate workflow if the culture is heterogeneous or does not scale well to large quantities. There are technological workarounds to enable imaging-based screens of cells that fall into this category but issues of cost and scalability of processes such as capturing z-stacks with many focal planes must be considered when choosing the assay platform. The simplest cell models to adapt into HCS are the ones where cells are highly homogenous and flat with large cytosolic regions.

As iPSC-derived cellular systems are beginning to reach yields tractable for microplate screening, a promising opportunity exists for increasing physiological relevance. In utilizing the resulting cell types, including neurons, macrophages, hepatocytes, and myocytes, a major consideration is the ability to pre-differentiate the iPSCs prior to plating in the microplates. Besides avoiding difficulty of culturing cells for weeks in a microplate well, pre-differentiation is important for reducing variability and maintaining tight quality controls. Other practical concerns in looking at HCS more broadly include transfectability and transducibility in cases where nucleic acid based delivery is essential (siRNA, shRNA, CRISPR/Cas9, cDNA overexpression screening, etc.). Although these

considerations seem straightforward, prior to engineering assays it is well worth checking the compatibility of your model system with your planned experiment such as building stable cell lines expressing multiple fluorescent reporters.

1.1.2 Controls Define the Assay but Won't Always Predict the Behavior of Bioactive Agents in a Screen

Out of necessity, HCS assay robustness is defined by the use of positive and negative controls, which in turn define key metrics such as Z' score and control CVs. Distinct from traditional HTS assay endpoints (single-parameter readouts such as luciferase expression), HCS generates a multiplexed dataset which opens a window to the wide range of effects that compounds or genetic manipulations can have on the properties of individual cells. This is both the inherent strength of HCS and the factor which requires much additional care during analysis. Within pilot screening runs, for example with small bioactive compound libraries, phenotypes are likely to be observed which were not predicted by the initial choice of positive and negative controls. Scientists familiar with traditional HTS assay development may be less attuned to the need to go through additional rounds of assay refinement after these datasets are acquired. Throughout the process of HCS assay development, we recommend visual inspection of actives and an iterative process of tuning the image analysis pipeline, in order to create more robust measures of activity or capture more relevant/descriptive phenotypes.

1.1.3 Always Be on the Lookout for False Positives Related to Toxicity

Many high-content phenotypes can be influenced by cytotoxicity from exogenous stimuli such as compounds or siRNAs. For example, assays measuring the co-localization of labeled proteins, or proteins and organelles, are convoluted by the rounding of unhealthy cells. Moreover, dying or stressed cells can exhibit artificially enhanced fluorescence of reporter proteins due to the non-specific concentration of fluorescent material. In the Parkin assay example using HeLa cells, we often observed that siRNA treatments would cause cells to become long and thin, so inclusion of cell morphometric image analysis measures are useful to quantify the phenomenon. When piloting high-content assays, we recommend stress testing a variety of cell stimuli to understand how unexpected cellular responses affect the robustness of the chosen analysis methodology. Luckily, the vast toolbox of image processing routines available in modern HCS software combined with the flexibility of reporter tools (dyes, fluorescent proteins, label-free brightfield imaging techniques, etc.) offers many paths to harden assays against specious phenotypic modulation. As a starting point, many HCS assays include nuclear staining for cell counting as a straightforward method to identify wells with reduced cell number. This can also help weed out false positives arising from normalization to a very small number of unhealthy cells but additional image segmentation guideposts can be put in place to gain a greater understanding of cell health.

1.1.4 Imaging Hardware: Balancing Throughput, Signal, and Resolution

Microscopists familiar with traditional low-throughput work on powerful confocal systems may often desire to maintain the resolution and imaging aesthetics when moving their assays to a high-content system. While current-generation high-content imagers (HCIs) are equipped with impressive optical capabilities, maintaining the visually stunning high magnification confocal microscopy methods comes at the expense of throughput and signal strength, which are likely to be critically important for the tractability of HCS. In many cases, lower magnification images that capture more cells (without the need for greater sampling), and thus allow for greater statistical power in the subsequent analysis, are more appropriate than high-resolution images capturing fewer cells. The optical power used should be sufficient to analyze the cellular substructures in question, but go no further: rare is the HCS assay that requires a 100× objective; 10× is often sufficient. The image analysis algorithms available in HCS software are often able to quantify changes with much less magnification than the human eye.

Some imaging assays require live-cell acquisition, either to sense cellular properties destroyed in fixation (e.g. pH or redox potential) or to measures the kinetics of cellular signaling events. As the HCS field moves towards the use of more physiological systems, many of the assays employed may require multiday imaging to track events such as neurite outgrowth, cell health, protein decay, etc. For such assays it is important to remember to utilize hardware with a live-cell chamber (most next-generation high-content imagers come equipped, but older generations often do not), and a robotically-linked plate hotel with temperature and CO_2 capabilities. Although live-cell and time-course assays are attractive and unavoidable for some questions, they come at an large cost to throughput. Image acquisition can take considerable amounts of time, ranging from minutes to hours for a 384 well plate depending on number of wavelengths, magnification, and fields per well. Looking forward, the throughput for these types of experiments will scale somewhat as a function of increased acquisition speed with ever-improving HCS platforms.

1.1.5 Managing High-Content Data: Invest in a Lot of Storage!

While data storage is an issue for all HTS campaigns, most other HTS assay formats do not come close to the data-storage requirements of image-based screening. Even modestly sized high-content imaging campaigns can generate terabytes of data rapidly (the amount will vary depending on resolution, number of fluorescent channels, fields captured, camera binning settings, etc.), and for a team or institution running many such screens, the data deluge will occur even more rapidly. The need for sufficient primary storage capacity, backup, and comprehensive data lifecycle management cannot be overstated. Users should coordinate with IT staff

regarding storage needs and develop general guidelines for how long data is kept "live" before entering an archival phase. Archiving is never an easy decision but if cost becomes an issue, consider storing only wells deemed "active" along with representative controls. Users should also be encouraged to remove images from optimization trials or failed experiments. A guiding principle can be the calculated cost of generating the dataset again versus the cost of archiving it over 5–10 years. Another core aspect of the HCS data management is annotation of the experiments and tracking metadata in a centralized database. Indexing the large volumes of images and linking them to specific protocols, users, and eNotebook entries through a metadata database is essential in building a sustainable HCS platform and implementing a successful data lifecycle policy.

1.1.6 Analyzing High-Content Data: Making a Mole-Hill from a Mountain?

Traditional HTS campaigns generate large numerical datasets, but analyzing high-content data is much more complex due to the need to extract useful content from images. Analysis traditionally occurs at two different levels: the primary analysis phase typically refers to image segmentation, and the software for this often accompanies the purchase of the high-content imager. In this step, the scientist uses the different channels of data collected to define cellular and subcellular "segments," and then uses this segmentation to capture intensity, morphological, and textural features relevant to the biology of interest. Most of these approaches begin by identifying nuclei and then working outward to define cell shape, cytosol, and organelles/spots of interest. Within each of these regions, different image properties can be calculated, and these values can be recombined with standard mathematical operators to define a vast array of potential parameters. During this analysis, it is important to note that one can identify oddly shaped cells at the edge of the well, fluorescent dust, and cells that are dying—these objects can be counted and/or removed, depending on the information that the scientist wishes to extract from each well. This step of "cell-level" analysis is one of the main advantages that HCS provides over traditional assay endpoints and can greatly improve data usefulness.

The user can then choose to bring a small number (e.g. one, such as a nuclear translocation parameter) or all of the resulting metrics into their "secondary analysis". This step, which typically occurs in specialized HCS analysis software, enables the calculation of traditional HTS assay performance metrics such as Z' scores and CVs. It will also quantify phenotypes of interest and potentially identify unexpected patterns in the cellular responses. A true "high-content" assay will make use of many different metrics to identify a range of phenotypes that go beyond the simplicity of a single measure of activation/inhibition around the biology of interest, although the majority of "high-content" screens to date have been

simpler in terms of data complexity [23]. For a given endpoint there can be hundreds of measures applied to describe the target phenotype but with carefully crafted assays, the four to seven channels supported by high-content imagers allow users to construct rich collections of endpoints. An example of this is the use of DAPI staining to quantify cell survival (UV channel), GFP-fusion proteins to track an intracellular signaling event (FITC channel), an Alexa-594 labeled antibody to determine the internalization of a cell surface protein, and a deep-red cellmask dye to capture changes in cell morphology (Cy5 channel). The example illustrates how by tracking multiple targets, one may explore how a compound or siRNA influences both the upstream and downstream events involved in the pathway of interest. Inclusion of additional content can help differentiate between desirable modulation in a target pathway and nonspecific/toxic effects by an exogenous agent.

With so many potential streams of data from each and every cell sampled (Table 1), a major concern in HCS is that the complexity of the aggregate dataset can make it very challenging to derive meaningful conclusions in a reasonable timeframe. For this reason, many microscopy-based assays are reduced to one or two variables, in order to save time and produce a list of actives in a straightforward manner. This likely also contributes to the prevalence of simpler imaging assays, such as total intensity measurement of a single target, given that they are easier to interpret. Image analysis algorithms that to distill the observed phenotypic mosaics down to a single parameter (e.g. principal component analysis) are an attempt to overcome this challenge, but their implementation by the broader screening community is still just beginning.

1.2 The Anatomy of a HCS Assay: Segmentation Strategy in the Parkin Assay Example

A core aspect of HCS is the design of microscopy assays to facilitate robust characterization of cellular phenotypes. Unlike most conventional microscopy where the translation of each channel image (DAPI, FITC, Texas Red/TxRed, Cy5, etc.) into numerical results is a manual process, the sheer volume of images in HCS requires that analysis be completely automated. Therefore, much attention in HCS is given to including guideposts in the assay scheme for image segmentation—essentially the process of helping the computer locate the biology of interest. Examples of segmentation include using a dye to stain the nuclei, cytoplasm, or cell membrane, and expressing a fluorescent protein targeted to mitochondria, lysosomes, or another specific cellular component. Successful HCS assays provide sufficient context for analysis software to identify signal patterns that relate to biological processes in questions (Table 2).

For the Parkin assay example detailed below, there were three core questions being asked for each cell of every well imaged:

1. Has GFP-Parkin translocated to the mitochondria of each cell or is there inhibition of translocation?
2. How much of the mitochondrial mass is present in each cell?
3. How many cells were remaining in the well at the end of the assay (i.e. did the siRNAs cause cytotoxity or accelerated cell division)?

In this relatively simple example, the first guidepost for segmentation needed to answer these questions is stained cell nuclei (in the UV/blue fluorescence channel) so that the software could identify cells (Fig. 2). The second is the RFP targeted to mitochondria that occupied the Texas Red channel in order to identify the networks in each cells. Once these segmentation tools are included in the assay, the software can then use them to define the regions within each cell to make measurements such as Pearson's correlations (co-localization) and total intensity.

Pilot screens—A key aspect to any HTS, let alone HCS, screening campaign is to ensure that the assay is reproducible. We recommend pilot screens employing several plates' worth of reagents (e.g., compound or siRNA) to be tested in replicate under optimized screening conditions. Ideally, replicates would be screened on both the same (technical replicates) and different days (biological replicates). Although there is no standard benchmark, a good assay would exhibit a Pearson correlation of >0.8 for biological replicates (*see* ref. 24 *and the NIH Assay Guidance Manual http://www.ncbi.nlm.nih.gov/books/NBK53196 for examples*). Pilot screens are also invaluable for a better understanding of signal window, signal distribution, the influence of toxicity on phenotype, and more.

2 Materials

The materials needed for a general HCS assay widely vary depending on the biology being measured. However, like most cell-based assays, HCS assays will begin with the generation of a cell line, primary cells, or iPSC-derived/differentiated material appropriate for the biological question. This implies that standard tissue-culture and cell cultivation methods apply. Like the Parkin translocation assay, many HCS assays involve fixing the cells in the microplates at an assay endpoint since the biological event being measured is transient. Additionally, fixing the cells facilitates many forms of cell staining and immunofluorescence techniques needed to illuminate a particular process. From the hardware perspective, there are many options for the entire HCS workflow. When processing more than a

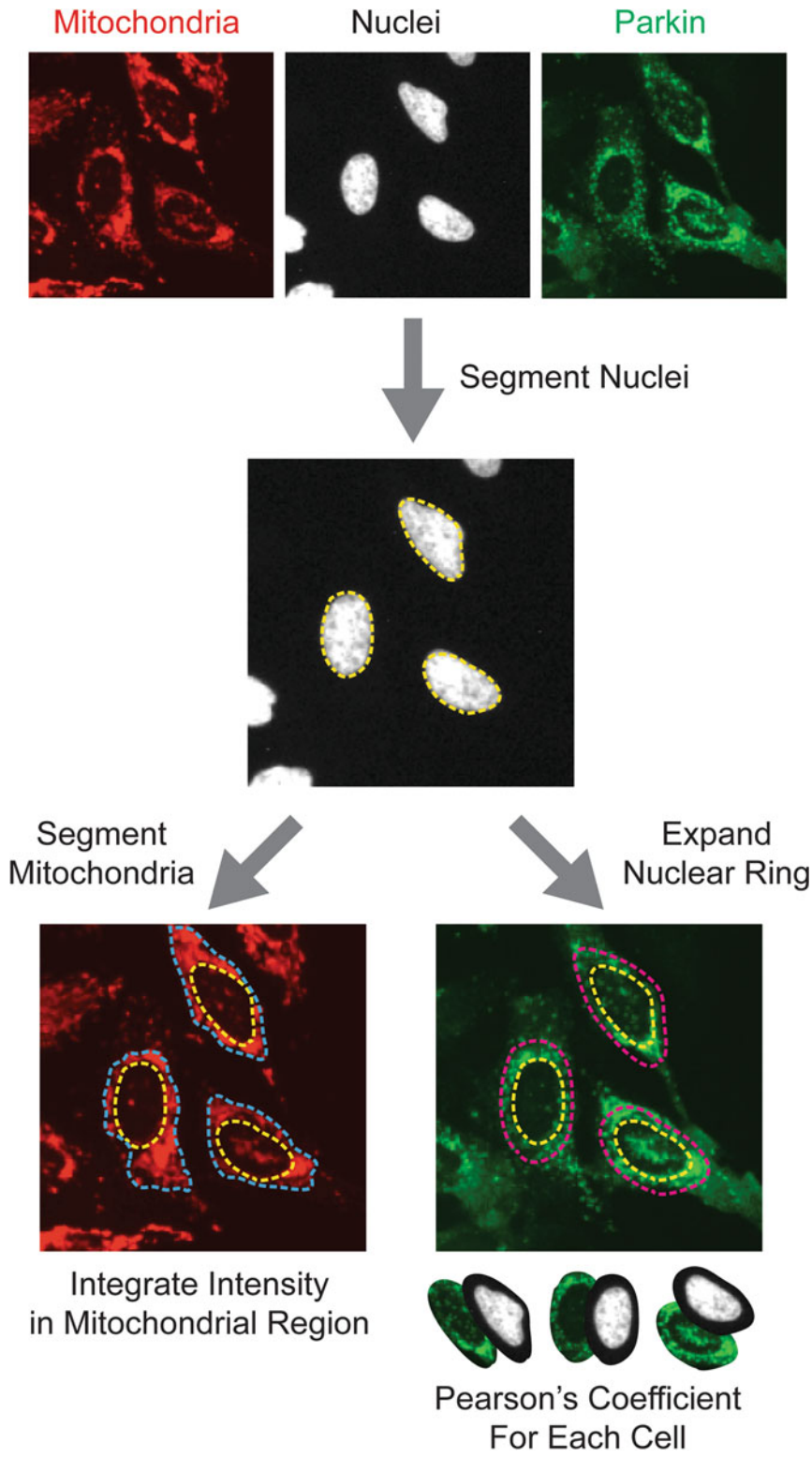

Fig. 2 The segmentation path used to quantify parameters in the Parkin assay. This diagram illustrates how the nuclear staining of the HeLa cells (DAPI channel, *greyscale*) is the foundation for the segmentation path for

few plates, integrated laboratory automation for plate and liquid handling is essential for consistent scheduling of time-sensitive steps. In terms of software, as with NextGen sequencing, HCS is a very data-intensive platform where each well of a screen can be hundreds of megabytes depending on the camera technology, wavelengths imaged, fields per well, and *z*-planes captured. Before embarking in HCS, it is strongly recommended to implement a data management hardware and software solution. Many HCS hardware vendors offer their own platforms typically integrated with analysis solutions. However, open-source alternatives do exist such as OMERO [25].

2.1 Cell Line Generation

1. All experiments should begin with a suitable adherent cell line for imaging such as HeLa that is mycoplasma-free and has been identity verified. Beginning the cell line generation with a low passage cell stock is recommended (*see* **Note 1**).
2. Appropriate culture media for the cultivation of the cell line. In this example, HeLa cells are cultivated in DMEM medium, ideally containing no phenol red, with 10 % certified FBS, 10 mM HEPES, 1× Non-Essential Amino Acids Solution, 1 mM Sodium pyruvate, and 2 mM L-Glutamine (or stabilized substitute such as GlutaMAX). The same batch/lot of FBS should be used for an entire screening campaign where possible.
3. Retroviral or lentiviral expression plasmid in addition to VSV-G, GAG, and POL accessory plasmids for packaging (*see* **Note 2**).
4. HEK293T cells as a host for retroviral or lentiviral packaging.
5. Human Parkin cDNA (PARK2, GeneID: 5071, see AddGene ID 59419, 59416, or 47560 for suitable templates).
6. cDNA for a monomeric green fluorescent protein such as AcGFP1.

Fig. 2 (continued) mitochondrial (mito-dsRed) content quantification (Texas red channel, *red*) and GFP-Parkin translocation (FITC channel, *green*). The segmentation masks from the individual cell nuclei (*dashed yellow lines*) are copied into the Texas red channel and signal thresholding algorithms segment an adjacent mass containing the mitochondrial network (collapsed around nucleus due to mitochondrial depolarization). Once the mitochondria mass in each cells have been segmented (area between *blue dashed line* and *yellow dashed lines*) pixel integration of the signal allows for a quantitative measurement of mitochondrial content. For GFP-Parkin translocation assessment, the DAPI channel nuclear masks are extended to include a small amount of adjacent cytosol and copied into the FITC channel. Subsequently a Pearson's correlation coefficient is executed on each cell between the DAPI channel and FITC channel within the expanded segmentation region

7. cDNA for a red fluorescent protein (RFP) such as dsRedExpress, dsRed2, or newer generation red fluorescent proteins (*see* **Note 3**).
8. If the selected red fluorescence protein template does not already contain a mitochondrial targeting sequence then a DNA template encoding a canonical mitochondrial leader sequence will be required. The first 29 amino acids of human cytochrome c oxidase subunit 8A is an example with a seven amino acid linker peptide (MSVLTPLLLRGLTGSARRLPVPRAKIHSLGDPPVAT) that was used in our dsRed2 fusion but many other strong targeting sequences such as the N-terminus of citrate synthase will also work.
9. Fluorescence-activated cell sorting (FACS) system capable of sorting cells at two simultaneous wavelengths that align with the appropriate green and red fluorescent proteins.

2.2 384-Well HCS Assay

1. Barcoded 384-well microplates designed for high-content imaging using plastic with low autofluorescence. In the case of the Parkin assay, HeLa cells grow well on a standard tissue-culture treated surface.
2. Library of siRNA reagents pre-spotted into the assay plates in a volume of 2 μL per well. The siRNA reagent stocks were dispensed into the dry wells at 400 nM in the Parkin translocation screens resulting in a 20 nM final concentration in the assay. Ideally, one would use siRNAs with off-target minimizing passenger-strand inactivation. Library plates can be spotted in plates in advance of siRNA screening sessions and frozen at −20 °C. Be sure to seal plates with nucleic-acid certified foil or heat-seals before freezing (*see* **Note 4**).
3. A suitable transfection reagent for the selected cell line (*see* **Note 5**).
4. Negative-control siRNA reagent that pairs with the reagent chemistry used for the larger siRNA screen. These non-targeting control (NTC) siRNAs are designed with sequences that are not complementary to any coding sequence in the genome of your cell line. However, given that many off-target gene expression perturbations can occur from the siRNA seed sequence alone, several reagents should be attempted to determine the one or two that do not interfere with the phenotypes being measured. Match the concentration of the negative control siRNAs with the chosen concentration of the library siRNAs and store in a similar manner.
5. Positive control siRNA in the form of a cell-death inducing reagent. Knockdown of genes involved in the cell-cycle such as WEE1 or PLK1 will induce a cytotoxic phenotype in

many cell lines. Match the concentration of the positive control siRNAs with the chosen concentration of the library siRNAs in a similar manner.

6. A second positive control siRNA which modifies the biology of interest. For the Parkin assay, we utilized a PINK1 siRNA to abrogate Parkin translocation and mitophagy. As with other controls, match the concentration of the positive control siRNAs with the chosen concentration of the library siRNAs in a similar manner.
7. Carbonyl cyanide 3-chlorophenylhydrazone (CCCP) dissolved in DMSO or Ethanol at 10 mM. Store aliquots at −20 °C.
8. An appropriate culture medium for the screening cell line, ideally containing no phenol red. In the Parkin assay, we use DMEM medium, with 10 % certified FBS, 10 mM HEPES, 1× on-Essential Amino Acids Solution, 1 mM Sodium pyruvate, and 2 mM L-Glutamine (or a stabilized substitute such as GlutaMAX) (*see* **Note 6**).
9. An appropriate serum-free transfection medium for the screening cell line containing no phenol red. In the Parkin assay, we use DMEM medium, no phenol red, 10 mM HEPES, 1× on-Essential Amino Acids Solution, 1 mM Sodium pyruvate, and 2 mM L-Glutamine (or stabilized substitute such as GlutaMAX) (*see* **Note 7**).
10. Microscopy grade Paraformaldehyde aqueous solution, typically 16–32 % (4 % working concentration), stored at room temperature.
11. Hoechst 33342 solution (20 mM), stored at 4 °C.
12. Phosphate buffer saline solution (1× PBS) pH 7.4 without Calcium or Magnesium (0.22 μm filtered), stored at room temperature.

2.3 Screening Hardware and Imaging

1. An integrated platform including plate and liquid handling with scheduling is recommended for medium to large-scale HCS. Assay development and small-scale screening (<10 plates) can be processed in a batch configuration but we find that scheduled automation allows for consistent timing of each step needed to achieve reproducible results. Given that most HCS campaigns utilize a fixed-cell endpoint for practicality, including the Parkin siRNA screening described here, the following modules should be present in the system: (a) plate washer, (b) bulk liquid dispensers such as peristaltic, syringe pump, and/or flying reagent dispensers, (c) on-line incubators, (d) a plate sealer and seal peeler, (e) a tip-based or acoustic liquid dispenser capable of quickly performing whole-plate and column/row-wise liquid transfers rapidly, (f) plate lidding and de-lidding stations (g), labware holders, (h) room-temperature

plate incubation stations, (i) HCS imager (*see* **item 2** below) (j) plate transport hardware such as robotic arms that connect the system modules together (*see* **Note 8**).

2. High-content screening-capable imager equipped with an LED or laser light source, at least four standard imaging excitation/emission channels (e.g. DAPI, FITC, TxRED, and Cy5) with minimally a 4× objective. The Parkin assay can be effectively quantified with 4× or 10× objectives but to support the multitude of biological questions asked in HCS, it is recommended that the HCS system be equipped with 4×–40× objectives. Additionally, the HCS imager should be equipped with a laser-autofocus system and calibrated for the chosen plate type. Importantly, to maximize the versatility of the analysis tools, the imager should support image output in 16-bit TIFF formats (or at least conversion into 16-bit TIFF formats) (*see* **Note 9**).

2.4 Image Processing and Data Analysis

1. Image-analysis software capable of supporting the plate-based imaging datasets generated instrument by the chosen imager. Specific to the Parkin assay, the software must facilitate the Pearson's correlation coefficient [26, 27] measurements in addition to intensity measurement for each segmented cell. The Parkin assay originally utilized Molecular Devices MetaXpress, though open-source tools such as CellProfiler [28] are capable of performing the analysis as well.
2. PC workstation (64-bit) or server capable of running the analysis software. The optimal specifications of this computer will depend on the scale of the HCS. In general, a major consideration that guides the optimal number of processor cores in the workstation or server is the number of concurrent threads supported by the analysis software. Additionally, HCS generates a large quantity of high-resolution images with a large bit-depth. Depending on the scale of HCS screening, redundant arrays of hard drives totaling 10–100+ TB of usable storage are recommended. In many cases, analysis software caches image sets into RAM to enhance processing speed so it is optimal to operate with at least 128 GB installed.

3 Methods

3.1 Cell Line Generation

1. Using PCR cloning methods, assemble the following construct in a standard cloning backbone such as pBluescript or pcDNA that is flanked on the 3′ and 5′ ends with restriction enzyme cut sites compatible with the multiple cloning site in the desired retroviral or Lentiviral transfer vector (*see* **Note 10**):

Option 1: 5′-GreenFluorophore-human Parkin cDNA-2A-mito-RedFluorophore-3′

Option 2: 5′-GreenFluorophore-human Parkin cDNA-IRES-mito-RedFluorophore-3′

2. Once the constructs have been sequence verified, subclone into the retroviral or lentiviral transfer vector of choice. Prepare a "maxi" scale of high purity DNA.
3. Using HEK293T cells, prepare retrovirus or lentivirus at a sufficient scale for transducing the chosen cell line using a packaging system (VSV-G, Gag, Pol, Rev). HeLa cells transduce relatively easily so viral supernatants from a 6-well plate are typically sufficient assuming a typical viral titer. Protocols and packaging systems are available from multiple manufactures or from Addgene.
4. With either viral supernatants or concentrated viral particles, determine the titer using established methods [29] and then transduce the target cell line at various multiplicity of infection levels (MOI, e.g. 0.1, 0.5, 1, 5 transducing units per cell).
5. In 3–7 days after transduction of the target cell line, analyze the fluorescence of both the Parkin and the mitochondrial marker directly in the tissue-culture vessel on a standard fluorescence microscope to determine an MOI level that has produced an abundance (>10 % of the population) of cells expressing a level suitable for low-exposure detection by microscopy. The signal from the cells will typically be quite heterogeneous in the unsorted cells.
6. Recover the cells from optimal microscopy MOI culture and FACS sort for cells displaying coincident GFP and RFP (or other appropriate channels based off of chosen fluorescent proteins) signals two to three relative fluorescent intensity (RFI) log-units above the untransduced cell background (*see* **Note 11**).
7. Examine the cultured cells again by fluorescence microscopy to gauge the brightness of the fluorescent protein expression. Repeat the FACS sorting, but this time set the gating to select a narrow range of RFI (0.1–0.3 log-unit gate widths around the target intensity) in both channels. The selected population of cells should now display minimal heterogeneity in fluorescent protein signal (*see* **Note 12**).
8. Expand the sorted cells, periodically examining with fluorescence microscopy to check signal variability, until it is possible to freeze enough aliquots to supply the entire screening campaign (*see* **Note 13**).

3.2 384-Well Plate HCS Assay

For screening in 384-well plates, assay optimization is the first order of business. In the case of siRNA screening, delivery of the siRNA into the cells is performed by reverse transfection when cells are added to the microplates. The workflow: thaw optical-grade plates with the frozen pre-arrayed siRNA reagents, add serum- free medium containing transfection reagent to generate complexes, and then dispense cells in culture medium to initiate the transfection in each well. Determining the optimal transfection reagent and the ratio of transfection reagent to siRNA is a critical step. The goal is to maximize the number of siRNA transfected cells (determined with cell-death inducing siRNA control reagent) while minimizing the amount of cytotoxicity generated by the transfection process (tracked by cell health and cell count in the untreated cells versus the NTC-transfected cells). When an ideal transfection reagent is titrated in the 384-well plate reverse transfections, there will be a dose displaying maximal transfection efficiency that is lower than the cytotoxic doses. In parallel, the imaging of the wells with the chosen high-content imager should begin to determine how well the assay performs in the microplate format.

1. Allow barcoded assay plates pre-arrayed with siRNA library reagents in columns 3–22 to thaw at room temperature and wipe away condensate. Clean plates with 70 % ethanol and remove plate seals in a tissue-culture hood. Cover plates with a plastic lid suitable for use with automation. At this point, plates can be processed in the tissue hood with off-line liquid handling or be loaded into an integrated automation system. The following steps described are applicable to either process.
2. If control siRNA reagents have not been added during the pre-arraying process, dispense 2 μL of 400 nM stocks into each well of the control columns (1, 2, 23, 24). For the Parkin translocation siRNA screens, we use 16 wells of NTC and 16 wells of PINK1 siRNA, and 16 wells of untreated cells. Optionally, the cell-death siRNA can be added to the remaining control wells as an indicator of transfection efficiency for each plate.
3. Add transfection reagent into serum-free transfection medium to create a large enough batch to fill all the plates in a given screening session. Each well of the 384-well plates receives 20 μL of this mix initiate siRNA-lipid complex formation. For the Parkin translocation siRNA screen, a lipid-based RNAiMax (Life Technologies) reagent was mixed at a 1:250 dilution into our serum-free DMEM-based transfection medium. Mix the complete transfection medium well by inversion or swirling the container gently (*see* **Note 14**).
4. Dispense 20 μL of the complete transfection mix into each well of the assay plates maintaining the load order of the plate series. Dispensing of the complete transfection mix can be executed

quickly and accurately using automated bulk reagent systems such as those based off of peristaltic pumps (commonly referred to as a multi-drop) or syringe pumps. Incubate plates at room temperature.

5. Once each plate has undergone an siRNA complexing incubation period optimal for the chosen transfection reagent (30 min for the Parkin translocation siRNA screen), deliver 20 μL of cell suspension (37,500 cells/mL) into each well using bulk dispensing instruments suitable for cell-based assays (we recommend automated peristaltic or syringe pump-based systems). The plate order for cell dispensing should follow the order that the plates received the transfection mix (*see* **Note 15**).
6. Incubate each plate for 30–60 min at room temperature to allow cells to begin attaching to the plate surface before transferring to the plate tissue-culture incubator (high humidity). The room temperature pre-incubation may help prevent edge-well effects by allowing cells to settle evenly (*see* **Note 16**).
7. After 48–72 h post siRNA transfection, plates can be inspected to check that the >90 % (for HeLa cells, the amount of cell death may be more or less in other cell lines due to varying maximal transfection efficiencies) of the cells have died in the cell death control wells. After spot-checking plates as a transfection quality control measure, the final stage of the assay begins.
8. Following the original plate load order, dispense 40 μL of 20 μM CCCP in culture medium to all the wells of each 384-well plate using a bulk liquid dispenser. The final concentration of the CCCP in the wells is 10 μM and causes rapid depolarization of HeLa cell mitochondrial membrane potential. Consistent timing and incubation for each plate is extremely important from this point forward (*see* **Note 17**).
9. After each plate has reached the linear range of GFP-Parkin translocation to mitochondria, the assay is terminated by the removal of 70 μL of liquid from the individual wells (plate washer) and replacement with 45 μL of 4 % PFA in PBS (bulk reagent dispenser). For our GFP-Parkin-IRES-mito-DsRed2 expressing HeLa cell line, the optimal incubation time was determined to be 2.5 h in order to capture gene knockdowns that could either accelerate or inhibit Parkin translocation to mitochondria in each cell. The time course and kinetics of Parkin translocation to depolarized mitochondria should be validated due to variations in cell line phenotypes (*see* **Note 18**).
10. Following the addition of chemical fixative, each plate is incubated for 10–15 min at room temperature. At the conclusion of the incubation, the plate washer is again used to aspirate 70 μL

of liquid in each well followed by two rounds of PBS washes (80 μL/well of PBS per wash).

11. Cell nuclei staining is then executed on each plate by first performing the same 70 μL plate-washer based aspiration on all wells. Next, a 40 μL/well dispense of 1× PBS containing Hoescht 33342 (5 μg/mL final concentration) is dispensed.
12. Following a 10 min incubation at room temperature, each assay plate is washed as in **step 10** with 1× PBS.
13. At the conclusion of the plate processing, each plate is sealed and stored at room temperature while in queue for imaging (<24 h) or 4 °C for longer term storage (>24 h before imaging) (*see* **Note 19**).

3.3 Screening Hardware and Imaging

1. For plate imaging, each channel (DAPI, FITC, TxRed filter sets) should be captured in the linear range of the camera with laser autofocus anchoring on the nuclei (DAPI) to find the focus. Due to variations in fluorescent protein signal, for each screening session, control wells in representative plates are used to adjust exposure times to achieve a consistent signal distribution across the entire screen. A few screening plates should also be spot-checked at various well sites to ensure good focus and exposure settings. At 10×, many large-CCD/CMOS chips can capture most cells in a given well (384-well plate). The Parkin assay can also be accurately analyzed at 4× as well (*representative images shown in* Fig. 3a). For more intricate biology captured in HCS assays, high magnification imaging (20×–60×) typically requires the acquisition of multiple fields to capture a statistically significant sample size. Prior to large-scale imaging, plate calibration and autofocus accuracy should be checked and adjusted accordingly. Often, laser autofocus-driven HCS instruments will allow for the specification of an autofocus offset for each channel that is not anchored to the autofocus process. These offsets can be adjusted so that the relevant biology (mitochondria, cytosol, etc.) is brought into focus after the laser finds the growth surface of the plate. For HeLa cells, a hybrid hardware-software autofocus system is not needed but these systems can be useful for biological features that have inconsistent positions in the *z*-axis (*see* **Note 20**).
2. Images captured from the wells of each barcoded plate should follow a logical naming scheme and be tracked through metadata stored in a central database. Plate barcodes are used to track plate processing throughout the screening and analysis process in addition to connecting image sets to particular siRNA library reagents (or compounds, biologics, etc.). As a best practice, images from each plate should be stored in a network location that is frequently backed-up.

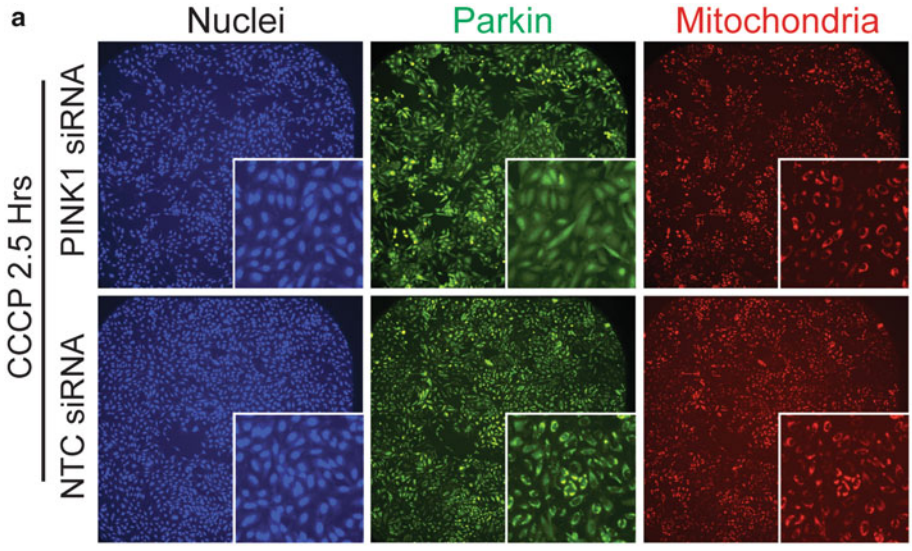

b

	1	2	3	4	5	6	7	8	9	10	11	12	13	14	15	16	17	18	19	20	21	22	23	24
A	1263	1210	918	1217	939	1210	989	1059	963	1621	1188	990	1121	833	1278	961	1096	2039	1048	1073	993	963	951	1279
B	1262	1157	1097	1215	999	1075	1655	1055	1073	758	1233	1018	956	1167	1426	1235	1147	1163	932	1090	1151	1410	995	1217
C	1197	1194	1385	1310	1326	1192	1204	1133	1228	1196	825	880	1090	974	1242	1277	1402	1210	1003	1035	1055	1038	998	1141
D	1336	1264	1216	1220	1153	1020	1082	1080	1052	1016	1067	1242	1121	1048	794	1297	1251	1173	1376	1258	1070	1220	1145	1460
E	1407	1172	1184	1090	1341	1061	1279	1220	919	1215	1026	1040	1166	1163	867	1254	1135	1073	1099	1178	942	954	975	1281
F	1278	1079	1010	1281	980	1161	1244	1032	962	1065	1164	1160	1014	1027	961	1263	1086	1364	1133	1242	1204	1079	910	1272
G	1349	1218	850	1292	1023	1086	1089	1182	1260	1164	1126	930	1147	1179	1247	995	1328	960	1247	1004	1328	1092	1030	1172
H	1318	1131	1006	1106	829	876	1300	890	906	1171	1165	809	833	1193	1033	785	1264	1100	1088	954	1138	918	947	1207
I	1557	1172	1331	1323	1170	1143	1218	1115	997	1037	1192	1056	1000	807	1072	1374	1083	1008	996	766	1105	993	943	1193
J	1208	1186	1173	1111	978	880	1364	1105	1165	932	834	1154	910	1100	1111	1227	968	871	1061	1003	1331	1185	890	1134
K	1218	1166	1172	1214	1122	1109	923	949	942	836	1043	1058	934	1074	920	1159	1145	1186	866	1191	1092	1088	957	1231
L	1221	1250	1151	1042	1015	955	1205	1236	914	1045	1032	1092	1209	910	958	1177	1046	1118	1152	1449	1083	1285	1092	1321
M	1341	1133	1050	1155	1047	837	1121	295	1089	1149	1148	1032	953	1098	1112	1208	942	943	987	1077	1155	1004	1073	1294
N	1339	1196	1188	1118	964	935	1255	1007	1311	966	1110	1120	941	1092	1090	1011	1056	1150	1121	1149	1240	1268	1065	1322
O	1386	1195	1134	886	996	1046	1333	1306	1007	1174	920	983	909	1222	1134	967	808	921	1022	1057	1208	1214	1130	1280
P	1218	1075	1118	1196	1246	1098	1113	1129	870	1198	932	990	1202	913	942	918	1336	927	1078	1019	1114	1112	1024	1166

CELL COUNT

	1	2	3	4	5	6	7	8	9	10	11	12	13	14	15	16	17	18	19	20	21	22	23	24
A	195	275	372	209	228	268	167	162	181	198	173	251	161	139	203	133	268	218	197	241	167	197	333	236
B	214	287	271	156	146	244	206	228	215	160	249	235	241	178	204	256	312	380	241	266	182	183	326	178
C	256	253	163	263	261	150	196	234	247	184	233	146	198	186	153	138	206	187	160	130	89.7	163	333	188
D	258	277	225	297	111	179	190	160	180	206	164	215	301	191	140	194	230	240	178	168	165	197	335	247
E	260	226	148	148	173	116	260	152	122	198	184	164	177	298	154	261	187	206	194	141	228	145	327	229
F	234	293	126	212	240	163	249	179	160	146	208	171	215	185	142	218	183	187	188	282	218	197	261	209
G	243	246	231	150	168	199	194	217	202	206	141	106	181	190	228	222	174	192	227	263	157	197	307	165
H	231	227	135	180	396	163	178	154	114	150	198	234	156	176	160	170	203	176	192	232	148	194	267	172
I	230	254	207	175	167	175	183	232	147	215	167	154	162	149	229	165	240	126	114	102	157	263	281	174
J	167	215	361	195	187	170	183	201	274	333	112	171	140	126	217	223	152	151	157	128	170	237	281	202
K	212	263	228	216	227	189	108	249	195	202	142	184	295	257	157	201	141	181	130	149	119	191	283	213
L	194	273	280	156	165	136	171	127	176	140	175	155	170	178	133	124	166	320	218	168	215	230	318	212
M	243	235	192	346	138	227	126	72	176	126	164	152	151	116	166	147	138	147	162	192	262	193	280	237
N	250	276	168	212	182	116	171	176	202	202	109	229	145	181	279	157	182	159	142	191	193	152	306	207
O	256	261	164	237	136	191	176	192	145	196	188	149	163	185	230	167	137	140	253	139	235	190	330	197
P	245	212	150	189	210	129	179	223	211	237	144	192	165	168	116	146	234	154	142	187	192	171	297	202

MITOCHONDRIAL MASS

	1	2	3	4	5	6	7	8	9	10	11	12	13	14	15	16	17	18	19	20	21	22	23	24
A	90	84	64	81	72	87	84	79	59	78	87	82	73	44	61	73	66	84	71	66	59	68	8	88
B	87	76	71	88	84	51	86	80	83	49	71	75	68	81	85	83	51	68	46	77	80	76	3	79
C	77	81	72	82	80	90	82	78	68	74	48	72	85	84	68	92	73	84	54	50	80	94	3	78
D	88	83	87	71	74	62	75	68	80	84	81	68	65	50	78	82	61	83	78	85	80	87	4	89
E	89	83	64	80	81	80	80	77	41	76	75	56	82	71	80	89	68	42	78	64	79	75	3	89
F	88	81	77	76	39	87	68	68	61	82	73	86	78	79	77	86	85	66	86	65	59	73	3	88
G	88	79	61	74	73	69	72	83	82	78	72	86	75	58	82	80	80	76	83	80	78	85	3	82
H	82	75	82	72	75	62	63	76	63	76	50	14	41	53	73	78	64	79	54	50	74	77	4	85
I	91	78	70	73	76	77	71	72	71	73	75	81	80	67	55	71	65	62	72	58	64	73	4	86
J	86	78	73	69	72	22	81	78	72	44	75	72	68	58	70	71	60	80	56	40	56	55	4	85
K	88	80	78	84	75	70	33	71	68	69	81	80	64	55	73	87	75	71	79	73	85	64	2	89
L	87	72	71	76	79	59	81	70	84	69	77	78	77	63	80	86	59	74	89	80	77	62	5	82
M	88	78	81	88	81	60	90	31	75	68	43	70	55	42	69	81	81	57	61	62	58	59	4	85
N	88	77	85	81	78	73	82	80	88	80	73	90	72	90	51	56	74	88	58	73	85	79	4	90
O	90	80	76	79	68	79	83	81	70	76	60	82	41	64	81	88	50	78	69	54	79	73	3	89
P	87	81	84	68	75	74	46	88	72	66	81	62	80	60	71	69	81	77	73	72	75	82	4	82

% CELLS WITH PARKIN TRANSLOCATION

Fig. 3 Expected data from the Parkin assay used in high-content siRNA screening. (**a**) Representative fields from control wells of a kinome siRNA screen imaged at 4×. Channels from the DAPI (Nuclei), FITC

3.4 Image Processing and Data Analysis

1. The image processing pipeline for the Parkin assay uses two segmentation processes to allow for the computation of all assay parameters. The first segmentation step for each cell is to delineate cell nuclei, and the second is identify the mitochondrial network that presents itself as a cohesive mass surrounding the nucleus at low magnifications (4×–10×). If imaging at higher magnifications (>10×), the second segmentation step should be of cytoplasmic volume (where the mitochondria reside) and can be accomplished approximately by extending a collar region from the shape of each segmented nuclei. For more exact segmentation of cytoplasmic regions, dyes staining the cytosol or cell membrane may be employed. Ultimately, the cytoplasmic segmentation is meant to define the compartment of each cell where the mitochondrial signal intensity should be measured.
2. To build a segmentation and analysis pipeline, begin by opening representative images from the NTC (high degree of translocation) and PINK1 siRNA (low degree of translocation) control wells in the chosen analysis software. Next, construct a segmentation scheme for the cell nuclei. Ideally, choose a DAPI-channel intensity over local background that generates segmented regions that closely follow the contours of each cell nuclei and that can delimit closely positioned nuclei as two separate entities. If nuclei separation proves challenging, it may be a sign that the cells are too confluent in the wells and the seeding density of cells at the start of the assay should be reduced. Once an effective nuclei segmentation scheme is found, the cell count in each well can be calculated (*see* Fig. 3b top panel *for example plate data from a kinome siRNA screen*) (*see* **Note 21**).
3. Quantification of the translocation of GFP-Parkin takes advantage of the apparent exit of the GFP signal from the nuclear region in non-confocal images after mitochondrial depolarization. This method is a surrogate readout for GFP-Parkin signal concentration onto the mitochondrial puncta as the translocation time course proceeds to completion. We found that measurement of GFP-Parkin signal in the region overlapping with

Fig. 3 (continued) (GFP-Parkin), and Texas Red/TxRed (Mitochondria) filters are shown after cells were fixed following a 2.5 h CCCP treatment. *Inset* regions for each field are digitally magnified 300 % to better demonstrate cellular phenotypes. (**b**) Numerical data extracts from the kinome screen plate with heatmaps. The *top heatmap* is the total number of segmented nuclei per well after image analysis and the *middle heatmap* is the mean mito-RFP signal per cell measured in each well. The *bottom heatmap* is the percentage of cells classified as translocation positive in each well. NTC siRNAs (negative controls) were present in all wells of column 2 and PINK1 siRNAs (positive control for Parkin translocation inhibition). Columns 1 and 24 of the plate were untreated. Columns 3–22 contained siRNAs to various kinases in the human genome

the nuclear stain is more resilient to changes in cell and mitochondrial morphology from siRNA or compound treatments. Essentially, the GFP-Parkin data layer from the screen reveals what fraction of the total cells in the imaged well failed to translocate the protein out of the region overlapping with the nuclei. In many HCS analysis software packages, a built-in nuclear translocation module will expedite the workflow development. A process to perform the quantification is to map the nuclear segmentation onto the FITC channel where the GFP-Parkin signal is captured for each cell (Region N). Next, Region N + C is defined by extending Region N by growing the nuclear segmentation shape by a pixel equivalent of 1/3rd the width of the nucleus of the particular cell where the measurement is being made. Region N + C also includes a 3 pixel gap extending from the edge of the nuclear segmentation mask to prevent overlapping signal measurements. The Pearson's correlation coefficient of DAPI signal and FITC signal in Region N + C in each cell is calculated to assess how far the emptying of the nuclear region has progressed [26, 27]. In the GFP-Parkin HeLa cell system, we use a correlation coefficient of 0.4 or less to score a cell as translocation positive (cell has majority of GFP-Parkin signal outside of the nuclear region). Likewise, a cell with a correlation coefficient greater than 0.4 is considered translocation negative (cell has a low difference between GFP-Parkin inside and outside of the nuclear region). At the well level, the aggregate percentage of cells scored as translocation positive is the score used to compare the Parkin translocation modulation by each siRNA reagent (*see* Fig. 3b bottom panel *for example plate data from a kinome siRNA screen*). Gene knockdowns that accelerate the process of GFP-Parkin translocation will have a greater "% translocation positive" score than the NTC controls. Gene knockdowns that inhibit the process of GFP-Parkin translocation will have a lesser "% translocation positive" score than the NTC controls (*see* **Note 22**).

4. The third measure in the analysis pipeline is to calculate the mitochondrial mass for each cell in a given well. This process again uses the segmentation defined by the DAPI channel image as a starting point. Given the mitochondria cluster around the nucleus upon CCCP treatment, cell shape or cytosolic volume algorithms built into most HCS analysis programs can be used for simple segmenting of the mitochondrial mass. Simple thresholding of the mito-RFP signal surrounding the nuclear segmentation is how we compute the region encompassing the mitochondrial network in each cell. Once an approximate region is determined, the integrated pixel intensity of Texas Red filter channel (mitochondria) signal in that region is recorded for each cell. To obtain a well score, the

mean integrated mito-RFP signal for all cells in the captured field(s) is calculated (*see* Fig. 3b middle panel *for example plate data from a kinome siRNA screen*). In a similar manner to the Parkin translocation score, the mitochondrial signal score can be used to determine if gene knockdowns are inducing a change in mitochondrial mass. Since higher or lower quantities of mitochondria may interfere with the quantification of Parkin translocation, this measure is useful to identify potentially artifactual results.

5. The next stage of the data analysis is in a plate-wise manner, to normalize the computed parameters to the negative control mean values on the plate. Therefore, the raw values for nuclei count, % translocation positive cells, and mitochondrial intensity in each well (mean of the cell population) are expressed as a fraction or percent of the NTC siRNA well median. This allows data from different plates to be aggregated into a master siRNA activity list and compared easily. The data can then be converted to more statistically interpretable metrics. For example, a useful plate normalization strategy for large-scale library screening (siRNA, small molecule, etc.) is the median absolute deviation (MAD) method [30]. MAD scoring links the normalized activity magnitude of a given well to the variation of all wells (excluding controls) in a plate.
6. For the determination of a final list of active siRNA reagents that cause modulation of the translocation phenotype, normalized cell counts and mitochondrial signal measurements are used to apply filters to remove those exhibiting cytotoxicity and/or mitochondrial depletion phenotypes.
7. Once a final active siRNA list is generated, the individual images for each of the actives should be inspected to assure that the algorithm has called an accelerator or inhibitor of Parkin translocation based on genuine phenotypes. There are some cases, particularly where cell morphology is drastically altered by siRNA-driven activity, that the processing algorithm may incorrectly score a change in the Parkin translocation.
8. After removing specious actives from the list of siRNAs modulating Parkin translocation, the siRNA multiplicity (screening of multiple unique reagents for each gene) in the screen is used to determine the confidence in each gene. The more active reagents (e.g. two out of three, or four out of five) for a given putative genetic regulator of Parkin translocation, the greater the chances that this gene is truly involved in the biology. For example, top "hit" candidates can be selected by looking for those that pass a predefined statistical threshold (e.g., $\pm$3MAD). For siRNA, or analogous screens using multiple reagents per gene, the activity of unique reagents targeting a

gene should be considered. At the most basic level, one could require a certain fraction of reagents to cross a specified MAD threshold for a gene to be considered a hit. A more elegant analysis would be to consider the activity of all reagents targeting a gene as compared to the entire screen population (e.g., redundant siRNA analysis, *see* ref. 31) (*see* **Note 23**).

4 Notes

1. The ideal cell line for HCS is one that has a flat morphology with a large cytosol. Many types of immortalized, iPSC/ES cell derived, or primary cells can be used in automated microscopy, however minimization of heterogeneity will increase confidence in morphometric measurements. Additionally, tightly adherent cells to tissue-culture plastic or coated microplate surfaces ensure that cultures growing in each well remain intact through liquid handling steps (e.g., washing, staining, and fixing). For non-adherent cells or spheroid colonies, imaging can be done with a semi-solid growth matrix or hanging drop arrays in microplate wells and 3D imaging with z-stacks. In the Parkin example, the cell line was also selected for the ability to be transfected easily with siRNA reagents.
2. As an alternative to viral-based cell line engineering, the emerging field of genome-editing offers powerful tools to increase the physiological relevance of a cell system used for an HCS assay. Using off-the-shelf reagents, transgenes can be inserted at precise genomic loci such as AAVS1 and ROSA safe-harbor regions to gain a greater control over the context of their integration. Genome editing also allows for one to knock-in epitope tags or fluorescent reporters in endogenous genes (or behind endogenous promoters) to avoid overexpression artifacts. Additionally, gene knock-out tools may be particularly useful for potentiating a pathway or creating a "clean system" to study the ability of an exogenous agent (siRNA, compound, etc.) to rescue a phenotype. Our experience has been that for HCS assays, fluorescent proteins inserted into the genome as single-copy knock-ins must be chosen carefully. Often such fluorescent protein knock-ins are not expressed at a sufficient level to produce tractable signal-to-background ratios for HCS microscopy. We recommend epitope tag knock-ins when tracking endogenously expressed proteins because of the potential for signal amplification in immunofluorescence based HCS assays.
3. As an alternative method to segment mitochondria, immunofluorescence can be performed with antibodies against mitochondrial proteins such as TOMM20 (outer membrane) or Pyruvate Dehydrogenase (matrix).

4. One of the most important principles in siRNA screening is reagent multiplicity. We recommend using at least three unique siRNA reagents for each gene in the library, whether it is a targeted subset or whole genome format. Each of the reagents should be arrayed into its own individual well. As off-target effects dominate siRNA-induced phenotypes [32], the ideal screen would include five to seven unique reagents per gene. Pooled siRNA reagents (optimally with non-overlapping sequences) can be treated as a single unique reagent and arrayed into an additional well. For screening, siRNAs are typically used at a final concentration of 10–50 nM, and for the original HeLa-based screens, we found that 20 nM was optimal. Overall, off-target effects can be generated at nearly any concentration but it is generally regarded that the lower the concentration of siRNA, the weaker the off-target profile. Lower siRNA doses will often reduce the on-target phenotypes as well, so the concentration is a balancing act. Most screens tend toward using high siRNA concentrations to ensure knockdown and maximize the potential of capturing any phenotype; off-target effects are mitigated by employing multiple arrayed reagents per gene. Chosen siRNA reagents are typically resuspended from lyophilized powders in water or manufacturer supplied resuspension buffer. Be sure to use RNAse free pipette tips, consumable reagents, resuspension reagents, labware, and plates. It is also best to have dedicated pipetting systems for RNA work. We recommend working with siRNA reagents in a tissue-culture enclosure wiped down with ethanol and RNAse-neutralizing solution to maintain sterility and to create a dedicated space for RNA work.
5. During assay development, we recommended trying multiple siRNA transfection reagents in the 384-well plate format to assure that transfection alone is not affecting the assay in addition to achieving the highest possible efficiency. The siRNA transfection reagents come in a variety of chemistries including lipids, polymers, and nanoparticles, so finding the optimal reagent that balances delivery vs. toxicity may involve screening through multiple types.
6. For large-scale screening it is highly recommended to generate a large batch of medium using the same lot of FBS and base components. Store at 4 °C.
7. OptiMEM is another commonly used serum-free medium to conduct the transfection reagent complexing but it will depend on the transfection reagent and the cell line.
8. Besides the image acquisition (plate reading), the main throughput bottlenecks in most high-content screens are typically the plate-washing and bulk reagent dispensing. Having multiple liquid handling systems and HCS readers will allow

the automated system to scale throughput and minimize plate traffic jams. Additionally, we recommend combination plate washers that include bulk liquid dispensing to minimize the need for plate transit in wash-dispense steps. The combination instruments are ideal because of efficient use of space on the deck as well. Finally, to support the overnight incubations at 4 °C common in immunofluorescent HCS assays, dedicated refrigerated on-line incubators can reduce the need to manually load and unload the automated system.

9. Support for a software autofocus following the laser-based acquisition of the plate bottom focal plane may be useful in some assays to refine the focus on a particular biology of interest or where there are large, 3D dimensional features.
10. Include a Kozak consensus sequence such as 5′-GCCACC-3′ immediately upstream of the start codon of the chosen Green Fluorophore (addressed as GFP for simplicity). The N-terminus of the Parkin cDNA should be fused to the Green-Fluorophore without the presence of a stop codon between the two proteins. Given that 2A sequences are smaller and generate stoichiometric amounts of the upstream and downstream translated product, we generally recommend them for multi-cistronic overexpression constructs. However, given that they add additional amino acids to N-terminus of the final proteins, an internal ribosome entry site (IRES) can also be used, although the trade-off may be poorer co-expression efficiency. For 2A sequences, a recommended version is GSGATNFSLLKQAGDVEENPGP [33] and should be fused in-frame with the last codon of the Parkin cDNA, before the stop codon. A stop codon should only be placed at the end of the Red Fluorophore. The mito-RedFluorophore (addressed as mito-RFP for simplicity) fusion should begin with the methionine immediately after the final proline in the 2A sequence. For an IRES option, we recommend the following sequence:

5′-GCCCCTCTCCCTCCCCCCCCCCTAACGTTACTGGC
CGAAGCCGCTTGGAATAAGGCCGGTGTGCGTTTGTC
TATATGTTATTTTCCACCATATTGCCGTCTTTTGGCAA
TGTGAGGGCCCGGAAACCTGGCCCTGTCTTCTTGAC
GAGCATTCCTAGGGGTCTTTCCCCTCTCGCCAAAGG
AATGCAAGGTCTGTTGAATGTCGTGAAGGAAGCAGTT
CCTCTGGAAGCTTCTTGAAGACAAACAACGTCTGTAG
CGACCCTTTGCAGGCAGCGGAACCCCCCACCTGGCG
ACAGGTGCCTCTGCGGCCAAAAGCCACGTGTATAAGA
TACACCTGCAAAGGCGGCACAACCCCAGTGCCACGTT
GTGAGTTGGATAGTTGTGGAAAGAGTCAAATGGCTCA
CCTCAAGCGTATTCAACAAGGGGCTGAAGGATGCCC
AGAAGGTACCCCATTGTATGGGATCTGATCTGGGGC
CTCGGTGCACATGCTTTACATGTGTTTAGTCGAGGT

TAAAAAACGTCTAGGCCCCCCGAACCACGGGGACGT
GGTTTTCCTTTGAAAAACACGATGATAAT-3′

11. Given various FACS sorter configurations, 3 RFI log-units may not be optimal for strong HCS microscope signals. The correlation between HCS instrument signal and FACS RFI ranges may have to be determined empirically. Collect RFP and GFP positive cells and culture for several passages to expand the population.
12. An alternative to the population based cell line development is to select individual clones and expand based off of optimal performance in fluorescence microscopy. While this method minimizes variability, it can introduce "clone-specific" phenotypic behaviors that are not ideal for screening. If clonal selection is used, multiple clones should be carefully characterized to determine that a particular clone is not an outlier in the biology of interest.
13. For HCS, it is important that the screening cell line be frozen in multiple aliquots at the same passage number to ensure the performance over the campaign. Test the final cell bank for mycoplasma contamination and analyze the relevant phenotype to make sure it can be generated as expected. In the case of the Parkin assay, with standard florescence microscopy we utilize the standard CCCP-mediated (10 μM final concentration in culture medium) collapse of mitochondrial membrane potential [10] to induce GFP-Parkin translocation to mitochondria in 1–3 h followed by the clearance of most mitochondrial bodies in each cell after a 24-h incubation with CCCP.
14. For large screening sessions, determine if the transfection reagent is stable in the chosen transfection medium over an extended period of time.
15. When preparing the cells for final dispensing into the plates, each source flask should be examined for contamination and checked for normal cell morphology before harvesting. The HeLa cultures should be 80–90 % confluent at the time of harvesting. We recommend expanding the cell line used for HCS in the same manner for each screening run. If the direct dispensing method is to be used, rigorous testing must be conducted to assure that the cell line is capable of recovering from the shock of freeze-thaw followed by immediate siRNA transfection. If a large batch of cells in suspension is prepared in advance for automated dispensing, gentle stirring of the cell suspension in the container is essential to achieving consistent cell densities in the plates. An optimal practice for cell dispensing over periods >60 min is to cool the stirring cells to prevent further clumping of the cells (if the cells are amenable to such temperature changes). To minimize the settling of cells in

automated dispenser lines, the chosen system should be purged and re-primed periodically as well. The selection of a cell seeding density for a given HCS assay generally follows the optimal cell density at the termination of the assay. Optimization of cell seeding densities should be performed during assay development to achieve a final cell density that is sub-confluent in negative control wells. The goal is to find a density that will allow for efficient segmentation of cells during the primary analysis and interrogation of the biology in question. Additionally, cell-cell contacts in confluent or even semi-confluent wells may change the nature of receptor localization, so it is advisable to characterize the assay performance at a range of cell densities.

16. If using an off-line tissue-culture incubator with shelves (not plate cassettes), do not stack plates on top of each other.
17. Depending on the cell line, CCCP may or may not be the most effective method to trigger mitochondrial depolarization and Parkin translocation. Alternatively, one may try mixes of oligomycin to block complex V ATPase activity and valinomycin (an alternative ionophore) or antimycin A (inhibits the electron transport chain). Note: Ideally, the media containing mitochondrial membrane potential abolishing compounds should be kept at 37 °C. This is to reduce the temperature change in the wells after this solution is dispensed. Given that maintaining liquid temperature is difficult in the lines of automated bulk liquid dispensers, we have not encountered issues dispensing room temperature solution into the plates and returning them immediately to the 37 °C tissue-culture incubator.
18. To perform a mitophagy assay, plates would remain at 37 °C for approximately 24 h, although this time should also be optimized for each cell line. At the completion of the mitophagy assay time course, >90 % of the mito-RFP signal should be depleted from each cell and GFP-Parkin will have lost the punctate localization. In the case that a particular cell line exhibits a high degree of cell death during the extended mitophagy assay, addition of 10–20 μM Q-VD-OPh (final) in the culture medium is typically an effective method to reduce cytotoxicity.
19. Plates should be warmed to room temperature before imaging. It is also advisable to clean the optical surface of the plates prior to imaging.
20. The number of cells to acquire per well should be determined based on the variability of the cell-to-cell phenotype, the magnitude of that change, and its frequency. Statistical methods are be employed to aid in the balance of achieving sufficiently

powered samples sizes, minimizing the image data volume, and increasing screening speed.

21. Due to fluctuations in fluorescent protein and dye signals between screening runs, it is important to re-optimize the algorithms on a run-to-run basis. Always check to make sure your analysis pipeline is working properly by spot-checking plate controls. Also, do not rely on the numerical outputs alone to check algorithm performance. We suggest that throughout the analysis process images should be examined with segmentation overlays to assure that the algorithm is properly capturing, the desired biology.
22. It is likely that the apparent GFP-Parkin signal in the nucleus is due to protein in the cytosol above and below the nuclear envelope.
23. Prior to the application of transformations such as calculating the MAD, it is important to determine if the data is normally distributed. If not, the application of such methods is not appropriate. Non-parametric methodologies, such as redundant siRNA analysis (screening many unique reagents that target a given gene, each one in a separate well), are not dependent upon normally distributed data.

Acknowledgements

We would like to thank Madhu Lal-Nag for assistance with image retrieval. This work was supported by the Intramural Research Program of the NIH, NINDS and the Trans-NIH RNAi initiative.

References

1. Lightowlers RN, Taylor RW, Turnbull DM (2015) Mutations causing mitochondrial disease: what is new and what challenges remain? Science 349(6255):1494–1499. doi:10.1126/science.aac7516
2. Wallace DC (2013) A mitochondrial bioenergetic etiology of disease. J Clin Invest 123 (4):1405–1412. doi:10.1172/JCI61398
3. Klein C, Westenberger A (2012) Genetics of Parkinson's disease. Cold Spring Harb Perspect Med 2(1):a008888. doi:10.1101/cshperspect.a008888
4. Nuytemans K, Theuns J, Cruts M, Van Broeckhoven C (2010) Genetic etiology of Parkinson disease associated with mutations in the SNCA, PARK2, PINK1, PARK7, and LRRK2 genes: a mutation update. Hum Mutat 31 (7):763–780. doi:10.1002/humu.21277
5. Pickrell AM, Youle RJ (2015) The roles of PINK1, parkin, and mitochondrial fidelity in Parkinson's disease. Neuron 85(2):257–273. doi:10.1016/j.neuron.2014.12.007
6. Kane LA, Lazarou M, Fogel AI, Li Y, Yamano K, Sarraf SA, Banerjee S, Youle RJ (2014) PINK1 phosphorylates ubiquitin to activate Parkin E3 ubiquitin ligase activity. J Cell Biol 205(2):143–153. doi:10.1083/jcb.201402104
7. Kazlauskaite A, Kondapalli C, Gourlay R, Campbell DG, Ritorto MS, Hofmann K, Alessi DR, Knebel A, Trost M, Muqit MM (2014) Parkin is activated by PINK1-dependent phosphorylation of ubiquitin at Ser65. Biochem J 460(1):127–139. doi:10.1042/BJ20140334
8. Koyano F, Okatsu K, Kosako H, Tamura Y, Go E, Kimura M, Kimura Y, Tsuchiya H, Yoshihara H, Hirokawa T, Endo T, Fon EA, Trempe JF,

Saeki Y, Tanaka K, Matsuda N (2014) Ubiquitin is phosphorylated by PINK1 to activate parkin. Nature 510(7503):162–166. doi:10.1038/nature13392

9. Lazarou M, Sliter DA, Kane LA, Sarraf SA, Wang C, Burman JL, Sideris DP, Fogel AI, Youle RJ (2015) The ubiquitin kinase PINK1 recruits autophagy receptors to induce mitophagy. Nature 524(7565):309–314. doi:10.1038/nature14893
10. Narendra D, Tanaka A, Suen DF, Youle RJ (2008) Parkin is recruited selectively to impaired mitochondria and promotes their autophagy. J Cell Biol 183(5):795–803. doi:10.1083/jcb.200809125
11. Narendra DP, Jin SM, Tanaka A, Suen DF, Gautier CA, Shen J, Cookson MR, Youle RJ (2010) PINK1 is selectively stabilized on impaired mitochondria to activate Parkin. PLoS Biol 8(1):e1000298. doi:10.1371/journal.pbio.1000298
12. Hasson SA, Kane LA, Yamano K, Huang CH, Sliter DA, Buehler E, Wang C, Heman-Ackah SM, Hessa T, Guha R, Martin SE, Youle RJ (2013) High-content genome-wide RNAi screens identify regulators of parkin upstream of mitophagy. Nature 504(7479):291–295. doi:10.1038/nature12748
13. Hartwell KA, Miller PG, Mukherjee S, Kahn AR, Stewart AL, Logan DJ, Negri JM, Duvet M, Jaras M, Puram R, Dancik V, Al-Shahrour F, Kindler T, Tothova Z, Chattopadhyay S, Hasaka T, Narayan R, Dai M, Huang C, Shterental S, Chu LP, Haydu JE, Shieh JH, Steensma DP, Munoz B, Bittker JA, Shamji AF, Clemons PA, Tolliday NJ, Carpenter AE, Gilliland DG, Stern AM, Moore MA, Scadden DT, Schreiber SL, Ebert BL, Golub TR (2013) Niche-based screening identifies small-molecule inhibitors of leukemia stem cells. Nat Chem Biol 9(12):840–848. doi:10.1038/nchembio.1367
14. Schulte J, Sepp KJ, Wu C, Hong P, Littleton JT (2011) High-content chemical and RNAi screens for suppressors of neurotoxicity in a Huntington's disease model. PLoS One 6(8):e23841. doi:10.1371/journal.pone.0023841
15. Shan J, Schwartz RE, Ross NT, Logan DJ, Thomas D, Duncan SA, North TE, Goessling W, Carpenter AE, Bhatia SN (2013) Identification of small molecules for human hepatocyte expansion and iPS differentiation. Nat Chem Biol 9(8):514–520. doi:10.1038/nchembio.1270
16. Nishiya N, Oku Y, Kumagai Y, Sato Y, Yamaguchi E, Sasaki A, Shoji M, Ohnishi Y, Okamoto H, Uehara Y (2014) A zebrafish chemical suppressor screening identifies small molecule inhibitors of the Wnt/beta-catenin pathway. Chem Biol 21(4):530–540. doi:10.1016/j.chembiol.2014.02.015
17. Taylor KL, Grant NJ, Temperley ND, Patton EE (2010) Small molecule screening in zebrafish: an in vivo approach to identifying new chemical tools and drug leads. Cell Commun Signal 8:11. doi:10.1186/1478-811X-8-11
18. Reisen F, Sauty de Chalon A, Pfeifer M, Zhang X, Gabriel D, Selzer P (2015) Linking phenotypes and modes of action through high-content screen fingerprints. Assay Drug Dev Technol 13(7):415–427. doi:10.1089/adt.2015.656
19. Sundaramurthy V, Barsacchi R, Chernykh M, Stoter M, Tomschke N, Bickle M, Kalaidzidis Y, Zerial M (2014) Deducing the mechanism of action of compounds identified in phenotypic screens by integrating their multiparametric profiles with a reference genetic screen. Nat Protoc 9(2):474–490. doi:10.1038/nprot.2014.027
20. Sutherland JJ, Low J, Blosser W, Dowless M, Engler TA, Stancato LF (2011) A robust high-content imaging approach for probing the mechanism of action and phenotypic outcomes of cell-cycle modulators. Mol Cancer Ther 10(2):242–254. doi:10.1158/1535-7163.MCT-10-0720
21. Gibson CC, Zhu W, Davis CT, Bowman-Kirigin JA, Chan AC, Ling J, Walker AE, Goitre L, Delle Monache S, Retta SF, Shiu YT, Grossmann AH, Thomas KR, Donato AJ, Lesniewski LA, Whitehead KJ, Li DY (2015) Strategy for identifying repurposed drugs for the treatment of cerebral cavernous malformation. Circulation 131(3):289–299. doi:10.1161/CIRCULATIONAHA.114.010403
22. Gustafsdottir SM, Ljosa V, Sokolnicki KL, Anthony Wilson J, Walpita D, Kemp MM, Petri Seiler K, Carrel HA, Golub TR, Schreiber SL, Clemons PA, Carpenter AE, Shamji AF (2013) Multiplex cytological profiling assay to measure diverse cellular states. PLoS One 8(12):e80999. doi:10.1371/journal.pone.0080999
23. Singh S, Carpenter AE, Genovesio A (2014) Increasing the content of high-content screening: an overview. J Biomol Screen 19(5):640–650. doi:10.1177/1087057114528537
24. Halder V, Kombrink E (2015) Facile high-throughput forward chemical genetic screening by in situ monitoring of glucuronidase-based reporter gene expression in Arabidopsis

thaliana. Front Plant Sci 6:13. doi:10.3389/fpls.2015.00013

25. Allan C, Burel JM, Moore J, Blackburn C, Linkert M, Loynton S, Macdonald D, Moore WJ, Neves C, Patterson A, Porter M, Tarkowska A, Loranger B, Avondo J, Lagerstedt I, Lianas L, Leo S, Hands K, Hay RT, Patwardhan A, Best C, Kleywegt GJ, Zanetti G, Swedlow JR (2012) OMERO: flexible, model-driven data management for experimental biology. Nat Methods 9(3):245–253. doi:10.1038/nmeth.1896
26. Adler J, Parmryd I (2010) Quantifying colocalization by correlation: the Pearson correlation coefficient is superior to the Mander's overlap coefficient. Cytometry A 77(8):733–742. doi:10.1002/cyto.a.20896
27. Vincent L (1993) Morphological grayscale reconstruction in image analysis: applications and efficient algorithms. IEEE Trans Image Process 2(2):176–201. doi:10.1109/83.217222
28. Kamentsky L, Jones TR, Fraser A, Bray MA, Logan DJ, Madden KL, Ljosa V, Rueden C, Eliceiri KW, Carpenter AE (2011) Improved structure, function and compatibility for Cell Profiler: modular high-throughput image analysis software. Bioinformatics 27(8):1179–1180. doi:10.1093/bioinformatics/btr095
29. Tiscornia G, Singer O, Verma IM (2006) Production and purification of lentiviral vectors. Nat Protoc 1(1):241–245. doi:10.1038/nprot.2006.37
30. Chung N, Zhang XD, Kreamer A, Locco L, Kuan PF, Bartz S, Linsley PS, Ferrer M, Strulovici B (2008) Median absolute deviation to improve hit selection for genome-scale RNAi screens. J Biomol Screen 13(2):149–158. doi:10.1177/1087057107312035
31. Konig R, Chiang CY, Tu BP, Yan SF, DeJesus PD, Romero A, Bergauer T, Orth A, Krueger U, Zhou Y, Chanda SK (2007) A probability-based approach for the analysis of large-scale RNAi screens. Nat Methods 4(10):847–849. doi:10.1038/nmeth1089
32. Sigoillot FD, King RW (2011) Vigilance and validation: keys to success in RNAi screening. ACS Chem Biol 6(1):47–60. doi:10.1021/cb100358f
33. Kim JH, Lee SR, Li LH, Park HJ, Park JH, Lee KY, Kim MK, Shin BA, Choi SY (2011) High cleavage efficiency of a 2A peptide derived from porcine teschovirus-1 in human cell lines, zebrafish and mice. PLoS One 6(4):e18556. doi:10.1371/journal.pone.0018556

INDEX

A

ABC transporters 227, 228
Absorbance 8, 9, 100, 102, 104–106, 112, 184, 186
Acceptor 8, 67, 78–81, 83, 84, 86–88, 90, 91, 96, 133, 134, 137, 159–161, 163, 165, 167, 264, 266, 268
Aequorin 9, 208, 263
AlamarBlue (AB) 182, 183, 187, 188, 192, 194, 246, 253
Allosteric inhibitors 14
AlphaLisa 9, 141
AlphaPlex 78
Anisotropy 116–118, 120, 121, 123, 128
Antagonism 23, 34, 35, 39
Antibiotics 201
Anti-fungal 172, 176
Antimicrobial 181, 195
Apoptosis 3, 228, 229, 233, 241, 242, 246, 249, 251, 252, 255–257, 259, 261, 274
Aspergillus fumigatus 171–178
Assay artifacts 88
Assay development 2, 4, 12–15, 17–27, 29, 52, 54, 55, 58, 61, 85–87, 89, 94, 119, 134, 144, 150, 151, 160, 208, 213–215, 217, 222, 225, 264, 265, 279, 287, 298, 301
Assay optimization 21–24, 85–87, 94, 122, 134, 222, 223, 290, 301
Assay performance 22, 28, 186, 192, 205, 218, 219, 224, 253, 257, 281, 301
Assay validation 27, 29
Atomic absorbance spectroscopy (AAS) 9
Autoactivation 159, 162
Automated Assay Optimization (AAO) 24
Automated microscopy 274, 295
Automation 3, 48, 62, 145, 149–151, 246, 259, 274, 285, 287, 290
Autophosphorylation 159, 160, 162, 163, 165–167

B

BacTiter-Glo (BTG) 182, 188, 189, 192, 194, 195
Beta-lactamase 9
Binding assays 18–20, 22, 34, 119, 120, 126, 128, 141, 198
Binding site 13, 15, 19, 33, 35, 40, 143
Bioassay 141, 172
Bioluminescence resonance energy transfer (BRET) 8, 263–270
BODIPY 118

C

Calcium fluorescent dye 200
Cell culture 20, 23, 210, 211, 234, 237, 247, 249–251, 253, 255, 256, 265, 267, 269
Cell-based assays 7–9, 13, 20, 21, 23, 207, 213, 245, 283, 291
Chemiluminescent 77, 78
Clustered regularly interspersed palindromic repeats (CRISPR) 5, 273, 278
Coefficient of variation (CV) 26, 103, 107, 109, 111, 186, 218
Commercially available compound 65–67, 69, 71–74
Competition binding 119, 126
Competition detection assays 125, 126
Competitive inhibitors 13, 15, 18, 126
Culture medium 199, 201, 209, 223, 240, 247, 250, 287, 290, 291, 300, 301
Cyclic AMP 232
Cytostatic 246, 260

D

DAPI 275, 282, 284, 288, 291, 293, 295
Data analysis 42, 101–103, 106, 107, 109, 112, 137, 152, 154, 190, 203, 268, 288, 294–296
Data handling 58, 59
Data processing 58, 67
Database 67, 74, 149, 155, 281, 291
Depolarization 117, 198, 256, 276, 285, 291, 294, 301
Detergent 22, 61, 89, 122, 135, 151, 220, 225
Dimethyl sulfoxide (DMSO) 21, 41, 43, 54–56, 73, 83–87, 90, 91, 93, 94, 104, 135, 148–150, 152, 153, 155, 156, 165, 166, 175, 176, 183, 185, 186, 189, 190, 192, 200–203, 206, 210, 211, 214–217, 222, 224, 234–236, 240, 242, 247–249, 252, 253, 258, 287
DMSO tolerance 122, 151, 155, 176, 213, 214
Docking 65, 67–69, 71, 73, 74

William P. Janzen (ed.), *High Throughput Screening: Methods and Protocols*, Methods in Molecular Biology, vol. 1439,
DOI 10.1007/978-1-4939-3673-1, © Springer Science+Business Media New York 2016

Donor 40, 67, 78–81, 83–88, 90, 91, 96, 133, 134, 137, 141, 159–161, 163, 165–167, 263, 264, 266, 268
Dual luciferase reporter gene assay 209
Dual-Glo luciferase 210–212, 224

E

Edge effect 21, 22, 193, 223, 251, 259, 261
Efflux inhibitors 229, 238, 241
Electrochemiluminescence (ECL) 9
Electrophysiology 197
Electrospray (ESI) 59, 73
Emission 78, 89, 116–118, 131–134, 165, 175, 177, 188, 202, 206, 264, 265, 267, 269, 288
Enzymatic assays 13–18, 85, 91, 92, 125–126, 134, 137, 141
Enzyme inhibition 33
Enzyme titration 151
Enzyme-linked immunosorbent assay (ELISA) 9, 274
Excitation 8, 78, 86–89, 94, 116, 117, 128, 131, 133, 146, 175, 177, 188, 202, 206, 237, 264, 267
Experimental testing 65, 66, 74

F

False-positive 2, 29, 59, 70, 88, 119, 124, 125, 131, 134, 166, 209, 220, 225, 239, 245, 254, 260, 270, 279
Firefly luciferase 208–217, 219–221, 224
FLIPR 9, 197–201, 203, 204, 206
Flow cytometer 234, 235, 237, 241, 243, 246, 249, 256, 257, 261
Flow cytometry 228, 229, 234–243, 246, 256
Fluorescein 118, 128, 133, 148
Fluorescence 8, 9, 12, 18, 82, 112, 115–122, 124, 127, 128, 131, 133, 146, 160, 188, 194, 198, 202, 203, 207, 267, 268, 274–276, 279, 283, 286, 289, 300
Fluorescence-activated cell sorting (FACS) 286, 289, 300
Fluorescence anisotropy 117, 118
Fluorescence polarization (FP) 18, 82, 115, 116, 118–126, 128, 132, 160
Fluorescent substrates 228
Fluorophores 115–117, 131–133, 239, 263, 268
Functional genomics 273
Fungus 171–176, 178

G

Glide score (G-score) 68, 70
Global fit analyses 36
G-protein-coupled receptors (GPCRs) 5
Gravimetric quality control 100–103
Green fluorescent protein (GFP) 207, 263, 275, 276, 285, 289, 294, 299, 300

H

H37Rv 182–187, 191, 192
High-content analysis (HCA) 274
High-content imaging 9, 280, 286
High-content screening 273, 275, 277–283, 285–291, 294–296, 298–302
High-throughput flow cytometry 228, 229, 234–243
Hippo signaling pathway 264
Histone methyltransferase 40
Hit 3, 7, 28, 29, 35, 40, 55, 65–67, 69, 70, 72–74, 88, 119, 124, 125, 128, 133, 162, 166, 178, 185, 189, 195, 209, 215, 218–222, 225, 296, 297
Hit confirmation 55, 222
Hit triage 68, 72, 209

I

IC_{50} replot 37–39
Image analysis 277–280, 282, 288, 294
Image processing 279, 288, 294–296
Imaging assays 280, 282
Immobilized metal-ion affinity based FP (IMAP) 8, 11
Induced pluripotent stem cell (IPSC) 3, 7, 20, 23, 278, 283, 295
Inward rectifying potassium channel (Kir) 198
Ion channels 5, 6, 9, 197, 198
Ionization 47, 59

K

K_i 13–15, 34, 35, 38, 40, 43, 127
Kinase 5, 11, 13, 18, 66, 71, 80, 125, 145, 150, 151, 163, 165, 275, 276
K_m 11, 13, 15, 17, 19, 22, 40, 55, 56, 62, 85, 91, 94, 142, 144, 148, 151–153

L

Lead 1–3, 5–7, 51, 66, 99, 172
Library 55, 59, 85–87, 94, 124, 185, 215, 216, 286, 291, 296, 298
Liquid handler 24, 99, 101, 102, 104–108, 111, 112, 134, 137, 166, 173, 175, 237, 267
Local curve fitting 36
Luciferase 9, 210–214, 264, 265, 269, 279
Luciferin 208, 220
Luminescence 8, 9, 115, 163–165, 167, 188, 190, 194, 208, 212–214, 219, 224, 225, 264, 268, 274
Luminescent 77

M

Mass charge (m/z) 50
Mass spectrometry (MS) 9, 14, 47–52, 55, 56, 58–60, 62, 162, 198
Matrix Assisted Laser Desorption Ionization (MALDI) 9, 47
Media 11, 23, 173–175, 177, 178, 182, 185, 186, 194, 215, 265, 267, 268, 285, 301
Membrane integrity (live/dead cells) 246
Microfluidic capillary electrophoresis 66, 70, 72
Mitochondrial integrity 246
Mixed inhibitor 14
Mobile phase 48, 49, 52, 58, 61, 62, 73
Multidrug resistance 227, 241
Multiple inhibitor 33, 35–40, 42, 43
Multiple reaction monitoring (MRM) 49, 51, 60
Multiplexing 53, 58
Mycobacterium tuberculosis (mtb) 181–191, 193–195

N

Nanoluc luciferase (NLuc) 264, 266, 267, 269
Natural products 5, 229
Non-specific binding (NSB) 19, 22
Nuclear hormone receptors 5, 6

P

Parkin 274, 276, 279, 282–291, 293–296, 299–302
Patch-clamp 9, 197
Phenotypic 1–4, 7, 9, 20, 172, 273, 277–279, 300
Photometric quality control 100, 102–108
Pin tool 83–85, 93
Plate reader 9, 41, 44, 83–87, 91, 100, 102, 104–106, 108, 109, 111, 112, 119, 120, 124, 128, 134, 136, 137, 175, 183, 188, 210, 212, 219, 220, 225, 246, 248, 249, 254–256, 259, 261, 265, 267–269
Polarization 115–117, 120, 126, 128
Procurement 2, 66, 67, 74
Product 7, 14, 18, 41, 43, 50–52, 55, 58–60, 62, 79–81, 83, 84, 87, 89, 94, 125, 132, 141, 142, 146, 147, 152, 155, 167, 173, 192, 208, 247, 299
Protein-protein interactions (PPI) 5, 6, 8, 77, 78, 81–87, 89, 90, 93, 94, 115, 132, 134, 136, 141, 264, 265, 270

Q

Quality control (QC) 2, 27, 73, 99–105, 107, 108, 112, 119, 124, 239, 275, 278, 291
Quench 9, 41, 88, 124, 127, 133, 212, 224, 254, 255, 260, 274

R

Radiometric assay 40
RapidFire™ 47–54, 57–59, 61, 62
Reference compound 56, 72, 150, 154, 164, 177
Renilla luciferase 208, 210, 212, 224, 264
Reporter gene 9, 211, 274
Resazurin 172, 173, 175–178, 246, 248, 253
RNAi 5

S

Scintillation proximity assay (SPA) 9, 19
Scoring functions 66
Screen 2, 4, 8, 11, 48, 56, 58, 61, 62, 65, 66, 77, 119, 121, 124, 159, 175, 176, 182, 189, 191, 193, 195, 228, 229, 252, 257–260, 278, 279, 285, 286, 290, 291, 293–296, 298
Screening 1–9, 11–29, 34, 55, 65–68, 70, 71, 74, 77, 88, 91, 93, 99, 115, 122, 131, 174, 175, 182, 197, 198, 208, 209, 215, 222, 224, 264, 273, 274, 276–280, 282, 283, 285–291, 293, 296, 298, 300, 302
Secreted alkaline phosphatase 9
Selectivity profiling 143–145, 147, 149–152, 154, 155
Serial dilution 44, 136, 137, 141, 148, 149, 151, 165, 185, 211, 221, 222, 266
Short hairpin ribonucleic acid (shRNA) 4, 273, 278
Signal to background ratio (S/B) 25–27, 120, 127, 128, 132, 133, 137, 138, 218, 295
Signal to noise 26
Small inhibitory ribonucleic acid (siRNA) 4, 273, 274, 276, 278, 279, 282, 283, 286, 287, 290, 291, 293–296, 298, 300, 302
Solvent tolerance 55
Stable cell lines 20, 208–210, 223, 279
Standard curve 52, 102, 104, 105, 112, 125
State-dependent blockers 197–201, 203, 204, 206
Stem cell 3, 20, 171, 227
Stokes shift 131, 133
Structural Protein-Ligand Interaction Fingerprints (SPLIF) 66–69, 71, 72

Structure-based virtual screening 65–67, 69, 71–74
Substrate 6, 8, 11, 13–15, 17, 18, 22, 33, 35, 37, 39–41, 43, 50, 55, 56, 58, 59, 62, 66, 72, 73, 78–80, 83, 85, 86, 91, 92, 94, 125, 141, 142, 146–149, 151–153, 155, 159, 160, 162, 163, 167, 208, 210–212, 219–225, 264, 268, 269
Substrate affinity 55
Substrate depletion 14, 17, 18, 62, 79, 83, 85, 92
Substrate inhibition 43
Synergism 34–36, 38, 39, 42

T

Tartrazine 100, 102, 104–108, 111, 112
TB. *See* Tuberculosis (TB)
Time-of-flight (ToF) 50
Time-resolved fluorescence assays 131–134, 136, 137, 141
Time-resolved fluorescence resonance energy transfer (TR-FRET) 8, 9, 11, 133, 134, 136–138, 140, 141, 160
Titration 85–87, 91–94, 96, 97, 120, 121, 123, 124, 126, 137, 138, 140, 141, 151, 152, 167, 184–185, 213–216
Tolerance 85–87, 93
Total cell counts 246
Total fluorescence intensity (FLINT) 116, 124, 128, 274
Toxicity 245–257, 259–261, 274, 277, 279, 283, 298
Transient expression 20, 222
Transient transfection 20, 208, 266, 267
Triage 66, 70, 209, 220–222, 225
Triple quadrupole (QqQ) 49–51, 58
TruHit 88
Tuberculosis (TB) 181, 194

U

Ultra high-throughput screening (uHTS) 210, 264
Uncompetitive inhibitors 13, 14, 18

V

Validation 4–7, 27
Viability 172, 176, 190, 205, 211, 214, 215, 229, 241, 246–248, 250, 251, 253, 254, 257, 274
Virtual screening (VS) 65–67, 69, 71–74, 124
Voltage-gated calcium channel (VGCC) 197–201, 203, 204, 206
Voltage-sensing dyes 9

Y

YAP-TEAD interaction 264, 265
Yonetani-Theorell 35, 36, 42

Z

Z′ factor 26, 27, 99, 239